frontiers | Research Topics

Cerebrospinal fluid dynamics and intracranial pressure elevation – novel insights on molecular and physiological mechanisms, and implications for neurological disease

Edited by
Adjanie Patabendige, Marcus Stoodley and Vegard Vinje

Published in
Frontiers in Molecular Neuroscience

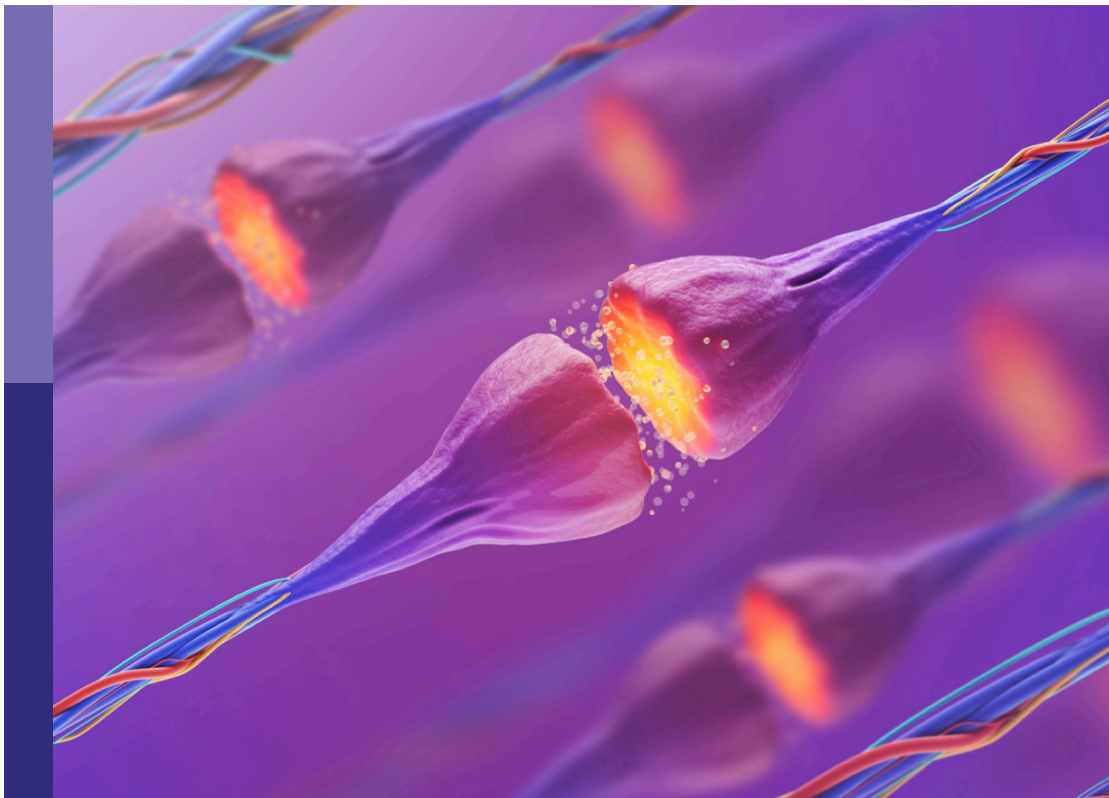

ISSN 1664-8714
ISBN 978-2-83251-309-5
DOI 10.3389/978-2-83251-309-5

About Frontiers

Frontiers is more than just an open access publisher of scholarly articles: it is a pioneering approach to the world of academia, radically improving the way scholarly research is managed. The grand vision of Frontiers is a world where all people have an equal opportunity to seek, share and generate knowledge. Frontiers provides immediate and permanent online open access to all its publications, but this alone is not enough to realize our grand goals.

Frontiers journal series

The Frontiers journal series is a multi-tier and interdisciplinary set of open-access, online journals, promising a paradigm shift from the current review, selection and dissemination processes in academic publishing. All Frontiers journals are driven by researchers for researchers; therefore, they constitute a service to the scholarly community. At the same time, the *Frontiers journal series* operates on a revolutionary invention, the tiered publishing system, initially addressing specific communities of scholars, and gradually climbing up to broader public understanding, thus serving the interests of the lay society, too.

Dedication to quality

Each Frontiers article is a landmark of the highest quality, thanks to genuinely collaborative interactions between authors and review editors, who include some of the world's best academicians. Research must be certified by peers before entering a stream of knowledge that may eventually reach the public - and shape society; therefore, Frontiers only applies the most rigorous and unbiased reviews. Frontiers revolutionizes research publishing by freely delivering the most outstanding research, evaluated with no bias from both the academic and social point of view. By applying the most advanced information technologies, Frontiers is catapulting scholarly publishing into a new generation.

What are Frontiers Research Topics?

Frontiers Research Topics are very popular trademarks of the *Frontiers journals series*: they are collections of at least ten articles, all centered on a particular subject. With their unique mix of varied contributions from Original Research to Review Articles, Frontiers Research Topics unify the most influential researchers, the latest key findings and historical advances in a hot research area.

Find out more on how to host your own Frontiers Research Topic or contribute to one as an author by contacting the Frontiers editorial office: frontiersin.org/about/contact

Cerebrospinal fluid dynamics and intracranial pressure elevation – novel insights on molecular and physiological mechanisms, and implications for neurological disease

Topic editors

Adjanie Patabendige — Edge Hill University, United Kingdom

Marcus Stoodley — Macquarie University, Australia

Vegard Vinje — Simula Research Laboratory, Norway

Citation

Patabendige, A., Stoodley, M., Vinje, V., eds. (2023). *Cerebrospinal fluid dynamics and intracranial pressure elevation – novel insights on molecular and physiological mechanisms, and implications for neurological disease*.

Lausanne: Frontiers Media SA. doi: 10.3389/978-2-83251-309-5

Table of contents

frontiers | Frontiers in Molecular Neuroscience

TYPE Editorial
PUBLISHED 28 December 2022
DOI 10.3389/fnmol.2022.1119980

OPEN ACCESS

EDITED AND REVIEWED BY
Detlev Boison,
The State University of New Jersey,
United States

*CORRESPONDENCE
Adjanie Patabendige
✉ Adjanie.Patabendige@edgehill.ac.uk

SPECIALTY SECTION
This article was submitted to
Brain Disease Mechanisms,
a section of the journal
Frontiers in Molecular Neuroscience

RECEIVED 09 December 2022
ACCEPTED 09 December 2022
PUBLISHED 28 December 2022

CITATION
Patabendige A, Vinje V and Stoodley M (2022) Editorial: Cerebrospinal fluid dynamics and intracranial pressure elevation–Novel insights on molecular and physiological mechanisms, and implications for neurological disease. *Front. Mol. Neurosci.* 15:1119980. doi: 10.3389/fnmol.2022.1119980

Editorial: Cerebrospinal fluid dynamics and intracranial pressure elevation–Novel insights on molecular and physiological mechanisms, and implications for neurological disease

Adjanie Patabendige[1,2,3]*, Vegard Vinje[4] and Marcus Stoodley[5]

[1]Brain Barriers Research Group, Department of Biology, Edge Hill University, Ormskirk, United Kingdom, [2]The School of Biomedical Sciences and Pharmacy, The University of Newcastle, Newcastle, NSW, Australia, [3]Department of Clinical Infection, Microbiology & Immunology, Institute of Infection, Veterinary, and Ecological Sciences, University of Liverpool, Liverpool, United Kingdom, [4]Simula Research Laboratory, Department of Numerical Analysis and Scientific Computing, Oslo, Norway, [5]Neurosurgery Unit, Faculty of Medicine, Health and Human Sciences, Macquarie University, Sydney, NSW, Australia

KEYWORDS

cerebrospinal fluid, intracranial pressure, ischaemic stroke, hydrocephalus, idiopathic intracranial hypertension, neurovascular unit

Editorial on the Research Topic
Cerebrospinal fluid dynamics and intracranial pressure elevation–Novel insights on molecular and physiological mechanisms, and implications for neurological disease

Cerebrospinal fluid (CSF) provides a protective cushioning to the brain and the spinal cord, and serves an important role in nutrient transport and waste removal, essential for maintaining normal neuronal function. Homeostatic feedback mechanisms are responsible for the strict regulation of CSF formation, composition, volume, turnover, and flow (Bothwell et al., 2019). Dysregulation of these homeostatic feedback mechanisms during certain neurological diseases such as stroke, brain trauma, hydrocephalus and idiopathic intracranial hypertension (IIH) can cause CSF volume to rise. This can be life threatening, as it leads to an increase in intracranial pressure (ICP). Control of ICP is achieved *via* highly invasive procedures. Development of non-invasive treatments such as pharmacological agents is hampered by a lack of suitable models and incomplete understanding of the underlying pathophysiology.

This Research Topic aimed to collect emerging evidence and novel perspectives on CSF dynamics and ICP elevation in neurological disease to highlight new developments in this field.

ICP elevation due to an increase in fluid build-up in the skull is experienced by patients with large malignant strokes, but this is not usually reported in minor-moderate strokes due to the need for highly invasive ICP measurement methods in the clinic (Helbok et al., 2014). Therefore, evidence for ICP elevation and underlying mechanisms in these strokes is mainly derived from pre-clinical stroke models (Omileke et al., 2021a,b). To further understand these mechanisms, Bothwell et al. explored cranial CSF clearance at cervical lymphatics using a tracer method to determine CSF movement into deep cervical lymph nodes and transit to the spinal subarachnoid space in a rat model of ischaemic stroke. The data suggested that a reduction in the CSF clearance through the cervical lymphatics may contribute to ICP elevation post ischaemic stroke. This was partially compensated by an increase in spinal CSF outflow as demonstrated by an increase in CSF transit to the spinal subarachnoid space. These findings could explain other studies which have reported increased resistance to CSF outflow post-stroke (Patabendige et al., 2019; Alshuhri et al., 2020), which indicate that a reduction in cranial CSF clearance is responsible for increased CSF outflow resistance in ischaemic stroke. According to the Monro–Kellie doctrine, the total volume of brain, blood and CSF is constant, and an increase in one of these components will cause a decrease in one or both of the other two components to maintain physiological ICP (Wilson, 2016). In their study of CSF micro-volume changes inside the spinal space, Klarica et al. introduced a new hypothesis that suggests an increase or decrease in ICP can occur due to small changes in spinal CSF volume without significant changes in CSF volume in the cranium. Their research points to a crucial role of the spinal subarachnoid space in controlling CSF pressure-that the spinal subarachnoid space plays a greater role than the intracranial space in compensating ICP fluctuations. However, others have also pointed towards the importance of considering the effect of epidural blood flow on the spinal pressures to fully understand the dynamics of CSF flow, especially during respiration (Lloyd et al., 2020).

Traditional views of CSF dynamics and ICP continue to be challenged as the field continues to evolve and new theories are formed, and novel models developed to study these complex mechanisms. Indeed, Eide and Hansson have provided a new perspective on the pathophysiology of IIH. While the pathophysiology of IIH is unknown, the authors challenged conventional studies that focus solely on intracranial CSF and venous pressures as main culprits. Their findings demonstrate that the majority of the patients included in their study had abnormal structural changes at the glia-neuro-vascular interface, suggesting capillary damage and blood-brain barrier (BBB) dysfunction as primary events in the pathophysiology of IIH. This suggests that BBB dysfunction and astrogliosis (Patabendige et al., 2021) could lead to an increase in brain volume and affect intracranial compliance, causing elevated ICP in IIH patients, while venous compression and increased CSF pressure may be secondary events. Furthermore, in their review, Yang et al. discuss the role of astrocytes in the pathophysiology of hydrocephalus, and stress the need for further studies, because astrocytes have not received the attention they deserve given their potentially important role in the pathophysiology of hydrocephalus. Others have demonstrated that "tissue compliance" could be an important factor, where neurons may also adaptively regulate their volume in diseases such as stroke in response to increased ICP, challenging the current dogma in pressure-volume relationships in neurological disease (Kalisvaart et al., 2020). A comprehensive review by Zhao et al. highlights the role played by aquaporins (AQP), which are highly expressed in astrocytic endfeet (AQP4) and choroid plexus epithelial cells (AQP1), in the pathophysiology of idiopathic normal pressure hydrocephalus, and outlined new targets for further research. Overall these studies and reviews demonstrate the important role played by the cells of the neurovascular unit in the pathophysiology of these diseases, and the need for further studies to determine their contribution to disease pathology. Other reviews in this topic discuss the role of the choroid plexus epithelium in neurological disease (Liu et al.) and the role of ependymal cilia in hydrocephalus (Ji et al.).

Finally, Hornkjøl et al. and Perera et al. have presented novel findings on CSF dynamics from a computational model and a non-invasive magnetic resonance imaging (MRI) technique respectively. Hornkjøl et al. demonstrated the importance of CSF dynamics on transport and clearance of substances, not only in the spinal subarachnoid space, but also deep into the brain. Research on the 'glymphatic system', a proposed waste clearance system of the brain, has mainly focused on fluid flow and transport within the brain (Iliff et al., 2012), while Hornkjøl et al. show that CSF flow in the spinal subarachnoid space may reduce characteristic clearance times of substances in the human brain from years to a few days. Perera et al. demonstrated the first ever application of a novel blood-cerebrospinal fluid barrier arterial spin labeling (BCSFB-ASL) MRI approach to determine BCSFB function in healthy and hypertensive rats. The findings suggest that BCSFB could be a key site vulnerable to systemic hypertension, leading to changes in CSF homeostasis in hypertensive subjects.

Overall, this Research Topic provides a cross-cutting perspective of CSF dynamics and ICP elevation, and showcases a range of thought-provoking approaches and models to study the complex underlying mechanisms. The novel discoveries

presented here will be exciting to follow as the field moves forward from traditional concepts of CSF dynamics.

Author contributions

Conceptualization and writing—original draft: AP. Writing—review and editing: AP, VV, and MS. All authors approved the submitted version.

Acknowledgments

Support from the Research Investment Fund by the Edge Hill University, UK to AP is acknowledged.

Conflict of interest

The authors declare that the research was conducted in the absence of any commercial or financial relationships that could be construed as a potential conflict of interest.

Publisher's note

References

Alshuhri, M. S., Gallagher, L., McCabe, C., and Holmes, W. M. (2020). Change in CSF dynamics responsible for ICP elevation after ischemic stroke in rats: a new mechanism for unexplained END? *Transl Stroke Res*. 11, 310–318. doi: 10.1007/s12975-019-00719-6

Bothwell, S. W., Janigro, D., and Patabendige, A. (2019). Cerebrospinal fluid dynamics and intracranial pressure elevation in neurological diseases. *Fluids Barriers CNS*. 16, 9. doi: 10.1186/s12987-019-0129-6

Helbok, R., Olson, D. M., Roux, P. D. L., Vespa, P., and The Participants in the International Multidisciplinary Consensus Conference on Multimodality Monitoring. (2014). Intracranial pressure and cerebral perfusion pressure monitoring in non-TBI patients: special considerations. *Neurocrit Care*. 21, S85–94. doi: 10.1007/s12028-014-0040-6

Iliff J. J., Wang, M., Liao, Y., Plogg, B. A., Peng, W., Gundersen, G. A., et al. (2012). A paravascular pathway facilitates CSF flow through the brain parenchyma and the clearance of interstitial solutes, including amyloid β. *Sci Transl Med*. 4, 147ra111. doi: 10.1126/scitranslmed.3003748

Kalisvaart, A. C. J., Wilkinson, C. M., Gu, S., Kung, T. F. C., Yager, J., Winship, I. R., et al. (2020). An update to the Monro-Kellie doctrine to reflect tissue compliance after severe ischemic and hemorrhagic stroke. *Sci Rep*. 10, 22013. doi: 10.1038/s41598-020-78880-4

Lloyd, R. A., Butler, J. E., Gandevia, S. C., Ball, I. K., Toson, B., Stoodley, M. A., et al. (2020). Respiratory cerebrospinal fluid flow is driven by the thoracic and lumbar spinal pressures. *J Physiol*. 598, 5789–5805. doi: 10.1113/JP279458

Omileke, D., Bothwell, S. W., Pepperall, D., Beard, D. J., Coupland, K., Patabendige, A. et al. (2021a). Decreased intracranial pressure elevation and cerebrospinal fluid outflow resistance: a potential mechanism of hypothermia cerebroprotection following experimental stroke. *Brain Sci*. 11,1589. doi: 10.3390/brainsci11121589

Omileke, D., Pepperall, D., Bothwell, S. W., Mackovski, N., Azarpeykan, S., Beard, J., et al. (2021b). Ultra-short duration hypothermia prevents intracranial pressure elevation following ischaemic stroke in rats. *Front. Neurol*. 12, 684353. doi: 10.3389/fneur.2021.684353

Patabendige, A., MacKovski, N., Pepperall, D., Hood, R., and Spartt, N. (2019). Correction to: A26 Cerebrospinal fluid outflow resistance is increased following small-moderate ischaemic stroke. *Fluids and Barriers of the CNS*. 16, 22. doi: 10.1186/s12987-019-0144-7

Patabendige, A., Singh, A., Jenkins, S., Sen, J., Chen, R. (2021). Astrocyte activation in neurovascular damage and repair following ischaemic stroke. *Int. J. Mol. Sci*. 22, 4280. doi: 10.3390/ijms22084280

Wilson, M. H. (2016). Monro-Kellie 2.0: The dynamic vascular and venous pathophysiological components of intracranial pressure. *J. Cereb. Blood Flow. Metab*. 36, 1338–1350. doi: 10.1177/0271678X16648711

frontiers in Molecular Neuroscience

ORIGINAL RESEARCH
published: 09 August 2021
doi: 10.3389/fnmol.2021.712779

Altered Cerebrospinal Fluid Clearance and Increased Intracranial Pressure in Rats 18 h After Experimental Cortical Ischaemia

Steven W. Bothwell[1,2], Daniel Omileke[1,2], Rebecca J. Hood[1,2], Debbie-Gai Pepperall[1,2], Sara Azarpeykan[1,2], Adjanie Patabendige[1,2,3]† and Neil J. Spratt[1,2,4]*†*

[1] The School of Biomedical Sciences and Pharmacy, The University of Newcastle, Newcastle, NSW, Australia, [2] Hunter Medical Research Institute, Newcastle, NSW, Australia, [3] Institute of Infection, Veterinary & Ecological Sciences, University of Liverpool, Liverpool, United Kingdom, [4] Hunter New England Local Health District, Newcastle, NSW, Australia

Oedema-independent intracranial pressure (ICP) rise peaks 20–22-h post-stroke in rats and may explain early neurological deterioration. Cerebrospinal fluid (CSF) volume changes may be involved. Cranial CSF clearance primarily occurs *via* the cervical lymphatics and movement into the spinal portion of the cranio-spinal compartment. We explored whether impaired CSF clearance at these sites could explain ICP rise after stroke. We recorded ICP at baseline and 18-h post-stroke, when we expect changes contributing to peak ICP to be present. CSF clearance was assessed in rats receiving photothrombotic stroke or sham surgery by intraventricular tracer infusion. Tracer concentration was quantified in the deep cervical lymph nodes *ex vivo* and tracer transit to the spinal subarachnoid space was imaged *in vivo*. ICP rose significantly from baseline to 18-h post-stroke in stroke vs. sham rats [median = 5 mmHg, interquartile range (IQR) = 0.1–9.43, $n = 12$, vs. −0.3 mmHg, IQR = −1.9–1.7, $n = 10$], $p = 0.03$. There was a bimodal distribution of rats with and without ICP rise. Tracer in the deep cervical lymph nodes was significantly lower in stroke with ICP rise (0 μg/mL, IQR = 0–0.11) and without ICP rise (0 μg/mL, IQR = 0–4.47) compared with sham rats (4.17 μg/mL, IQR = 0.74–8.51), $p = 0.02$. ICP rise was inversely correlated with faster CSF transit to the spinal subarachnoid space ($R = -0.59$, $p = 0.006$, Spearman's correlation). These data suggest that reduced cranial clearance of CSF via cervical lymphatics may contribute to post-stroke ICP rise, partially compensated *via* increased spinal CSF outflow.

Keywords: cerebrospinal fluid, infarct expansion, neurological deterioration, ischaemia, intracranial pressure, stroke, lymphatics, spinal clearance

Abbreviations: ICP, Intracranial pressure; CSF, Cerebrospinal fluid; IQR, Interquartile range; MCAo, Middle cerebral artery occlusion; SD, Standard deviation; SEM, Standard error of the mean; dcLN, Deep cervical lymph nodes.

OPEN ACCESS

Edited by:
Arianna Bellucci, University of Brescia, Italy

Reviewed by:
Giuseppe Pignataro, University of Naples Federico II, Italy
Jan Wenzel, University of Lübeck, Germany
Marina Rubio, Institut National de la Santé et de la Recherche Médicale (INSERM), France

***Correspondence:**
Adjanie Patabendige
Adjanie@liverpool.ac.uk
Neil J. Spratt
Neil.spratt@health.nsw.gov.au

† These authors have contributed equally to this work

Specialty section:
This article was submitted to Brain Disease Mechanisms, a section of the journal Frontiers in Molecular Neuroscience

Received: *21 May 2021*
Accepted: *16 July 2021*
Published: *09 August 2021*

Citation:
Bothwell SW, Omileke D, Hood RJ, Pepperall D-G, Azarpeykan S, Patabendige A and Spratt NJ (2021) Altered Cerebrospinal Fluid Clearance and Increased Intracranial Pressure in Rats 18 h After Experimental Cortical Ischaemia. Front. Mol. Neurosci. 14:712779. doi: 10.3389/fnmol.2021.712779

INTRODUCTION

Ischaemic stroke is a leading cause of death and disability worldwide (Mathers and Loncar, 2006). Stroke severity is variable, and some patients present with relatively minor stroke. While occlusion of small branch vessels accounts for many of those with minor symptoms, it is now recognised that some patients with minor symptoms may have large vessel occlusion (Smith et al., 2005). Around 10–20% of patients with minor stroke or transient ischaemic attack will experience early recurrent stroke and infarct expansion, and the vast majority of these occur in the initially ischaemic vascular territory (Asdaghi et al., 2011; Coutts et al., 2012).

The most likely cause of infarct expansion is failure of leptomeningeal collateral vessels. Failure of initially good collateral blood flow is associated with infarct growth following ischaemic stroke (Campbell et al., 2013). The cause of collateral vessel failure has not been definitively established. However, after stroke, blood flow in these vessels is largely driven by cerebral perfusion pressure, which is sensitive to changes in intracranial pressure (ICP) (Czosnyka and Pickard, 2004). In support of this, our previous work showed that elevation of ICP during middle cerebral artery occlusion (MCAo) in rats caused a linear reduction of collateral blood flow (Beard et al., 2015). We previously identified a dramatic rise in ICP present at 24 h after minor ischaemic stroke in rats, which peaked at 20–22 h (Murtha et al., 2014a; Beard et al., 2016). Other labs have shown that ICP is elevated around 24 h post-stroke in both small and large experimental ischaemia (Kotwica et al., 1991; Silasi et al., 2009). Clinical observations of stroke patients also found elevated ICP at 24 h (Kovacs et al., 2017). The time point of this ICP rise, taken with our understanding of how ICP influences collateral blood flow, suggests a possible mechanism of collateral failure and infarct expansion.

Our understanding of the underlying mechanisms of this ICP rise is limited. Tissue, blood, and cerebrospinal fluid (CSF) volume all determine ICP. We know that oedema (tissue volume) is not the primary cause (Murtha et al., 2015) and pilot data from our lab suggest that there is no contribution of cerebral blood volume (McLeod et al., 2014). Emerging evidence suggests that CSF volume is increased post-stroke. Resistance to CSF outflow is increased 18 h post-stroke in a rat model of cortical ischaemia and 24 h post-stroke in a model of striatal stroke (Patabendige et al., 2019; Alshuhri et al., 2020). These studies indicate that increased CSF volume may contribute to ICP rise after stroke.

We are only now beginning to understand the importance and complexities of CSF dynamics (Bothwell et al., 2019). Traditional textbook explanations of CSF clearance describe the movement of CSF into the superior sagittal sinus *via* arachnoid projections (Weed, 1914; Davson and Segal, 1996). However, our understanding has now shifted in line with a large body of work that describes CSF drainage from the subarachnoid space to the deep cervical lymphatics in multiple species (Boulton et al., 1999; Mollanji et al., 2001a,b; Mathieu et al., 2013; Ma et al., 2017; Maloveska et al., 2018). There are two primary mechanisms hotly debated in contemporary discussions of CSF clearance to the lymphatics system. The first describes the clearance of CSF from the subarachnoid space into the nasal mucosa along the perineural sheathes of olfactory nerves (Faber, 1937; Jackson et al., 1979; Walter et al., 2006; Ma et al., 2017; Norwood et al., 2019). These nerves cross the cribriform plate and once in the nasal mucosa, CSF moves to lymphatic vessels of the submucosa and onto the deep cervical lymphatics (Bradbury and Westrop, 1983; Zakharov et al., 2004; Proulx, 2021). The second mechanism describes the uptake of CSF into lymphatic vessels located in the dura mater, described as the "meningeal lymphatics," with some evidence that the basal cisterns are hotspots of CSF uptake (Aspelund et al., 2015). In this model, the meningeal lymphatics support direct clearance of CSF into the deep cervical lymphatics that is distinct from lymphatic uptake at the nasal mucosa (Louveau et al., 2015). Either way, clearance is directed to the cervical lymphatics.

Our lab previously implicated CSF clearance into the nasal mucosa as a major outflow pathway in rats, along with drainage into the spinal canal (Murtha et al., 2014b). In rodents, CSF has been shown to travel along the spinal subarachnoid space and canal before moving into lymphatic vessels of the sacral spine (Ma et al., 2019). In this study, we aimed to determine whether cranial CSF clearance is altered in an animal model of ischaemic stroke, and whether alterations are likely to contribute to ICP rise after stroke.

MATERIALS AND METHODS

Animals

Procedures were carried out on male outbred Wistar rats aged between 8 and 12 weeks ($n = 31$) weighing between 280 and 320 g. All experimental animal procedures used in this project were in accordance with the Australian Code of Practice for the Care and Use of Animals for Scientific Purposes and were approved by the Animal Care and Ethics Committee of the University of Newcastle (A-2013-343).

Animals were excluded from experiments if they presented with congenital deformities that obstructed surgical laminectomy to expose the imaging window, or if technical errors preventing accurate penetration of the ventricles and infusion of Evans blue dye occurred. Animals were only included in the final analysis after confirmation of stroke, and ventricle penetration of infusion catheter by histology.

Animals were assigned to stroke or sham groups prior to intervention. Blinding was not possible during experimental procedures; however, the investigator was blinded at the time of data extraction and analysis: each animal was assigned an experiment number and analysis was carried out on all data in one sitting with no indication of experimental stroke status.

Anaesthesia and Monitoring

Rats were anaesthetised with isoflurane (5% induction, 2–2.5% maintenance) in 50:50% N_2:O_2. Incision sites were injected subcutaneously with 2 mg/kg 0.05% Bupivacaine (Pfizer, Sydney, Australia). Core body temperature was regulated and maintained at 37°C *via* a thermocouple rectal probe (RET-2, Physitemp

Instruments Inc., Clifton, NJ, United States) and heat mat. Blood gases and pH were measured in a fast blood analyser (i-STAT 1; Abbott, Australia) at baseline prior to stroke and prior to Evans blue dye infusion from 0.1 mL blood samples taken from a femoral arterial line. This line was also used for arterial blood pressure monitoring. Prior to recovery, an additional Bupivacaine injection (0.3 mL, 0.05%, subcutaneous) and rectal paracetamol (250 mg/kg; GlaxoSmithKline, Brentford, United Kingdom) were administered for overnight pain relief. Saline was administered intraperitoneally (2 × 1.5 mL) to replace fluid loses. Following surgery, animals were returned to their cages with free access to food and water. Cages were placed half over a heat mat to allow animals to thermoregulate during recovery.

ICP Measurement

ICP (mmHg) was measured using a fibre-optic pressure sensor (Opsens Solutions, Quebec, Canada). Rats were fixed in a stereotaxic frame with ear bars in and a burr hole was made −1.8 mm lateral and −2 mm posterior to Bregma on the left parietal bone. A hollow polyether ether ketone (PEEK) screw (5 mm long, 1 mm internal diameter) was fixed in the burr hole. The screw was filled with saline and the pressure sensor wire was sealed 5 mm deep so that the sensor was sitting above the dura. Correct positioning was confirmed when a trace of pulse and respiratory oscillations were observed after the wire was sealed in place. Baseline ICP was recorded for 30 min prior to photothrombotic stroke, and average ICP was recorded from 17.5 to 18 h post-stroke in all animals. ICP was recorded up to 21 h in some animals but not all as experiment timing restricted our ability to correct displacements of the ICP probe that occurred after CSF tracer infusion.

Photothrombotic Stroke

A light source (100,000 LUX, 5 mm diameter, Olympus Corporation LG-PS2, Tokyo, Japan) was placed over the right parietal bone 0.5 mm from the skull surface, 1.2 mm posterior to Bregma. While the light source was concentrated on the skull, Rose bengal in saline (0.01 g/kg; Sigma, St. Louis, MO, United States) was infused into the right femoral vein followed by 1 mL saline. The light source remained constant for 20 min after Rose bengal infusion. Sham animals received only saline + light exposure.

Laminectomy

Laminectomy was carried out as previously described (Walker et al., 2015). Briefly, an incision was made from the back of the head caudally to the mid-thoracic region. The connective tissue was blunt dissected away and a cut was made through the midline of each muscle layer. The paraspinous muscles were retracted to expose the spinal column and connective tissue was blunt dissected. A dental drill (Saeshin Precision, Paho-dong, Korea) was used to thin the laminae of the C7 and T1 vertebrae. The laminae were then cut and removed at these points to expose the spinal cord.

Evans Blue Dye Infusion

After stroke, two additional PEEK screws were fixed −1.8 mm lateral and −0.8 mm posterior to Bregma on each parietal bone to guide ventricle catheter penetration. The opening of the screw was sealed using caulking material (Silagum) prior to recovery of the animal after stroke and was only removed prior to lateral ventricle infusion 18 h post-stroke.

At 18 h post-stroke, a 27G neonatal lumbar needle (Becton, Dickinson and Company, NJ, United States) connected to PE-10 tubing (internal diameter 0.381 mm; SAI) and a syringe containing Evan's blue dye (2% w/v in artificial CSF) was sealed 9 mm deep into each screw (5 mm screw length + 4 mm lateral ventricle depth) so that it would pierce the lateral ventricles. Evans blue dye was infused bilaterally into the lateral ventricles (20 μL total volume, 2 μL/min total with 1 μL/min in each ventricle). Infusion was controlled by a syringe driver (Harvard Apparatus, Holliston, MA, United States). Penetration of the ventricles was later confirmed by histology.

Image Acquisition and Analysis of CSF Transit Speed

White light images were acquired using a microscopic eyepiece (DEM130, CMOS chip, Scopium) connected to a stereo microscope (Olympus SZX7). The eyepiece was connected to a PC running pre-installed image acquisition software. An image was captured every minute for 90 min. These images were then loaded into ImageJ as a sequence. The images were converted to an 8-bit format with the colour channels split; only the red channel was used for analysis as this minimized contrast from blood vessels. Two regions of interest were selected: the spinal cord and a small region of tissue lateral to the spinal cord to correct for background noise. Difference between each image and baseline were calculated to show contrast development (Evans blue dye build up at the C7-T1 CSF space). Values for 100% maximum contrast were determined as the maximum contrast observed throughout the imaging period and this was used to determine 50% maximum contrast. Average area under the curve (AUC) of contrast development and time taken to reach 50% maximum contrast (T50%max) were used as an indicator of spinal CSF transit speed. Contrast development at the spinal CSF space is shown in **Figure 1A**.

Quantification of Evans Blue Dye in Deep Cervical Lymph Nodes

The first bilateral deep cervical lymph nodes of each animal were removed following sacrifice and were frozen at −80°C until formamide extraction. Formamide extraction of Evans blue dye from the lymph node tissue was carried out as previously described but with some minor modifications (Krzyzanowska et al., 2010). Briefly, deep cervical lymph nodes were removed from the freezer and thawed. Once thawed, samples were dried in a 56°C oven for 1.5 h. Dried samples were added to an Eppendorf containing 50 μL of formamide, care was taken to ensure the entire tissue sample was submerged. The Eppendorfs containing both sample and formamide were placed back into the 56°C oven for 48 h to allow for Evans blue dye extraction into the solution.

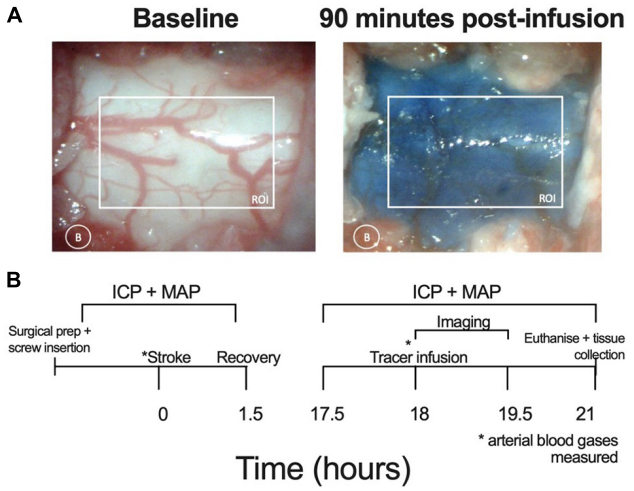

FIGURE 1 | (A) Representative images showing the respective absence and presence of Evans blue dye at baseline and 90 min post-infusion at the C7-T1 region in a stroke animal without ICP rise. The white box represents the region of interest (ROI) for quantifying contrast and the white circle indicates lateral measurement of background (B) changes. **(B)** Experimental timeline. Lateral ventricle screw insertion and physiological variable recordings were carried out prior to stroke. Evans blue dye was infused 18 h post-stroke and imaging was carried out 0–90 min post-infusion. Post-stroke physiological variables were recorded from 17.5 to 21 h post-stroke. Deep cervical lymph nodes were extracted following euthanasia. ICP, intracranial pressure; MAP, mean arterial pressure, * time point at which arterial blood gases (ABG) measured.

Following extraction of Evans blue dye from the deep cervical lymph nodes into formamide, each sample was placed into a well of a 96-well plate, which contained three rows of standard curve solution (starting concentration 128 μg/mL formamide with a 1:2 dilution for each step, ending with 0.5 μg/mL formamide). Absorbance was determined at 620 nm in a spectrophotometer (SPECTROstar Nano plate reader, BMG Labtech) and the standard curve was used to determine concentration from absorbance within the program. Concentration of Evans blue dye in both the ipsilateral and contralateral deep cervical lymph nodes was assessed and these were averaged to obtain a single value for each animal.

Histological Analysis

Animals were euthanised at 3 h post-infusion and transcardially perfused with 0.9% saline. The brains were then fixed in neutral-buffered formalin before being processed and paraffin embedded. Coronal sections of 5 and 10 μm were cut and stained with haematoxylin and eosin. Images were scanned using a digital slide scanner (Aperio Technologies, Vista, CA, United States) and image analysis was carried out within the Aperio program. Image analysis was confirmed by an independent investigator and any cases with >10% discrepancy were flagged for review. Infarct volume (corrected for oedema) was determined by subtracting the measured interhemispheric volume difference (oedema volume, ipsilateral–contralateral) from the measured infarct volume for each slice.

Experimental Design

The experimental timeline is outlined in **Figure 1B**. Physiological variables were recorded at baseline, prior to photothrombotic stroke and at 18 h post stroke, prior to dye infusion. Screws were placed over the lateral ventricles and a dental cap was fitted after photothrombotic stroke. A C7-T1 laminectomy was performed at 17.5 h post-stroke to expose this area of the spinal cord. Bilateral infusion of 10 μL (1 μL per minute) Evans blue dye into both lateral ventricles (20 μL total) took place at 18 h post-stroke. Cisterna magna injection was not possible due to restricted access with the imaging set-up. White light images were acquired of the C7-T1 spinal cord every minute from 0 to 90 min post-infusion and images were analysed using ImageJ software (NIH). The animals were sacrificed at 3 h post-infusion and deep cervical lymph nodes were extracted and frozen at −80°C until formamide extraction and spectrophotometric analysis took place.

We previously reported a transient ICP rise that peaks 20–22 h post-stroke (Murtha et al., 2015; Beard et al., 2016). In this experiment, we chose 18 h post-stroke as our time point for this investigation. This is because we hypothesised that changes to CSF flow would be present at this earlier time point, which would contribute to the ICP rise we observe later. If we investigated CSF changes at 20–22 h, there is a high likelihood of missing these changes, as we would expect the system to begin to return to baseline levels at this point.

Our initial experiments demonstrating ICP rise utilised the MCAo model of stroke in rats (Murtha et al., 2014a, 2015). We and others have shown that MCAo can cause damage to the choroid plexus, which may influence CSF volume (Ennis and Keep, 2006; Beard et al., 2016). We aimed to pursue a line of investigation (contributions of CSF to ICP rise) using a rat model of stroke that does not cause choroid plexus damage. We have shown in two studies that ICP rise also occurs after photothrombotic stroke (Beard et al., 2016; Patabendige et al., 2019). Therefore, we chose to continue using this model for our study. Use of photothrombotic stroke also minimises surgical intervention, particularly around the cervical region, to prevent interference with lymphatic vessels.

Statistical Analysis

Sample size calculations based on pilot data were conducted on G*Power 3.1.9.2 and indicated that five stroke animals and five sham animals were required to detect a 30% change in CSF tracer transit between stroke and sham animals with 80% power and α error probability of 0.05 ($SD = 6.2$). The bimodal distribution of stroke animals with and without ICP rise prompted us to increase the number of animals so that we could compare changes to CSF flow in the presence and absence of ICP rise.

Statistical analyses were carried out using GraphPad Prism 7 (GraphPad Software, La Jolla, CA, United States). Data were tested for normal distribution using a D'Agostino and Pearson normality test. Comparisons between two groups were analysed by unpaired Student's *t*-test for normally distributed data and by Mann-Whitney *U* test for non-normally distributed data. Area under the curve analysis was used to determine differences in

contrast development over time. These values were presented as mean ± standard error of the mean (SEM) to allow for a comparison of average differences observed at each time point.

Additional statistical analyses were conducted *post hoc* to more accurately determine the association of spinal CSF flow and cervical lymphatic tracer transit with ICP elevation, since some stroke animals did not have a significant ICP rise. In these analyses, comparisons between three or more groups were carried out using one-way ANOVA for normally distributed data and using a non-parametric Kruskal-Wallis test for non-normally distributed data. A *post hoc* Bonferroni test was conducted after ANOVA and a Dunn's test was conducted after Kruskal-Wallis test to identify differences between groups. All normally distributed data values are presented graphically as average ± standard deviation (SD) and non-normally distributed data as median and interquartile range (IQR), 25 and 75% percentile, unless otherwise stated. Relationships were determined by Pearson correlation for normally distributed data and Spearman correlation for non-normally distributed data.

RESULTS

Physiological Parameters

Physiological parameters measured at baseline and 18 h post-stroke are presented for each group in **Table 1**.

Exclusions

All excluded animals were from the sham group.

Three animals were excluded from experimentation as they presented with congenital deformities to the spinal column that prevented laminectomy. Four animals were excluded due to errors in surgical placement of screws or problems with infusion, and one animal died before imaging was complete. One sham animal received Evans blue dye infusion, but it was later found that ventricular penetration did not take place due to misalignment of screws, this animal was excluded from the analysis. All stroke animals demonstrated tissue infarction; therefore, none were excluded.

There Was a Bimodal Distribution of Stroke Animals With and Without ICP Rise

Baseline ICP was not significantly different between stroke (5.23 ± 1.8 mmHg, $n = 12$) and sham (4.6 ± 1.88 mmHg, $n = 8$) groups, $t(20) = 0.79$, $p = 0.44$ (**Figure 2A**). We used + 4.4 mmHg as the determinant of ICP rise (baseline to 18 h) as it represents twice the standard deviation of ΔICP of sham animals. ICP rose significantly in stroke animals (5.0 mmHg, IQR = 0.1–9.4, $n = 12$) but not in sham animals (−0.3 mmHg, IQR = −1.9 to 1.7, $n = 10$; $U = 27$, $p = 0.03$; **Figure 2B**) from baseline to 18 h post-stroke. There was a bimodal distribution of stroke animals with and without ICP rise with 7/12 stroke animals showing ICP rise greater than +4.4 mmHg between baseline (pre-photothrombotic stroke) and 18 h post-stroke. For subsequent analyses to determine whether there was an association between ICP rise and CSF tracer outflow, we separated stroke animals into two groups depending on whether they had an ICP rise or not. Average infarct volume was 8.67 ± 4.8 mm^3. Tissue infarct is shown in **Figure 2C**. ICP change between baseline and 17.5–21 h post-stroke is shown for stroke rats with ICP rise ($n = 5$), stroke rats without ICP rise ($n = 5$), and sham rats ($n = 7$) in **Figure 2D**.

Oedema Is Not the Cause of ICP Rise 18 h After Photothrombotic Stroke

There was no significant correlation between infarct volume and ΔICP from baseline to 18 h post-stroke (**Figure 3A**), $R = 0.55$, $p = 0.07$, Spearman's correlation.

Oedema was not correlated with ΔICP between baseline and 18 h post-stroke (**Figure 3B**), $R = 0.41$, $p = 0.18$, Spearman's correlation. Average oedema volume was 1.12 ± 2.26 mm^3.

TABLE 1 | Comparison of physiological parameters between baseline and 18 h post-stroke within each group, paired *t*-test.

	Stroke with ICP rise		Stroke without ICP rise		Sham	
	Baseline	**18 h**	**Baseline**	**18 h**	**Baseline**	**18 h**
Respiratory rate (per minute)	62 ± 3	60 ± 3*†	68 ± 6	69 ± 6	64 ± 3	69 ± 7
Heart rate (BPM)	436 ± 20	421 ± 33	453 ± 10†	427 ± 34	428 ± 12†	414 ± 26
Mean arterial pressure (mmHg)	92.9 ± 4.8	90.4 ± 5.4	90 ± 9.2	98.5 ± 6.4††	87.4 ± 7	87.2 ± 6.4
SpO_2 (%)	97.9 ± 1.0	98.0 ± 2.4	96.7 ± 2.9	97.8 ± 2.6	98.7 ± 1.1	98 ± 2.5
paO_2 (mmHg)	185 ± 23 ($n = 6$)†	200 ± 25 ($n = 6$)	164 ± 28	193 ± 40	148 ± 23 ($n = 9$)	196 ± 22 ($n = 9$)***
$paCO_2$ (mmHg)	61.2 ± 8.2 ($n = 6$)	62.2 ± 9.8 ($n = 6$)	52.3 ± 9.2†	60.4 ± 5.9	63.5 ± 5.5 ($n = 9$)	61.6 ± 7.4 ($n = 9$)**
pH	7.28 ± 0.03 ($n = 6$)	7.32 ± 0.03 ($n = 6$)	7.31 ± 0.03†††	7.32 ± 0.02	7.25 ± 0.01 ($n = 9$)	7.3 ± 0.04 ($n = 9$)*

Comparison between stroke with ICP rise (n = 7), stroke without ICP rise (n = 5), and sham (n = 10) at baseline and 18 h post-stroke, one-way ANOVA with post hoc Bonferroni test (stroke groups vs. sham).
$p \leq 0.05$.
**$p \leq 0.01$.*
***$p \leq 0.001$, paired t-test of baseline vs. 18 h post-stroke.*
†$p \leq 0.05$.
††$p \leq 0.01$.
†††$p \leq 0.001$, one way ANOVA with post hoc Bonferroni test of stroke with/without ICP rise vs. sham.
BPM, beats per minute.

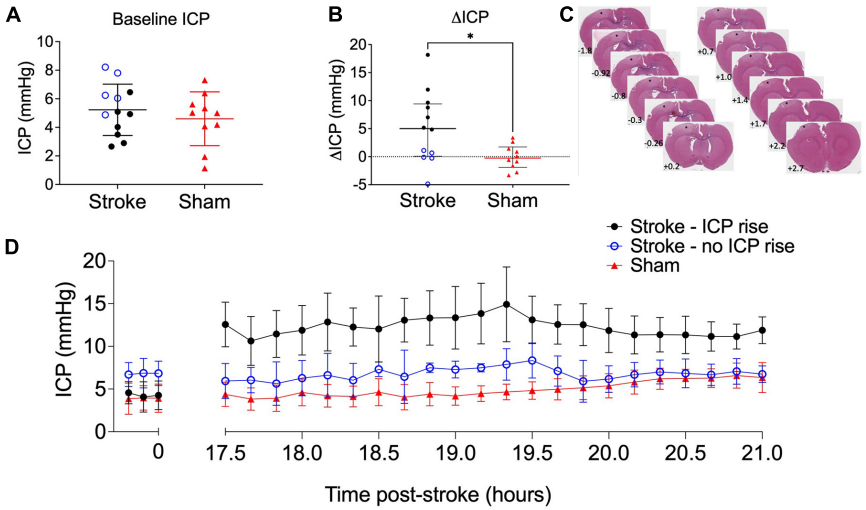

FIGURE 2 | (A) Baseline intracranial pressure (ICP; mmHg) in stroke ($n = 12$; black closed circles and blue open circles) and sham ($n = 10$; red triangles) rats, Student's *t*-test. **(B)** Change in ICP from baseline to 18 h post-stroke in stroke rats and in sham rats. *$p \leq 0.05$, Mann-Whitney *U* test presented as median and interquartile range. Blue open circles indicate animals that did not have an ICP rise above +4.4 mmHg. All animals were included in statistical analysis. **(C)** Representative image of cortical ischaemia after H&E staining, Bregma +2.7 to −1.8. * indicates infarct. **(D)** Temporal profile of mean ICP at baseline and between 17.5 and 21 h post-stroke. Nb. For all graphs stroke rats with ICP rise greater than +4.4 mmHg ($n = 5$; black circles), stroke rats without ICP rise ($n = 5$; blue open circles), and sham rats ($n = 7$; red triangles).

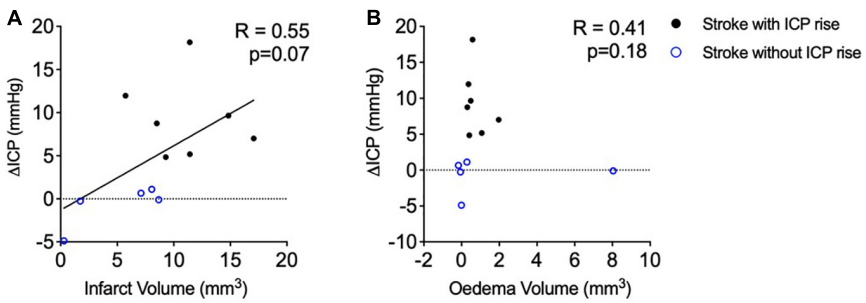

FIGURE 3 | (A) Relationship between infarct volume (mm^3) and intracranial pressure rise (ΔICP; mmHg). Black closed circles represent stroke animals with an ICP rise greater than +4.4 mmHg ($n = 7$) and blue open circles represent those without ICP rise ($n = 5$). **(B)** Relationship between oedema volume (mm^3) and ΔICP. A Spearman correlation was used for analyses. Black closed circles represent stroke animals with an ICP rise greater than +4.4 mmHg ($n = 7$) and blue open circles represent those without ICP rise ($n = 5$).

Cranial Clearance of Evans Blue Dye to the Deep Cervical Lymph Nodes Was Reduced in Stroke Animals but Was Not Correlated With ΔICP

Evans blue dye concentration was not significantly different between ipsilateral and contralateral lymph nodes for all groups (2.74 ± 4.76 μg/mL formamide vs. 3.08 ± 4.53 μg/mL formamide), $t(42) = 0.24$, $p = 0.81$. Therefore, we averaged ipsilateral and contralateral values to obtain one value per animal to compare between groups. The concentration of Evans blue dye extracted from the deep cervical lymph nodes was significantly different between groups, $p = 0.02$ (**Figure 4A**). Stroke animals with ICP rise (0 μg/mL formamide, IQR = 0–0.11) were similar to stroke animals without ICP rise (0 μg/mL formamide, IQR = 0–4.47), and both had a lower concentration when compared to sham animals (4.17 μg/mL formamide, IQR = 0.74–8.51). A *post hoc* Dunn's test found a significant difference between sham animals and stroke animals with ICP rise, $p = 0.03$, but no significant difference between sham animals and stroke animals without ICP rise, $p = 0.1$.

Cervical lymph node concentration of Evans blue dye was not correlated with ΔICP, $R = 0.27$, $p = 0.23$ (**Figure 4B**), infarct volume, $R = -0.19$, $p = 0.55$, or oedema volume, $R = -0.22$, $p = 0.5$.

Spinal CSF Transit Speed Was Correlated With ICP Rise

Average contrast development (Arbitrary Units; AU) ± SEM over time (minutes) for each group is shown in **Figure 5A**. AUC of contrast development was greater in stroke animals with

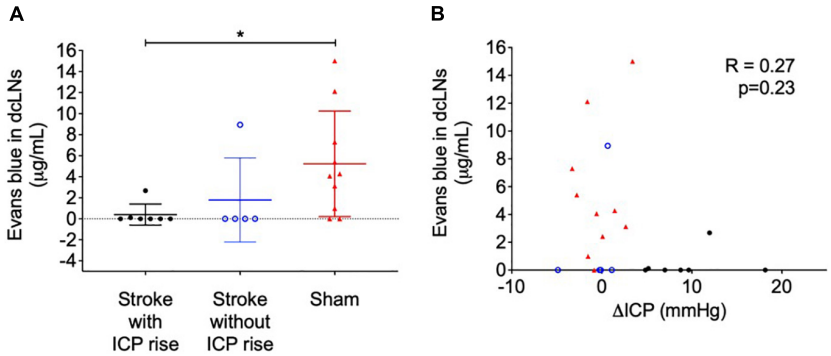

FIGURE 4 | (A) Concentration of Evans blue dye extracted into formamide (µg/mL) from deep cervical lymph nodes (dcLNs) of stroke animals with intracranial pressure (ICP) rise greater than +4.4 mmHg (black closed circles), stroke without ICP rise (blue open circles), and sham (red triangles) animals. *$p \leq 0.05$, Kruskal-Wallis test with *post hoc* Dunn's test between groups. **(B)** Relationship between ΔICP (mmHg) and the concentration of Evans blue dye in dcLNs. A Spearman correlation was used for analyses.

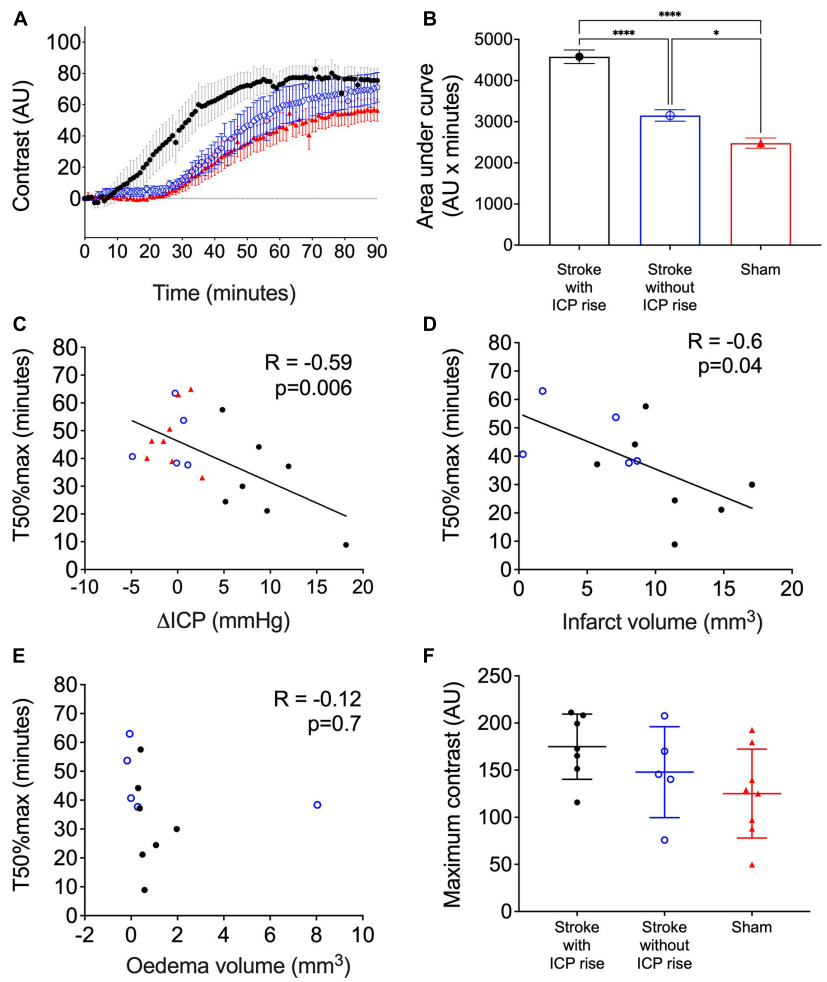

FIGURE 5 | (A) Average contrast development (arbitary units; AU) over time (minutes) for stroke rats with intracranial pressure (ICP) rise greater than +4.4 mmHg (black closed circles), stroke rats with no ICP rise (blue open circles), and sham rats (red triangles). Presented as mean ± standard error of the mean (SEM). **(B)** Area under the curve (AU × minutes) presented for each group as mean ± SEM, ANOVA with *post hoc* Bonferroni test. **(C)** Relationship between ΔICP (mmHg) and time to reach 50% maximum contrast (T50%max; minutes). A Spearman correlation was used to determine the relationship. **(D)** Relationship between infarct volume (mm^3) and T50%max, Pearson correlation. **(E)** Relationship between oedema volume (mm^3) and T50%max, Pearson correlation. **(F)** Maximum contrast (AU) observed in each group, mean ± standard deviation.

ICP rise (mean = 4,579, SEM = 164 AU × minutes, $n = 7$), compared with stroke animals without ICP rise (mean = 3,152, SEM = 138.4 AU × minutes, $n = 5$), and sham animals (mean = 2,481, SEM = 124.9 AU × minutes, $n = 8$), $F(2, 17) = 59.8$, $p < 0.0001$ (**Figure 5B**). A *post hoc* Bonferroni test confirmed a significant difference between stroke animals with ICP rise and sham animals [$p < 0.0001$, $t(17) = 10.82$], and stroke animals without ICP rise and sham animals [$p = 0.02$, $t(17) = 3.14$].

There was a significant inverse correlation between ΔICP and T50%max. Animals with a higher ΔICP reached 50% maximum contrast faster than those with a lower ΔICP, $R = -0.59$, $p = 0.006$, Spearman's correlation (**Figure 5C**).

Infarct Volume but Not Oedema Correlates With Faster Spinal CSF Transit

There was a significant inverse correlation between infarct volume and T50%max, which demonstrates faster transit of Evans blue dye to the C7-T1 spinal subarachnoid space in animals with larger infarct volumes (**Figure 5D**), $R = -0.6$, $p = 0.04$.

Oedema volume was not correlated with T50%max (**Figure 5E**), $R = -0.12$, $p = 0.7$.

Maximum Change in Contrast Was Not Different Between Groups

The maximum change in contrast from 0 to 90 min post-infusion did not significantly differ between stroke animals with ICP rise (174.9. ± 34.6 AU, $n = 7$), stroke animals without ICP rise (147.9 ± 48.2 AU, $n = 5$), and sham animals (125.1 ± 47.15 AU, $n = 8$), $F(2, 17) = 2.45$, $p = 0.11$ (**Figure 5F**).

A Correlation Between Spinal CSF Transit Speed and Clearance to the Deep Cervical Lymphatics Could Not Be Determined

Cranial CSF clearance to the deep cervical lymphatics was reduced in stroke animals with and without ICP rise and spinal CSF transit speed was faster in animals with ICP rise (**Figure 6**). There was no correlation between these variables, $R = -0.24$, $p = 0.3$.

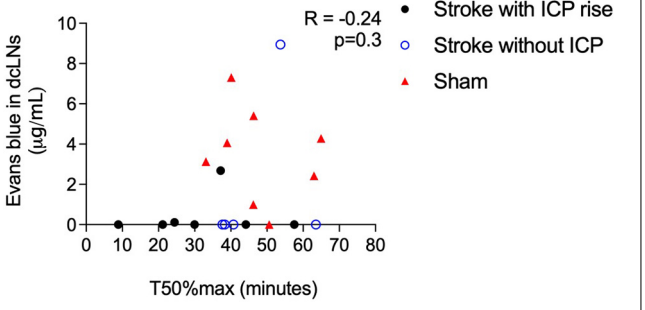

FIGURE 6 | Correlation between speed of CSF transit to the spinal subarachnoid space (T50%max) and concentration of Evans blue dye in deep cervical lymph nodes (dcLNs; µg/ml) in stroke animals with intracranial pressure (ICP) rise greater than +4.4 mmHg (black closed circles), without ICP rise (blue open circles), and sham animals (red triangles). A Spearman correlation was used for analyses.

DISCUSSION

We previously found an oedema independent ICP rise that peaks 20–22 h after experimental ischaemia. Here, we report that it can be detected as early as 18 h. We showed that clearance of cranial CSF tracer into the deep cervical lymphatics is reduced, and there is faster movement of tracer into the spinal subarachnoid space 18 h after photothrombotic stroke in rats. Prior work has shown resistance to CSF outflow is increased after experimental ischaemia (Patabendige et al., 2019; Alshuhri et al., 2020). This work suggests that cranial clearance of CSF is reduced, which may explain increased outflow resistance. Further, we found impaired cranial clearance in animals with and without ICP rise. Animals with increased ICP had increased spinal CSF transit speed, suggesting this pathway is utilised as a compensatory mechanism when both cranial clearance is reduced and ICP is elevated.

All but two stroke animals had no Evans blue dye in their deep cervical lymph nodes after intraventricular infusion and 3-hour circulation. This indicates a significant disruption of CSF clearance 18 h after stroke. Resistance to CSF outflow in the spine is greater than resistance to CSF outflow in the cranium (Bozanovic-Sosic et al., 2001). Therefore, when cranial clearance pathways are impaired, we would expect an overall increase in resistance to CSF outflow across the whole cranio-spinal compartment. We previously demonstrated this increased resistance to CSF outflow 18 h after photothrombotic stroke in rats (Patabendige et al., 2019) and another group reported similar findings 24 h after MCAo (Alshuhri et al., 2020). The current results indicate that reduction in cranial CSF clearance may contribute to increased resistance.

Impaired CSF clearance to the deep cervical lymphatics was previously shown in response to neurological injury (Bolte et al., 2020). Therefore, we hypothesised that this pathway would provide insight into the underlying mechanisms of ICP rise 18 h post-stroke. The almost complete reduction of CSF clearance to deep cervical lymph nodes in stroke animals likely impeded our ability to detect a correlation with ICP rise, since that distribution was non-linear (**Figure 4B**). Animals without ICP rise still had impaired cranial CSF clearance. These observations may be explained by the time point of our experiments. Here, we aimed to capture changes to CSF dynamics and ICP at 18 h post-stroke but we previously reported peak ICP rise between 20 and 22 h (Beard et al., 2016). ICP values in this current study were smaller than those previously reported, due to the earlier time point of our experiments (Murtha et al., 2015; Beard et al., 2016). We expect that ICP would have continued to rise and peak at 20–22 h post-stroke. We speculate that disruptions to CSF flow may pre-empt ICP rise, which means it may be possible that the disruption to CSF flow we observed in the absence of ICP rise could be indicative of a delayed ICP rise that we did not capture due to our experimental timing. Despite these observations, we

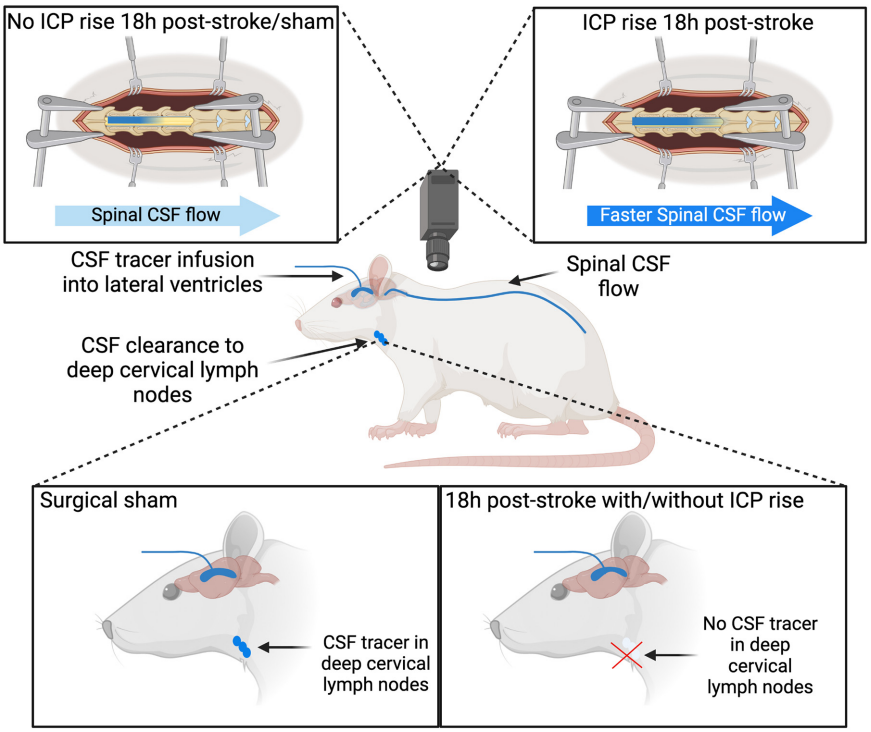

FIGURE 7 | Cerebrospinal fluid (CSF) tracer movement into the deep cervical lymph nodes and spinal CSF space. Stroke animals have impaired CSF clearance to deep cervical lymph nodes 18 h post-stroke with and without intracranial pressure (ICP) rise. Increased ICP 18 h post-stroke is associated with faster CSF tracer movement into the spinal CSF space, compared to stroke animals without ICP rise and sham animals.

found that increased ICP was associated with increased spinal CSF transit. This suggests that movement of cranial CSF along this pathway is utilised as a compensatory mechanism in response to elevated ICP when direct cranial clearance pathways are absent (**Figure 7**). Similar observations of increased ICP, reduced cranial clearance, and increased spinal clearance of CSF were previously reported after subarachnoid haemorrhage related hydrocephalus in rabbits (Griebel et al., 1989). Further, previous work found that sealing of the cribriform plate in dogs prevented CSF tracer flow into the deep cervical lymphatics and instead promoted tracer accumulation in lymphatic vessels associated with spinal CSF drainage (Galkin, 1930). Recently, Proulx's group demonstrated a predominant role for lymphatics at the sacral spine in spinal CSF clearance, although the proportion of CSF clearance at this site was minimal relative to that at the cervical lymphatics (Ma et al., 2019). We did not examine the sacral lymphatics in this study, but our current findings suggest that future investigations of CSF clearance post-stroke should include examination of spinal lymphatics to understand its contribution to overall clearance of CSF from the cranio-spinal compartment.

Our findings that oedema volume did not correlate with either ΔICP or T50%max are consistent with our previous report that oedema does not correlate with ICP rise 24 h after transient MCAo, and with work showing similar observations after permanent MCAo (Murtha et al., 2015; Alshuhri et al., 2020). Oedema volumes were assessed early and would likely be greater at later time points. However, we still observe ICP rise from 18 to 21 h, which suggests that mechanisms other than oedema contribute to ICP rise after photothrombotic stroke. We also found that ICP rise did not significantly correlate with infarct size, which is in line with our previous observations that ICP rise at 24 h is not an indicator of large infarct volume (Murtha et al., 2015; Beard et al., 2016). This is in contrast to ICP rise observed after large infarct 3–5 days post-stroke in animal models (Kotwica et al., 1991; Silasi et al., 2009) and in humans (Schwab et al., 1996).

In this study, we infused the CSF tracer, Evans Blue dye, directly into the lateral ventricles of rats (Boulton et al., 1999; Maloveska et al., 2018; Norwood et al., 2019). This type of intervention has the potential to disturb normal CSF dynamics; however, this technique is widely used and we took care to limit the infusion rate to lower than that of CSF production (normally 2.66–2.84 μL/min in rats) to maintain the integrity of the system as much as possible (Chiu et al., 2012). We also monitored ICP during infusion to ensure there were no significant changes. We used the low molecular weight, lipophobic tracer, Evans blue dye, for our studies to investigate cranial clearance of CSF since tracer movement differs depending on molecular size and weight (Yang et al., 2013), and we wished to approximate movement of fluid, rather than larger molecular weight, and potentially immunogenic, proteins within the fluid. No Evans blue dye was present (i.e., blue staining) around the infarct or surrounding brain tissue, which indicates that extravasation of CSF tracer to blood *via* the area of

stroke due to blood-brain barrier breakdown is unlikely. Our choice of anaesthetic was advantageous to our study of CSF clearance. Anaesthetic-related hypercapnia was previously shown to impair glymphatic flow after intraparenchymal injection of tracer, while lymphatic clearance remained unaltered after direct infusion into CSF (Goodman and Iliff, 2020). This means that there was likely reduced parenchymal uptake of tracer in our study, allowing our findings to be largely representative of bulk CSF clearance pathways. Reduced $paCO_2$ can reduce ICP by inducing vasoconstriction of the cerebral resistance arterioles, which reduces cerebral blood volume (Godoy et al., 2017). Stroke rats without ICP rise had a significantly lower baseline $paCO_2$, and consequently reduced pH, when compared to sham animals in this study, although animals did not reach levels of hypocapnia (<24.75 mmHg) (Young et al., 1991). This is unlikely to explain the absence of ICP rise in this group as $paCO_2$ was similar between all groups 18 h post-stroke. Further, if our observations of ICP were explained solely by CO_2 then we would expect a greater ICP rise in this group as animals had a larger increase in $paCO_2$ from baseline compared to other groups. We utilised photothrombotic stroke as the preferred model for this study to maintain choroid plexus integrity throughout our experiments. MCAo reduces blood flow to the choroid plexus by around 62% and causes choroidal oedema leading to reduced blood-CSF barrier integrity and increased CSF secretion (Ennis and Keep, 2006). Histology confirmed that ischaemia was restricted to the cortex in this current study.

It is important to consider the differences in CSF clearance between humans and animal models. Animal studies demonstrating CSF clearance pathways are relatively abundant when compared to human studies, largely due to their invasive nature. However, evidence of lymphatic drainage in humans was previously found in cadavers and imaging studies have shown CSF tracer movement into the nasal mucosa and deep cervical lymphatics of humans (de Leon et al., 2017; Eide et al., 2018; Proulx, 2021). It is important to remember that we have not yet arrived at a consensus regarding the relative proportion of CSF clearance attributed to lymphatic outflow pathways in humans. Nevertheless, the consequences of impaired CSF clearance are multi-faceted, potentially contributing to increased ICP, reduced cerebral blood flow, protein accumulation and aggregation, and cognitive decline (Griebel et al., 1989; Bolte et al., 2020).

CONCLUSION

In this study we have shown that CSF tracer clearance into the cervical lymphatics is impaired 18 h post-stroke in a rat photothrombotic stroke model, and there is a compensatory increase in CSF transit to the spinal subarachnoid space. Taken with previous observations of increased resistance to CSF outflow after experimental ischaemia, we believe changes to CSF clearance post-stroke may contribute to changes in the regulation of ICP.

DATA AVAILABILITY STATEMENT

The raw data supporting the conclusions of this article will be made available by the authors, without undue reservation.

ETHICS STATEMENT

The animal study was reviewed and approved by the University of Newcastle Animal Care and Ethics Committee.

AUTHOR CONTRIBUTIONS

SB carried out the surgical components of the study, analysed and interpreted the data, performed statistical analysis, and drafted the manuscript. DO and RH helped with interpretation of the data and manuscript drafting. D-GP and DO helped with the histology and image analysis. SA helped with the deep cervical lymph node extraction and subsequent quantification of Evans blue dye. NS and AP participated in the concept and design of the study, helped with interpretation of the data, and drafting the manuscript. All authors read and approved the final manuscript.

FUNDING

This study was supported by an HDR scholarship to SB by the University of Newcastle, Australia. AP was supported by the NSW Ministry of Health under the NSW Health Early-Mid Career Fellowships Scheme. NS was supported by a co-funded Australian NHMRC/National Heart Foundation Career Development/Future Leader Fellowship (GNT1110629/100827).

ACKNOWLEDGMENTS

Thanks to Brett Graham at the University of Newcastle for demonstrating the laminectomy technique and to Nikolce Mackovski for training SB in surgical procedures and providing technical assistance throughout experiments. We would like to thank Christopher Oldmeadow, of the CReDITSS Unit, Hunter Medical Research Institute, for biostatistical advice. **Figure 7** was created with BioRender.com.

REFERENCES

Alshuhri, M. S., Gallagher, L., Mccabe, C., and Holmes, W. M. (2020). Change in CSF dynamics responsible for ICP elevation after ischemic stroke in rats: a new mechanism for unexplained end? *Transl. Stroke Res.* 11, 310–318. doi: 10.1007/s12975-019-00719-6

Asdaghi, N., Hameed, B., Saini, M., Jeerakathil, T., Emery, D., and Butcher, K. (2011). Acute perfusion and diffusion abnormalities predict early new MRI lesions 1 week after minor stroke and transient ischemic attack. *Stroke* 42, 2191–2195. doi: 10.1161/strokeaha.110.611376

Aspelund, A., Antila, S., Proulx, S. T., Karlsen, T. V., Karaman, S., Detmar, M., et al. (2015). A dural lymphatic vascular system that drains brain interstitial

fluid and macromolecules. *J. Exp. Med.* 212, 991–999. doi: 10.1084/jem.20142290

Beard, D. J., Logan, C. L., Mcleod, D. D., Hood, R. J., Pepperall, D., Murtha, L. A., et al. (2016). Ischemic penumbra as a trigger for intracranial pressure rise–a potential cause for collateral failure and infarct progression? *J. Cereb. Blood Flow Metab.* 36, 917–927. doi: 10.1177/0271678x15625578

Beard, D. J., Mcleod, D. D., Logan, C. L., Murtha, L. A., Imtiaz, M. S., Van Helden, D. F., et al. (2015). Intracranial pressure elevation reduces flow through collateral vessels and the penetrating arterioles they supply. A possible explanation for 'collateral failure' and infarct expansion after ischemic stroke. *J. Cereb. Blood Flow Metab.* 35, 861–872. doi: 10.1038/jcbfm.2015.2

Bolte, A. C., Dutta, A. B., Hurt, M. E., Smirnov, I., Kovacs, M. A., Mckee, C. A., et al. (2020). Meningeal lymphatic dysfunction exacerbates traumatic brain injury pathogenesis. *Nat. Commun.* 11:4524.

Bothwell, S. W., Janigro, D., and Patabendige, A. (2019). Cerebrospinal fluid dynamics and intracranial pressure elevation in neurological diseases. *Fluids Barriers CNS* 16:9.

Boulton, M., Flessner, M., Armstrong, D., Mohamed, R., Hay, J., and Johnston, A. M. (1999). Contribution of extracranial lymphatics and arachnoid villi to the clearance of a CSF tracer in the rat. *Am. J. Physiol.* 276, R818–R823.

Bozanovic-Sosic, R., Mollanji, R., and Johnston, M. G. (2001). Spinal and cranial contributions to total cerebrospinal fluid transport. *Am. J. Physiol. Regul. Integr. Comp. Physiol.* 281, R909–R916.

Bradbury, M. W., and Westrop, R. J. (1983). Factors influencing exit of substances from cerebrospinal fluid into deep cervical lymph of the rabbit. *J. Physiol.* 339, 519–534. doi: 10.1113/jphysiol.1983.sp014731

Campbell, B. C., Christensen, S., Tress, B. M., Churilov, L., Desmond, P. M., Parsons, M. W., et al. (2013). Failure of collateral blood flow is associated with infarct growth in ischemic stroke. *J. Cereb. Blood Flow Metab.* 33, 1168–1172. doi: 10.1038/jcbfm.2013.77

Chiu, C., Miller, M. C., Caralopoulos, I. N., Worden, M. S., Brinter, T., Gordon, Z. N., et al. (2012). Temporal course of cerebrospinal fluid dynamics and amyloid accumulation in the aging rat brain from three to thirty months. *Fluids Barriers CNS* 9:3. doi: 10.1186/2045-8118-9-3

Coutts, S. B., Modi, J., Patel, S. K., Aram, H., Demchuk, A. M., Goyal, M., et al. (2012). What causes disability after transient ischemic attack and minor stroke?: results from the CT and MRI in the triage of TIA and minor cerebrovascular events to identify high risk patients (CATCH) study. *Stroke* 43, 3018–3022. doi: 10.1161/strokeaha.112.665141

Czosnyka, M., and Pickard, J. D. (2004). Monitoring and interpretation of intracranial pressure. *J. Neurol. Neurosurg. Psychiatry* 75, 813–821. doi: 10.1136/jnnp.2003.033126

Davson, H., and Segal, M. B. (1996). *Physiology of the CSF and Blood-Brain Barriers*. Boca Raton, FL: CRC Press.

de Leon, M. J., Li, Y., Okamura, N., Tsui, W. H., Saint-Louis, L. A., Glodzik, L., et al. (2017). Cerebrospinal fluid clearance in Alzheimer disease measured with dynamic PET. *J. Nucl. Med.* 58, 1471–1476. doi: 10.2967/jnumed.116.187211

Eide, P. K., Vatnehol, S. A. S., Emblem, K. E., and Ringstad, G. (2018). Magnetic resonance imaging provides evidence of glymphatic drainage from human brain to cervical lymph nodes. *Sci. Rep.* 8:7194.

Ennis, S. R., and Keep, R. F. (2006). The effects of cerebral ischemia on the rat choroid plexus. *J. Cereb. Blood Flow Metab.* 26, 675–683. doi: 10.1038/sj.jcbfm.9600224

Faber, W. M. (1937). The nasal mucosa and the subarachnoid space. *Am. J. Anat.* 62, 121–148. doi: 10.1002/aja.1000620106

Galkin, W. S. (1930). Über die Bedeutung der "Nasenbahn" für den Abfluß aus dem Subarachnoidalraum. *Z. Gesamte. Exp. Med.* 72, 65–71.

Godoy, D. A., Seifi, A., Garza, D., Lubillo-Montenegro, S., and Murillo-Cabezas, F. (2017). Hyperventilation therapy for control of posttraumatic intracranial hypertension. *Front. Neurol.* 8:250. doi: 10.3389/fneur.2017.00250

Goodman, J. R., and Iliff, J. J. (2020). Vasomotor influences on glymphatic-lymphatic coupling and solute trafficking in the central nervous system. *J. Cereb. Blood Flow Metab.* 40, 1724–1734. doi: 10.1177/0271678x19874134

Griebel, R. W., Black, P. M., Pile-Spellman, J., and Strauss, W. H. (1989). The importance of "Accessory" outflow pathways in hydrocephalus after experimental subarachnoid hemorrhage. *Neurosurgery* 24, 187–192. doi: 10.1227/00006123-198902000-00006

Jackson, R. T., Tigges, J., and Arnold, W. (1979). Subarachnoid space of the CNS, nasal mucosa, and lymphatic system. *Arch. Otolaryngol.* 105, 180–184. doi: 10.1001/archotol.1979.00790160014003

Kotwica, Z., Hårdemark, H. G., and Persson, L. (1991). Intracranial pressure changes following middle cerebral artery occlusion in rats. *Res. Exp. Med. (Berl.)* 191, 99–104. doi: 10.1007/bf02576664

Kovacs, T., Murtha, L. A., Beard, D. J., Mcleod, D. D., Hood, R. J., and Garcia-Esperon, C. (2017). Intracranial pressure rises 24 hours after mile-moderate ischaemic stroke–a potential trigger for early neurological deterioration? *Eur. Stroke J.* 2, 98–478.

Krzyzanowska, A., Martin, Y., Avendaño, C., and Piedras, M. J. (2010). Evaluation of Evans Blue extravasation as a measure of peripheral inflammation. [Preprint]. *Protoc. Exch.* doi: 10.1038/protex.2010.209

Louveau, A., Smirnov, I., Keyes, T. J., Eccles, J. D., Rouhani, S. J., Peske, J. D., et al. (2015). Structural and functional features of central nervous system lymphatic vessels. *Nature* 523, 337–341. doi: 10.1038/nature14432

Ma, Q., Decker, Y., Muller, A., Ineichen, B. V., and Proulx, S. T. (2019). Clearance of cerebrospinal fluid from the sacral spine through lymphatic vessels. *J. Exp. Med.* 216, 2492–2502. doi: 10.1084/jem.20190351

Ma, Q., Ineichen, B. V., Detmar, M., and Proulx, S. T. (2017). Outflow of cerebrospinal fluid is predominantly through lymphatic vessels and is reduced in aged mice. *Nat. Commun.* 8:1434.

Maloveska, M., Danko, J., Petrovova, E., Kresakova, L., Vdoviakova, K., Michalicova, A., et al. (2018). Dynamics of Evans blue clearance from cerebrospinal fluid into meningeal lymphatic vessels and deep cervical lymph nodes. *Neurol. Res.* 40, 372–380. doi: 10.1080/01616412.2018.1446282

Mathers, C. D., and Loncar, D. (2006). Projections of global mortality and burden of disease from 2002-2030. *PLoS Med.* 3:e442. doi: 10.1371/journal.pmed.0030442

Mathieu, E., Gupta, N., Macdonald, R. L., Ai, J., and Yücel, Y. H. (2013). In vivo imaging of lymphatic drainage of cerebrospinal fluid in mouse. *Fluids Barriers CNS* 10, 35–35. doi: 10.1186/2045-8118-10-35

McLeod, D. D., Hood, R. J., Murtha, L. A., Beard, D. J., and Spratt, N. J. (2014). *Cerebral Blood Volume and ICP Rise 18 Hours Post-Stroke* [Unpublished manuscript]. Callaghan, NSW: School of Biomedical Sciences and Pharmacy, University of Newcastle.

Mollanji, R., Bozanovic-Sosic, R., Silver, I., Li, B., Kim, C., Midha, R., et al. (2001a). Intracranial pressure accommodation is impaired by blocking pathways leading to extracranial lymphatics. *Am. J. Physiol. Regul. Integr. Comp. Physiol.* 280, R1573–R1581.

Mollanji, R., Papaiconomou, C., Boulton, M., Midha, R., and Johnston, M. (2001b). Comparison of cerebrospinal fluid transport in fetal and adult sheep. *Am. J. Physiol. Regul. Integr. Comp. Physiol.* 281, R1215–R1223.

Murtha, L. A., Mcleod, D. D., Mccann, S. K., Pepperall, D., Chung, S., Levi, C. R., et al. (2014a). Short-duration hypothermia after ischemic stroke prevents delayed intracranial pressure rise. *Int. J. Stroke* 9, 553–559. doi: 10.1111/ijs.12181

Murtha, L. A., Mcleod, D. D., Pepperall, D., Mccann, S. K., Beard, D. J., Tomkins, A. J., et al. (2015). Intracranial pressure elevation after ischemic stroke in rats: cerebral edema is not the only cause, and short-duration mild hypothermia is a highly effective preventive therapy. *J. Cereb. Blood Flow Metab.* 35, 592–600. doi: 10.1038/jcbfm.2014.230

Murtha, L. A., Yang, Q., Parsons, M. W., Levi, C. R., Beard, D. J., Spratt, N. J., et al. (2014b). Cerebrospinal fluid is drained primarily via the spinal canal and olfactory route in young and aged spontaneously hypertensive rats. *Fluids Barriers CNS* 11, 12. doi: 10.1186/2045-8118-11-12

Norwood, J. N., Zhang, Q., Card, D., Craine, A., Ryan, T. M., and Drew, P. J. (2019). Anatomical basis and physiological role of cerebrospinal fluid transport through the murine cribriform plate. *Elife* 8:e44278.

Patabendige, A., Mackovski, N., Pepperall, D., Hood, R., and Spratt, N. (2019). Correction to: A26 cerebrospinal fluid outflow resistance is increased following small-moderate ischaemic stroke. *Fluids Barriers CNS* 16:22.

Proulx, S. T. (2021). Cerebrospinal fluid outflow: a review of the historical and contemporary evidence for arachnoid villi, perineural routes, and dural lymphatics. *Cell Mol. Life Sci.* 78, 2429–2457. doi: 10.1007/s00018-020-03706-5

Schwab, S., Aschoff, A., Spranger, M., Albert, F., and Hacke, W. (1996). The value of intracranial pressure monitoring in acute hemispheric stroke. *Neurology* 47, 393–398. doi: 10.1212/wnl.47.2.393

Silasi, G., Maclellan, C. L., and Colbourne, F. (2009). Use of telemetry blood pressure transmitters to measure intracranial pressure (ICP) in freely moving rats. *Curr. Neurovasc. Res.* 6, 62–69. doi: 10.2174/156720209787466046

Smith, E. E., Abdullah, A. R., Petkovska, I., Rosenthal, E., Koroshetz, W. J., and Schwamm, L. H. (2005). Poor outcomes in patients who do not receive intravenous tissue plasminogen activator because of mild or improving ischemic stroke. *Stroke* 36, 2497–2499. doi: 10.1161/01.str.0000185798.78817.f3

Walker, M. J., Walker, C. L., Zhang, Y. P., Shields, L. B., Shields, C. B., and Xu, X. M. (2015). A novel vertebral stabilization method for producing contusive spinal cord injury. *J. Vis. Exp.* 20:e50149.

Walter, B. A., Valera, V. A., Takahashi, S., and Ushiki, T. (2006). The olfactory route for cerebrospinal fluid drainage into the peripheral lymphatic system. *Neuropathol. Appl. Neurobiol.* 32, 388–396. doi: 10.1111/j.1365-2990.2006.00737.x

Weed, L. H. (1914). Studies on cerebro-spinal Fluid. No. III : the pathways of escape from the Subarachnoid Spaces with particular reference to the Arachnoid Villi. *J. Med. Res.* 31, 51–91.

Yang, L., Kress, B. T., Weber, H. J., Thiyagarajan, M., Wang, B., Deane, R., et al. (2013). Evaluating glymphatic pathway function utilizing clinically relevant intrathecal infusion of CSF tracer. *J. Transl. Med.* 11:107. doi: 10.1186/1479-5876-11-107

Young, W. L., Barkai, A. I., Prohovnik, I., Nelson, H., and Durkin, M. (1991). Effect of PaCO2 on cerebral blood flow distribution during halothane compared with isoflurane anaesthesia in the rat. *Br. J. Anaesth.* 67, 440–446. doi: 10.1093/bja/67.4.440

Zakharov, A., Papaiconomou, C., and Johnston, M. (2004). Lymphatic vessels gain access to cerebrospinal fluid through unique association with olfactory nerves. *Lymphat. Res. Biol.* 2, 139–146. doi: 10.1089/lrb.2004.2.139

Conflict of Interest: The authors declare that the research was conducted in the absence of any commercial or financial relationships that could be construed as a potential conflict of interest.

Publisher's Note: All claims expressed in this article are solely those of the authors and do not necessarily represent those of their affiliated organizations, or those of the publisher, the editors and the reviewers. Any product that may be evaluated in this article, or claim that may be made by its manufacturer, is not guaranteed or endorsed by the publisher.

frontiers | Frontiers in Molecular Neuroscience

REVIEW
published: 12 July 2022
doi: 10.3389/fnmol.2022.927479

Ependymal Cilia: Physiology and Role in Hydrocephalus

Weiye Ji[1,2,3,4†], Zhi Tang[1†], Yibing Chen[2,3,4], Chuansen Wang[2,3,4], Changwu Tan[2,3,4], Junbo Liao[2,3,4], Lei Tong[2,3,4] and Gelei Xiao[2,3,4]*

[1] Department of Neurosurgery, Hunan Cancer Hospital and the Affiliated Cancer Hospital of Xiangya School of Medicine, Central South University, Changsha, China, [2] Department of Neurosurgery, Xiangya Hospital, Central South University, Changsha, China, [3] Diagnosis and Treatment Center for Hydrocephalus, Xiangya Hospital, Central South University, Changsha, China, [4] National Clinical Research Center for Geriatric Disorders, Xiangya Hospital, Central South University, Changsha, China

Cerebrospinal fluid (CSF), a colorless liquid that generally circulates from the lateral ventricles to the third and fourth ventricles, provides essential nutrients for brain homeostasis and growth factors during development. As evidenced by an increasing corpus of research, CSF serves a range of important functions. While it is considered that decreased CSF flow is associated to the development of hydrocephalus, it has recently been postulated that motile cilia, which line the apical surfaces of ependymal cells (ECs), play a role in stimulating CSF circulation by cilia beating. Ependymal cilia protrude from ECs, and their synchronous pulsing transports CSF from the lateral ventricle to the third and fourth ventricles, and then to the subarachnoid cavity for absorption. As a result, we postulated that malfunctioning ependymal cilia could disrupt normal CSF flow, raising the risk of hydrocephalus. This review aims to demonstrate the physiological functions of ependymal cilia, as well as how cilia immobility or disorientation causes problems. We also conclude conceivable ways of treatment of hydrocephalus currently for clinical application and provide theoretical support for regimen improvements by investigating the relationship between ependymal cilia and hydrocephalus development.

Keywords: ependymal cilia, hydrocephalus, cerebrospinal fluid, pathogenesis, treatment

OPEN ACCESS

Edited by:
Adjanie Patabendige,
Edge Hill University, United Kingdom

Reviewed by:
Lance Lee,
Sanford Research, United States
Ville Leinonen,
Kuopio University Hospital, Finland

***Correspondence:**
Gelei Xiao
xiaogelei@csu.edu.cn

† These authors have contributed equally to this work and share first authorship

Specialty section:
This article was submitted to Brain Disease Mechanisms, a section of the journal Frontiers in Molecular Neuroscience

Received: *24 April 2022*
Accepted: *20 June 2022*
Published: *12 July 2022*

Citation:
Ji W, Tang Z, Chen Y, Wang C, Tan C, Liao J, Tong L and Xiao G (2022) Ependymal Cilia: Physiology and Role in Hydrocephalus. Front. Mol. Neurosci. 15:927479. doi: 10.3389/fnmol.2022.927479

INTRODUCTION

Hydrocephalus is a neurological disease caused by an excess of cerebrospinal fluid (CSF) in the ventricles (Filis et al., 2017). The classic definition of hydrocephalus refers to two types: communicating and non-communicating (also known as obstructive) (Shim et al., 2019; Zhang J. X. et al., 2020). Excess fluid is present in communicating hydrocephalus due to abnormalities in CSF secretion, motility, and/or absorption (Finn et al., 2014; Shim et al., 2019). Blockage of the CSF flow during circulation causes obstructive hydrocephalus (Højlund et al., 2018). Headache, lower-limb weakness, starting or gait instability, urine incontinence, ataxia, and progressive loss of autonomic language and physical activity are also typical symptoms (Filis et al., 2017). It could be congenital

or the result of excessive CSF production, malabsorption, or obstruction due to trauma, infection, venous occlusion, tumors, intracranial hemorrhage, or motile cilia dysfunction (Shim et al., 2019).

Cerebrospinal fluid is a transparent, colorless liquid found in the ventricle and subarachnoid region. It is primarily produced by the choroid plexus in the lateral ventricle, third ventricle, and fourth ventricle, with some directionality in its flow (Berliner et al., 2019; Lloyd et al., 2020). CSF is created, absorbed, and returned to the vein on a constant basis. In the central nervous system, it functions similarly to lymph. It provides specific nutrients to brain cells, transfers metabolites from brain tissue, and maintains the acid-base balance of the central nervous system. To relieve pressure on the brain and spinal cord, cerebrospinal fluid (CSF) surrounds and supports them.

Heart and cilia are two power sources of the circulation of CSF. Cilia are highly conserved organelles that protrude from the surface of nearly every cell type and are classified into two types: motile and primary cilia (Mitchison and Valente, 2017; Zhang J. et al., 2020). Respiratory epithelial cells, oviduct cells, node cells, and ECs all have mobile cilia (Zhang J. et al., 2020). Ependymal cilia, a long process that can swing out of the free surface of ECs, are found in the central nervous system (CNS) (Dur et al., 2020) and extend into the myelocoele. Normal ependymal cilia are uniformly distributed on ECs and have a constant length. The special unique plane polarity of cilia guarantees that they swing in a stable direction during movement, promoting directed CSF circulation in the brain (Kumar et al., 2021; Yamada et al., 2021).

As a result, it goes without saying that cilia play an irreplaceable role in the development of hydrocephalus. The aberrant accumulation of CSF in the ventricle is caused by the malfunction of ependymal cilia, which obstructs the normal flow of CSF, resulting in an imbalance between CSF production and absorption (Al Omran et al., 2017). Despite the fact that the physiology and significance of ependymal cilia in hydrocephalus has aroused researchers' curiosity, there are still some limits in this field. Thus, we'll focus on the physiological activities of ependymal cilia in this review, as well as the mechanism of cilia immobility, or cilia disorientation, which leads to disorders. Furthermore, we attempt to decipher the process of hydrocephalus development based on factors that cause pathophysiology of motile cilia, such as alcohol abuse, degenerative neuropathology, PCD, and brain injury, and thus propose conceivable treatment options for hydrocephalus, which may provide new theoretical support for future research by examining the relationship between ependymal cilia and hydrocephalus development.

Abbreviations: CSF, cerebrospinal fluid; ECs, ependymal cells; PCD, primary ciliary dyskinesia; CNS, central nervous system; BBs, basal bodies; BF, basal feet; PM, plasma membrane; ODF, outer dense fiber; CCNO, Cyclin O; NME7, non-metastatic cell 7; γTuRC, γ-tubulin ring complex; MT, microtubule; HTT, Huntington protein; HAP1, Huntington-associated protein 1; PCM1, perinuclear matter 1 protein; HD, Huntington disease; CP, central pair; PMTs, peripheral microtubules; ODA, outer dynein arm; IDA, inner dynein arm; DNAAFs, dynein axonemal assembly factors; ODA7, outer dynein arm 7; LRRC50, leucine-rich repeat-containing protein 50; KTU, kintoun; LRRC6, leucine-rich repeat-containing protein 6; CCDC151, coiled-coil domain-containing protein 151; CFAP221, cilia-and flagella-associated protein 221; PCDP1, primary ciliary dyskinesia protein 1; CFAP54, cilia-and flagella-associated protein 54; PCP, planar cell polarity; DVLs, disheveled); DVL2, disheveled 2; AD, Alzheimer's disease; NPH, normal pressure hydrocephalus; N-DRCs, nexin-dynein regulatory complexes; RS, radial spoke.

PHYSIOLOGICAL FUNCTIONS OF EPENDYMAL CILIA

Ependymal cilia, which are found in the ventricular system of the brain (Ringers et al., 2020), serve an important role in maintaining appropriate CSF flow (Chiani et al., 2019). Ependymal cilia ensure CSF flow and are necessary for CSF homeostasis and directional migration of neural cells.

Ependymal Cilia Propelling the Circulation of Cerebrospinal Fluid

The directional flow of CSF depends directly on ependymal cilia within the ventricular system (Lee, 2013; Kumar et al., 2021). Ependymal cilia can be found on ECs all across the brain, projecting up to 20 microns from the cell (Zhang J. et al., 2020). As CSF circulation requires a powerful and accurate pressure from the exterior (Kumar et al., 2021), the synchronized beats of ependymal cilia that plays an indispensable role in the flow of CSF from the lateral ventricles to the third and fourth ventricles, and then toward the subarachnoid space for absorption (Vidovic et al., 2018). This mechanism was recently confirmed by Alexia Mahuzier's experiment, which looked at mice with mutations in genes important for cilia development.

Ependymal cells have about 50 motile cilia per cell, which aid in directing CSF flow through the ventricular system. The rotating organization of the basal bodies (BBs) is required for the coordinated beat of ependymal cilia. Rotational polarity refers to the unidirectional arrangement of all basal feet (BF) on each EC. BF protrude unilaterally from the BB barrel, affecting CSF flow direction (Mirzadeh et al., 2010; Wallingford, 2010; Ohata et al., 2014; Ryu et al., 2021). It is clear that cilia motion is indispensable for initiating and maintaining apical actin enrichment at the apex of centriolar plaque. The apical enrichment of actin in centriolar plaques in adult ECs helps to the maintenance of the optimum number and spacing of centrioles, allowing ECs to maintain an ideal number of motile cilia and hence ensure effective CSF flow in the ventricles (Mahuzier et al., 2018).

Furthermore, the continual beating of ependymal cilia aids in CSF nutrition exchange and waste clearance (Xiong et al., 2014; Fame and Lehtinen, 2020), assisting in the maintenance of CSF homeostasis.

Ependymal Cilia Regulating Neuroblast Migration

Previous study has revealed that ependymal cilia in the brain ventricles direct neuroblast migration in both adult and mouse development (Marshall and Nonaka, 2006; Sawamoto et al., 2006). The beating of ependymal cilia can propel CSF flow and form a concentration gradient of the guiding molecules, facilitating the orientation of neuroblast migration (Hirschner et al., 2007). Interestingly, a recent study found that the Xenopus

neuroblast also relies on ependymal cilia-driven CSF flow, owing to the ability of the polarized ependymal cilia to create a polarized flow (Dur et al., 2020; **Figure 1**, Functions of ependymal cilia).

LACK OF EPENDYMAL CILIA

Ciliary abnormalities include the absence of cilia, cilia immobility, and alterations in planar polarity that shift the direction of the cilia's beat (Wu et al., 2020). The relationship between cilia failure and gene mutations has been actively explored in humans thanks to developments in research methodologies, and genetic analysis of human hydrocephalus cases have been continuously reported. As a result, we've compiled a list of linked pathogenic genes discovered in hydrocephalus induced by ependymal cilia abnormalities.

Although numerous gene mutations that we have known can cause loss of ependymal cilia to varying degrees, we will review genes that cause cilia deletion according to a novel concept in this review. Cilia are derived from BBs, and the centrioles are the primary structure of the BBs. As a result, numerous dysfunctions of the centriole will interfere with the normal proliferation of ependymal cilia, resulting in cilia loss. Therefore, we'll focus on the genes linked to ciliary loss caused by centriole dysfunctions.

FoxJ1 is a transcription factor that is required for ciliogenesis in multiciliated cells (MCCs) of the mouse (Lewis and Stracker, 2021). The expression of γ-tubulin, dynein, and kinesin motor proteins is severely lacking in FoxJ1-deficient mice, resulting in the inability of centriole to be transported to the surface of ECs, impairing the formation of ependymal cilia (Jacquet et al., 2009). Human patients with the FoxJ1 mutation have recently shown motor cilia abnormalities caused by BBs injury in MCCs (Lewis and Stracker, 2021).

Mcidas (Mci or Idas), Geminin protein, GemC1 (also known as Gmnc or Lynkeas), and FoxJ1 are transcription regulators that play a pivotal role in the formation of ECs. Both GemC1 and Mcidas have been found in studies to induce MCC differentiation in the brain. Mcidas, in combination with transcription factors such as TAp73, c-Myb, E2F4 and E2F5, increases the development and maturation of BBs according to several studies (Omiya et al., 2021). However, Mcidas-deficient mouse developed morphologically discernible MCCs in the brain, which can express early transcription factors such as p73 and FoxJ1, but cannot extend centrioles, thus resulting in the loss of ependymal cilia (Lewis and Stracker, 2021).

NHERF1/EBP50 is an adapter protein found mostly in the apical plasma membrane of human epithelial cells. NHERF1-deficient mice's lateral ventricle, third ventricle, and fourth ventricle swelled, indicating the formation of non-obstructive hydrocephalus and it can be either mild or severe. NHERF1 expression was highest at the apical of plasma membrane (PM) of ECs, and was involved in the emergence of non-obstructive hydrocephalus through the disruption of ciliary movement of ECs, according to brain sections (Georgescu et al., 2015).

Odf2 is a gene that encodes a highly stable fibrous structure in the sperm tail and was first discovered as one of the main components of the outer dense fiber (ODF). When exons 6 and 7 of Odf2 are deleted, mice's cilia lose a considerable amount of their basal feet. This structure is linked to the basal body triad and aids in the formation of BBs. Furthermore, it has been demonstrated by immunofluorescence that the number of cilia per cell decreased in $Odf2^{\Delta Ex6,7/\Delta Ex6,7}$ MCCs in the ventricle (Kunimoto et al., 2012).

Cyclin O, encoded by CCNO, is a member of the cyclin family that regulates ciliogenesis and apoptosis. CCNO mutations have recently been discovered in human patients and animal models, and they can result in the entire loss or severe decrease of ependymal cilia. CCNO is required for the proper production and maintenance of deuterostomes, a cytoplasmic structure responsible for the expansion of centrioles, which attach on the plasma membrane during cilia formation to form BBs, which serve as a platform for the growth of ciliary axonemes. The CCNO mutation causes Ccno deficit, which causes deuterostomes to fail to form correctly, resulting in a decrease in the number of centrioles and the inability to grow cilia regularly, thus leading to the loss or insufficient number of ependymal cilia (Wallmeier et al., 2014; Funk et al., 2015; Núnez-Ollé et al., 2017).

NME7, also known as non-metastatic cell 7 or nucleoside diphosphate kinase 7, is a member of the NME family of proteins that modulates the nucleation activity of γ-tubulin ring complex (γTuRC) and helps to regulate the microtubule (MT) organizing center. The γTuRC is the principal MT nucleator in animal cells and plays a crucial role in MT organization. Inhibition of NME7 expression in ependymal cilia suppresses centrosome-based MT nucleation (Liu et al., 2014; Šedová et al., 2021), impairing the normal development of centrioles and therefore resulting in the loss of ependymal cilia.

Huntington protein (HTT) is a gene that regulates ciliogenesis by interacting with Huntington-associated protein 1 (HAP1) and perinuclear matter 1 protein (PCM1). The depletion of HTT in ECs caused ciliary layer alterations in mice. HTT or HAP1 deficiency caused PCM1 to scatter from centrosomes, resulting in impaired ciliogenesis *in vivo* and hydrocephalus in mice. In Huntington Disease (HD), aberrant ependymal cilia disrupt CSF flow and interfere with neuroblast migration, disrupting brain homeostasis and speeding up disease progression (Keryer et al., 2011).

IMMOBILITY OF CILIA

According to previous research, each ependymal cilium has a central pair of singlet MTs known as the central pair (CP) complex and nine parallel doublet MTs known as peripheral microtubules (PMTs), forming a so-called '9 + 2' structure. Additionally, the outer component is known as the outer dynein arm (ODA), whereas the inner structure is known as the inner dynein arm (IDA). A radial spoke structure in each PMT regulates motility by connecting the CP to the dynein arms (Marshall and Nonaka, 2006; Sawamoto et al., 2006). As a result, there is little question that if the ependymal cilia are structurally

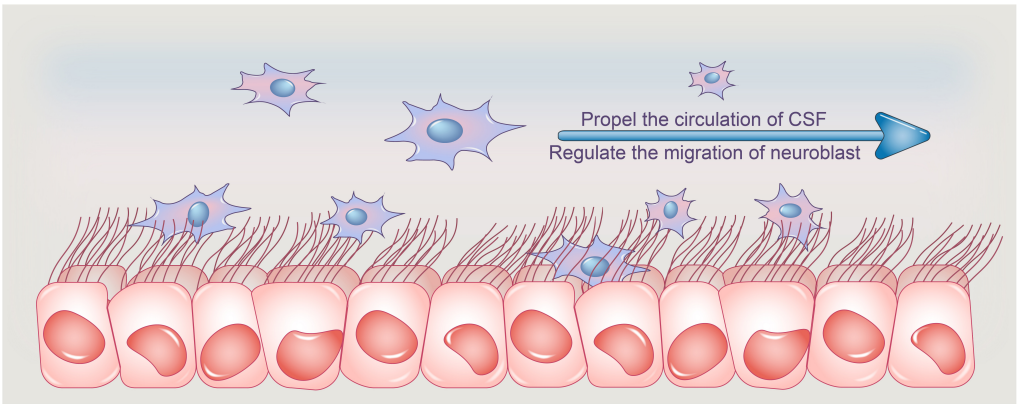

FIGURE 1 | Functions of ependymal cilia. Ependymal cilia protrude from ependymal cells, and their synchronized pulsing transports CSF from the lateral ventricle to the third and fourth ventricles, where it is absorbed. Adult ependymal cells' apical enrichment of actin in centriolar plaques aids in the maintenance of the optimal number and spacing of centrioles, allowing ependymal cells to maintain an ideal number of motile cilia and thus aid in CSF nutrition exchange and waste clearance, assisting in CSF homeostasis. Furthermore, the beating of ependymal cilia can propel CSF flow and create a concentration gradient of guiding molecules, which aids neuroblast migration orientation. CSF, cerebrospinal fluid.

abnormal, they will be unable to swing normally, eventually affecting the normal circulation of CSF.

Altered Structure of Axonemes

Mice lacking the Jhy gene ($Jhy^{lacZ/lacZ}$) developed dilated lateral ventricles and juvenile hydrocephalus as early as 1.5 days after birth. The ependymal cilia lining the lateral ventricles of $Jhy^{lacZ/lacZ}$ animals are sparser, shorter, more irregular, and disoriented at higher magnification, implying that they may have no function. The '9 + 2' MTs in the cilia of $Jhy^{lacZ/lacZ}$ animals were disorganized, rather, most of the cilia of $Jhy^{lacZ/lacZ}$ animals formed axonemes with '9 + 0' or '8 + 2' MTs, according to ultrastructural studies. Ciliary motility is assumed to be dependent on the CP of '9 + 2' cilia, which also controls the direction of the beat. The aberrant ependymal cilia have '9 + 0' confirmation, suggesting that $Jhy^{lacZ/lacZ}$ '9 + 0' cilia are nearly immotile. As a result of Jhy gene mutations, these aberrant ependymal cilia are unable to maintain sufficient CSF flow, which appears to be the cause of hydrocephalus in $Jhy^{lacZ/lacZ}$ mice (Appelbe et al., 2013; Muniz-Talavera and Schmidt, 2017).

Altered Structure of Dynein Arms

Dynein axonemal assembly factors (DNAAFs), which refer to a group of proteins, are involved in the preassembly of ODA complexes. The basic structures of ciliary movement are dynein arms. By hydrolyzing ATP, ODA provides the right mechanical force for ciliary beat, whereas IDA controls the ciliary beating mode. ODA complexes are preassembled in the cytoplasm before being transported to ciliated axons. DNAAF1 [also known as outer dynein arm 7 (ODA7) or leucine-rich repeat-containing protein 50 (LRRC50)], DNAAF2 [also known as PF13 or kintoun (KTU)], DNAAF3 (also known as PF22), and DNAAF4 (also known as DYX1C1) are the four types that have been discovered so far (Inaba et al., 2016). DNAAFs work with molecular chaperones to ensure that ODA subunits fold correctly, allowing ependymal cilia to move normally. The preassembly of ODA was impaired when DNAAFs mutated, making the ependymal cilia unable to swing normally (Ha et al., 2016).

Except DNAAFs, leucine-rich repeat-containing protein 6 (LRRC6) is also required for the transport of the ODA complex from the cytoplasm to the cilia. The structure of ependymal cilia remains intact in the absence of LRRC6, but they are entirely immobile. The '9 + 2' structure of MTs remains normal in mice lacking LRRC6, but ODA proteins that should be carried to the ciliary axonemes remain in the cytoplasm and are not delivered to the ciliary axonemes, according to studies. The cilia in the ependymal cilia lack ODAs, which are necessary for cilia movement, resulting in cilia immobility (Inaba et al., 2016).

The inner and outer dynein arms, as previously stated, are essential components for cilia movement. The coiled-coil domain-containing protein 151 (CCDC151) gene encodes a coiled-coil protein that aids in the assembly of the ODA complex and ensures that it is appropriately linked to MTs. Since we already know that dynein's mechanical force aids in the synchronous beating of ependymal cilia, a recent experiment confirms our previous findings by showing that the loss of CCDC151 causes complete loss of ODA in axonemes, resulting in severe ciliary dyskinesia, and most of the ependymal cilia around the ventricle were immobile (Chiani et al., 2019).

DNA Polλ, commonly known as Polβ2, is a key gene for IDA assembly and belongs to the PolX family. Aside from electron microscopy, investigations have indicated that in mice lacking DNA Polλ, the dynein arms of cilia from the EC layer are defective. Furthermore, ependymal cilia without ODAs can beat slowly, but IDAs appear to be essential. As a result, it appears that ciliary immobility seems to be blamed to defective IDAs, which are induced by DNA Polλ mutants (Kobayashi et al., 2002). However, there is still considerable disagreement. Zariwala et al. (2004) recently looked into the deletion construct further and discovered that in the mouse model, the expression of a new gene called DPCD was also likely affected. Furthermore, in a second

experiment, mice with deletion of only the catalytic domain of Polλ had a normal phenotype. As a result, the PCD phenotype found in Polλ knockout mice by Kobayashi et al. (2002) is most likely attributable to the loss of DPCD (Zariwala et al., 2004).

DISORIENTATION OF EPENDYMAL CILIA

We know from the preceding description that the aberrant quantity and structure of ependymal cilia can impair CSF. Furthermore, abnormal cilia function in the ependyma will result in the abnormal accumulation of CSF.

Normal ependymal cilia swing in a set polarity direction, moving CSF from the lateral ventricle to the third ventricle, and then through the midbrain aqueduct into the fourth ventricle. When the polarity of ependymal cilia is compromised due to a variety of causes, the equilibrium mode of directional CSF flow will be disrupted, causing CSF to accumulate in the ventricle and prevent it from being evacuated on time.

Reduction in Ciliary Movement Frequency

Primary cilia are usually '9 + 0' type, whereas motile cilia are '9 + 2.' The most obvious structure to identify the two is CP, which is absolutely necessary for maintaining the function of the motile cilia in the brain (Dawe et al., 2007). The CP apparatus is a complicated structure made up of at least seven distinct protein projections that regulate dynein motion forces and allow the dynein arm to maintain normal ciliary motion (Lee et al., 2008; Brown et al., 2012; McKenzie et al., 2015). As a result, in this review, we concentrate on genes linked to reduction in ciliary movement frequency, which is mainly driven by CP dysfunction.

Hydin is located in the CP of brain and is required for appropriate cilia motility. In Hydin mutant mice, early hydrocephalus symptoms such as enlargement of the lateral ventricle and third ventricle were observed, which is related to aberrant CSF accumulation caused by defective ciliary activity. The ependymal cilia will be unable to bend appropriately due to the lack of a particular projection in Hydin, resulting in a decrease in cilia beating frequency and cilia stagnation (Dawe et al., 2007; Al Omran et al., 2017).

Cilia-and flagella-associated protein 221 (CFAP221), also known as primary ciliary dyskinesia protein 1 (PCDP1), is a CP protein that regulates ependymal ciliary motility and is located to the C1d projection of the CP apparatus. The CFAP221 expression being suppressed will result in a reduction in ependymal ciliary beat frequency (McKenzie and Lee, 2020).

The C1d projection complex is encoded by cilia-and flagella-associated protein 54 (CFAP54), a crucial component of the C1d assembly mechanism. Mutations in CFAP54 cause reduced ependymal ciliary beating frequency (Lee et al., 2008) and loss of the C1d projection (McKenzie and Lee, 2020), leading in CSF flow disruption and accumulation, similar to CFAP221 (McKenzie et al., 2015).

Planar Cell Polarity Disorder

In ECs, PCP, also known as tissue polarity (Tissir et al., 2010), takes two forms: translational polarity and rotational polarity. The stability of ependymal ciliary motion is dependent on both intracellular and intercellular polarity coordination (Ohata et al., 2014).

The human DAPLE gene determines the direction of CSF flow and regulates the orientation of ependymal cilia (Yamada et al., 2021). DAPLE deficiency impairs horizontal polarization in ECs (Takagishi et al., 2017) as well as the beat of ependymal cilia.

Disheveled (DVLs) are also necessary for preserving the polarity of the EC plane. In ECs, the application of dominant negative disheveled 2 (DVL2) has been found to impair the rotational arrangement of cilia. Furthermore, in adult mice, selectively induced DVLs removal resulted in ependymal cilia with a faulty intracellular rotational configuration. Reduced frequency of ependymal ciliary beat and aberrant CSF accumulation may occur if rotational polarity is disrupted (Ohata et al., 2014).

Calaxin, a Ca2 + binding dynein-related protein that controls cilia motility, binds to ODA directly in a Ca2 + -dependent way. Ependymal cilia in mice lacking the EFCAB1 gene encoding Calaxin had somewhat lower fluid flow rates driven by ependymal cilia than normal ependymal cilia, according to Sasaki et al. (2019). Calaxin deficiency may thereby disrupt the rotational polarity of ependymal cilia, leading to absonant cilia movement (Sasaki et al., 2019; **Figure 2**, Abnormalities of ependymal cilia).

FACTORS CAUSING PATHOPHYSIOLOGY OF MOTILE CILIA IN HYDROCEPHALUS

Although it has previously been stated that defects in the structure or function of ependymal cilia can clearly lead to hydrocephalus, here we thoroughly discuss some factors that may be linked to abnormal motile cilia, including alcohol abuse, degenerative neuropathology such as Alzheimer's disease (AD), PCD, and brain injury (Drielsma et al., 2012; Jiménez et al., 2014; Yamada et al., 2021).

Alcohol Abuse

Chronic alcohol consumption can have a number of negative effects on the brain, including a 31–71% rise in ventricular size, which is a sign of hydrocephalus (de la Monte, 1988; Zahr et al., 2014). Al Omran et al. (2017) recently found that treating brain slices *in vitro* with 0.25% ethanol reduced the beating frequency of cilia, resulting in a decrease in CSF movement speed. More notably, their research found that ethanol consumption decreased ependymal ciliary pulsation and function in the lateral and third ventricles in rats by reporting three distinct types of ependymal cilia named type-I, type-II, and type-III. These three types were classified based on their frequency and angle of beating, distinct localization in the mouse brain (Al Omran et al., 2017). Ethanol lowers the frequency of ependymal cilia oscillations in rat models, according to findings (Yamada et al., 2021). It can be concluded that ethanol can impair the normal movement of the ependymal cilia in the ventricle, causing hydrocephalus by blocking the circulation of CSF (Saternos and AbouAlaiwi, 2019).

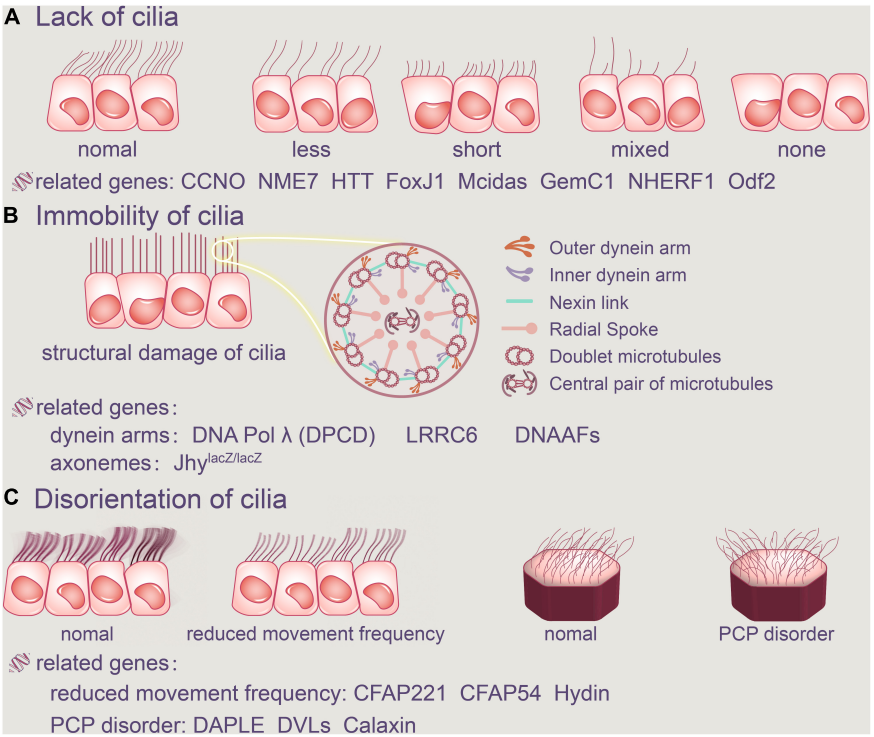

FIGURE 2 | Abnormalities of ependymal cilia. The absence of cilia, cilia immobility, and changes in planar polarity that modify the direction of the cilia's beat are all examples of ciliary disorders. **(A)** Cilia loss occurs when the number of ependymal cilia decreases, their length decreases, or there are no cilia at all. FoxJ1, Mcidas, GemC1, NHERF1, Odf2, CCNO, NME7, and HTT are all related genes. **(B)** Furthermore, the structure of the original normal cilia is destroyed, as is the aberrant function of the dynein arms and axonemes, resulting in ependymal cilia immobility. DNAAFFs, CCDC151, and DNA Polλ (DPCD) are all related genes. In addition, aberrant cilia function in the ependyma causes inappropriate CSF accumulation. **(C)** Ciliary movement frequency will be reduced by Hydin, CFAP221 and CFAP54, and regular PCP disorder will be harmed. CCNO, Cyclin O; NME7, non-metastatic cell 7; HTT, Huntington protein; LRRC6, leucine-rich repeat-containing protein 6; DNAAFs, dynein axonemal assembly factors; CFAP221, cilia-and flagella-associated protein 221; CFAP54, cilia-and flagella-associated protein 54; DVLs, disheveled.

One of the major causes of congenital hydrocephalus is alcohol abuse during pregnancy. Long-term drinking can also have a variety of negative consequences on adults' brains, including hydrocephalus (Al Omran et al., 2017).

Alzheimer's Disease

Normal pressure hydrocephalus (NPH) is a common neurological disease. Hakim's triad of clinical symptoms includes dementia, gait problem, and urinary incontinence (Johanson et al., 2008; Tan et al., 2021). With aging, the ability of CP epithelial cells to generate CSF decreased. As the rate of CSF formation declines by 50% or more throughout the development of disease, the absorption rate of CSF slows down, resulting in a consequently increase of the concentration of toxic substance. AD is a progressive neurological illness that affects adults over the age of 70 and is characterized by memory disorders, executive dysfunction, and comprehensiveness including dementia, personality changes and behavioral changes (Inaba et al., 2016; Xiao et al., 2021). Because NPH is frequently detected in people with Alzheimer's disease, the current hypothesis proposes that NPH is the outcome of neurodegenerative alterations in AD patients. The removal of toxic molecules such as Aβ is aided by the circulation of CSF (Zhan et al., 2020).

More ependymal cilia fall off in the ventricle as the aging of the CNS, and the circulation of CSF flow is reduced, resulting in decreased clearance of potentially toxic metabolites, contributing to AD. The poisonous molecule cannot be eliminated quickly enough in AD patients, and it is deposited in the meninges, increasing CSF outflow resistance, inhibiting CSF absorption and accumulating in the ventricle, leading to NPH (Keryer et al., 2011).

Recently, Wilson and Williams believe that iNPH can now be categorized as a reversible dementia since our understanding of the disease has improved. Because the symptoms of iNPH are so similar to those of AD or PD, the majority of patients will be misdiagnosed or go undiscovered. As a result, some scholars have questioned the existence of iNPH (Yang et al., 2021). Even though occurrences of AD-caused hydrocephalus are uncommon, the incidence cannot be ruled out and scholars should delve deeper into this topic.

Primary Ciliary Dyskinesia

Primary ciliary dyskinesia, formerly known as immobile cilia syndrome, is caused by defects in the structure and function of cilia. Chronic sinusitis, otitis media, infertility, inverted position, and hydrocephalus are among the symptoms that patients may

experience. However, the incidence of these related diseases varies greatly among patients with PCD. According to recent reports, the incidence of hydrocephalus in patients with PCD is relatively low when compared to chronic sinusitis, otitis media, male infertility, or inverted position. Hydrocephalus, on the other hand, is a common occurrence in mice with PCD (Lee, 2013). A link between PCD and hydrocephalus has been established by numerous studies (Mulroy et al., 2020).

Due to structural malfunction, the ependymal cilia of PCD patients are unable to beat at a regular frequency, often contributing to the impairment of normal CSF circulation. As a result, accumulated CSF enlarges the ventricle, eventually develops into hydrocephalus.

Brain Injury

Brain injury is an organic injury to the brain tissue induced by head trauma. When the cranium is struck, the CSF in the ventricle can act as a shock absorber, reducing the risk of brain tissue injury. The continual beating of ependymal cilia contributes to CSF circulation and is the foundation of nutrient exchange and waste elimination, as we already know. Therefore, the sharp reduction of ependymal cilia caused by brain injury may have serious pathological repercussions.

In the study of Williamson et al. (2018), collagenase caused intracerebral hemorrhage in the rat model, according to Xiong et al. (2014), concussion brain injury produces rapid shedding of ventricular ependymal cilia and lowers the frequency of CSF flow (Bothwell et al., 2019, 2021). Furthermore, on the surface of the lateral ventricle 1 week after concussion, there were essentially no ependymal cilia (Xiong et al., 2014). Because of the rapid decrease in the number of ependymal cilia induced by brain damage, CSF will accumulate, resulting in hydrocephalus (**Figure 3**, Pathophysiology of motile cilia in hydrocephalus).

TREATMENT OF HYDROCEPHALUS BY TARGETING EPENDYMAL CILIA

The abnormal collection of CSF in the ventricle causes hydrocephalus (Zhan et al., 2020). Ependymal cilia dysfunction can obstruct CSF circulation, causing a discrepancy between CSF production and absorption (Al Omran et al., 2017). The two types of hydrocephalus are communicating and obstructive, with the former being more common. Communicating hydrocephalus may be due to excessive CSF secretion or secondary to reduced CSF absorption.

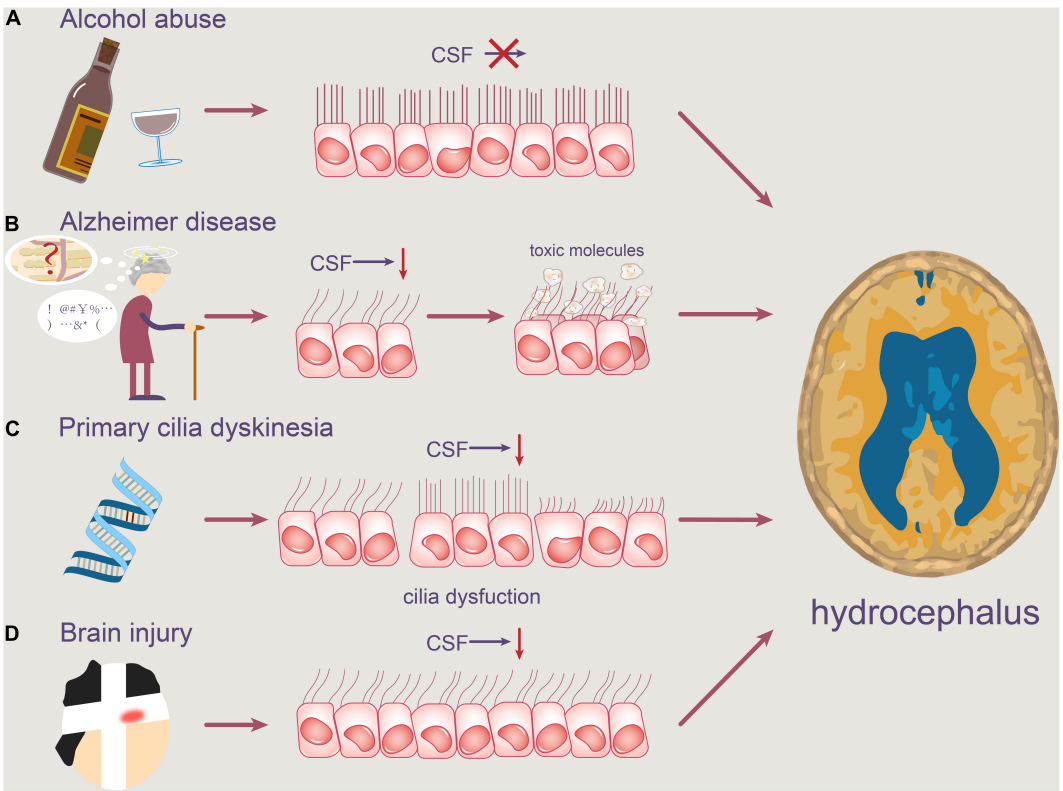

FIGURE 3 | Pathophysiology of motile cilia in hydrocephalus. Abnormal motile cilia can be caused by a variety of reasons. **(A)** Alcohol abuse may reduce the beating frequency of cilia, resulting in slower CSF flow. **(B)** Degenerative neuropathologies, such as Alzheimer's disease, can obstruct the clearance of toxic molecules like Aβ, causing them to accumulate in the ventricle. **(C)** Furthermore, PCD patients' ependymal cilia are unable to beat at a regular frequency, which contributes to a disruption in normal CSF circulation. **(D)** Concussion brain injury also contributes to the rapid shedding of ventricular ependymal cilia and the reduction of CSF flow frequency.

TABLE 1 | A comprehensive list of ependymal cilia dysfunction-related genes.

Gene	Protein localization/Function	Structural defect in ependymal cilia	Typical functional defect in ependymal cilia	References
FoxJ1	Transcription factor	Inability of centrioles to be transported to the surface of ECs	Lack of ependymal cilia	Jacquet et al., 2009; Lewis and Stracker, 2021
Mcidas	Transcription factor	Inability to extend centrioles	Lack of ependymal cilia	Lewis and Stracker, 2021; Omiya et al., 2021
GemC1	Transcription factor	Inability to extend centrioles	Lack of ependymal cilia	Lewis and Stracker, 2021; Omiya et al., 2021
NHERF1	Apical cytoplasm	Inability to establishes protein complexes at the apical PM	Lack of ependymal cilia	Georgescu et al., 2015
Odf2	BF in the polarized organization	Inability of formation of BF	Lack of ependymal cilia	Kunimoto et al., 2012
CCNO	Apical cytoplasm	The reduction of the number of centrioles	Lack of ependymal cilia	Wallmeier et al., 2014; Funk et al., 2015; Núnez-Ollé et al., 2017
NME7	MT organizing center	The reduction of the number of centrioles	Lack of ependymal cilia	Liu et al., 2014; Šedová et al., 2021
Jhy	Unknown	Altered structure of axonemes	Immotile ependymal cilia	Appelbe et al., 2013; Muniz-Talavera and Schmidt, 2017
DNAAF1/LRRC50/ODA7	Cytoplasmic, DA assembling	ODA + IDA defect	Immotile ependymal cilia	Duquesnoy et al., 2009; Loges et al., 2009; Ha et al., 2016
DNAAF2/PF13/KTU	Cytoplasmic, DA assembling	ODA + IDA defect	Immotile ependymal cilia	Omran et al., 2008; Ha et al., 2016
DNAAF3/PF22	Cytoplasmic, DA assembling	ODA + IDA defect	Immotile ependymal cilia	Mitchison et al., 2012; Ha et al., 2016
DNAAF4/DYX1C1	Cytoplasmic, DA assembling	ODA + IDA defect	Immotile ependymal cilia	Chandrasekar et al., 2013; Ha et al., 2016; Cho et al., 2018
LRRC6	Cytoplasmic, DA assembling	ODA + IDA defect	Immotile ependymal cilia	Kott et al., 2012; Inaba et al., 2013, 2016
CCDC151	ODA targeting and docking	ODA defect	Immotile ependymal cilia	Alsaadi et al., 2014; Hjeij et al., 2014; Chiani et al., 2019
DNAI1	ODA	ODA defect	Immotile ependymal cilia	Horváth et al., 2005; Zariwala et al., 2006; Failly et al., 2008; Ziêtkiewicz et al., 2010; Mazor et al., 2011; Wildung et al., 2019; Bhushan et al., 2021
DNAI2	ODA	ODA defect	Immotile ependymal cilia	Rocca et al., 2008, 2020
ZMYND10	Cytoplasmic, DA assembling	ODA + IDA defect	Immotile ependymal cilia	Rocca et al., 2008; Moore et al., 2013; Zariwala et al., 2013; Cho et al., 2018
CCDC39	Nexin-dynein regulatory complexes (N-DRCs)	MT disorganization and IDA defect	Short and immotile ependymal cilia	Merveille et al., 2011; Abdelhamed et al., 2018; Emmert et al., 2019
DNA Polλ	DNA repair polymerase	IDA defect	Immotile ependymal cilia	Kobayashi et al., 2002
RSPH9	Radial spokes (RSs)	MT disorganization (CP-RS defect)	Lower beating amplitude and disorientation of ependymal cilia	Castleman et al., 2009; Ziêtkiewicz et al., 2012; Kott et al., 2013; Zou et al., 2020
Hydin	CP	Reduction of ciliary movement frequency	Disorientation of ependymal cilia	Dawe et al., 2007; Al Omran et al., 2017
CFAP221/PCDP1	CP	Reduction of ciliary movement frequency	Disorientation of ependymal cilia	Lee et al., 2008; DiPetrillo and Smith, 2010; McKenzie et al., 2018; McKenzie and Lee, 2020
CFAP54	CP	Reduction of ciliary movement frequency	Disorientation of ependymal cilia	Lee et al., 2008; McKenzie et al., 2015, 2018; McKenzie and Lee, 2020
DAPLE	Anterior side of the apical membrane	PCP disorder	Disorientation of ependymal cilia	Takagishi et al., 2017
DVLs	Unknown	PCP disorder	Disorientation of ependymal cilia	Ohata et al., 2014; Yamada et al., 2021
EFCAB1	Unknown	PCP disorder	Disorientation of ependymal cilia	Sasaki et al., 2019

Medical treatments and surgical management are now used to treat hydrocephalus (Wang et al., 2021). Drug treatment is generally only applicable to patients with mild hydrocephalus and mild hydrocephalus under the age of two. Acetazolamide, as well as dehydration medicines and diuretics including mannitol, hydrochlorothiazide, amino pteridine, and furosemide, are preferred to decrease CSF secretion. A lateral ventricle and third ventricle fistula, a ventricle subarachnoid shunt, repeated puncture of the ventricle through drilling, suboccipital decompression, and other surgical treatments are available (Bhushan et al., 2021).

Despite the fact that surgery is still the most effective treatment for hydrocephalus, it can cause a variety of major problems, including shunt system blockage and infection, as well as a poor prognosis (Johanson et al., 2008; Wu et al., 2020). As a result, it is urgent to find a better treatment.

The moving cilia are recognized to be directly responsible for the unidirectional flow of CSF. The coordinated beating of cilia in a certain direction causes powerful CSF movement, and ependymal cilia dysfunction can be caused by a variety of gene mutations. We summarized the findings from human and experimental animal models from this perspective. We categorized them into several kinds based on many types of ciliary deficiency phenotypes found in various models: reduced ciliary number, shorter cilia, ciliary structural flaws, and ciliary polarity disorder (Lee, 2013; Kumar et al., 2021). Different phenotypes share a common characteristic: they disrupt the normal movement of ependymal cilia, causing further harm to the CSF circulation and resulting in hydrocephalus. We hope that by focusing on these harmful genes, we may be able to develop targeted therapies for specific mutation locations or action pathways, to further correct ependymal cilia defects and alleviate hydrocephalus. **Table 1** lists the genes that have been identified as playing a role or that may play a role in ependymal cilia, as well as their relationship with ependymal ciliary dysfunction (**Table 1**, A comprehensive list of ependymal cilia dysfunction-related genes).

CONCLUSION

We outlined the primary physiological activities of ependymal cilia in this review, which include aiding CSF circulation and regulating neuroblast migration. Recent results related to ciliogenesis dysfunctions, on the other hand, have provided new insights into how it causes disorders like AD and HD.

Furthermore, the abnormalities of ependymal cilia are linked to the occurrence of hydrocephalus, whose mechanism is currently understood as a disruption of normal CSF flow, which leads to aberrant accumulation in the brain. The relationship between phenotypes and genotypes of ependymal cilia should be clarified from a broad perspective. As a result, we've identified the linked causative genes associated with hydrocephalus in **Table 1** for future research. The discovery of these genes will not only aid in the genetic knowledge of cilia-related hydrocephalus, but it may also provide a unique latent point for future hydrocephalus diagnostic and therapy strategies.

In conclusion, we think that this review will be useful in determining the precise mechanism of cilia-caused hydrocephalus. Despite the fact that our current understanding is still superficial, it is expected that more basic and clinical research will emerge in the future, which will assist people all around the world.

AUTHOR CONTRIBUTIONS

WYJ and ZT collected the related manuscript. WYJ, ZT, YBC, CSW, JBL, LT, and CWT drafted and revised the manuscript. GX participated in the design of the review and helped to draft and revise the manuscript. All authors read and approved the final manuscript.

FUNDING

This work was supported by National Natural Science Foundation of China (No. 82171347), Hunan Provincial Natural Science Foundation of China (Nos. 2022JJ70107 and 2022JJ30971), the Scientific Research Project of Hunan Provincial Health Commission of China (No. 202204040024), and the Students Innovations in Central South University of China (Nos. 20210033020055, 20210033020036, and 2021003302004).

ACKNOWLEDGMENTS

We would like to express my gratitude to all those who helped us during the writing of this manuscript and thanks to all the peer reviewers for their opinions and suggestions.

REFERENCES

Abdelhamed, Z., Vuong, S. M., Hill, L., Shula, C., Timms, A., Beier, D., et al. (2018). A mutation in Ccdc39 causes neonatal hydrocephalus with abnormal motile cilia development in mice. *Development* 145:dev154500. doi: 10.1242/dev.154500

Al Omran, A. J., Saternos, H. C., Althobaiti, Y. S., Wisner, A., Sari, Y., Nauli, S. M., et al. (2017). Alcohol consumption impairs the ependymal cilia motility in the brain ventricles. *Sci. Rep.* 7:13652. doi: 10.1038/s41598-017-13947-3

Alsaadi, M. M., Erzurumluoglu, A. M., Rodriguez, S., Guthrie, P. A., Gaunt, T. R., Omar, H. Z., et al. (2014). Nonsense mutation in coiled-coil domain containing 151 gene (CCDC151) causes primary ciliary dyskinesia. *Hum. Mutat.* 35, 1446–1448. doi: 10.1002/humu.22698

Appelbe, O. K., Bollman, B., Attarwala, A., Triebes, L. A., Muniz-Talavera, H., Curry, D. J., et al. (2013). Disruption of the mouse Jhy gene causes abnormal ciliary microtubule patterning and juvenile hydrocephalus. *Dev. Biol.* 382, 172–185. doi: 10.1016/j.ydbio.2013.07.003

Berliner, J. A., Woodcock, T., Najafi, E., Hemley, S. J., Lam, M., Cheng, S., et al. (2019). Effect of extradural constriction on CSF flow in rat spinal cord. *Fluids Barriers CNS* 16:7. doi: 10.1186/s12987-019-0127-8

Bhushan, B., Sardana, V., Shringi, P., Yadav, S. R., and Maheshwari, D. (2021). Role of surgical procedures (VP Shunt and ETV) in tuberculous meningitis with

hydrocephalus (TBMH): a systematic review. *J. Pediatr. Neurosci.* 16, 106–112. doi: 10.4103/jpn.JPN_286_20

Bothwell, S. W., Janigro, D., and Patabendige, A. (2019). Cerebrospinal fluid dynamics and intracranial pressure elevation in neurological diseases. *Fluids Barriers CNS* 16:9. doi: 10.1186/s12987-019-0129-6

Bothwell, S. W., Omileke, D., Patabendige, A., and Spratt, N. J. (2021). CSF secretion is not altered by NKCC1 nor TRPV4 antagonism in healthy rats. *Brain Sci.* 11:1117. doi: 10.3390/brainsci11091117

Brown, J. M., Dipetrillo, C. G., Smith, E. F., and Witman, G. B. (2012). A FAP46 mutant provides new insights into the function and assembly of the C1d complex of the ciliary central apparatus. *J. Cell Sci.* 125(Pt 16), 3904–3913. doi: 10.1242/jcs.107151

Castleman, V. H., Romio, L., Chodhari, R., Hirst, R. A., de Castro, S. C. P., Parker, K. A., et al. (2009). Mutations in radial spoke head protein genes RSPH9 and RSPH4A cause primary ciliary dyskinesia with central-microtubular-pair abnormalities. *Am. J. Hum. Genet.* 84, 197–209. doi: 10.1016/j.ajhg.2009.01.011

Chandrasekar, G., Vesterlund, L., Hultenby, K., Tapia-Páez, I., and Kere, J. (2013). The zebrafish orthologue of the dyslexia candidate gene DYX1C1 is essential for cilia growth and function. *PLoS One* 8:e63123. doi: 10.1371/journal.pone.0063123

Chiani, F., Orsini, T., Gambadoro, A., Pasquini, M., Putti, S., Cirilli, M., et al. (2019). Functional loss of *Ccdc1 51* leads to hydrocephalus in a mouse model of primary ciliary dyskinesia. *Dis. Model. Mech.* 12:dmm038489. doi: 10.1242/dmm.038489

Cho, K. J., Noh, S. H., Han, S. M., Choi, W.-I., Kim, H.-Y., Yu, S., et al. (2018). ZMYND10 stabilizes intermediate chain proteins in the cytoplasmic pre-assembly of dynein arms. *PLoS Genet.* 14:e1007316. doi: 10.1371/journal.pgen.1007316

Dawe, H. R., Shaw, M. K., Farr, H., and Gull, K. (2007). The hydrocephalus inducing gene product, Hydin, positions axonemal central pair microtubules. *BMC Biol.* 5:33. doi: 10.1186/1741-7007-5-33

de la Monte, S. M. (1988). Disproportionate atrophy of cerebral white matter in chronic alcoholics. *Arch. Neurol.* 45, 990–992. doi: 10.1001/archneur.1988.00520330076013

DiPetrillo, C. G., and Smith, E. F. (2010). Pcdp1 is a central apparatus protein that binds Ca(2+)-calmodulin and regulates ciliary motility. *J. Cell Biol.* 189, 601–612. doi: 10.1083/jcb.200912009

Drielsma, A., Jalas, C., Simonis, N., Désir, J., Simanovsky, N., Pirson, I., et al. (2012). Two novel CCDC88C mutations confirm the role of DAPLE in autosomal recessive congenital hydrocephalus. *J. Med. Genet.* 49, 708–712. doi: 10.1136/jmedgenet-2012-101190

Duquesnoy, P., Escudier, E., Vincensini, L., Freshour, J., Bridoux, A.-M., Coste, A., et al. (2009). Loss-of-function mutations in the human ortholog of *Chlamydomonas reinhardtii ODA7* disrupt dynein arm assembly and cause primary ciliary dyskinesia. *Am. J. Hum. Genet.* 85, 890–896. doi: 10.1016/j.ajhg.2009.11.008

Dur, A. H., Tang, T., Viviano, S., Sekuri, A., Willsey, H. R., and Tagare, H. D. (2020). In Xenopus ependymal cilia drive embryonic CSF circulation and brain development independently of cardiac pulsatile forces. *Fluids Barriers CNS* 17:72. doi: 10.1186/s12987-020-00234-z

Emmert, A. S., Iwasawa, E., Shula, C., Schultz, P., Lindquist, D., Dunn, R. S., et al. (2019). Impaired neural differentiation and glymphatic CSF flow in the Ccdc39 rat model of neonatal hydrocephalus: genetic interaction with L1cam. *Dis. Model. Mech.* 12:dmm040972. doi: 10.1242/dmm.040972

Failly, M., Saitta, A., Muñoz, A., Falconnet, E., Rossier, C., Santamaria, F., et al. (2008). DNAI1 mutations explain only 2% of primary ciliary dykinesia. *Respiration* 76, 198–204. doi: 10.1159/000128567

Fame, R. M., and Lehtinen, M. K. (2020). Emergence and developmental roles of the cerebrospinal fluid system. *Dev. Cell* 52, 261–275. doi: 10.1016/j.devcel.2020.01.027

Filis, A. K., Aghayev, K., and Vrionis, F. D. (2017). Cerebrospinal fluid and hydrocephalus: physiology, diagnosis, and treatment. *Cancer Control* 24, 6–8. doi: 10.1177/107327481702400102

Finn, R., Evans, C. C., and Lee, L. (2014). Strain-dependent brain defects in mouse models of primary ciliary dyskinesia with mutations in Pcdp1 and Spef2. *Neuroscience* 277, 552–567. doi: 10.1016/j.neuroscience.2014.07.029

Funk, M. C., Bera, A. N., Menchen, T., Kuales, G., Thriene, K., Lienkamp, S. S., et al. (2015). Cyclin O (Ccno) functions during deuterosome-mediated centriole amplification of multiciliated cells. *EMBO J.* 34, 1078–1089. doi: 10.15252/embj.201490805

Georgescu, M.-M., Yell, P., Mobley, B. C., Shang, P., Georgescu, T., Wang, S.-H. J., et al. (2015). NHERF1/EBP50 is an organizer of polarity structures and a diagnostic marker in ependymoma. *Acta Neuropathol. Commun.* 3:11. doi: 10.1186/s40478-015-0197-z

Ha, S., Lindsay, A. M., Timms, A. E., and Beier, D. R. (2016). Mutations in Dnaaf1 and Lrrc48 cause hydrocephalus, laterality defects, and sinusitis in mice. *G3* 6, 2479–2487. doi: 10.1534/g3.116.030791

Hirschner, W., Pogoda, H.-M., Kramer, C., Thiess, U., Hamprecht, B., Wiesmüller, K.-H., et al. (2007). Biosynthesis of Wdr16, a marker protein for kinocilia-bearing cells, starts at the time of kinocilia formation in rat, and wdr16 gene knockdown causes hydrocephalus in zebrafish. *J. Neurochem.* 101, 274–288. doi: 10.1111/j.1471-4159.2007.04500.x

Hjeij, R., Onoufriadis, A., Watson, C. M., Slagle, C. E., Klena, N. T., Dougherty, G. W., et al. (2014). CCDC151 mutations cause primary ciliary dyskinesia by disruption of the outer dynein arm docking complex formation. *Am. J. Hum. Genet.* 95, 257–274. doi: 10.1016/j.ajhg.2014.08.005

Højlund, M., Hansen, P., Krone, W., and Høgh, L. (2018). Obstructive hydrocephalus caused by colloid cyst presenting as a schizophrenia-like psychosis. *BMJ Case Rep.* 2018:bcr2017223037. doi: 10.1136/bcr-2017-223037

Horváth, J., Fliegauf, M., Olbrich, H., Kispert, A., King, S. M., Mitchison, H., et al. (2005). Identification and analysis of axonemal dynein light chain 1 in primary ciliary dyskinesia patients. *Am. J. Respir. Cell Mol. Biol.* 33, 41–47. doi: 10.1165/rcmb.2004-0335OC

Inaba, Y., Shinohara, K., Botilde, Y., Nabeshima, R., Takaoka, K., Ajima, R., et al. (2013). LRRC6 mutation causes primary ciliary dyskinesia with dynein arm defects. *PLoS One* 8:e59436. doi: 10.1371/journal.pone.0059436

Inaba, Y., Shinohara, K., Botilde, Y., Nabeshima, R., Takaoka, K., Ajima, R., et al. (2016). Transport of the outer dynein arm complex to cilia requires a cytoplasmic protein Lrrc6. *Genes Cells* 21, 728–739. doi: 10.1111/gtc.12380

Jacquet, B. V., Salinas-Mondragon, R., Liang, H., Therit, B., Buie, J. D., Dykstra, M., et al. (2009). FoxJ1-dependent gene expression is required for differentiation of radial glia into ependymal cells and a subset of astrocytes in the postnatal brain. *Development* 136, 4021–4031. doi: 10.1242/dev.041129

Jiménez, A. J., Domínguez-Pinos, M. D., Guerra, M. M., Fernández-Llebrez, P., and Pérez-Fígares, J. M. (2014). Structure and function of the ependymal barrier and diseases associated with ependyma disruption. *Tissue Barriers* 2:e28426. doi: 10.4161/tisb.28426

Johanson, C. E., Duncan, J. A. III, Klinge, P. M., Brinker, T., Stopa, E. G., and Silverberg, G. D. (2008). Multiplicity of cerebrospinal fluid functions: new challenges in health and disease. *Cerebrospinal Fluid Res.* 5:10. doi: 10.1186/1743-8454-5-10

Keryer, G., Pineda, J. R., Liot, G., Kim, J., Dietrich, P., Benstaali, C., et al. (2011). Ciliogenesis is regulated by a huntingtin-HAP1-PCM1 pathway and is altered in Huntington disease. *J. Clin. Invest.* 121, 4372–4382. doi: 10.1172/JCI57552

Kobayashi, Y., Watanabe, M., Okada, Y., Sawa, H., Takai, H., Nakanishi, M., et al. (2002). Hydrocephalus, situs inversus, chronic sinusitis, and male infertility in DNA polymerase lambda-deficient mice: possible implication for the pathogenesis of immotile cilia syndrome. *Mol. Cell. Biol.* 22, 2769–2776. doi: 10.1128/MCB.22.8.2769-2776.2002

Kott, E., Duquesnoy, P., Copin, B., Legendre, M., Dastot-Le Moal, F., Montantin, G., et al. (2012). Loss-of-function mutations in LRRC6, a gene essential for proper axonemal assembly of inner and outer dynein arms, cause primary ciliary dyskinesia. *Am. J. Hum. Genet.* 91, 958–964. doi: 10.1016/j.ajhg.2012.10.003

Kott, E., Legendre, M., Copin, B., Papon, J.-F., Dastot-Le Moal, F., Montantin, G., et al. (2013). Loss-of-function mutations in RSPH1 cause primary ciliary dyskinesia with central-complex and radial-spoke defects. *Am. J. Hum. Genet.* 93, 561–570. doi: 10.1016/j.ajhg.2013.07.013

Kumar, V., Umair, Z., Kumar, S., Goutam, R. S., Park, S., and Kim, J. (2021). The regulatory roles of motile cilia in CSF circulation and hydrocephalus. *Fluids Barriers CNS* 18:31. doi: 10.1186/s12987-021-00265-0

Kunimoto, K., Yamazaki, Y., Nishida, T., Shinohara, K., Ishikawa, H., Hasegawa, T., et al. (2012). Coordinated ciliary beating requires Odf2-mediated polarization of basal bodies via basal feet. *Cell* 148, 189–200. doi: 10.1016/j.cell.2011.10.052

Lee, L. (2013). Riding the wave of ependymal cilia: genetic susceptibility to hydrocephalus in primary ciliary dyskinesia. *J. Neurosci. Res.* 91, 1117–1132. doi: 10.1002/jnr.23238

Lee, L., Campagna, D. R., Pinkus, J. L., Mulhern, H., Wyatt, T. A., Sisson, J. H., et al. (2008). Primary ciliary dyskinesia in mice lacking the novel ciliary protein Pcdp1. *Mol. Cell. Biol.* 28, 949–957. doi: 10.1128/MCB.00354-07

Lewis, M., and Stracker, T. H. (2021). Transcriptional regulation of multiciliated cell differentiation. *Semin. Cell Dev. Biol.* 110, 51–60. doi: 10.1016/j.semcdb.2020.04.007

Liu, P., Choi, Y. K., and Qi, R. Z. (2014). NME7 is a functional component of the γ-tubulin ring complex. *Mol. Biol. Cell* 25, 2017–2025. doi: 10.1091/mbc.E13-06-0339

Lloyd, R. A., Butler, J. E., Gandevia, S. C., Ball, I. K., Toson, B., Stoodley, M. A., et al. (2020). Respiratory cerebrospinal fluid flow is driven by the thoracic and lumbar spinal pressures. *J. Physiol.* 598, 5789–5805. doi: 10.1113/JP279458

Loges, N. T., Olbrich, H., Becker-Heck, A., Häffner, K., Heer, A., Reinhard, C., et al. (2009). Deletions and point mutations of LRRC50 cause primary ciliary dyskinesia due to dynein arm defects. *Am. J. Hum. Genet.* 85, 883–889. doi: 10.1016/j.ajhg.2009.10.018

Mahuzier, A., Shihavuddin, A., Fournier, C., Lansade, P., Faucourt, M., Menezes, N., et al. (2018). Ependymal cilia beating induces an actin network to protect centrioles against shear stress. *Nat. Commun.* 9:2279. doi: 10.1038/s41467-018-04676-w

Marshall, W. F., and Nonaka, S. (2006). Cilia: tuning in to the cell's antenna. *Curr. Biol.* 16, R604–R614. doi: 10.1016/j.cub.2006.07.012

Mazor, M., Alkrinawi, S., Chalifa-Caspi, V., Manor, E., Sheffield, V. C., Aviram, M., et al. (2011). Primary ciliary dyskinesia caused by homozygous mutation in DNAL1, encoding dynein light chain 1. *Am. J. Hum. Genet.* 88, 599–607. doi: 10.1016/j.ajhg.2011.03.018

McKenzie, C. W., Craige, B., Kroeger, T. V., Finn, R., Wyatt, T. A., Sisson, J. H., et al. (2015). CFAP54 is required for proper ciliary motility and assembly of the central pair apparatus in mice. *Mol. Biol. Cell* 26, 3140–3149. doi: 10.1091/mbc.E15-02-0121

McKenzie, C. W., and Lee, L. (2020). Genetic interaction between central pair apparatus genes CFAP221, CFAP54, and SPEF2 in mouse models of primary ciliary dyskinesia. *Sci. Rep.* 10:12337. doi: 10.1038/s41598-020-69359-3

McKenzie, C. W., Preston, C. C., Finn, R., Eyster, K. M., Faustino, R. S., and Lee, L. (2018). Strain-specific differences in brain gene expression in a hydrocephalic mouse model with motile cilia dysfunction. *Sci. Rep.* 8:13370. doi: 10.1038/s41598-018-31743-5

Merveille, A.-C., Davis, E. E., Becker-Heck, A., Legendre, M., Amirav, I., Bataille, G., et al. (2011). CCDC39 is required for assembly of inner dynein arms and the dynein regulatory complex and for normal ciliary motility in humans and dogs. *Nat. Genet.* 43, 72–78. doi: 10.1038/ng.726

Mirzadeh, Z., Han, Y.-G., Soriano-Navarro, M., García-Verdugo, J. M., and Alvarez-Buylla, A. (2010). Cilia organize ependymal planar polarity. *J. Neurosci.* 30, 2600–2610. doi: 10.1523/JNEUROSCI.3744-09.2010

Mitchison, H. M., Schmidts, M., Loges, N. T., Freshour, J., Dritsoula, A., Hirst, R. A., et al. (2012). Mutations in axonemal dynein assembly factor DNAAF3 cause primary ciliary dyskinesia. *Nat. Genet.* 44, s1–s2. doi: 10.1038/ng.1106

Mitchison, H. M., and Valente, E. M. (2017). Motile and non-motile cilia in human pathology: from function to phenotypes. *J. Pathol.* 241, 294–309.

Moore, D. J., Onoufriadis, A., Shoemark, A., Simpson, M. A., Zur Lage, P. I., de Castro, S. C., et al. (2013). Mutations in ZMYND10, a gene essential for proper axonemal assembly of inner and outer dynein arms in humans and flies, cause primary ciliary dyskinesia. *Am. J. Hum. Genet.* 93, 346–356. doi: 10.1016/j.ajhg.2013.07.009

Mulroy, E., Latorre, A., Magrinelli, F., and Bhatia, K. P. (2020). Ciliary dysfunction: the hairy explanation of normal pressure hydrocephalus? *Mov. Disord. Clin. Pract.* 7, 30–31. doi: 10.1002/mdc3.12880

Muniz-Talavera, H., and Schmidt, J. V. (2017). The mouse Jhy gene regulates ependymal cell differentiation and ciliogenesis. *PLoS One* 12:e0184957. doi: 10.1371/journal.pone.0184957

Ohata, S., Nakatani, J., Herranz-Pérez, V., Cheng, J., Belinson, H., Inubushi, T., et al. (2014). Loss of Dishevelleds disrupts planar polarity in ependymal motile cilia and results in hydrocephalus. *Neuron* 83, 558–571. doi: 10.1016/j.neuron.2014.06.022

Omiya, H., Yamaguchi, S., Watanabe, T., Kuniya, T., Harada, Y., Kawaguchi, D., et al. (2021). BMP signaling suppresses Gemc1 expression and ependymal differentiation of mouse telencephalic progenitors. *Sci. Rep.* 11:613. doi: 10.1038/s41598-020-79610-6

Omran, H., Kobayashi, D., Olbrich, H., Tsukahara, T., Loges, N. T., Hagiwara, H., et al. (2008). Ktu/PF13 is required for cytoplasmic pre-assembly of axonemal dyneins. *Nature* 456, 611–616. doi: 10.1038/nature07471

Ringers, C., Olstad, E. W., and Jurisch-Yaksi, N. (2020). The role of motile cilia in the development and physiology of the nervous system. *Philos. Trans. R. Soc. Lond. B Biol. Sci.* 375:20190156.

Rocca, M. S., Piatti, G., Michelucci, A., Guazzo, R., Bertini, V., Vinanzi, C., et al. (2008). DNAI2 mutations cause primary ciliary dyskinesia with defects in the outer dynein arm. *Am. J. Hum. Genet.* 83, 547–558.

Rocca, M. S., Piatti, G., Michelucci, A., Guazzo, R., Bertini, V., Vinanzi, C., et al. (2020). A novel genetic variant in DNAI2 detected by custom gene panel in a newborn with primary ciliary dyskinesia: case report. *BMC Med. Genet.* 21:220. doi: 10.1186/s12881-020-01160-5

Ryu, H., Lee, H., Lee, J., Noh, H., Shin, M., Kumar, V., et al. (2021). The molecular dynamics of subdistal appendages in multi-ciliated cells. *Nat. Commun.* 12:612. doi: 10.1038/s41467-021-20902-4

Sasaki, K., Shiba, K., Nakamura, A., Kawano, N., Satouh, Y., Yamaguchi, H., et al. (2019). Calaxin is required for cilia-driven determination of vertebrate laterality. *Commun. Biol.* 2:226.

Saternos, H. C., and AbouAlaiwi, W. A. (2019). Commentary: alcohol consumption impairs the ependymal cilia motility in the brain ventricles. *J. Neurol. Neuromedicine* 4, 20–21. doi: 10.29245/2572.942X/2019/2.1250

Sawamoto, K., Wichterle, H., Gonzalez-Perez, O., Cholfin, J. A., Yamada, M., Spassky, N., et al. (2006). New neurons follow the flow of cerebrospinal fluid in the adult brain. *Science* 311, 629–632.

Šedová, L., Buková, I., Bažantová, P., Petrezsélyová, S., Prochazka, J., Školníková, E., et al. (2021). Semi-lethal primary ciliary dyskinesia in rats lacking the Nme7 gene. *Int. J. Mol. Sci.* 22:3810. doi: 10.3390/ijms22083810

Shim, J. W., Territo, P. R., Simpson, S., Watson, J. C., Jiang, L., Riley, A. A., et al. (2019). Hydrocephalus in a rat model of Meckel Gruber syndrome with a TMEM67 mutation. *Sci. Rep.* 9:1069. doi: 10.1038/s41598-018-37620-5

Takagishi, M., Sawada, M., Ohata, S., Asai, N., Enomoto, A., Takahashi, K., et al. (2017). Daple coordinates planar polarized microtubule dynamics in ependymal cells and contributes to hydrocephalus. *Cell Rep.* 20, 960–972. doi: 10.1016/j.celrep.2017.06.089

Tan, C., Wang, X., Wang, Y., Wang, C., Tang, Z., Zhang, Z., et al. (2021). The pathogenesis based on the glymphatic system, diagnosis, and treatment of idiopathic normal pressure hydrocephalus. *Clin. Interv. Aging* 16, 139–153. doi: 10.2147/CIA.S290709

Tissir, F., Qu, Y., Montcouquiol, M., Zhou, L., Komatsu, K., Shi, D., et al. (2010). Lack of cadherins Celsr2 and Celsr3 impairs ependymal ciliogenesis, leading to fatal hydrocephalus. *Nat. Neurosci.* 13, 700–707. doi: 10.1038/nn.2555

Núnez-Ollé, M. N., Jung, C., Terré, B., Balsiger, N. A., Plata, C., Roset, R., et al. (2017). Constitutive Cyclin O deficiency results in penetrant hydrocephalus, impaired growth and infertility. *Oncotarget* 8, 99261–99273. doi: 10.18632/oncotarget.21818

Vidovic, D., Davila, R. A., Gronostajski, R. M., Harvey, T. J., and Piper, M. (2018). Transcriptional regulation of ependymal cell maturation within the postnatal brain. *Neural Dev.* 13:2.

Wallingford, J. B. (2010). Planar cell polarity signaling, cilia and polarized ciliary beating. *Curr. Opin. Cell Biol.* 22, 597–604.

Wallmeier, J., Al-Mutairi, D. A., Chen, C.-T., Loges, N. T., Pennekamp, P., Menchen, T., et al. (2014). Mutations in CCNO result in congenital mucociliary clearance disorder with reduced generation of multiple motile cilia. *Nat. Genet.* 46, 646–651. doi: 10.1038/ng.2961

Wang, C., Wang, X., Tan, C., Wang, Y., Tang, Z., Zhang, Z., et al. (2021). Novel therapeutics for hydrocephalus: insights from animal models. *CNS Neurosci. Ther.* 27, 1012–1022.

Wildung, M., Esser, T. U., Grausam, K. B., Wiedwald, C., Volceanov-Hahn, L., Riedel, D., et al. (2019). Transcription factor TAp73 and microRNA-449 complement each other to support multiciliogenesis. *Cell Death Differ.* 26, 2740–2757. doi: 10.1038/s41418-019-0332-7

Williamson, M. R., Wilkinson, C. M., Dietrich, K., and Colbourne, F. Acetazolamide mitigates intracranial pressure spikes without affecting

functional outcome after experimental hemorrhagic stroke. *Transl. Stroke Res.* 10, 428–439. doi: 10.1007/s12975-018-0663-6

Wu, K.-Y., Tang, F.-L., Lee, D., Zhao, Y., Song, H., Zhu, X.-J., et al. (2020). Ependymal Vps35 promotes ependymal cell differentiation and survival, suppresses microglial activation, and prevents neonatal hydrocephalus. *J. Neurosci.* 40, 3862–3879. doi: 10.1523/JNEUROSCI.1520-19.2020

Xiao, G., Chen, Q., and Zhang, X. (2021). MicroRNA-455-5p/CPEB1 pathway mediates Aβ-related learning and memory deficits in a mouse model of Alzheimer's disease. *Brain Res. Bull.* 177, 282–294. doi: 10.1016/j.brainresbull.2021.10.008

Xiong, G., Elkind, J. A., Kundu, S., Smith, C. J., Antunes, M. B., Tamashiro, E., et al. (2014). Traumatic brain injury-induced ependymal ciliary loss decreases cerebral spinal fluid flow. *J. Neurotrauma* 31, 1396–1404. doi: 10.1089/neu.2013.3110

Yamada, S., Ishikawa, M., and Nozaki, K. (2021). Exploring mechanisms of ventricular enlargement in idiopathic normal pressure hydrocephalus: a role of cerebrospinal fluid dynamics and motile cilia. *Fluids Barriers CNS* 18:20. doi: 10.1186/s12987-021-00243-6

Yang, H. W., Lee, S., Yang, D., Dai, H., Zhang, Y., Han, L., et al. (2021). Deletions in CWH43 cause idiopathic normal pressure hydrocephalus. *EMBO Mol. Med.* 13:e13249.

Zahr, N. M., Mayer, D., Rohlfing, T., Hsu, O., Vinco, S., Orduna, J., et al. (2014). Rat strain differences in brain structure and neurochemistry in response to binge alcohol. *Psychopharmacology* 231, 429–445. doi: 10.1007/s00213-013-3253-z

Zariwala, M., O'Neal, W. K., Noone, P. G., Leigh, M. W., Knowles, M. R., and Ostrowski, L. E. (2004). Investigation of the possible role of a novel gene, DPCD, in primary ciliary dyskinesia. *Am. J. Respir. Cell Mol. Biol.* 30, 428–434. doi: 10.1165/rcmb.2003-0338RC

Zariwala, M. A., Gee, H. Y., Kurkowiak, M., Al-Mutairi, D. A., Leigh, M. W., Hurd, T. W., et al. (2013). ZMYND10 is mutated in primary ciliary dyskinesia and interacts with LRRC6. *Am. J. Hum. Genet.* 93, 336–345.

Zariwala, M. A., Leigh, M. W., Ceppa, F., Kennedy, M. P., Noone, P. G., Carson, J. L., et al. (2006). Mutations of DNAI1 in primary ciliary dyskinesia: evidence of founder effect in a common mutation. *Am. J. Respir. Crit. Care Med.* 174, 858–866. doi: 10.1164/rccm.200603-370OC

Zhan, C., Xiao, G., Zhang, X., Chen, X., Zhang, Z., Liu, J., et al. (2020). Decreased MiR-30a promotes TGF-β1-mediated arachnoid fibrosis in post-hemorrhagic hydrocephalus. *Transl. Neurosci.* 11, 60–74. doi: 10.1515/tnsci-2020-0010

Zhang, J., Chandrasekaran, G., Li, W., Kim, D.-Y., Jeong, I. Y., Lee, S.-H., et al. (2020). Wnt-PLC-IP(3)-Connexin-Ca(2+) axis maintains ependymal motile cilia in zebrafish spinal cord. *Nat. Commun.* 11:1860. doi: 10.1038/s41467-020-15248-2

Zhang, J. X., Shi, X. Y., Tang, Z. X., Sun, H., Shen, Z., and Wan, S. (2020). Acute communicating hydrocephalus caused by extravasation of digital subtraction angiography contrast medium: a case report and literature review. *J. Int. Med. Res.* 48:300060520945504. doi: 10.1177/0300060520945504

Ziêtkiewicz, E., Bukowy-Bieryłło, Z., Voelkel, K., Klimek, B., Dmeńska, H., Pogorzelski, A., et al. (2012). Mutations in radial spoke head genes and ultrastructural cilia defects in East-European cohort of primary ciliary dyskinesia patients. *PLoS One* 7:e33667. doi: 10.1371/journal.pone.0033667

Ziêtkiewicz, E., Nitka, B., Voelkel, K., Skrzypczak, U., Bukowy, Z., Rutkiewicz, E., et al. (2010). Population specificity of the DNAI1 gene mutation spectrum in primary ciliary dyskinesia (PCD). *Respir. Res.* 11:174. doi: 10.1186/1465-9921-11-174

Zou, W., Lv, Y., Liu, Z. I., Xia, P., Li, H., and Jiao, J. (2020). Loss of Rsph9 causes neonatal hydrocephalus with abnormal development of motile cilia in mice. *Sci. Rep.* 10:12435. doi: 10.1038/s41598-020-69447-4

Conflict of Interest: The authors declare that the research was conducted in the absence of any commercial or financial relationships that could be construed as a potential conflict of interest.

Publisher's Note: All claims expressed in this article are solely those of the authors and do not necessarily represent those of their affiliated organizations, or those of the publisher, the editors and the reviewers. Any product that may be evaluated in this article, or claim that may be made by its manufacturer, is not guaranteed or endorsed by the publisher.

frontiers | Frontiers in Molecular Neuroscience

ORIGINAL RESEARCH
published: 12 July 2022
doi: 10.3389/fnmol.2022.900057

A New Perspective on the Pathophysiology of Idiopathic Intracranial Hypertension: Role of the Glia-Neuro-Vascular Interface

Per Kristian Eide[1,2*] *and Hans-Arne Hansson*[3]

[1] *Department of Neurosurgery, Oslo University Hospital—Rikshospitalet, Oslo, Norway,* [2] *Institute of Clinical Medicine, Faculty of Medicine, University of Oslo, Oslo, Norway,* [3] *Institute of Biomedicine, University of Gothenburg, Göteborg, Sweden*

Idiopathic intracranial hypertension (IIH) is a neurological disease characterized by symptoms and signs of increased intracranial pressure (ICP) of unknown cause. Most attention has been given to the role of cerebrospinal fluid (CSF) disturbance and intracranial venous hypertension caused by sinus vein stenosis. We previously proposed that key pathophysiological processes take place within the brain at the glia-neuro-vascular interface. However, the relative importance of the proposed mechanisms in IIH disease remains unknown. Modern treatment regimens aim to reduce intracranial CSF and venous pressures, but a substantial proportion of patients experience lasting complaints. In 2010, the first author established a database for the prospective collection of information from individuals being assessed for IIH. The database incorporates clinical, imaging, physiological, and biological data, and information about treatment/outcome. This study retrieved information from the database, asking the following research questions: In IIH subjects responding to shunt surgery, what is the occurrence of signs of CSF disturbance, sinus vein stenosis, intracranial hypertension, and microscopic evidence of structural abnormalities at the glia-neuro-vascular interface? Secondarily, do semi-quantitative measures of abnormal ultrastructure at the glia-neurovascular differ between subjects with definite IIH and non-IIH (reference) subjects? The study included 13 patients with IIH who fulfilled the diagnostic criteria and who improved following shunt surgery, i.e., patients with definite IIH. Comparisons were done regarding magnetic resonance imaging (MRI) findings, pulsatile and static ICP scores, and immune-histochemistry microscopy. Among these 13 IIH subjects, 6/13 (46%) of patients presented with magnetic resonance imaging (MRI) signs of CSF disturbance (empty sella and/or distended perioptic subarachnoid spaces), 0/13 (0%) of patients with IIH had MRI signs of sinus vein stenosis, 13/13 (100%) of patients with IIH presented with abnormal preoperative pulsatile ICP [overnight mean ICP wave amplitude (MWA) above thresholds], 3/13 (23%) patients showed abnormal static ICP (overnight mean ICP above threshold), and 12/13 (92%) of patients with IIH showed abnormal structural changes at the glia-neuro-vascular interface. Comparisons of semi-quantitative structural variables between

OPEN ACCESS

Edited by:
Adjanie Patabendige,
Edge Hill University, United Kingdom

Reviewed by:
Erdem Tüzün,
Istanbul University, Turkey
Brian John Sweeney,
Cork University Hospital, Ireland

***Correspondence:**
Per Kristian Eide
p.k.eide@medisin.uio.no

Specialty section:
This article was submitted to Brain Disease Mechanisms, a section of the journal Frontiers in Molecular Neuroscience

Received: *19 March 2022*
Accepted: *07 June 2022*
Published: *12 July 2022*

Citation:
Eide PK and Hansson H-A (2022) A New Perspective on the Pathophysiology of Idiopathic Intracranial Hypertension: Role of the Glia-Neuro-Vascular Interface. Front. Mol. Neurosci. 15:900057. doi: 10.3389/fnmol.2022.900057

IIH and aged- and gender-matched reference (REF) subjects showed IIH abnormalities in glial cells, neurons, and capillaries. The present data suggest a key role of disease processes affecting the glia-neuro-vascular interface.

Keywords: idiopathic intracranial hypertension, pseudotumor cerebri, benign intracranial hypertension, pathophysiology, intracranial pressure, astrocytes, capillaries

INTRODUCTION

Idiopathic intracranial hypertension (IIH), also denoted pseudotumor cerebri (PTC) or benign intracranial hypertension (BIH), is a neurological disease characterized by symptoms and signs indicative of increased intracranial pressure (ICP), including headache, impaired vision, diplopia, and visual field findings of papilledema and reduced visual field, as well as dizziness, tinnitus, and fatigue (Ball and Clarke, 2006; Mollan et al., 2016). The prevalence of the disease is highest in fertile women who are overweight but may as well occur in children, normal-weight adults, and in men. Severe consequences are lasting visual impairment and blindness, and substantial negative effects on the quality of life. It is well-documented that the disease represents a great burden to those affected (Kleinschmidt et al., 2000). Patients with IIH are usually young and experience impaired occupational capacity which, also results in increased costs to society (Friesner et al., 2011). The occurrence of the disease is on the rise, probably related to the increasing weight in the population of the Western world (Kesler and Gadoth, 2001; Curry et al., 2005; Raoof et al., 2011; Kesler et al., 2014).

The pathophysiology of IIH is unknown (Mollan et al., 2016). Traditionally, most attention has been given to the role of cerebrospinal fluid (CSF) circulation failure, though the role of increased cerebral venous pressure caused by sinus vein obstruction has attracted interest more recently (Mollan et al., 2018). The current treatment options do not target the cause of disease, but focus on reducing ICP: Weight decline reduces abdominal pressure and thereby central venous pressure that may secondarily reduce ICP. Medications, e.g., acetazolamide and topiramate, reduce CSF production and CSF diversion surgery (shunt surgery) reduces CSF pressure by establishing an alternative route for CSF efflux. Given radiological evidence of sinus vein stenosis, stenting of dural veins, which lowers ICP by reducing back pressure caused by increased intracranial vein pressure proximal to the stenosis, has provided successful outcomes (Albuquerque et al., 2011; Kalyvas et al., 2020).

However, despite the best available treatments, a substantial proportion of the patients with IIH have lasting symptoms, a particularly disabling headache that extensively affects daily life (Friedman et al., 2017; Burkett and Ailani, 2018). Even mortality risk is increased in IIH (Hermes et al., 2020). One previous study estimated that annual costs for IIH in the USA in 2007 were 444 million USD, primarily related to frequent hospital admissions, unsatisfactory treatment options, and lost productivity (Friesner et al., 2011). The costs probably increase as weight is increasing in the population (Mollan et al., 2019). A 2015 Cochrane review concluded that there is a lack of evidence to guide medical or interventional treatment of IIH (Piper et al., 2015). Accordingly, there is a great need for a deeper knowledge of the pathophysiology of IIH for health care personnel to provide disease-specific treatment.

The first author since 2010 established a database (Neurovascular-Cerebrospinal fluid Quality registry, reg. no 2011/6692) that includes consecutive and prospective patients examined for IIH, as well as other patients with neurovascular and/or CSF disturbances. The database incorporates information from clinical management (clinical information, management data, and ICP measurements) and information obtained as part of research (analysis of brain biopsy specimens, intrathecal contrast-enhanced MRI assessing the glymphatic function).

The present study asked which of the variables indicative of IIH pathophysiology are most prevalent in IIH subjects who respond to CSF diversion surgery; specifically what is the occurrence of signs of CSF disturbance, sinus vein stenosis, intracranial hypertension, and ultrastructural abnormalities at the glia-neuro-vascular interface in patients with IIH? The main components of this anatomical location are glial cells (astrocytes and microglia), neurons pericytes, and, capillaries (**Figure 1**). This entity is also denoted as the neurovascular unit or coupling. Secondarily, a semi-quantitative measure of ultrastructural change was compared with a reference group from the same database. Study variables were retrieved from the already established database.

MATERIALS AND METHODS

Database, Approvals, and Study Design

Since 2010, the Neurovascular-Cerebrospinal fluid quality control database has enrolled patients with neurovascular and CSF disturbances, including patients with IIH. The database has been approved by the Institutional Data Protection Official at Oslo university hospital (approval no. 2011/6692). The registry of patients with IIH stores prospectively collected information about the clinical status (preoperative symptoms and outcome results), imaging findings, overnight ICP scores, and results of

Abbreviations: A, astrocyte; AQP4, aquaporin-4; BBB, blood-brain-barrier; BIH, benign intracranial hypertension; BM, basement membrane; BMI, body mass index; CD68, Cluster of differentiation 68; CSF, cerebrospinal fluid; CRP, C-reactive protein; EC, endothelial cell; EF, endfoot; ER, endoplasmic reticulum; GFAP, glial fibrillary acidic protein; ICP, intracranial pressure; IIH, Idiopathic intracranial hypertension; IL, interleukin; iNPH: idiopathic normal pressure hydrocephalus; LM, light microscopy; LP, lumboperitoneal; M, mitochondria; MERC, mitochondria-endoplasmic reticulum contact; MRI, magnetic resonance imaging; MWA, mean ICP wave amplitude; N, neuron; NF-H, neurofilament-heavy; P, pericytes; Pp, pericyte process; PSD, postsynaptic density; PTC, pseudo-tumor cerebri; REF, reference; TEM, transmission electron microscopy, TNF, tumor necrosis factor; VP, ventriculoperitoneal.

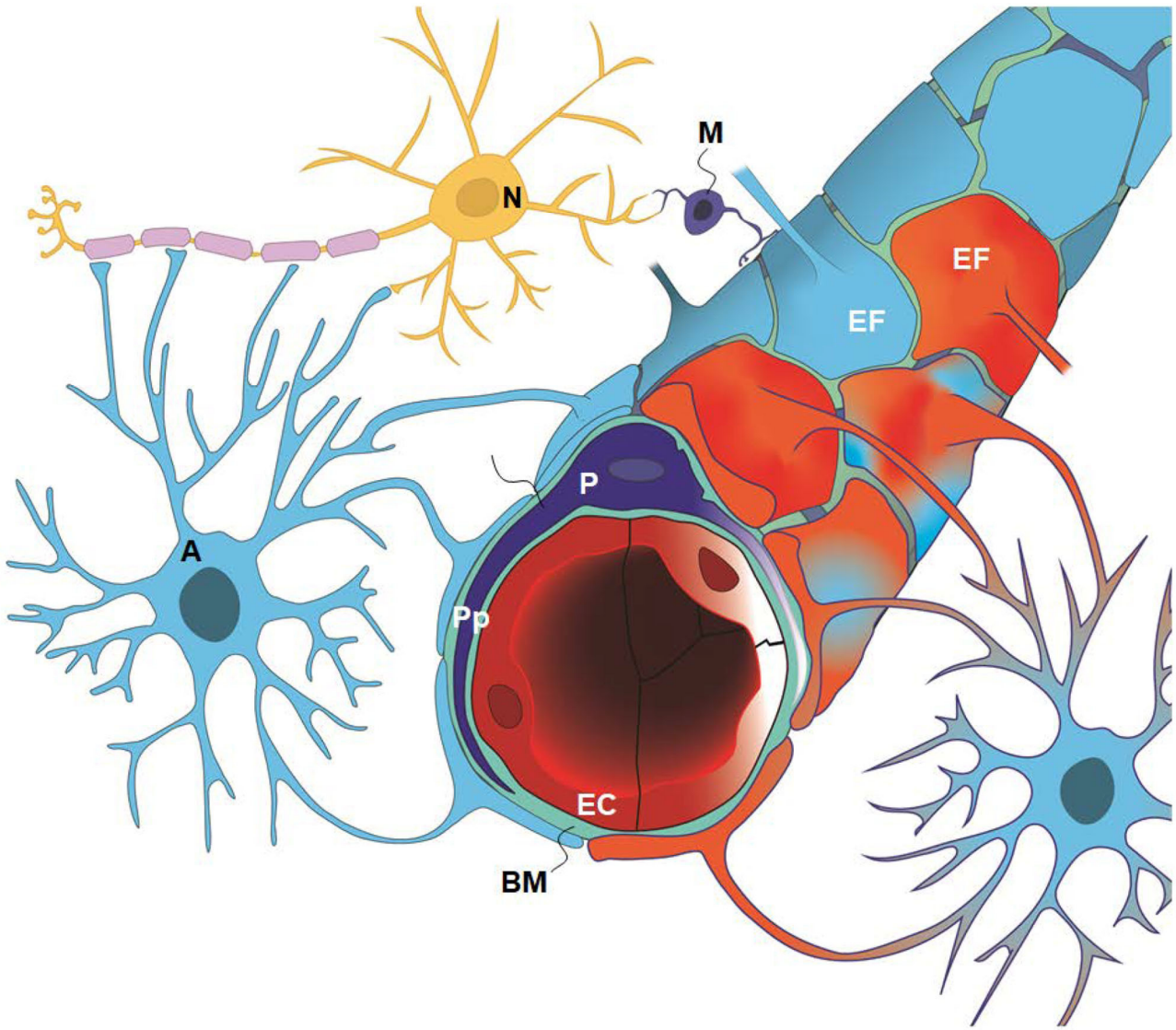

FIGURE 1 | The glia-neuro-vascular interface (also denoted the glia-neuro-vascular unit/coupling) incorporates the capillary wherein its circumference consists of endothelial cells (ECs) having tight junctions and pericytes (P) with processes (Pp). The relationship between the endothelial cells and pericytes in humans is 1:1–3:1, decreasing with age and in diseases. The basement membrane (BM) is a loose matrix between endothelial cells (ECs) and pericytes (Ps) and the astrocytic end-feet (EF). The astrocytic end-feet processes create a donut shaped structure enclosing the basement membrane (BM). There are inter-end-feet-gaps between the endfoot (EF) processes enabling passage of molecules to the interstitial tissue. Normal end-feet (EF) are indicated in blue to the left while pathological end-feet (EF) in red color to the right. Other components are the astrocytes (A), neurons (N) and microglia (M). In IIH, there is patchy astrogliosis, causing changes to the normal configuration of astrocytes. Moreover, there is loss of integrity of the BBB with degeneration of basement membrane and pericyte processes, and BBB leakage of the blood proteins fibrinogen and fibrin. Extra-vascular fibrin(ogen) is not demonstrable in normal adult brains and is prominently pro-inflammatory. Our present disclosure of blood-brain-dysfunction in IIH subjects indicates that the glia-neuro-vascular unit is likely associated with the pathogenesis of the disease. Illustration: Ine Eriksen, University of Oslo.

ultrastructural analyses from cortical brain biopsies. The clinical information, overnight ICP recordings, and imaging data were included in the registry as part of routine clinical work-up in patients with IIH prior to shunt surgery. The morphological information about alterations at the glia-neuro-vascular interface was obtained as part of a research project approved by The Regional Committee for Medical and Health Research Ethics of Health Region South-East, Norway (Approvals no. REK 2009/2060, 2012/1157, and 2011/2306) and by Oslo University Hospital (Approvals no. 10/6806 and 2011/19311). The study was performed by the ethical standards as laid down in the 1964 Declaration of Helsinki and its later amendments, and patients were included after oral and written informed consent.

The design of the present study was to compare different variables addressing the pathophysiology of IIH, particularly measures of CSF disturbance, sinus vein stenosis, intracranial

hypertension, and structural abnormalities from brain biopsy specimens. Data were retrieved from the prospectively collected database.

The primary research question was: In IIH subjects responding to shunt surgery, what is the occurrence of signs of CSF disturbance, sinus vein stenosis, intracranial hypertension, and microscopic evidence of structural changes at the glia-neuro-vascular interface?

The secondary research question was: Do semi-quantitative measures of abnormal ultrastructure at the glia-neurovascular differ between subjects with definite IIH and non-IIH (reference; REF) subjects, the latter individuals being matched with IIH subjects according to gender and age.

Inclusion criteria: (1) The patients with IIH included in the study fulfilled the IIH diagnostic criteria and had a definite clinical response to shunt surgery (i.e., improvement of visual function and at least partial improvement of headache). (2) The non-IIH (Reference; REF) subjects retrieved from the database were closest in age and gender to the IIH subjects. (3) This study was limited to IIH and REF subjects in the database who had analysis results of ultrastructural examinations and overnight preoperative ICP scores.

Variables Retrieved From the Database

Demographic and Clinical Data

The demographic and clinical data retrieved from the database were age, gender, body mass index (BMI), preoperative symptoms, and management/outcome data. Moreover, they had undergone the routine management in this department, which is primarily placement of a ventriculoperitoneal (VP), or secondarily a lumboperitoneal (LP) shunt. For VP shunt, we apply HAKIM^{TM} Programmable Valve Shunt System (Codman & Shurtleff, Inc., Medos S.A. Rue Girardet 29, CH 2400 Le Locle, Switzerland), and for LP shunt we use an Orbis-Sigma Valve II shunt (Integra Inc, Plainsboro, NJ, USA).

The REF subjects closest in age to the patients with IIH were also retrieved from the Neurovascular-Cerebrospinal fluid database to compare ultrastructure at the glia-neuro-vascular interface. The database includes results from analysis of apparently normal brain tissue from individuals undergoing planned brain surgery in whom removal of normal brain tissue is required as part of treatment. This includes brain tissue resection for epilepsy, brain tissue resection during elective clipping of cerebral aneurysm (no prior bleeds) in whom minor tissue resection was required during the clipping procedure, and brain tissue from patients undergoing tissue resection for parenchymal brain tumors.

Imaging Signs of CSF Disturbance

The MRI biomarkers of CSF disturbance retrieved from the database included the presence of empty sella (**Figure 2A**) and distension of the perioptic subarachnoid spaces (**Figure 2B**).

Imaging Signs of Sinus Vein Stenosis

Imaging data about signs of sinus vein stenosis retrieved from the database included MRI with venography (**Figures 2C–F**). This hospital has no routine for venous pressure recordings or measurements of pressure gradients over a suspected sinus vein stenosis. Therefore, MRI/MRI venography was utilized for visualization of sinus vein stenosis and signs of intracranial venous hypertension.

Continuous Overnight ICP Measurements

Results of overnight ICP monitoring retrieved from the database included an overnight average of pulsatile ICP (mean ICP wave amplitude; MWA), a percentage of MWA $>$ 5 mmHg, and an average of static ICP (mean ICP), and a percentage of mean ICP $>$ 15 mmHg.

The procedure of ICP monitoring has been described before (Eide and Kerty, 2011). In short, an ICP sensor (Codman MicroSensor^{TM}, Johnson & Johnson, Raynham, MA, USA) was introduced 1–2 cm into the frontal cortex parenchyma in local anesthesia *via* a skin incision frontally on the right side, a small burr hole, and a minor opening in the dura. In the present IIH patients, overnight ICP monitoring had been performed as previously described (Eide and Kerty, 2011), utilizing a computerized software (Sensometrics software, dPCom, Oslo). The ICP signals were sampled at 200 Hz, providing an online analysis of the pulsatile ICP as mean ICP wave amplitude (MWA), and the static ICP (mean ICP) every consecutive 6-s time window (**Figure 3**). The software provides online trend plots and average values of the ICP scores. In general, as an indication for shunt surgery, the department's routine is the use of results of diagnostic ICP monitoring in addition to the patient history, clinical and neuro-ophthalmological findings, and imaging findings. Regarding ICP thresholds, we have defined abnormal static ICP as the average mean ICP during over-night monitoring being $>$15 mmHg (Eide and Kerty, 2011) or $>$15 mmHg in $>$50% of recording time, and abnormal pulsatile ICP during over-night monitoring as average MWA $>$ 4 mmHg and/or MWA $>$ 5 mmHg in $>$10% of recording time (Eide and Sorteberg, 2010; Eide and Kerty, 2011).

Ultrastructural Examinations of Brain Biopsy Samples

The results from histopathological analyses of brain tissue specimens from IIH and REF subjects retrieved from the database specifically addressed changes in the cell types constituting the glia-neuro-vascular interface: Glial cells, AQP4 expression at astrocytic end-feet, neurons, pericytes, basement membrane, and BBB integrity.

We described previously the surgical procedure of obtaining a brain biopsy (Eide et al., 2016). In short, a minor opening was made in the dura and a biopsy (0.9 $\times$ 10 mm) aspirated through a disposable Nashold Biopsy Needle (Integra Radionics, Burlington, MA, USA), introduced immediately below the cortical surface. This biopsy procedure provides for atraumatic and standardized biopsy sections. The brain biopsies were prepared for both light microscopy (LM) and transmission electron microscopy (TEM). The cortical biopsy was obtained at the same site where the ICP sensor or ventricular catheter was introduced.

The technical procedures concerning the handling of the brain biopsies and analysis of ultrastructure at the glia-neuro-vascular

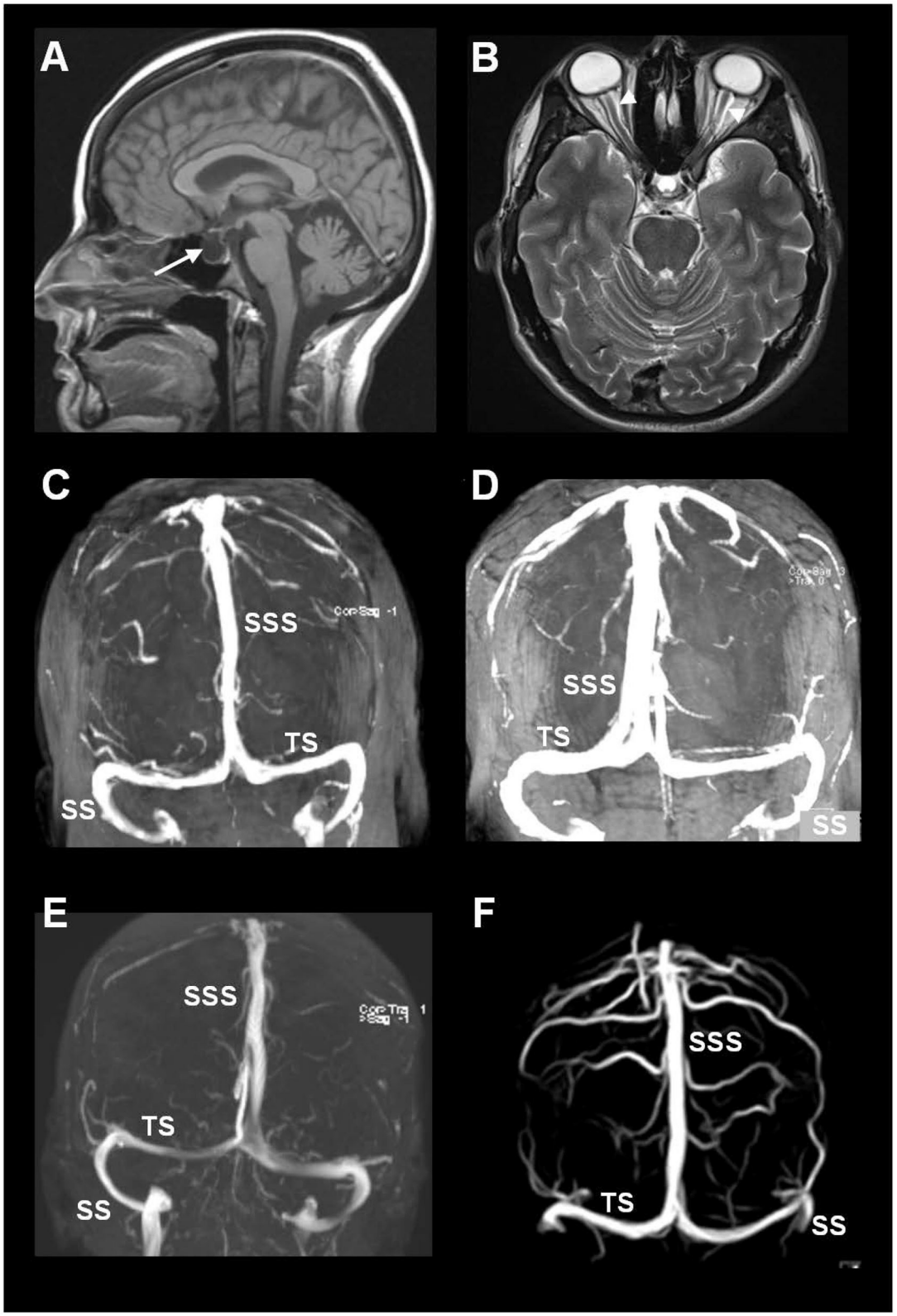

FIGURE 2 | MRI biomarkers indicative of CSF disturbance in IIH include the presence of **(A)** empty sella (arrow) and **(B)** distension of the perioptic subarachnoid spaces (arrowheads). **(C–F)** Sinus vein stenosis was assessed using MRI venography, here illustrated by MRI venography from four of the included patients with IIH. The image shows the transverse sinus (TS), sigmoid sinus (SS), and the superior sagittal sinus (SSS).

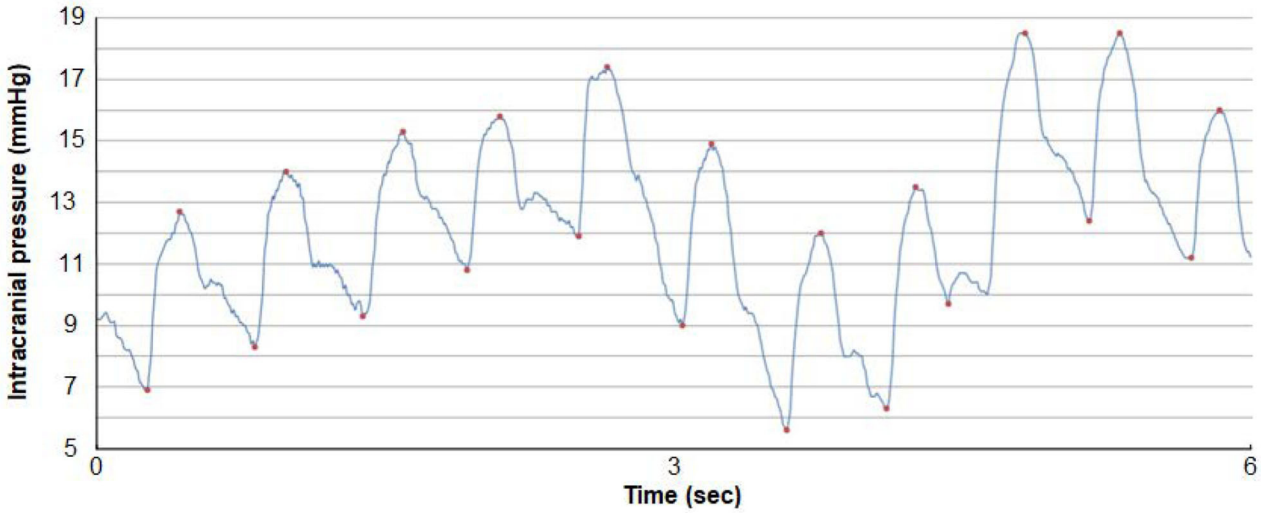

FIGURE 3 | A continuous ICP signal measured from an ICP sensor placed in the frontal parenchyma of an individual with IIH. The level of ICP is shown on the y-axis and time on the x-axis. Both the pulsatile and static ICP are derived from the same ICP signal. The pulsatile ICP is described as the Mean Wave Amplitude (MWA) that refers to the pressure changes occurring during the cardiac cycle, that is, the increase in pressure from diastolic minimum pressure to systolic maximum pressure (here illustrated by the red dots). The mean ICP refers to the static ICP, that is, the absolute pressure measured against a reference pressure. The MWA and the mean ICP are determined over consecutive 6-s time windows; here mean ICP is 12.2 mmHg and MWA 6.4 mmHg. Image: Sensometrics Analytics, dPCom, Oslo, Norway.

interface have previously been described in detail (Eide et al., 2016, 2021a; Eidsvaag et al., 2018; Hasan-Olive et al., 2019c).

Light Microscopy

The technical procedures for handling, processing, and analysis of brain tissue for LM have been described before (Eide et al., 2016; Hasan-Olive et al., 2019c). The tissue specimens comprising the superficial three cortical layers (Layers 1–3) were fixed in buffered 4% paraformaldehyde for 2 days in the cold, dehydrated, and embedded in paraffin. Tissue blocks were sectioned at a thickness of 6 μm. After deparaffinization and rehydration, the sections were immersed in aqueous hydrogen peroxide for about 10 min to quench endogenous peroxidase activity. Antigen retrieval was done by immersion in proteinase K working solution for 10 min at pH 8.0; the subsequent blocking was achieved with normal horse serum before incubation overnight with the primary antibody at 4°C. After rinsing, a biotinylated antibody was applied overnight at 4°C (Vectastain Universal Elite Kit; Vector Labs. Inc., Burlingame, CA, USA), followed by an avidin-biotin complex. Visualization was obtained with a 3,3′-diaminobezidine peroxidase substrate kit (Vector). The sections were counterstained with hematoxylin and examined by LM after mounting and being cover-glassed.

Astrocytes were identified by their expression of the anti-gliofibrillary acidic protein (GFAP) and aquaporin-4 (AQP4), activated inflammatory cells (microglia) by the antibody Cluster of Differentiation 68 (CD68), nerve cell damage by the antibody neurofilament heavy (NF-H), and extravasated fibrin(ogen) was detected by an antibody revealing both fibrinogen and fibrin (polyclonal, 1:400, Dako, A0080) as a measure of BBB dysfunction. The following primary antibodies were used: anti-gliofibrillary acidic protein (GFAP; 1:3000, mouse monoclonal clone GA5, Sigma); anti-AQP4 (polyclonal produced in rabbit against a recombinant protein tag, 1:1000, Sigma); anti-neurofilament heavy (NF-H, monoclonal against phosphorylated and non-phosphorylated neurofilaments, clone N52,1:500, Sigma); anti-CD68 (monoclonal clone KP1, 1:200;DAKO); and anti-fibrin(ogen) (polyclonal, 1:400, A0080, Dako A/S, Glostrup, Denmark). Reference sections had been processed in parallel, and the specificity of the immunohistochemical reaction was checked by the omission of the primary antibody.

Glial cells were examined for the presence of astrogliosis, astrocyte hypertrophy, and loss of astrocyte domains (**Figures 4–6**). Furthermore, the expression of AQP4 perivascular, as well as in neuropil, was determined (**Figure 7**). Semi-quantification of AQP4 expression was done using densitometry analysis that provides an estimate of transmitted light, expressed as anarbitrary units (**Figure 8**). Lower arbitrary units imply increased AQP4 expression. Nerve cell bodies could be disclosed to be extensively delimited by astrocyte membranes with high AQP4IR (**Figure 7**).

Morphometry was done to determine the percentage area of either GFAP or CD68 immunoreactivity (3 areas per biopsy specimen, 273 × 410 μm), utilizing a Nikon Eclipse Ni microscope, a DS-Ri2 camera, and NIS element B.V4.3 program (Nikon, Tokyo, Japan), and a Leica QWin Pro system (Leica Biosystems GmbH, Wetzlar, Germany).

The semi-quantification and morphometry procedures were performed by one person (HAH) who was blinded to the diagnosis of the patients.

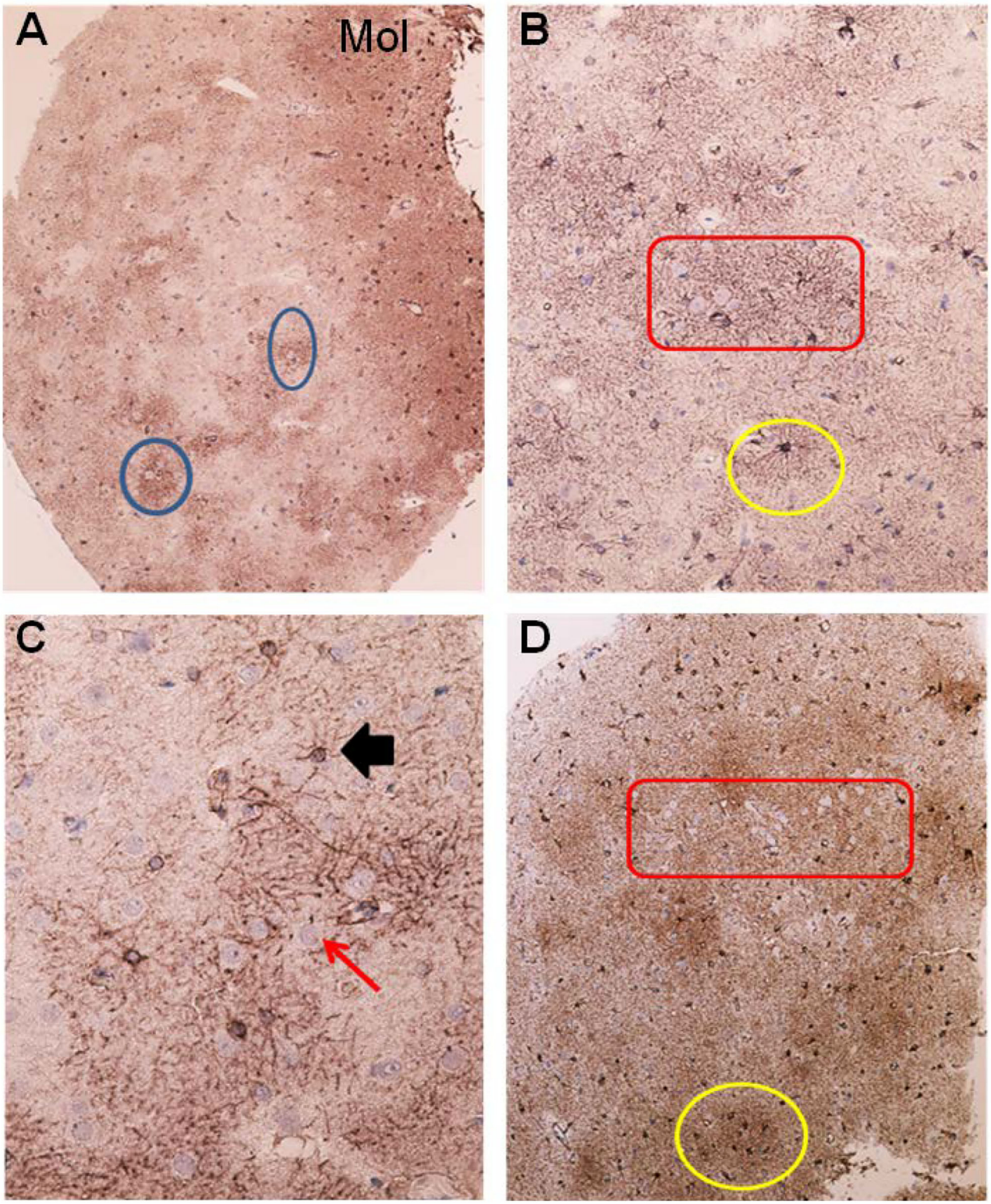

FIGURE 4 | Astrocytes visualized by GFAP IR in brain cortex biopsies from IIH patients. **(A)** Low magnification of a section of brain biopsy reveals a high prevalence of astrocytes in the subpial molecular layer (Mol; layer 1, also named Chaslin's layer) looking like clusters of dark dots. Patches of astrocytes enclosing neurons are seen in cortical layers 2/3 (blue circles). **(B)** Clusters of hypertrophic astrocytes are seen enclosing unstained neurons (encircled by a red line). An apparently normal-looking astrocyte (outlined by yellow circle) with radiating slender processes without having any processes from adjacent glial cells entering its domain. **(C)** Neurons (red arrow) *(Continued)*

FIGURE 4 | in the center of the specimen are enclosed by astrocytes. Note that processes from adjacent astrocytes enter their neighbors' domains as well as having increased branching (black arrow). The GFAP-IR expression is low outside the patch of neurons and astrocytes. **(D)** A low magnification micrograph of the superficial cortex layers shows a cluster of neurons forming a patch surrounded by mainly glia cells (encircled by a red line). Adjacent cluster of astrocytes enclose only few neurons (yellow circle).

Neuronal changes were assessed by the expression of neurofilament-H (NF-H) and by the identification of synaptic stripping. The NF-H IR was indicative of axonal damage characteristic for damaged neurons, while the lack of NF-H IR was typical for normal neurons (**Figure 6D**). Synaptic stripping was characterized by nerve cell bodies being delimited by a GFAP IR membrane enclosing at least half of the nerve cell body sectioned through the nucleus (**Figure 5C**).

Alterations in capillaries were examined by identifying degenerating pericytes processes and degeneration of the basement membrane visualized as vacuolization and degenerative splitting. A cortical capillary was defined as a vascular structure with an inner diameter $<8\,\mu m$ with the lumen bordered by a thin layer of endothelial cells (1–2 per circumference), delimited abluminally by a basement membrane (BM), and enclosed by pericytes (cell body and/or processes) (Mathiisen et al., 2010; Alberts et al., 2014; Winkler et al., 2014; Sweeney et al., 2016). Signs of degeneration included degenerating pericytes, and increased occurrence of vacuoles was graded as follows: None = 0, slight = 1–2, moderate 3–4; severe $\geq$ 5, and/or vacuoles enclosed more than half of the circumference of the capillaries. The astrocytic perivascular processes were identified by their position along the abluminal border of the basement membrane, enclosing the microvessels. Leakage of the BBB was examined by determining the area of fibrin(ogen) immunoreactivity in the neuropil (**Figure 9**).

Transmission Electron Microscopy

We have described the routine for TEM in IIH (Eidsvaag et al., 2018; Eide et al., 2021a). The tissue specimens comprising at least the three deeper layers of the cerebral cortex (Layers 4-6) were immersion fixed in 0.1-M phosphate buffer containing 4% paraformaldehyde and 0.25% glutaraldehyde and kept in a fridge (4°C) overnight. Then, they were transferred to the same fixative diluted 1/10 in phosphate buffer and stored in the solution until further processing. Small blocks from the biopsies were cut, undergoing freeze substitution and infiltration in a Lowicryl HM20 resin (Polysciences Inc., Warrington, PA, USA, Cat15924). The sections were counterstained with uranyl acetate during the cryosubstitution steps before the Lowicryl embedding. Using a Reichert ultramicrotome (Wien, Austria), sections of 80 nm were cut, and mounted on nickel grids. An FEI Tecnai^{TM} 12 transmission electron microscope (FEI Company, Hillsboro, OR, USA) was applied for TEM recording; images were acquired with the analySIS image analysis software (Soft Imaging Systems GmbH, Münster, Germany).

The AQP4 expression was analyzed as the linear density of AQP4 toward endothelium (**Figure 10A**), as previously described (Hasan-Olive et al., 2019c). Mitochondrial-ER contact sites (MERCs) were analyzed as the length of the ER toward the mitochondrion (**Figure 10B**), as previously described (Eide et al., 2021a). The shortest distances between ER and mitochondria were measured at equal distances along with this contact site. For each individual, the length of mitochondria/ER contact was measured, and the average distance between mitochondria and ER was calculated for the particular length. The average of the measurements of the distance between mitochondria to ER was referred to as MERCs distance. Shortened distance between mitochondria and ER is indicative of pathology (Leal et al., 2018; Stacchiotti et al., 2018). Postsynaptic densities (PSDs) were identified in dendritic spines and measured by their length of electron-dense appearance (**Figure 10C**), as previously described (Eide et al., 2021a). The postsynaptic density is a measure of synaptic strength.

Statistical Analysis

The statistical analyses were done with the SPSS software version 27 (IBM Corporation, Armonk, NY). Differences between IIH and REF cohorts were determined using independent sample *t*-tests for continuous data, and by Pearson's chi-square test for categorical data. The statistical significance was accepted at the 0.05 level.

RESULTS

Occurrence of Indices in Patients With IIH About the Underlying Pathophysiology

The study included 13 consecutive patients with IIH (11 female and two male; average age 33.1 $\pm$ 10.7 years) who fulfilled the inclusion criteria. An overview of variables retrieved from the database is provided in **Table 1**. The included patients with IIH fulfilled the diagnostic criteria of IIH (Friedman et al., 2013; Mollan et al., 2018): (A) Papilledema. (B) Normal neurological examination (except for 6th cranial nerve affection). (C) Normal magnetic resonance imaging (MRI), i.e., absence of hydrocephalus, mass, structural lesions, or meningeal enhancement, with the exclusion of venous thrombosis. (D) Normal CSF composition. (E) Elevated lumbar opening pressure (>25 mmH_2O). Notably, subjective cognitive impairment was reported by 6/13 (46%) of patients with IIH.

The IIH cohort had a disease history of 5.1 $\pm$ 3.4 years. Before surgical workup, they had undergone conservative measures, including weight reduction, and medical treatment (acetazolamide in 10/13 patients, topiramate in 2/13 of patients, and furosemide in 2/13 patients).

Magnetic resonance imaging (MRI) evidence of CSF disturbance indicated by empty sella and/or distended perioptic subarachnoid spaces were observed in 6/13 (46%) of patients with IIH (**Table 1**). Most importantly, in this series of 13 patients

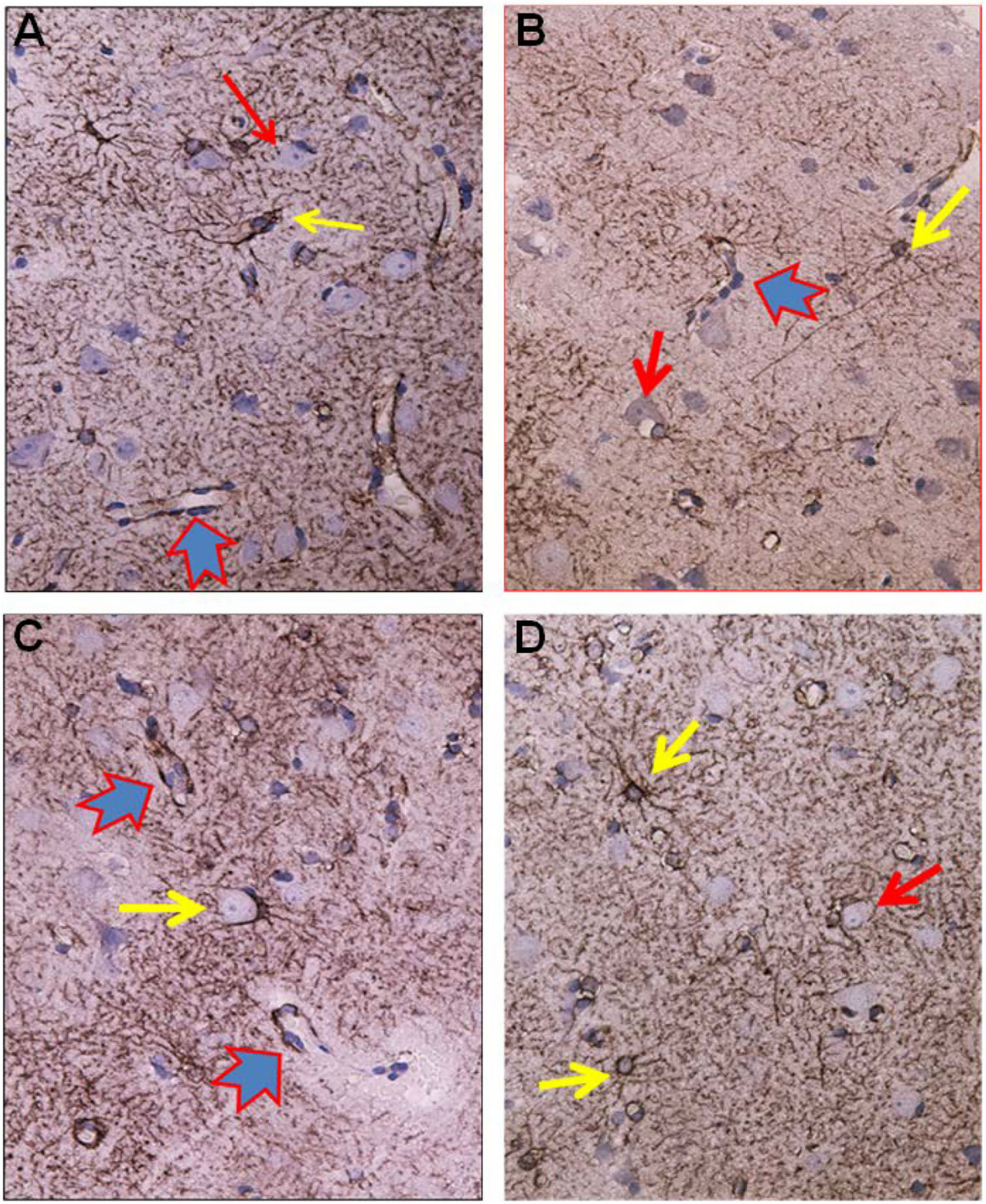

FIGURE 5 | Visualization of astrocytes by GFAP-IR in cerebral cortex of IIH patients. **(A)** GFAP-IR *is* demonstrable forming an elaborated meshwork of processes and membranes. Note the swelling of the perivascular astrocytic end-feet along small blood vessels (red-blue arrow). Nerve cell marked by red arrow and astrocytes marked by yellow arrow. **(B)** Enlarged astrocyte end-feet, filled up by GFAP-IR material, were demonstrable along small blood vessel. The function, effects and importance of such enlarged GFAP-IR end-feet accumulations require further investigation. **(C)** The large nerve cell in the center (yellow arrow) is delimited by astrocyte membranes along its cell body. This is characteristic for synaptic stripping where the GFAP IR membrane continuously encloses half of the perikaryal circumference of the nerve cell body. Note that GFAP-IR profiles are demonstrable in only parts of the cortex specimen. Enlarged GFAP-IR end-feet marked by red-blue arrows. **(D)** Examples of close approximation between the astrocyte processes and the nerve cells. Further, the intensely stained GFAP-IR processes radiate from the astrocyte cell body, divide, and additionally entered neighbor cell domains. Red arrow toward nerve cell and yellow arrows toward astrocytes.

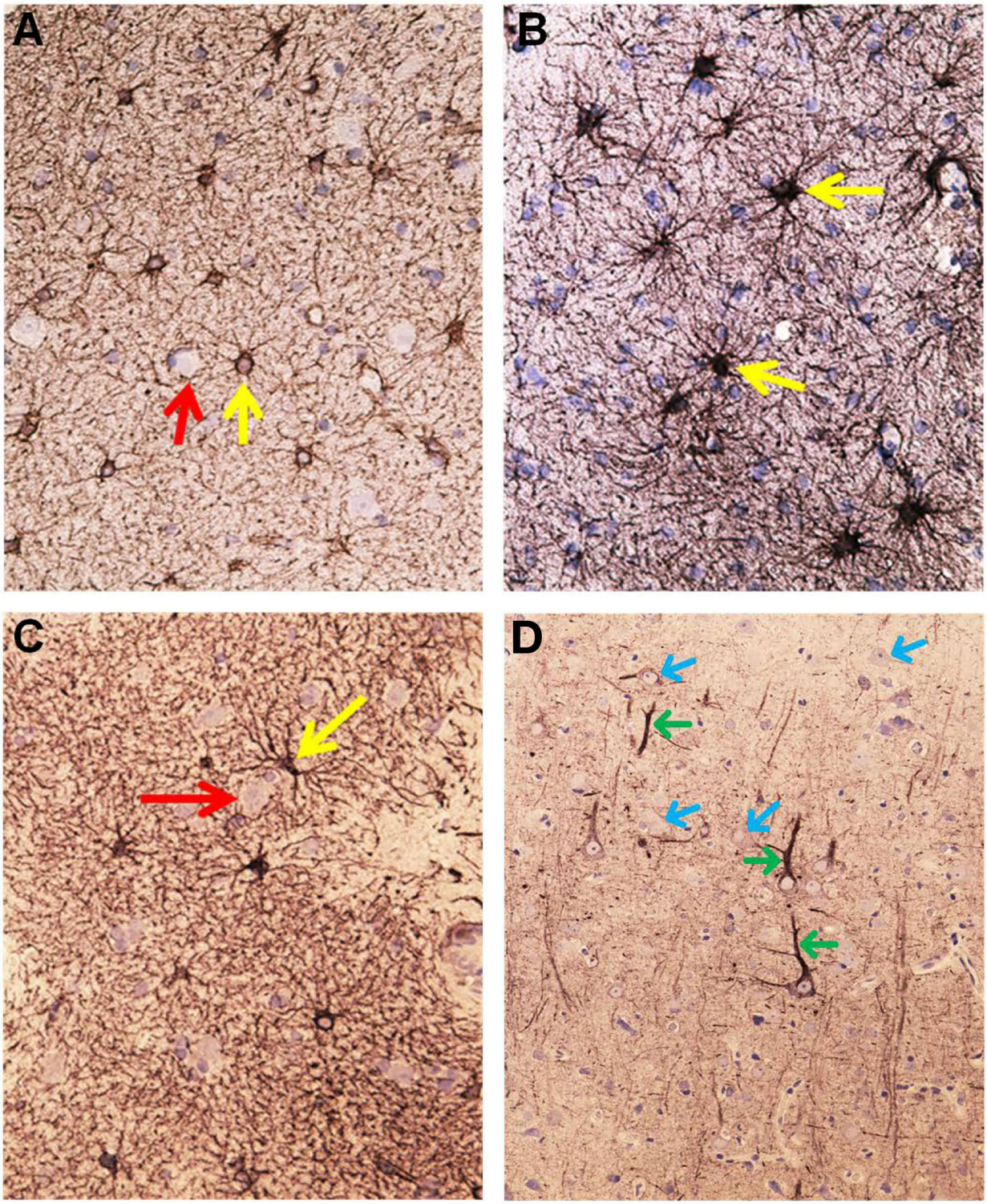

FIGURE 6 | Aspects on the dynamics of astrocytes and neurons in the cerebral cortex of IIH patients. **(A)** Section of the subpial molecular cortex layer, which is dominated by astrocytes and have only scattered nerve cells. The GFAP-IR astrocytes (yellow arrow) are star-shaped with mainly slender radiating and non-dividing processes. Scattered nerve cells (red arrow) are seen in the neuropil. This illustrates the normal structure of cortex layer 1. **(B)** The astrocytes in this specimen of layer 1 are hypertrophic and their processes have abundancy of glio-filament (yellow arrow). The density of the GFAP-IR meshwork is increased in **(B)** as compared to **(A)**. **(C)** A dense network of branching and prominently GFAP-IR processes of impressive density. **(D)** In cortex layers 2/3 of an IIH subject, NF-H-IR expression occurs in damaged or dying neurons (green arrows), while living neurons remain colorless (blue arrows). This indicates neuronal damage in IIH.

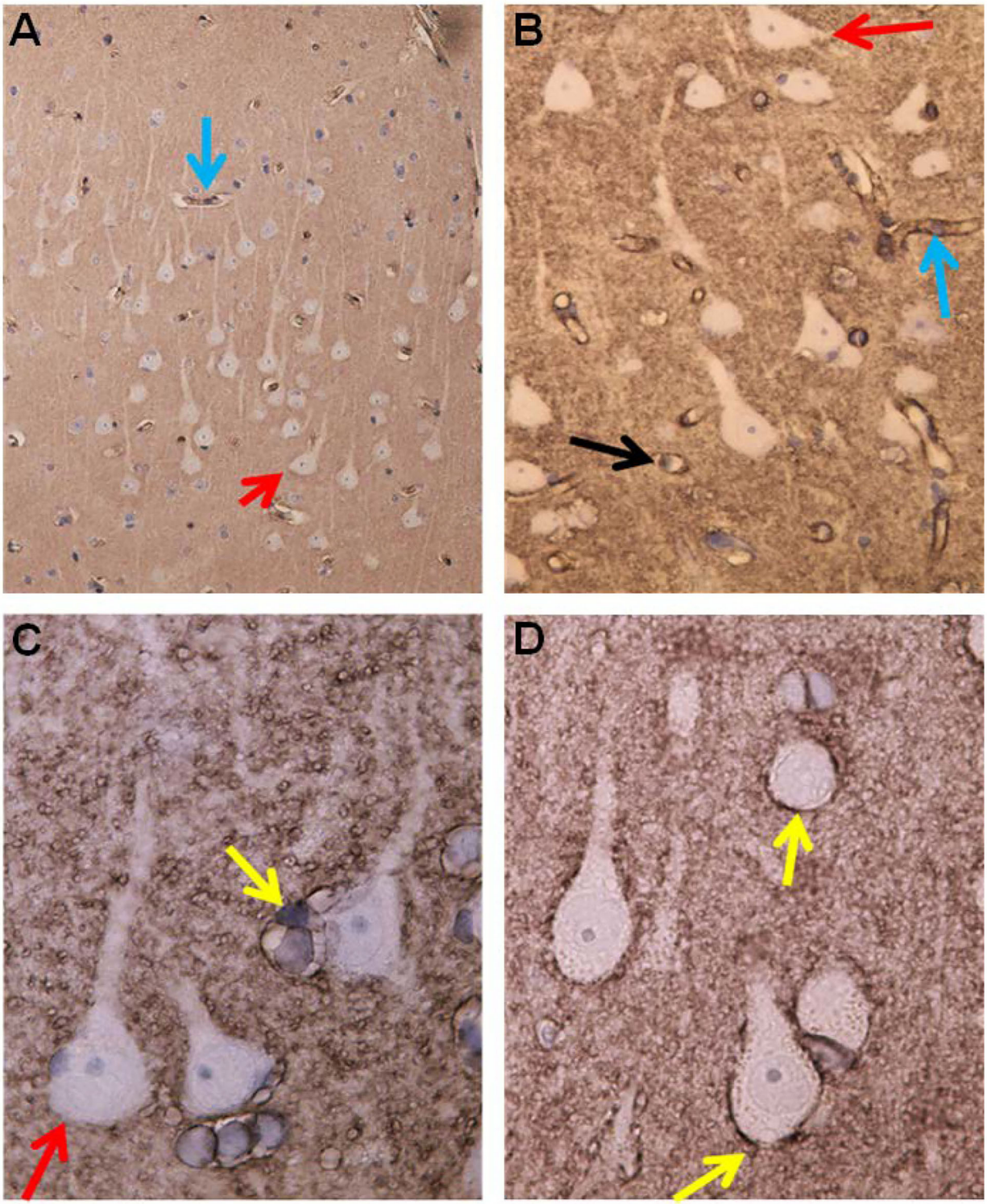

FIGURE 7 | Aquaporin 4 (AQP4)—IR in cerebral cortex of IIH subjects. **(A)** In cortex layers 2/3 the neurons (red arrow) lack AQP4-IR. In contrast, the cell bodies and processes of astrocytes show moderate to strong AQP4-IR. Small blood vessels are distinctly outlined due to high AQP4 IR in the astrocyte end-feet (blue arrow). **(B)** This Figure illustrates that the small cerebral vessels are distinctly outlined due to the prominent AQP4-IR in astrocyte end-feet. Note that the perivascular end feet lining blood vessels are more intensely reactive than the neuropil. **(C)** Pyramidal nerve cells (red arrow) could be observed outlined by seemingly continuous AQP4-IR along the neurilemma, as noticed for many neurons (reference patient). In contrast, no enclosing continuous rim of AQP4-IR was observed in IIH. **(D)** The significance of the different patterns of AQP4 IR in end-feet in different locations ought to be further elucidated.

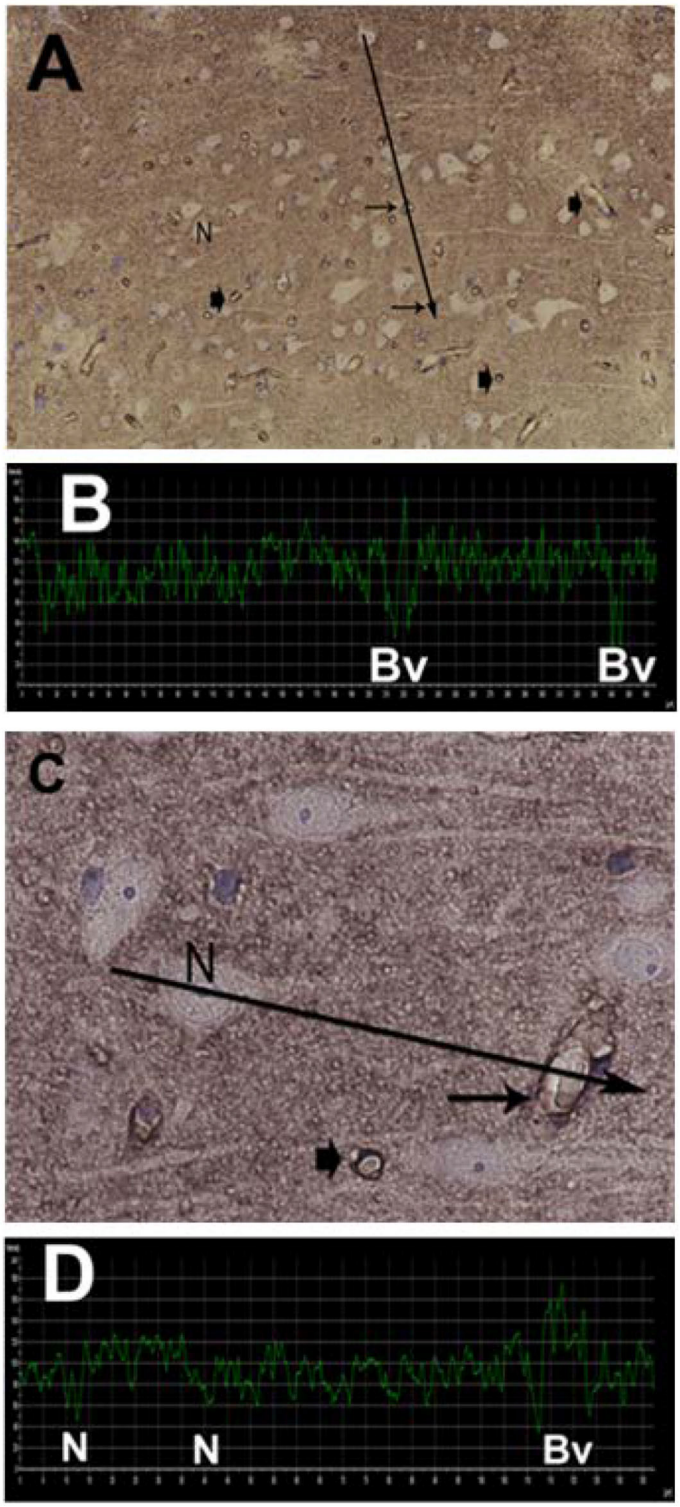

FIGURE 8 | Semi quantitative densitometry determination of AQP4 IR in cerebral biopsies in IIH patients. **(A)** The pattern of AQP4 IR is revealed. The densitometric measurement in **(A)** along a line is shown in **(B)**. Low transmission of light discloses strong AQP4 IR. The nerve cells are non-immunoreactive contrasting to the prominent AQP4-IR in the neuropil. Densitometric analysis enables mapping of the sites with reactive and non-reactive cell structures. **(C)** The relative intensity of the AQP4 IR can be mapped at the cellular level enabling more detailed analysis. The neurons are non-reactive. The perivascular astrocytic end-feet show prominent AQP4 IR. **(D)** The densitometric measurement.

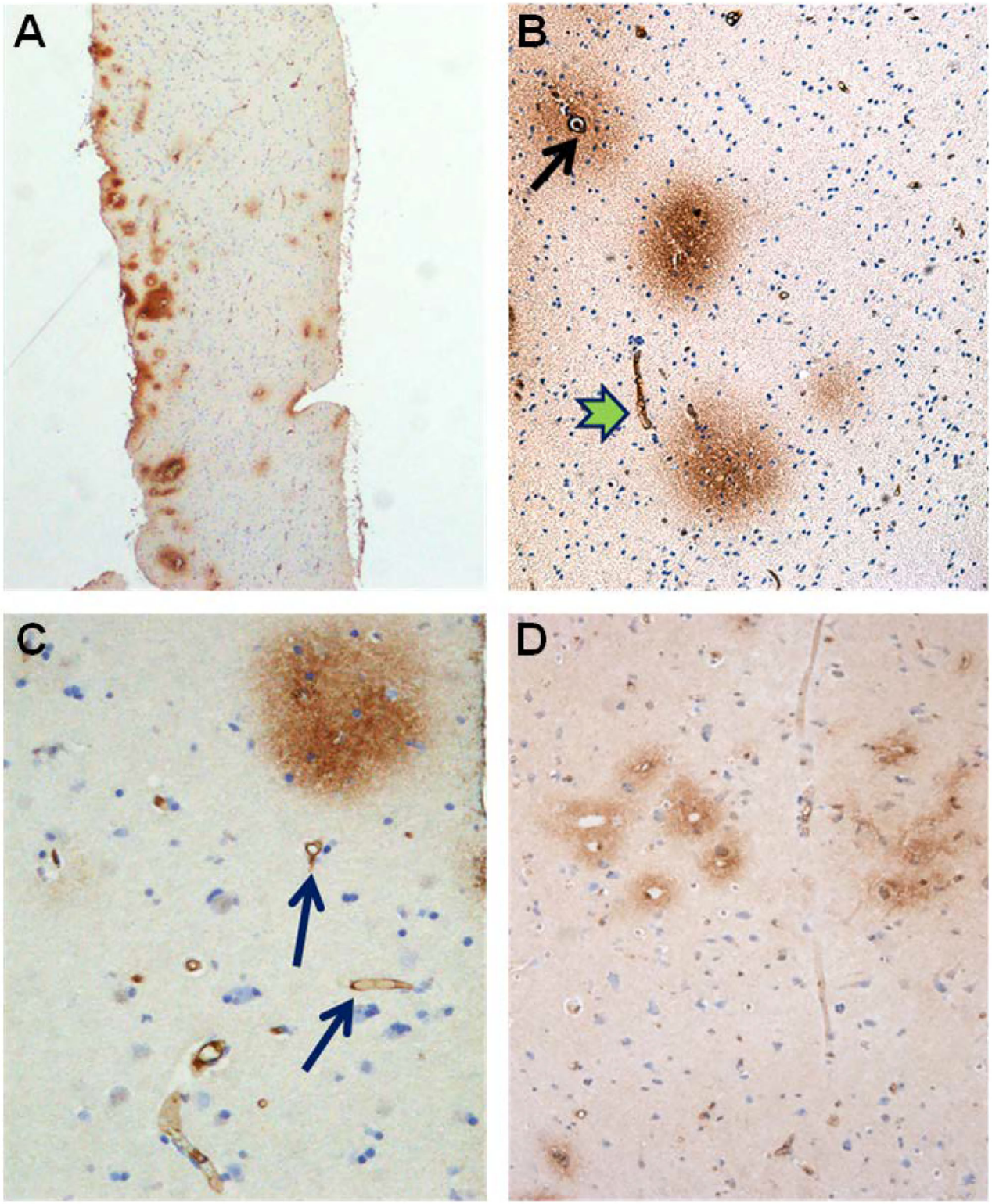

FIGURE 9 | Evidence of BBB dysfunction in IIH subjects. **(A)** The cerebral cortex biopsies comprised cortex tissue that was dissected and fixed by immersion within minutes to achieve best possible preservation. Extravasations of blood products were revealed by immunohistochemical demonstration of both fibrin and fibrinogen, i.e., the blood proteins detected by the used antibody. **(B)** Leakage from a small blood vessel (black arrow) in the center of extravasated fibrin(ogen). Note the vessel wall at the top is retaining blood proteins. **(C)** Fibrin (ogen) is demonstrable both extravasated (upper right corner) and in the walls of small brain vessels (arrow). **(D)** A cluster of small blood vessels is surrounded by leaked fibrin (ogen).

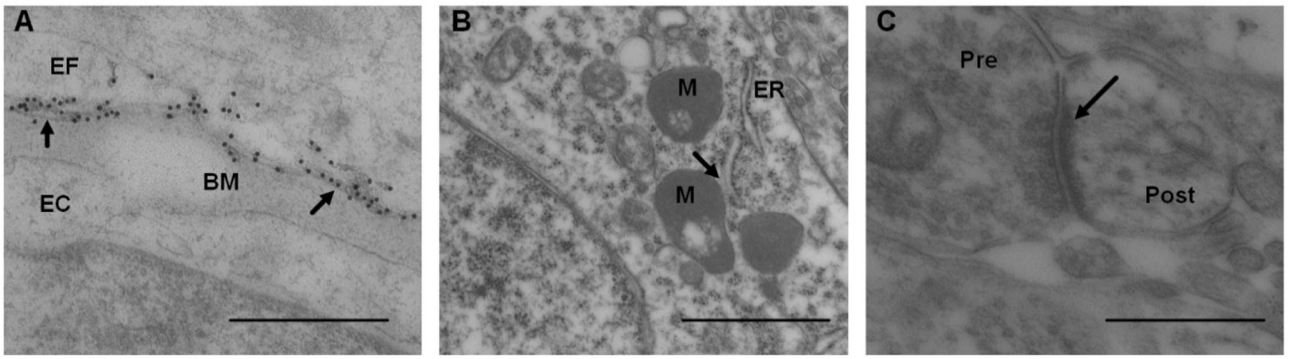

FIGURE 10 | Transmission electron microscopy images of biopsy from right frontal cortex of IIH patients. **(A)** Expression of AQP4 was shown by immunogold labeling of AQP4 in perivascular astrocytic end-feet (EF) facing basement membrane (BM) and endothelial cells (EC); arrows indicate contact toward BM. Scale bar 500 nm. **(B)** Distance between mitochondria (M) and endoplasmic reticulum (ER) in patients with IIH, denoted mitochondria-ER-contact sites (MERCs; arrow). Shortened distance is indicative of pathology. Scale bar 1 μm **(C)** Post-synaptic density (PSD) length (arrow) in IIH, with pre (Pre) and post-synaptic (Post) nerve terminals. Reduced PSD length is indicative of pathology. Scale bar 500 nm.

with definite IIH, none presented with MRI signs of sinus vein stenosis (**Table 1**).

There were abnormal pulsatile ICP in 13/13 (100%) IIH subjects, shown as overnight MWA scores of >4 mmHg (**Figure 11A**) or overnight percentage of MWA > 5 mmHg in > 10% of recording time (**Figure 11B**). Abnormal mean ICP, either defined as overnight mean ICP >15 mmHg (**Figure 11C**) or overnight mean ICP > 15 mmHg in >50% of recording time (**Figure 11D**), was observed in 3/13 (23%) of IIH subjects.

The brain biopsies were not accompanied by adverse consequences. Abnormal ultrastructure at the glia-neurovascular interface was demonstrated in 12/13 (92%) of patients with IIH; only case #4 presented with no apparent abnormal ultrastructure. **Table 1** provides an overview of some ultrastructural findings in the patients with definite IIH. Continuous variables cannot be dichotomized as abnormal/normal and were not included in **Table 1**. The brain biopsies were obtained from right frontal gray matter in the 13 patients with IIH. The 12 REF subjects had undergone surgery for epilepsy ($n = 9$), clipping of a cerebral aneurysm ($n = 2$), or resection of a malignant brain tumor ($n = 1$). The reference tissue specimens were obtained from the gray matter of the frontal cortex in three, temporal cortex in seven, parietal cortex in one, and occipital cortex in one subject.

Comparisons of Semi-quantitative Ultrastructural Variables

The semi-quantitative variables of ultrastructural change at the glia-neuro-vascular interface retrieved from the database were compared between 13 Patients with IIH and 12 REF subjects, who were comparable in age and gender (**Table 2**). The IIH and REF cohorts differed significantly in BMI and the occurrence of the symptoms, such as headache, papilledema/visual impairment, and tinnitus (**Table 2**). Furthermore, the female/male distribution was 11/2 among IIH and 7/5 among REF subjects, even though the difference was non-significant.

A comparison of morphology between IIH and REF subjects showed a significantly increased area of GFAP immunoreactivity, higher occurrence of patchy astrogliosis, and loss of astrocyte domains in IIH subjects (**Table 3**).

As evaluated by LM, AQP4 immunoreactivity at perivascular borders was increased as visualized by LM, but this was not verified by TEM-utilizing immunogold labeling of AQP4 (**Table 3**). These observations confirm that the perivascular expression of AQP4 is not reduced in IIH subjects. regarding the possible role of neuroinflammation and microglia in IIH, no difference in CD68 expression was seen in IIH subjects (**Table 3**).

As indicated in **Table 3**, impaired neuronal function in IIH was indicated by reduced MERCs distance, as well as reduced post-synaptic density length.

Furthermore, the semi-quantitative comparisons indicated that patients with IIH present with alterations at the capillary level. The IIH subjects were characterized by more frequent degeneration of pericytes processes, as well as signs of vacuolization and degeneration of the basement membrane (**Table 3**). Moreover, there was marked evidence of blood-brain-barrier leakage in IIH, shown as an increased area of fibrin(ogen) immunoreactivity (**Table 3**).

DISCUSSION

The major observation of this study was that the present 13 patients with definite IIH demonstrated MRI signs of CSF disturbance in 6/13 (46%) of patients, signs of sinus vein stenosis in 0/13 (0%), abnormal pulsatile ICP in 13/13 (100%) of patients, abnormal static ICP in 3/13 (23%) of patients with IIH, and ultrastructural changes indicative of pathology at the glia-neuro-vascular interface in 12/13 (92%) of patients with IIH. Furthermore, comparisons of semi-quantitative variables of ultrastructural changes at the glia-neuro-vascular interface demonstrated abnormalities for variables

TABLE 1 | Variables indicative of idiopathic intracranial hypertension (IIH) pathophysiology in the 13 patients with definite IIH.

	IIH patient												
	1	**2**	**3**	**4**	**5**	**6**	**7**	**8**	**9**	**10**	**11**	**12**	**13**
Demographic													
Gender	F	F	F	F	F	F	F	F	F	M	F	F	M
Age (yrs)	38	30	22	34	24	48	37	47	22	21	24	52	31
BMI (kg/m^2)	29	33	29	34	28	23	26	33	38	35	37	39	23
Symptoms													
Headache	1	1	1	1	1	1	1	1	1	1	1	1	1
Papilledema/Visual deficits	1	1	1	1	1	1	1	1	1	1	1	1	1
Tinnitus	–	–	1	1	1	–	–	–	–	–	–	1	1
Cognitive impairment	1	1	–	–	1	1	1	–	–	–	–	1	–
MRI-evidence of CSF disturbance													
Empty sella/distended													
Perioptic subarachnoid space	1	–	–	–	1	1	–	–	1	–	–	1	1
MRI-Evidence of venous obstruction													
Sinus vein stenosis	–	–	–	–	–	–	–	–	–	–	–	–	–
Overnight ICP													
Abnormal MWA	1	1	1	1	1	1	1	1	1	1	1	1	1
Abnormal mean ICP	1	–	–	–	–	1	–	–	–	–	–	–	1
Ultrastructural abnormality at the glia-neuro-vascular interface													
Glial cells													
Astrocyte hypertrophy/loss of astrocyte domains	1	1	1	–	1	1	–	1	1	1	1	1	1
Patchy astrogliosis	1	1	–	–	–	1	–	–	1	–	1	1	–
Neurons													
Neurofilament-H	1	1	–	–	–	1	–	–	–	–	1	–	–
Synaptic stripping	1	–	–	–	–	1	–	1	1	–	1	–	–
Capillaries													
Degeneration of pericyte processes	1	–	–	–	1	1	1	1	1	1	1	–	–
BM vesicles/splitting	1	–	–	–	1	1	1	1	1	1	1	–	–
BBB leakage	1	–	–	–	1	1	1	1	1	1	1	1	1

BBB, blood-brain-barrier; BM, Basement membrane; BMI, body mass index; ICP, Intracranial pressure; MWA, mean; ICP, wave amplitude.

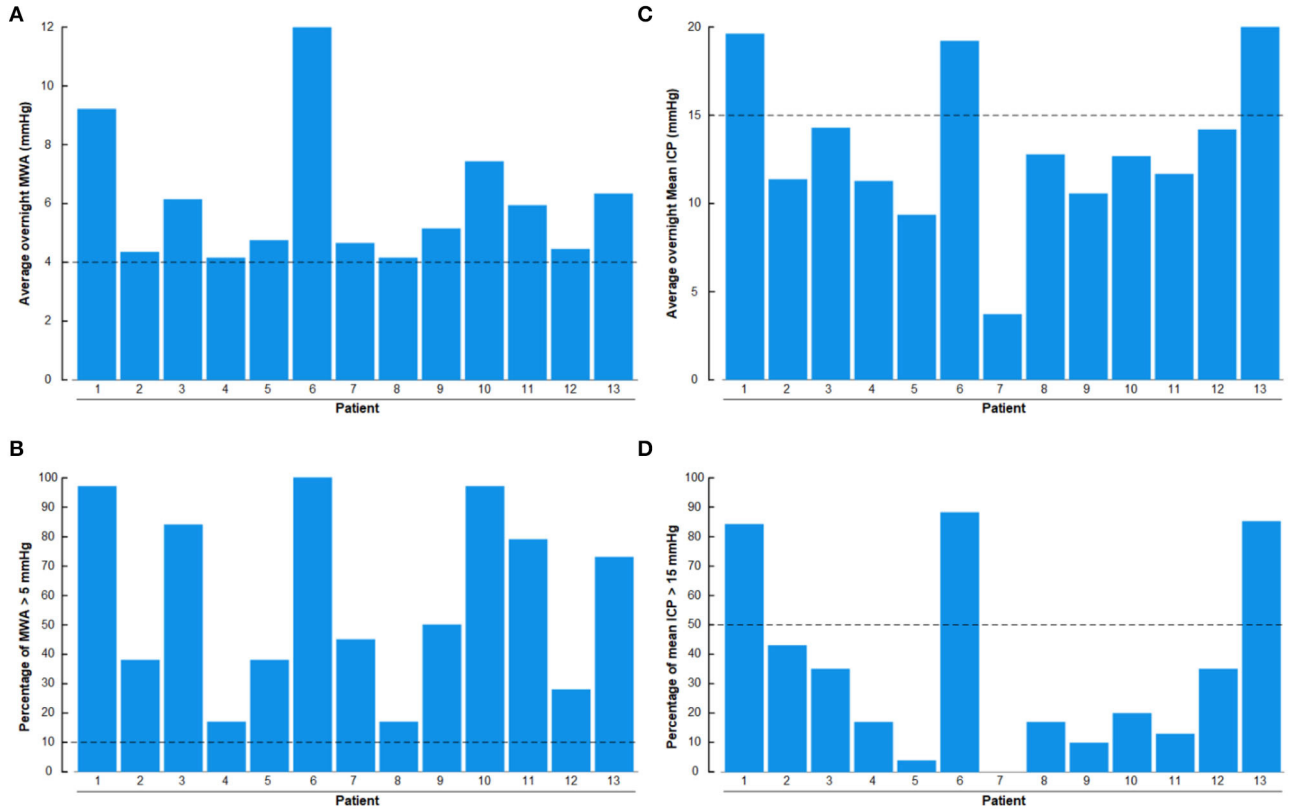

FIGURE 11 | The overnight recordings of MWA and mean ICP in the 13 Patients with IIH included in the study are shown on an individual basis. **(A)** Overnight average of MWA. **(B)** Overnight percentage of MWA > 5 mmHg. **(C)** Overnight average of mean ICP. **(D)** Overnight percentage of mean ICP > 15 mmHg. The horizontal lines indicate upper normal thresholds as defined by the first author: **(A)** Overnight MWA > 4 mmHg. **(B)** Overnight 10% of MWA > 5 mmHg. **(C)** Overnight Mean ICP > 15 mmHg. **(D)** Overnight 50% of Mean ICP > 15 mmHg.

related to glial cells, neurons pericytes, and capillaries in patients with IIH.

Patients With IIH

The present cohort of 13 patients with IIH may be considered *Definite* patients with IIH. Before shunt surgery, they fulfilled the diagnostic criteria of IIH (Friedman et al., 2013; Mollan et al., 2018), and responded with clinical improvement (visual improvement and at least partial improvement of headache) following shunt surgery. It should be noted that cognitive impairment is frequently reported in IIH (Kharkar et al., 2011; Yri et al., 2014), and was reported by 6/13 (46%) of patients with IIH in this study. There is evolving evidence for olfactory dysfunction in IIH (Schmidt et al., 2012; Kunte et al., 2013; Bershad et al., 2014), but this cranial nerve dysfunction was not recorded in our registry. The present cohort included non-selected and consecutive patients with IIH, who are representative of patients with IIH referred to neurosurgery. These patients with IIH may, however, not be representative of a general cohort of patients with IIH as these patients are primarily treated conservatively before referral to neurosurgery. This IIH cohort had been treated conservatively 5.1 ± 3.4 years before neurosurgical treatment.

CSF Disturbance in IIH

In this IIH cohort, MRI evidence for CSF disturbance visualized as empty sella or distended perioptic subarachnoid spaces was observed in 6/13 (46%) of patients. Traditionally, CSF circulation failure has been considered the main mechanism behind IIH, related to excessive CSF production and/or reduced CSF efflux. This is as well the main rationale behind the medical treatment of reducing CSF production. Hence, the medications acetazolamide and topiramate reduce CSF production by inhibiting carbonic anhydrase. It should be noted, however, that even though acetazolamide is the most widely used medication for IIH, a recent Cochrane review concluded that there is insufficient evidence to recommend or reject the efficacy of this medication (Piper et al., 2015). Among the present IIH subjects, at the time of ICP/biopsy, 10/13 (77%) used acetazolamide and 2/13 (15%) topiramate, but with lasting symptoms, and abnormal pulsatile ICP in all patients (**Figure 11B**; **Tables 1**, **2**).

On the other hand, the strongest evidence in favor of CSF disturbance in IIH is the clinical response to

TABLE 2 | Material of patients with definite IIH and REF subjects.

	IIH	REF	Significance
Number	13	12	
Gender (F/M)	11/2	7/5	ns
Age mean at inclusion (yrs.)	33.1 ± 10.7	37.9 ± 11.7	ns
BMI (kg/m^2)	31.2 ± 5.4	25.8 ± 4.3	$P = 0.012$
Co-Morbidity			
Arterial hypertension, *n* (%)	1 (7.7%)	2 (16.7%)	ns
Diabetes mellitus, *n* (%)	1 (7.7%)	0	ns
Pre-Operative symptoms			
Headache	13 (100%)	2 (17%)	$P < 0.001$
Papilledema/visual impairment	13 (100%)	0	$P < 0.001$
Tinnitus	5 (39%)	0	$P = 0.016$
Cognitive impairment	6 (46%)	4 (33%)	ns

BMI, Body mass index; F, Female; M, Male. Continuous data are presented as mean ± standard deviation, and categorical data as numbers (with percentages in parenthesis). Significant differences between continuous variables were determined by independent samples t-test, and differences between categorical data were determined by Pearson's chi square test. Ns, non-significant.

CSF diversion surgery, either ventriculoperitoneal or lumbo-peritoneal shunting. All the present patients with IIH had normalization of visual impairment following shunt surgery and at least partial improvement of headache. Hence, reducing CSF pressure by shunting effectively improves visual function, even though lasting complaints with headaches are frequent, and the shunt revision rate in IIH is high (McGirt et al., 2004; Eide and Kerty, 2011; Eide et al., 2016). Therefore, given that normalization of CSF pressure may not be accompanied by improved headache (Eide, 2021), other mechanisms than CSF pressure, *per se,* seems to be at play. Today, there is a tendency toward treating headaches associated with IIH as migraine and recommend anti-migraine medications.

Intracranial Venous Hypertension and Obesity in IIH

The diagnostic criteria of IIH require imaging studies demonstrating normal brain parenchyma with no hydrocephalus, mass lesions, structural lesions, meningeal enhancement, or evidence of venous thrombosis (Friedman et al., 2013; Mollan et al., 2018). These MRI findings were confirmed in the present patients with IIH.

An important hypothesis regarding IIH pathophysiology is intracranial venous hypertension caused by sinus vein stenosis (Mollan et al., 2018). It even has been proposed that the notation "idiopathic" should be omitted, based on the reasoning that intracranial venous hypertension is the main cause of the disease (Fargen, 2020). It is, however, complicating that the diagnostic criteria for the presence of significant sinus vein stenosis vary. Based on MRI venography, none of the present patients with IIH showed evidence of sinus vein stenosis and accompanying intracranial venous obstruction. Moreover, static ICP was neither markedly increased; merely 3/13 (23%) of patients with IIH presented with overnight mean ICP > 15 mmHg or overnight percentage of mean ICP > 15 mmHg in >50% of observations. Significant venous obstruction caused by sinus vein stenosis would be expected to increase the static ICP. Therefore, the present data do not add support the assumption that sinus vein stenosis is a significant player in IIH pathophysiology.

Intracranial venous hypertension may, however, be increased for other reasons in IIH. The incidence of IIH in the general adult population was 1–2 in 100,000 whereas, in adult obese fertile women, the incidence was 12–32 in 100,000 people (Kesler et al., 2014). Based on an assumption that being overweight leads to increased abdominal pressure and, thereby, increased venous pressure that subsequently increases ICP, weight reduction is the first-line treatment. In line with this, a low-energy diet in women with IIH was accompanied by less severe symptoms, reduced papilledema, and lowered ICP (Sinclair et al., 2010). In the present IIH cohort, BMI was significantly increased, and a BMI of >30 kg/m^2 was found in 7/13 (54%) of patients.

ICP Measurements in IIH

The present observations in shunt-responsive IIH subjects of abnormal pulsatile ICP in 13/13 (100%) of subjects, but abnormal static ICP in 3/13 (23%) patients compared with previous observations in patients with IIH refractory to conservative-medical treatment, namely abnormal pulsatile ICP despite normalized static ICP (Eide and Kerty, 2011; Eide, 2021). For years, we have recorded ICP in IIH and have measured ICP *via* a sensor placed in the brain parenchyma since parenchymal ICP measurements may be considered the gold standard. Using dedicated software, we have determined the overnight pulsatile ICP as the mean ICP wave amplitude (MWA), in addition to the static ICP (mean ICP). From this experience, we have established upper normal thresholds for MWA (Eide and Kerty, 2011; Eide, 2021). Since few studies have reported the results of continuous over-night ICP monitoring in IIH, we have adopted upper normal thresholds of mean ICP from the experience of others; usually a mean ICP of <15 mmHg has been considered normal (Corbett and Mehta, 1983; Whiteley et al., 2006; Bono and Quattrone, 2007), but ICP has been estimated from measurements of lumbar CSF opening pressure with the patient in the lateral decubitus position. The upper normal pressure values ranging between 200 and 250 mm H_2O (14.7–18.4 mm Hg) (Corbett and Mehta, 1983). UK physicians treating IIH consider a gray zone between 250 and 300-mm CSF to be disease defining (Wakerley et al., 2020). Even though the diagnosis of IIH relies on lumbar CSF pressure (Mollan et al., 2018), it is important to bear in mind that there are definite limitations to estimating ICP from lumbar puncture (Eftekhari et al., 2019). The lumbar CSF pressure depends on many factors; for example, the position of the lumbar region relative to the head causes hydrostatic pressure differences to affect the lumbar CSF pressure. In addition, breath-holding hyperventilation or Valsalva related to pain, discomfort, and anxiety all affect the lumbar CSF pressure. Furthermore, since the lumbar CSF pressure changes over time, it has been suggested to measure lumbar CSF pressure over longer periods (Torbey et al., 2004). Therefore, the ICP and lumbar CSF pressure are not identical, even with the patient in the horizontal position

TABLE 3 | Comparisons of structural differences at glia-neuro-vascular interface of patients with definite IIH and reference (REF) subjects.

	IIH	REF	Significance
Glial cells			
Astrocytes			
Area of GFAP immunoreactivity (%)	13.2 ± 3.1	7.3 ± 2.7	$P < 0.001$
Patchy astrogliosis (yes/no)	6/7	1/10	$P = 0.047$
Distinct astrocyte domains (yes/no)	3/10	9/2	$P = 0.004$
Perivascular astrocytic end-feet			
AQP4 at membranes facing endothelial cells			
LM–Arbitrary units	48.7 ± 15.4	68.5 ± 7.4	$P = 0.001$
TEM–Linear gold particle density (particles/μm)	18.3 ± 3.1	17.9 ± 4.2	ns
AQP4 at membranes facing neuropil			
LM–Arbitrary units	116.5 ± 3.9	115.3 ± 7.7	ns
TEM–Linear gold particle density (particles/μm)	8.2 ± 3.6	8.1 ± 2.5	ns
Microglia			
Area of CD68 immunoreactivity (%)	0.45 ± 0.23	0.70 ± 0.45	ns
EM markers of abnormal neuronal function			
Neuronal soma			
MERCs distance (μm)	0.05 ± 0.001	0.24 ± 0.04	$P = 0.008$
Post-Synaptic density			
Post-Synaptic density length (μm)	0.35 ± 0.05	0.63 ± 0.09	$P = 0.001$
Microvascular alterations			
Pericyte process degeneration			
Category (normal/focal/extensive)	0/8/0	4/4/0	$P = 0.021$
Basement membrane abnormality			
Vacuolization (none/slight/moderate/severe)	0/6/2/0	4/1/2/1	$P = 0.036$
Degeneration splitting (Y/N)	8/0	4/4	$P = 0.021$
Blood-brain-Barrier leakage			
Area of fibrin(ogen) immunoreactivity	11.2 ± 7.9	0.8 ± 1.1	$P < 0.001$

AQP4, Aquaporin-4; CD68, Cluster of differentiation 68; EM, Electron microscopy; GFAP, Glial fibrillary acidic protein; LM, Light microscopy; MERC distance, Mitochondria-endoplasmic reticulum distance. Continuous data presented as mean ± standard deviation, and categorical data as numbers. Lower arbitrary units are accompanied with higher AQP4 expression. Significant differences between groups were determined by independent samples t-test for continuous data and by Pearson's Chi-Square test for categorical data (ns, non-significant).

and absence of CSF blocks. In line with this, simultaneous measurements of the CP from a parenchymal sensor and from the lumbar CSF compartment demonstrated different pulsatile and static ICP scores (Eide and Brean, 2006). Accordingly, the present overnight ICP measurements provide a reliable picture of ICP alterations in the present patients with IIH.

The Glia-Neuro-Vascular Interface

This present work draws attention to the glia-neuro-vascular interface in IIH. The estimated total perfused length of capillaries in the human brain is about 600–700 km, covering a total surface area of 20 m^2 and a median inter-capillary distance of 50 μm (Winkler et al., 2014; Sweeney et al., 2016). There is one capillary for each neuron in the brain; the distance between a capillary and a neuron is about 10 μm. The astrocytes have processes that approach both the neuropil and the capillaries, the latter constituting the perivascular astrocytic end-feet that surround the entire capillary as a donut with end-feet gaps, estimated to about 20 nm toward the interstitial tissue (Mathiisen et al., 2010). The end-feet facing the basement membrane is covered by the water channel aquaporin-4 (AQP4), covering about 50% of the area of end-feet (Nagelhus and Ottersen, 2013). In adult humans, the glial cells, including the astrocytes, constitute about half of the total number of brain cells and half of the brain volume (Verkhratsky and Butt, 2013; Winters and Kleinschmidt-Demasters, 2015). The astrocytes are instrumental in bridging the functional connection between neurons and brain capillaries and play a key role in brain metabolism (Howarth, 2014). In particular, the perivascular astrocytic end-feet exhibit signaling patterns that are crucial, for e.g., vasomotion and water and fluid homeostasis (Amiry-Moghaddam and Ottersen, 2003; Mulligan and MacVicar, 2004; Boulay et al., 2017; Langer et al., 2017), and for maintenance of blood-brain barrier (BBB) function (Haddad-Tovolli et al., 2017).

A seminal study from 2012 coined the perivascular fluid circulation through brain parenchyma "the glymphatic system," serving as a pseudo-lymphatic system within the brain (Iliff et al., 2012). The glymphatic system is a perivascular transport system for fluids and solutes, hypothesizing that waste products from cerebral metabolism are transported antegrade at the arterial side of the capillary network, *via* interstitial tissue, with efflux antegrade along the venous side of the capillaries. The system

depends on AQP4 at the astrocytic end-feet, is regulated by sleep, and becomes impaired with increasing age (Nedergaard and Goldman, 2020). We recently provided evidence of impaired glymphatic function in patients with IIH (Eide et al., 2021b).

Figure 12 demonstrates in a shunt-responsive IIH patient the extravascular enrichment within brain parenchyma of an MRI contrast agent (gadobutrol, molecular size 604 Da), serving as CSF tracer after injection to the lumbar subarachnoid space. This tracer is hydrophilic and does not pass the BBB and is transported outside the capillaries. Hence, the abnormal extravascular passage of this CSF tracer previously shown in patients with IIH (Eide et al., 2021b) should draw our attention toward the glia-neuro-vascular interface, wherein the basement membrane represents a loose matrix for solute transport, and wherein the function of astrocytic end-feet would be expected to affect molecular transport *via* inter-end-feet gaps and along the capillaries.

IIH Is Characterized by Alterations at the Glia-Neuro-Vascular Interface

In this study, ultrastructural changes at the glia-neuro-vascular interface were observed in 12/13 (92%) of IIH subjects, despite no imaging signs of sinus vein stenosis, and overnight mean ICP of >15 mmHg in merely 3/13 (23%) of IIH subjects. On the other hand, abnormal pulsatile ICP was seen in 13/13 of patients with IIH.

The present IIH subjects were shunt responders and demonstrated patchy astrogliosis in cortical gray matter, including cell hypertrophy, and loss of astrocyte domains, which compares with previous observation in non-selected patients with IIH treated surgically or conservatively (Eide et al., 2016). Astrogliosis was visualized by increased expression of the glial fibrillary acidic protein (GFAP). In general, an astrogliosis is a non-specific event of astrocytes, which may occur secondary to a wide range of causes, such as noxious agents, chemokines, cytokines, trauma, infections, and inflammations (Oberheim et al., 2012; Verkhratsky and Butt, 2013; Winters and Kleinschmidt-Demasters, 2015). Astrogliosis also affects the end-feet processes and their molecular composition (Eid et al., 2005; Heuser et al., 2012).

An important observation in the patients with IIH is that the perivascular expression of AQP4 was not reduced, as opposed to the dementia subtype idiopathic normal pressure hydrocephalus (iNPH), which presented with loss of perivascular AQP4 expression (Eide and Hansson, 2018; Hasan-Olive et al., 2019a). It is, therefore, of note that *in vivo* evidence suggests impaired glymphatic function in IIH (Eide et al., 2021b), even though perivascular AQP4 expression was not reduced. On the contrary, in IIH subjects the degree of perivascular AQP4 expression correlated positively with the degree of astrogliosis, i.e., an increasing degree of astrogliosis was accompanied with an increasing degree of AQP4 expression (Eide et al., 2016). This may be interpreted as indicative of a compensatory increase of AQP4 at perivascular astrocytic end-feet.

In the astrocytic processes close to the perivascular end-foot membrane, 3-dimensional (3D) EM showed bundles of mitochondria (Mathiisen et al., 2010). We used transmission electron microscopy (TEM) to study mitochondria in astrocytes and found an increased frequency of pathological mitochondria within the perivascular astrocytic end-feet of IIH subjects (Eide et al., 2021a). Furthermore, the degree of astrogliosis correlated positively with a number of pathological mitochondria in duplicate samples from the same patient; i.e., more astrogliosis and more pathological mitochondria. It has previously been shown that mitochondrial dysfunction is associated with reactive cortical astrogliosis (Fiebig et al., 2019).

Regarding neuronal dysfunction in IIH, in the present IIH shunt responders, there were shortened mitochondria-endoplasmic reticulum contact (MERC) distance in neuronal soma and shortened post-synaptic density (PSD) length. The role of MERCs is complex (Giacomello and Pellegrini, 2016). We interpret our observations of increased occurrence of pathological structures in neuronal soma of patients with IIH as indicative of abnormal cellular metabolism in neurons (Eide et al., 2021a). Comparable observations were previously made in individuals with the neurodegenerative disease and dementia subtype idiopathic normal pressure hydrocephalus (Leal et al., 2018; Hasan-Olive et al., 2019b). Moreover, the observation of reduced post-synaptic density length in IIH shunt responders is suggestive of impaired synaptic strength. This observation is of interest, given reports of cognitive impairment being prevalent in patients with IIH (Kharkar et al., 2011; Yri et al., 2014). In line with this, we previously reported an increased frequency of pathological mitochondria in pre- and post-synaptic nerve terminals, indicative of impaired mitochondrial trafficking (Eide et al., 2021a). Due to the high-energy demand in the pre- and post-synaptic terminals, a sufficient number of functional mitochondria is a prerequisite to maintaining synaptic function (Hollenbeck, 2005; Yu and Yu, 2017). Another piece of evidence of neuronal dysfunction was the finding of synaptic stripping in 5/13 (54%) of patients with IIH. The phenomenon of synaptic stripping is a process by which microglia selectively remove synapses from injured neurons (Blinzinger and Kreutzberg, 1968). Taken together, there is accumulating evidence for neuronal dysfunction in IIH disease.

The present observations confirmed structural changes in capillaries of patients with IIH responding to shunt surgery. Capillary damage was indicated by the frequent occurrence of caveolae and endothelial cytoplasmic vesicles, with the basement membrane being folded, tortuous, and irregular with signs of splitting, as previously shown in non-selected patients with IIH, treated conservatively or surgically (Eidsvaag et al., 2018). Of note, the pericyte processes in IIH were degenerating despite structurally intact pericyte cell bodies. It has previously been shown that intact pericytes are crucial for the development, establishment, and maintenance of the BBB (Liwnicz et al., 1990; Farkas and Luiten, 2001; Sagare et al., 2013; Andreone et al., 2017; Erdo et al., 2017; Kisler et al., 2017; Montagne et al., 2017; Liebner et al., 2018; Sweeney et al., 2018). Experimental studies show that pericyte dysfunction causes neurovascular and metabolic dysfunction (Kisler et al., 2017) and enhances neurodegeneration (Sagare et al., 2013; Sweeney et al., 2016). Furthermore, loss and degeneration of pericytes may result in BBB dysfunction

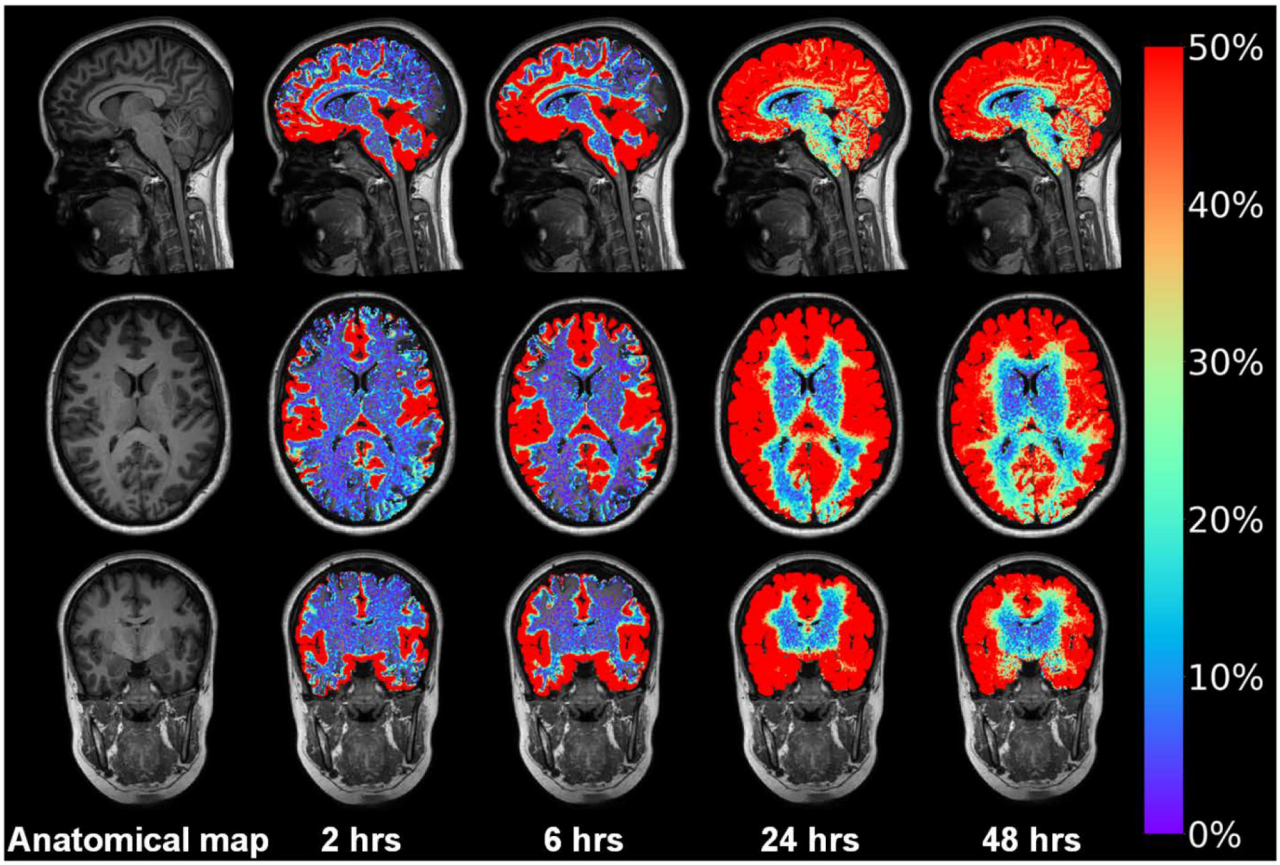

FIGURE 12 | Intrathecal contrast-enhanced MRI in one subject with IIH provides evidence for a glymphatic system in patients with IIH. Intrathecal injection of the MRI contrast agent gadobutrol (Gadovist[tm], Bayer Pharma AG, Berlin, Germany) in a dose 0.5 mmol, serves as a CSF tracer molecule. Gadobutrol has a molecular size of about 604 Da and is highly hydrophilic, making it suitable for transport within the CSF. After arriving to the subarachnoid CSF, the tracer is contained outside the blood vessels since it does not pass the BBB. Using FreeSurfer, tracer in CSF spaces is subtracted, only showing enrichment of tracer in brain parenchyma over time in this IIH patient responding to shunt surgery. The tracer enriched in the interhemispheric fissure and Sylvian fissure and medial temporal where the large vessels resides anterior middle cerebral and posterior cerebral arteries, respectively. Moreover, the tracer enriched in a centripetal fashion; at 24 h the entire brain had enriched with tracer that lasted at 48 h. *In vivo* evidence for impaired glymphatic function in IIH has been given before (Eide et al., 2021b). Illustration: Lars Magnus Valnes, Department of neurosurgery, Oslo university hospital, Oslo, Norway.

and disturbed cerebral microcirculation (van Vliet et al., 2015; Sweeney et al., 2018). In this regard, it is of interest to note the occurrence of leakage of the blood glycoprotein fibrin (ogen) in IIH shunt responders, as well as in patients with IIH treated surgically or conservatively (Hasan-Olive et al., 2019c). Fibrin (ogen) has a molecular weight of 340 kDa and is a marker of BBB integrity. Outside the blood vessels, fibrinogen is transformed into fibrin. These blood products are pro-inflammatory, and extravasated fibrin (ogen) promotes inflammation (Alafuzoff et al., 1985; Paul et al., 2007; Zlokovic, 2008; Sengillo et al., 2013; Sweeney et al., 2016; Liebner et al., 2018). There was a positive correlation between the degree of the astrogliosis and degree of BBB leakage (Hasan-Olive et al., 2019c). Considering the microvascular changes seen in IIH, it should be noted that patients with IIH have a substantially increased cardiovascular risk (Fric et al., 2017; Adderley et al., 2019), and female patients a with IIH have higher prevalence of diabetes and arterial hypertension as compared to the general population (Fric et al., 2017).

Some limitations regarding comparisons between IIH and REF subjects should be noted. Gender differences between groups might play a minor role (female/male ratio 11/2 vs. 7/5). The IIH and REF groups also differed concerning BMI. Differences regarding the location of brain biopsy and minor differences in the layers assessed might as well play a role. Whether or not long-term treatment with acetazolamide or topiramate for IIH cause histological changes is to our knowledge unknown. In the epilepsy REF subjects, long-term treatment with anticonvulsants might have affected the histochemical findings. Abnormal changes in REF samples would rather be expected to reduced differences toward IIH. Even though our REF subjects were not healthy in all respects, the tissues samples were gathered from brain not affected by the primary diseases, but that anyway had to be removed as part of treatment.

Role of Neuro-Inflammation in IIH

While BBB leakage of blood proteins are pro-inflammatory and the patchy astrogliosis of IIH may be caused by inflammation, this study revealed no increased CD68 expression. CD68 is an indicator of microglia activation (Eide et al., 2016). Microglia is a glial cell type that may become activated in neurodegenerative diseases. Hence, serum and CSF of IIH subjects showed pro-inflammatory cytokines, including interleukin (IL)-1β, IL-8, and tumor necrosis factor (TNF)-α (Edwards et al., 2013; Samanci et al., 2017). In this context, the recent observations of anti-glial autoimmunity may have relevance. In multiple sclerosis patients, the immuno-modulating treatment daclizumab resulted in secondary GFAP autoimmunity (Luessi et al., 2018). A GFAP-antibody positive meningo-encephalitis is a steroid-responsive encephalitis that may be accompanied with meningitis, myelitis, and optic disc edema and evidence of inflammation in CSF (Fang et al., 2016; Flanagan et al., 2017; Shan et al., 2018). Some patients with this entity share similarities with IIH, such as visual impairment, papilledema, visual field defects, and intracranial hypertension (Flanagan et al., 2017; Chen et al., 2018). A subset of patients with IIH were positive toward GFAP-antibody, which might in some IIH subjects result in astrocyte dysfunction (Yetimler et al., 2021). Therefore, further focus on neuro-inflammation in IIH is warranted.

New Perspectives on the Pathophysiology of IIH

The authors suggest that the present observations provide new perspectives on the pathophysiology of IIH. In a possible cascade, capillary damage and BBB disruption may be primary events, possibly related to overweight, medication, or even genetic factors. Leakage of blood products, such as fibrin and fibrinogen, may induce inflammatory responses and astrogliosis that may affect capillary-mediated energy supply and peri-capillary clearance of metabolic waste causing energy failure and altered metabolism in astrocytes and neurons. Notably, astrogliosis in Patients with IIH may as well be triggered by obesity (Horvath et al., 2010; Hao et al., 2016). Altered BBB function and astrogliosis may in turn increase brain volume and impair the intracranial pressure-volume reserve (i.e., intracranial compliance) and even increase the ICP. In this model, venous compression and increased CSF pressure are secondary events.

In particular, the astrogliosis may be crucial for the cranial nerve dysfunction that characterizes IIH. Previously, the optic nerve path between the chiasm and the eye globe in adult humans was mapped (Hayreh, 1984) and demonstrated the tight-fitting passage of the optic nerve through the bony optic canal, a location where the nerve is susceptible to compression and distortion. Impairment of the glial cells that support the function of the optic nerve axons leads to axonal and eventually nerve cell body degeneration (Lee et al., 2012). The observed astrogliosis in IIH may therefore be accompanied with reduced glial metabolic support to the optic nerve, which may contribute to the impairment of visual function. We found in patients with IIH with visual impairment significantly higher GFAP immunoreactivity (and perivascular AQP4 expression) than in those without visual impairment (Eide et al., 2016). Furthermore, the increased optic nerve volume and subarachnoid CSF accumulation (Alperin et al., 2013) may be relieved by surgical fenestration of the optic sheath, which in some patients with IIH counteract the visual impairment (Feldon, 2007). Since all cranial nerves escape the cranial vault *via* openings in the scull base, minor volume increase might underlie the cranial nerve dysfunction characterizing IIH, e.g., visual failure, reduced olfactory function, tinnitus, and hearing loss (Jindal et al., 2009; Schmidt et al., 2012; Kunte et al., 2013; Bershad et al., 2014; Reitsma et al., 2015; Mollan et al., 2016).

With regard to the abnormal pulsatile ICP, characterizing IIH (Eide, 2021), dysfunction of the perivascular astrocytic end-feet may be crucial. Even though the water channel AQP4 covers about 50% of the astrocytic end-feet facing the basement membrane, the exact role of the AQP4 channel is unknown. Tentatively, it may be suggested that AQP4 enables variable influx of water to the end-feet processes, thereby regulating the volume and structure of the end-foot, which secondarily regulates the size of the inter-end-feet gaps. In turn, this enables variable efflux of molecules from the basement membrane to the interstitial space. Volume regulation of donut-shaped perivascular astrocytic end-feet may also enable a cushioning effect of the pulsatile pressure changes created by the capillary pulsations at the arterial (and venous) side. Hypothetically, dysfunctional astrocytic end-feet forming a donut around the capillaries may be a less efficient pressure pulsation absorber, thereby, explaining the elevated pulsatile ICP in patients with IIH. Furthermore, dysfunctional astrocytic end-feet may be a biological cause of the impaired pulsation absorber mechanisms and abnormal pulsatile ICP seen in other diseases, such as idiopathic normal pressure hydrocephalus (Park et al., 2012).

CONCLUSION

Our knowledge about IIH has evolved since its first description in 1937, with current pathophysiological thinking focusing primarily on the intracranial CSF and venous pressures. The results presented here suggest that events occurring at the glia-neuro-vascular interface are important players in IIH pathophysiology. The role of sinus vein stenosis is questionable. Understanding the underlying molecular events might pave the way toward more specific treatment of the IIH disease.

DATA AVAILABILITY STATEMENT

The original contributions presented in the study are included in the article/supplementary material, further inquiries can be directed to the corresponding author.

ETHICS STATEMENT

The studies involving human participants were reviewed and approved by the Regional Committee for Medical and Health Research Ethics of Health Region South-East, Norway (Approvals no. REK 2009/2060, 2012/1157, and 2011/2306). The

patients/participants provided their written informed consent to participate in this study.

AUTHOR CONTRIBUTIONS

PE: conceptualization, design, writing—original draft, supervision, administration, correspondence, and material requests. PE and H-AH: data analysis, review, editing, and approval of the final manuscript. Both authors contributed to the article and approved the submitted version.

FUNDING

The work involving histopathological assessment of brain tissue specimens was supported by grants from Health South-East, Norway (Grant Nos. 2012016 and 2016027).

REFERENCES

Adderley, N. J., Subramanian, A., Nirantharakumar, K., Yiangou, A., Gokhale, K. M., Mollan, S. P., et al. (2019). Association between idiopathic intracranial hypertension and risk of cardiovascular diseases in women in the United Kingdom. *JAMA Neurol.* 76, 1088–1098. doi: 10.1001/jamaneurol.2019.1812

Alafuzoff, I., Adolfsson, R., Grundke-Iqbal, I., and Winblad, B. (1985). Perivascular deposits of serum proteins in cerebral cortex in vascular dementia. *Acta Neuropathol.* 66, 292–298. doi: 10.1007/BF00690961

Alberts, B., Johnson, A., Lewis, J., Raff, M., Roberts, K., and Walter, P. (2014). *Molecular Biology of the Cell.* New York, NY: Garland Science.

Albuquerque, F. C., Dashti, S. R., Hu, Y. C., Newman, C. B., Teleb, M., McDougall, C. G., et al. (2011). Intracranial venous sinus stenting for benign intracranial hypertension: clinical indications, technique, and preliminary results. *World Neurosurg.* 75, 648-52; discussion 592–5. doi: 10.1016/j.wneu.2010.11.012

Alperin, N., Ranganathan, S., Bagci, A. M., Adams, D. J., Ertl-Wagner, B., Saraf-Lavi, E., et al. (2013). MRI evidence of impaired CSF homeostasis in obesity-associated idiopathic intracranial hypertension. *Am. J. Neuroradiol.* 34, 29–34. doi: 10.3174/ajnr.A3171

Amiry-Moghaddam, M., and Ottersen, O. P. (2003). The molecular basis of water transport in the brain. *Nat. Rev. Neurosci.* 4, 991–1001. doi: 10.1038/nrn1252

Andreone, B. J., Chow, B. W., Tata, A., Lacoste, B., Ben-Zvi, A., Bullock, K., et al. (2017). Blood-Brain barrier permeability is regulated by lipid transport-dependent suppression of caveolae-mediated transcytosis. *Neuron* 94, 581–594.e5. doi: 10.1016/j.neuron.2017.03.043

Ball, A. K., and Clarke, C. E. (2006). Idiopathic intracranial hypertension. *Lancet Neurol.* 5, 433–442. doi: 10.1016/S1474-4422(06)70442-2

Bershad, E. M., Urfy, M. Z., Calvillo, E., Tang, R., Cajavilca, C., Lee, A. G., et al. (2014). Marked olfactory impairment in idiopathic intracranial hypertension. *J. Neurol. Neurosur. Psychiatry* 85, 959–964. doi: 10.1136/jnnp-2013-307232

Blinzinger, K., and Kreutzberg, G. (1968). Displacement of synaptic terminals from regenerating motoneurons by microglial cells. *Cell Tissue Res.* 85, 145–157. doi: 10.1007/BF00325030

Bono, F., and Quattrone, A. (2007). CSF opening pressure: reference interval and the effect of body mass index. *Neurology* 68, 1439; author reply 40. doi: 10.1212/01.wnl.0000265411.84472.61

Boulay, A. C., Saubaméa, B., Adam, N., Chasseigneaux, S., Mazar,é N., Gilbert, A., et al. (2017). Translation in astrocyte distal processes sets molecular heterogeneity at the gliovascular interface. *Cell Discov.* 3, 17005. doi: 10.1038/celldisc.2017.5

Burkett, J. G., and Ailani, J. (2018). An up to date review of pseudotumor cerebri syndrome. *Curr. Neurol. Neurosci. Rep.* 18, 33. doi: 10.1007/s11910-018-0839-1

Chen, J. J., Aksamit, A. J., McKeon, A., Pittock, S. J., Weinshenker, B. G., Leavitt, J. A., et al. (2018). Optic disc edema in glial fibrillary acidic protein autoantibody-positive meningoencephalitis. *J. Neuroophthalmol.* 38, 276–281. doi: 10.1097/WNO.0000000000000593

Corbett, J. J., and Mehta, M. P. (1983). Cerebrospinal fluid pressure in normal obese subjects and patients with pseudotumor cerebri. *Neurology* 33, 1386–1388. doi: 10.1212/WNL.33.10.1386

Curry, W. T. Jr., Butler, W. E., and Barker, F. G. II. (2005). Rapidly rising incidence of cerebrospinal fluid shunting procedures for idiopathic intracranial hypertension in the United States, 1988-2002. *Neurosurgery* 57, 97–108; discussion 97. doi: 10.1227/01.NEU.0000163094.23923.E5

Edwards, L. J., Sharrack, B., Ismail, A., Tench, C. R., Gran, B., Dhungana, S., et al. (2013). Increased levels of interleukins 2 and 17 in the cerebrospinal fluid of patients with idiopathic intracranial hypertension. *Am. J. Clin. Exp. Immunol.* 2, 234–244.

Eftekhari, S., Westgate, C. S. J., Uldall, M. S., and Jensen, R. H. (2019). Preclinical update on regulation of intracranial pressure in relation to idiopathic intracranial hypertension. *Fluids Barriers CNS* 16, 35. doi: 10.1186/s12987-019-0155-4

Eid, T., Lee, T. S., Thomas, M. J., Amiry-Moghaddam, M., Bjornsen, L. P., Spencer, D. D., et al. (2005). Loss of perivascular aquaporin 4 may underlie deficient water and K+ homeostasis in the human epileptogenic hippocampus. *Proc. Natl. Acad. Sci. U.S.A.* 102, 1193–1198. doi: 10.1073/pnas.0409308102

Eide, P., and Brean, A. (2006). Lumbar cerebrospinal fluid pressure waves versus intracranial pressure waves in idiopathic normal pressure hydrocephalus. *Br. J. Neurosurg.* 20, 407–414. doi: 10.1080/02688690601047312

Eide, P. K. (2021). Abnormal intracranial pulse pressure amplitude despite normalized static intracranial pressure in idiopathic intracranial hypertension refractory to conservative medical therapy. *Life* 11, 537. doi: 10.3390/life11060537

Eide, P. K., Eidsvaag, V. A., Nagelhus, E. A., and Hansson, H. A. (2016). Cortical astrogliosis and increased perivascular aquaporin-4 in idiopathic intracranial hypertension. *Brain Res.* 1644, 161–175. doi: 10.1016/j.brainres.2016.05.024

Eide, P. K., and Hansson, H. A. (2018). Astrogliosis and impaired aquaporin-4 and dystrophin systems in idiopathic normal pressure hydrocephalus. *Neuropathol. Appl. Neurobiol.* 44, 474–490. doi: 10.1111/nan.12420

Eide, P. K., Hasan-Olive, M. M., Hansson, H. A., and Enger, R. (2021a). Increased occurrence of pathological mitochondria in astrocytic perivascular endfoot processes and neurons of idiopathic intracranial hypertension. *J. Neurosci. Res.* 99, 467–480. doi: 10.1002/jnr.24743

Eide, P. K., and Kerty, E. (2011). Static and pulsatile intracranial pressure in idiopathic intracranial hypertension. *Clin. Neurol. Neurosurg.* 113, 123–128. doi: 10.1016/j.clineuro.2010.10.008

Eide, P. K., Pripp, A. H., Ringstad, G., and Valnes, L. M. (2021b). Impaired glymphatic function in idiopathic intracranial hypertension. *Brain Commun.* 3, fcab043. doi: 10.1093/braincomms/fcab043

Eide, P. K., and Sorteberg, W. (2010). Diagnostic intracranial pressure monitoring and surgical management in idiopathic normal pressure hydrocephalus: a 6-year review of 214 patients. *Neurosurgery* 66, 80–91. doi: 10.1227/01.NEU.0000363408.69856.B8

Eidsvaag, V. A., Hansson, H. A., Heuser, K., Nagelhus, E. A., and Eide, P. K. (2018). Cerebral microvascular abnormalities in patients with idiopathic intracranial hypertension. *Brain Res.* 1686, 72–82. doi: 10.1016/j.brainres.2018.02.017

Erdo, F., Denes, L., and de Lange, E. (2017). Age-associated physiological and pathological changes at the blood-brain barrier: a review. *J. Cereb. Blood Flow Metab.* 37, 4–24. doi: 10.1177/0271678X16679420

Fang, B., McKeon, A., Hinson, S. R., Kryzer, T. J., Pittock, S. J., Aksamit, A. J., et al. (2016). Autoimmune glial fibrillary acidic protein astrocytopathy: a novel meningoencephalomyelitis. *JAMA Neurol.* 73, 1297–1307. doi: 10.1001/jamaneurol.2016.2549

Fargen, K. M. (2020). Idiopathic intracranial hypertension is not idiopathic: proposal for a new nomenclature and patient classification. *J. Neurointerv. Surg.* 12, 110–114. doi: 10.1136/neurintsurg-2019-015498

Farkas, E., and Luiten, P. G. (2001). Cerebral microvascular pathology in aging and Alzheimer's disease. *Prog. Neurobiol.* 64, 575–611. doi: 10.1016/S0301-0082(00)00068-X

Feldon, S. E. (2007). Visual outcomes comparing surgical techniques for management of severe idiopathic intracranial hypertension. *Neurosurg. Focus*. 23, E6. doi: 10.3171/FOC-07/11/E6

Fiebig, C., Keiner, S., Ebert, B., Schaffner, I., Jagasia, R., Lie, D. C., et al. (2019). Mitochondrial dysfunction in astrocytes impairs the generation of reactive astrocytes and enhances neuronal cell death in the cortex upon photothrombotic lesion. *Front. Mol. Neurosci*. 12, 40. doi: 10.3389/fnmol.2019.00040

Flanagan, E. P., Hinson, S. R., Lennon, V. A., Fang, B., Aksamit, A. J., Morris, P. P., et al. (2017). Glial fibrillary acidic protein immunoglobulin G as biomarker of autoimmune astrocytopathy: analysis of 102 patients. *Ann. Neurol*. 81, 298–309. doi: 10.1002/ana.24881

Fric, R., Pripp, A. H., and Eide, P. K. (2017). Cardiovascular risk factors in chiari malformation and idiopathic intracranial hypertension. *Brain Behav*. 7, e00677. doi: 10.1002/brb3.677

Friedman, D. I., Liu, G. T., and Digre, K. B. (2013). Revised diagnostic criteria for the pseudotumor cerebri syndrome in adults and children. *Neurology* 81, 1159–1165. doi: 10.1212/WNL.0b013e3182a55f17

Friedman, D. I., Quiros, P. A., Subramanian, P. S., Mejico, L. J., Gao, S., McDermott, M., et al. (2017). Headache in idiopathic intracranial hypertension: findings from the idiopathic intracranial hypertension treatment trial. *Headache* 57, 1195–1205. doi: 10.1111/head.13153

Friesner, D., Rosenman, R., Lobb, B. M., and Tanne, E. (2011). Idiopathic intracranial hypertension in the USA: the role of obesity in establishing prevalence and healthcare costs. *Obes. Rev*. 12, e372–e380. doi: 10.1111/j.1467-789X.2010.00799.x

Giacomello, M., and Pellegrini, L. (2016). The coming of age of the mitochondria-ER contact: a matter of thickness. *Cell Death Differ*. 23, 1417–1427. doi: 10.1038/cdd.2016.52

Haddad-Tovolli, R., Dragano, N. R. V., Ramalho, A. F. S., and Velloso, L. A. (2017). Development and function of the blood-brain barrier in the context of metabolic control. *Front. Neurosci*. 11, 224. doi: 10.3389/fnins.2017.00224

Hao, S., Dey, A., Yu, X., and Stranahan, A. M. (2016). Dietary obesity reversibly induces synaptic stripping by microglia and impairs hippocampal plasticity. *Brain Behav. Immun*. 51, 230–239. doi: 10.1016/j.bbi.2015.08.023

Hasan-Olive, M. M., Enger, R., Hansson, H. A., Nagelhus, E. A., and Eide, P. K. (2019a). Loss of perivascular aquaporin-4 in idiopathic normal pressure hydrocephalus. *Glia* 67, 91–100. doi: 10.1002/glia.23528

Hasan-Olive, M. M., Enger, R., Hansson, H. A., Nagelhus, E. A., and Eide, P. K. (2019b). Pathological mitochondria in neurons and perivascular astrocytic end-feet of idiopathic normal pressure hydrocephalus patients. *Fluids Barriers CNS* 16, 39. doi: 10.1186/s12987-019-0160-7

Hasan-Olive, M. M., Hansson, H. A., Enger, R., Nagelhus, E. A., and Eide, P. K. (2019c). Blood-Brain barrier dysfunction in idiopathic intracranial hypertension. *J. Neuropathol. Exp. Neurol*. 78, 808–818. doi: 10.1093/jnen/nlz063

Hayreh, S. S. (1984). The sheath of the optic nerve. *Ophthalmologica* 189, 54–63. doi: 10.1159/000309386

Hermes, S. M., Miller, N. R., Waslo, C. S., Benes, S. C., and Tanne, E. (2020). Mortality among patients with idiopathic intracranial hypertension enrolled in the IH registry. *Neurology* 95, e921–e929. doi: 10.1212/WNL.0000000000009312

Heuser, K., Eid, T., Lauritzen, F., Thoren, A. E., Vindedal, G. F., Tauboll, E., et al. (2012). Loss of perivascular Kir4.1 potassium channels in the sclerotic hippocampus of patients with mesial temporal lobe epilepsy. *J. Neuropathol. Exp. Neurol*. 71, 814–825. doi: 10.1097/NEN.0b013e318267b5af

Hollenbeck, P. J. (2005). Mitochondria and neurotransmission: evacuating the synapse. *Neuron* 47, 331–333. doi: 10.1016/j.neuron.2005.07.017

Horvath, T. L., Sarman, B., Garcia-Caceres, C., Enriori, P. J., Sotonyi, P., Shanabrough, M., et al. (2010). Synaptic input organization of the melanocortin system predicts diet-induced hypothalamic reactive gliosis and obesity. *Proc. Natl. Acad. Sci. U.S.A*. 107, 14875–14880. doi: 10.1073/pnas.1004282107

Howarth, C. (2014). The contribution of astrocytes to the regulation of cerebral blood flow. *Front. Neurosci*. 8, 103. doi: 10.3389/fnins.2014.00103

Iliff, J. J., Wang, M., Liao, Y., Plogg, B. A., Peng, W., Gundersen, G. A., et al. (2012). A paravascular pathway facilitates CSF flow through the brain parenchyma and the clearance of interstitial solutes, including amyloid beta. *Sci. Transl. Med*. 4, 147ra11. doi: 10.1126/scitranslmed.3003748

Jindal, M., Hiam, L., Raman, A., and Rejali, D. (2009). Idiopathic intracranial hypertension in otolaryngology. *Eur. Arch. Otorhinolaryngol*. 266, 803–806. doi: 10.1007/s00405-009-0973-0

Kalyvas, A., Neromyliotis, E., Koutsarnakis, C., Komaitis, S., Drosos, E., Skandalakis, G. P., et al. (2020). A systematic review of surgical treatments of idiopathic intracranial hypertension (IIH). *Neurosurg. Rev*. 44, 773–792. doi: 10.1007/s10143-020-01288-1

Kesler, A., and Gadoth, N. (2001). Epidemiology of idiopathic intracranial hypertension in Israel. *J. Neuroophthalmol*. 21, 12–14. doi: 10.1097/00041327-200103000-00003

Kesler, A., Stolovic, N., Bluednikov, Y., and Shohat, T. (2014). The incidence of idiopathic intracranial hypertension in Israel from 2005 to 2007: results of a nationwide survey. *Eur. J. Neurol*. 21, 1055–1059. doi: 10.1111/ene.12442

Kharkar, S., Hernandez, R., Batra, S., Metellus, P., Hillis, A., Williams, M. A., et al. (2011). Cognitive impairment in patients with pseudotumor cerebri syndrome. *Behav. Neurol*. 24, 143–148. doi: 10.1155/2011/630475

Kisler, K., Nelson, A. R., Rege, S. V., Ramanathan, A., Wang, Y., Ahuja, A., et al. (2017). Pericyte degeneration leads to neurovascular uncoupling and limits oxygen supply to brain. *Nat. Neurosci*. 20, 406–416. doi: 10.1038/nn.4489

Kleinschmidt, J. J., Digre, K. B., and Hanover, R. (2000). Idiopathic intracranial hypertension. Relationship to depression, anxiety, and quality of life. *Am. J. Ophthalmol*. 129, 831. doi: 10.1016/S0002-9394(00)00507-9

Kunte, H., Schmidt, F., Kronenberg, G., Hoffmann, J., Schmidt, C., Harms, L., et al. (2013). Olfactory dysfunction in patients with idiopathic intracranial hypertension. *Neurology* 81, 379–382. doi: 10.1212/WNL.0b013e31829c5c9d

Langer, J., Gerkau, N. J., Derouiche, A., Kleinhans, C., Moshrefi-Ravasdjani, B., Fredrich, M., et al. (2017). Rapid sodium signaling couples glutamate uptake to breakdown of ATP in perivascular astrocyte end-feet. *Glia* 65, 293–308. doi: 10.1002/glia.23092

Leal, N. S., Dentoni, G., Schreiner, B., Kamarainen, O. P., Partanen, N., Herukka, S. K., et al. (2018). Alterations in mitochondria-endoplasmic reticulum connectivity in human brain biopsies from idiopathic normal pressure hydrocephalus patients. *Acta Neuropathol. Commun*. 6, 102. doi: 10.1186/s40478-018-0605-2

Lee, Y., Morrison, B. M., Li, Y., Lengacher, S., Farah, M. H., Hoffman, P. N., et al. (2012). Oligodendroglia metabolically support axons and contribute to neurodegeneration. *Nature* 487, 443–448. doi: 10.1038/nature11314

Liebner, S., Dijkhuizen, R. M., Reiss, Y., Plate, K. H., Agalliu, D., and Constantin, G. (2018). Functional morphology of the blood-brain barrier in health and disease. *Acta Neuropathol*. 135, 311–336. doi: 10.1007/s00401-018-1815-1

Liwnicz, B. H., Leach, J. L., Yeh, H. S., and Privitera, M. (1990). Pericyte degeneration and thickening of basement membranes of cerebral microvessels in complex partial seizures: electron microscopic study of surgically removed tissue. *Neurosurgery* 26, 409–420. doi: 10.1227/00006123-199003000-00006

Luessi, F., Engel, S., Spreer, A., Bittner, S., and Zipp, F. (2018). GFAPα IgG-associated encephalitis upon daclizumab treatment of MS. *Neurol. Neuroimmunol. Neuroinflamm*. 5, e481. doi: 10.1212/NXI.0000000000000481

Mathiisen, T. M., Lehre, K. P., Danbolt, N. C., and Ottersen, O. P. (2010). The perivascular astroglial sheath provides a complete covering of the brain microvessels: an electron microscopic 3D reconstruction. *Glia* 58, 1094–1103. doi: 10.1002/glia.20990

McGirt, M. J., Woodworth, G., Thomas, G., Miller, N., Williams, M., and Rigamonti, D. (2004). Cerebrospinal fluid shunt placement for pseudotumor cerebri-associated intractable headache: predictors of treatment response and an analysis of long-term outcomes. *J. Neurosurg*. 101, 627–632. doi: 10.3171/jns.2004.101.4.0627

Mollan, S. P., Aguiar, M., Evison, F., Frew, E., and Sinclair, A. J. (2019). The expanding burden of idiopathic intracranial hypertension. *Eye* 33, 478–485. doi: 10.1038/s41433-018-0238-5

Mollan, S. P., Ali, F., Hassan-Smith, G., Botfield, H., Friedman, D. I., and Sinclair, A. J. (2016). Evolving evidence in adult idiopathic intracranial hypertension: pathophysiology and management. *J. Neurol. Neurosurg. Psychiatry* 87, 982–992. doi: 10.1136/jnnp-2015-311302

Mollan, S. P., Davies, B., Silver, N. C., Shaw, S., Mallucci, C. L., Wakerley, B. R., et al. (2018). Idiopathic intracranial hypertension: consensus guidelines on management. *J. Neurol. Neurosurg. Psychiatry* 89, 1088–1100. doi: 10.1136/jnnp-2017-317440

Montagne, A., Zhao, Z., and Zlokovic, B. V. (2017). Alzheimer's disease: a matter of blood-brain barrier dysfunction? *J. Exp. Med.* 214, 3151–3169. doi: 10.1084/jem.20171406

Mulligan, S. J., and MacVicar, B. A. (2004). Calcium transients in astrocyte end-feet cause cerebrovascular constrictions. *Nature* 431, 195–199. doi: 10.1038/nature02827

Nagelhus, E. A., and Ottersen, O. P. (2013). Physiological roles of aquaporin-4 in brain. *Physiol. Rev.* 93, 1543–1562. doi: 10.1152/physrev.00011.2013

Nedergaard, M., and Goldman, S. A. (2020). Glymphatic failure as a final common pathway to dementia. *Science* 370, 50–56. doi: 10.1126/science.abb8739

Oberheim, N. A., Goldman, S. A., and Nedergaard, M. (2012). Heterogeneity of astrocytic form and function. *Methods Mol. Biol.* 814, 23–45. doi: 10.1007/978-1-61779-452-0_3

Park, E. H., Eide, P. K., Zurakowski, D., and Madsen, J. R. (2012). Impaired pulsation absorber mechanism in idiopathic normal pressure hydrocephalus: laboratory investigation. *J. Neurosurg.* 117, 1189–1196. doi: 10.3171/2012.9.JNS121227

Paul, J., Strickland, S., and Melchor, J. P. (2007). Fibrin deposition accelerates neurovascular damage and neuroinflammation in mouse models of Alzheimer's disease. *J. Exp. Med.* 204, 1999–2008. doi: 10.1084/jem.20070304

Piper, R. J., Kalyvas, A. V., Young, A. M., Hughes, M. A., Jamjoom, A. A., and Fouyas, I. P. (2015). Interventions for idiopathic intracranial hypertension. *Cochrane Database Syst. Rev.* 2015, CD003434. doi: 10.1002/14651858.CD003434.pub3

Raoof, N., Sharrack, B., Pepper, I. M., and Hickman, S. J. (2011). The incidence and prevalence of idiopathic intracranial hypertension in Sheffield, UK. *Eur. J. Neurol.* 18, 1266–1268. doi: 10.1111/j.1468-1331.2011.03372.x

Reitsma, S., Stokroos, R., Weber, J. W., and van Tongeren, J. (2015). Pediatric idiopathic intracranial hypertension presenting with sensorineural hearing loss. *Ann. Otol. Rhinol. Laryngol.* 124, 996–1001. doi: 10.1177/0003489415591999

Sagare, A. P., Bell, R. D., Zhao, Z., Ma, Q., Winkler, E. A., Ramanathan, A., et al. (2013). Pericyte loss influences Alzheimer-like neurodegeneration in mice. *Nat. Commun.* 4, 2932. doi: 10.1038/ncomms3932

Samanci, B., Samanci, Y., Tüzün, E., Altiokka-Uzun, G., Ekizoglu, E., Içöz, S., et al. (2017). Evidence for potential involvement of pro-inflammatory adipokines in the pathogenesis of idiopathic intracranial hypertension. *Cephalalgia* 37, 525–531. doi: 10.1177/0333102416650705

Schmidt, C., Wiener, E., Hoffmann, J., Klingebiel, R., Schmidt, F., Hofmann, T., et al. (2012). Structural olfactory nerve changes in patients suffering from idiopathic intracranial hypertension. *PLoS ONE* 7, e35221. doi: 10.1371/journal.pone.0035221

Sengillo, J. D., Winkler, E. A., Walker, C. T., Sullivan, J. S., Johnson, M., and Zlokovic, B. V. (2013). Deficiency in mural vascular cells coincides with blood-brain barrier disruption in Alzheimer's disease. *Brain Pathol.* 23, 303–310. doi: 10.1111/bpa.12004

Shan, F., Long, Y., and Qiu, W. (2018). Autoimmune glial fibrillary acidic protein astrocytopathy: a review of the literature. *Front. Immunol.* 9, 2802. doi: 10.3389/fimmu.2018.02802

Sinclair, A. J., Burdon, M. A., Nightingale, P. G., Ball, A. K., Good, P., Matthews, T. D., et al. (2010). Low energy diet and intracranial pressure in women with idiopathic intracranial hypertension: prospective cohort study. *BMJ* 341, c2701. doi: 10.1136/bmj.c2701

Stacchiotti, A., Favero, G., Lavazza, A., Garcia-Gomez, R., Monsalve, M., and Rezzani, R. (2018). Perspective: mitochondria-ER contacts in metabolic cellular stress assessed by microscopy. *Cells* 8, 5. doi: 10.3390/cells8010005

Sweeney, M. D., Ayyadurai, S., and Zlokovic, B. V. (2016). Pericytes of the neurovascular unit: key functions and signaling pathways. *Nat. Neurosci.* 19, 771–783. doi: 10.1038/nn.4288

Sweeney, M. D., Sagare, A. P., and Zlokovic, B. V. (2018). Blood-brain barrier breakdown in Alzheimer disease and other neurodegenerative disorders. *Nat. Rev. Neurol.* 14, 133–150. doi: 10.1038/nrneurol.2017.188

Torbey, M. T., Geocadin, R. G., Razumovsky, A. Y., Rigamonti, D., and Williams, M. A. (2004). Utility of CSF pressure monitoring to identify idiopathic intracranial hypertension without papilledema in patients with chronic daily headache. *Cephalalgia* 24, 495–502. doi: 10.1111/j.1468-2982.2004.00688.x

van Vliet, E. A., Aronica, E., and Gorter, J. A. (2015). Blood-brain barrier dysfunction, seizures and epilepsy. *Semin. Cell Dev. Biol.* 38, 26–34. doi: 10.1016/j.semcdb.2014.10.003

Verkhratsky, A., and Butt, A. (2013). *Glial Physiology and Pathophysiology*. Oxford: Wiley-Blackwell. doi: 10.1002/9781118402061

Wakerley, B. R., Mollan, S. P., and Sinclair, A. J. (2020). Idiopathic intracranial hypertension: update on diagnosis and management. *Clin. Med.* 20, 384–388. doi: 10.7861/clinmed.2020-0232

Whiteley, W., Al-Shahi, R., Warlow, C. P., Zeidler, M., and Lueck, C. J. (2006). CSF opening pressure: reference interval and the effect of body mass index. *Neurology* 67, 1690–1691. doi: 10.1212/01.wnl.0000242704.60275.e9

Winkler, E. A., Sagare, A. P., and Zlokovic, B. V. (2014). The pericyte: a forgotten cell type with important implications for Alzheimer's disease? *Brain Pathol.* 24, 371–386. doi: 10.1111/bpa.12152

Winters, H. V., and Kleinschmidt-Demasters, B. K. (2015). "General pathology of the central nervous system," in *Greenfield's Neuropathology, 9th edn*, eds S. Love, H. Budka, J. W. Ironside, A. Perry (London: CRC Press), 1–58.

Yetimler, B., Tzartos, J., Sengül, B., Dursun E, Ulukan, Ç., Karagiorgou, K., et al. (2021). Serum glial fibrillary acidic protein (GFAP)-antibody in idiopathic intracranial hypertension. *Int. J. Neurosci.* 131, 775–779. doi: 10.1080/00207454.2020.1758084

Yri, H. M., Fagerlund, B., Forchhammer, H. B., and Jensen, R. H. (2014). Cognitive function in idiopathic intracranial hypertension: a prospective case-control study. *BMJ Open* 4, e004376. doi: 10.1136/bmjopen-2013-004376

Yu, L., and Yu, Y. (2017). Energy-efficient neural information processing in individual neurons and neuronal networks. *J. Neurosci. Res.* 95, 2253–2266. doi: 10.1002/jnr.24131

Zlokovic, B. V. (2008). The blood-brain barrier in health and chronic neurodegenerative disorders. *Neuron* 57, 178–201. doi: 10.1016/j.neuron.2008.01.003

Conflict of Interest: Figure 3 is from Sensometrics analytical software, which is used for digital recording of continuous pressure (ICP, ABP, and CSF pressure) signals. PE has a financial interest in the software company, dPCom AS, which manufactures this software.

The remaining author declares that the research was conducted in the absence of any commercial or financial relationships that could be construed as a potential conflict of interest.

Publisher's Note: All claims expressed in this article are solely those of the authors and do not necessarily represent those of their affiliated organizations, or those of the publisher, the editors and the reviewers. Any product that may be evaluated in this article, or claim that may be made by its manufacturer, is not guaranteed or endorsed by the publisher.

frontiers | Frontiers in Molecular Neuroscience

TYPE Original Research
PUBLISHED 02 September 2022
DOI 10.3389/fnmol.2022.964632

OPEN ACCESS

EDITED BY
Adjanie Patabendige,
Edge Hill University, United Kingdom

REVIEWED BY
Li Zhao,
Zhejiang University, China
Harald E. Möller,
Max Planck Institute for Human Cognitive and Brain Sciences, Germany

*CORRESPONDENCE
Charith Perera
c.perera@ucl.ac.uk

SPECIALTY SECTION
This article was submitted to Brain Disease Mechanisms, a section of the journal Frontiers in Molecular Neuroscience

RECEIVED 08 June 2022
ACCEPTED 02 August 2022
PUBLISHED 02 September 2022

CITATION
Perera C, Tolomeo D, Baker RR, Ohene Y, Korsak A, Lythgoe MF, Thomas DL and Wells JA (2022) Investigating changes in blood-cerebrospinal fluid barrier function in a rat model of chronic hypertension using non-invasive magnetic resonance imaging. *Front. Mol. Neurosci.* 15:964632. doi: 10.3389/fnmol.2022.964632

Investigating changes in blood-cerebrospinal fluid barrier function in a rat model of chronic hypertension using non-invasive magnetic resonance imaging

Charith Perera[1]*, Daniele Tolomeo[1], Rebecca R. Baker[1], Yolanda Ohene[2,3], Alla Korsak[4], Mark F. Lythgoe[1], David L. Thomas[5,6,7] and Jack A. Wells[1]

[1]Division of Medicine, UCL Centre for Advanced Biomedical Imaging, University College London, London, United Kingdom, [2]Division of Neuroscience and Experimental Psychology, University of Manchester, Manchester, United Kingdom, [3]Geoffrey Jefferson Brain Research Centre, University of Manchester, Manchester, United Kingdom, [4]Centre for Cardiovascular and Metabolic Neuroscience, Neuroscience, Physiology and Pharmacology, University College London, London, United Kingdom, [5]Neuroradiological Academic Unit, Department of Brain Repair and Rehabilitation, UCL Queen Square Institute of Neurology, London, United Kingdom, [6]Dementia Research Centre, UCL Queen Square Institute of Neurology, London, United Kingdom, [7]Wellcome Centre for Human Neuroimaging, UCL Queen Square Institute of Neurology, University College London, London, United Kingdom

Chronic hypertension is a major risk factor for the development of neurodegenerative disease, yet the etiology of hypertension-driven neurodegeneration remains poorly understood. Forming a unique interface between the systemic circulation and the brain, the blood-cerebrospinal fluid barrier (BCSFB) at the choroid plexus (CP) has been proposed as a key site of vulnerability to hypertension that may initiate downstream neurodegenerative processes. However, our ability to understand BCSFB's role in pathological processes has, to date, been restricted by a lack of non-invasive functional measurement techniques. In this work, we apply a novel Blood-Cerebrospinal Fluid Barrier Arterial Spin Labeling (BCSFB-ASL) Magnetic resonance imaging (MRI) approach with the aim of detecting possible derangement of BCSFB function in the Spontaneous Hypertensive Rat (SHR) model using a non-invasive, translational technique. SHRs displayed a 36% reduction in BCSFB-mediated labeled arterial water delivery into ventricular cerebrospinal fluid (CSF), relative to normotensive controls, indicative of down-regulated choroid plexus function. This was concomitant with additional changes in brain fluid biomarkers, namely ventriculomegaly and changes in CSF composition, as measured by T1 lengthening. However, cortical cerebral blood flow (CBF) measurements, an imaging biomarker of cerebrovascular health, revealed no measurable change between the groups. Here, we provide the first demonstration of BCSFB-ASL in the rat brain, enabling non-invasive

assessment of BCSFB function in healthy and hypertensive rats. Our data highlights the potential for BCSFB-ASL to serve as a sensitive early biomarker for hypertension-driven neurodegeneration, in addition to investigating the mechanisms relating hypertension to neurodegenerative outcomes.

KEYWORDS

choroid plexus (CP), arterial spin labelling (ASL), hypertension, blood-cerebrospinal fluid barrier (BCSFB), spontaneous hypertensive rat (SHR), MRI, preclinical studies, imaging

Introduction

The latest figures provided by the World Health Organization estimate that 1.28 billion adults suffer from hypertension (Zhou et al., 2021). Hypertension is an established risk factor for the onset of neurodegenerative conditions such as Alzheimer's Disease (AD) (Iadecola et al., 2016). However, there is a limited understanding of the complex changes occurring in the brain under systemic hypertension that lead to downstream neurodegeneration. Moreover, as well as building understanding, it is important to also work toward development of biomarkers for the early detection of brain pathology as a consequence of sustained hypertension.

Disruption of the cerebral vasculature has been well established to originate from the effects of hypertension, e.g., impairment of blood brain barrier (BBB) integrity and reductions in cerebral blood flow (CBF) (Wardlaw et al., 2003). However, the responsibility of mediating the complex interplay between blood and the brain, a key mechanism for central nervous system (CNS) homeostasis, is not limited to only the role of the BBB alone. This responsibility is also attributed to the blood-cerebrospinal fluid barrier (BCSFB) at the choroid plexus (CP)—a relatively understudied barrier within the brain's cerebrospinal fluid-filled ventricles (Lun et al., 2015) which display a selective vulnerability toward hypertension-driven damage. Prior evidence points to the extent of hypertension-induced damage being more pronounced at the BCSFB than the BBB, which manifests as increased BCSFB leakiness and an altered cerebrospinal fluid (CSF) homeostasis in a manner akin to that observed in AD (Al-Sarraf and Philip, 2003; Castañeyra-Perdomo et al., 2010). The limited study of BCSFB functionality *in-vivo*, due to the reliance on invasive methodologies (Prinzen and Bassingthwaighte, 2000; Hubert et al., 2019), has hindered exploration of pathophysiological changes at the BCSFB that may catalyze neurodegenerative processes, particularly under hypertension.

We have recently developed a translational Magnetic resonance imaging (MRI) technique for the non-invasive assessment of BCSFB function, known as "BCSFB Arterial Spin Labeling (ASL)" (Evans et al., 2020). BCSFB-ASL quantifies the rate of BCSFB-mediated delivery of endogenous arterial blood water to ventricular CSF, thereby providing a surrogate measure of BCSFB function (Evans et al., 2020; Perera et al., 2021). This non-invasive approach may help to better elucidate the BCSFB's role in the onset of downstream neurodegeneration in the hypertensive brain. Here we present the application of this technique to probe BCSFB functional changes under systemic hypertension, as well as demonstrating the first application in the rat brain.

Spontaneous hypertensive rats (SHR) provide a well-characterized model of human hypertension and present with markers of neurodegeneration such as amyloid-β accumulation, cognitive impairment, cerebral atrophy, BBB dysfunction, and brain fluid dysregulation (Kaiser et al., 2014; Mestre et al., 2018; Wang et al., 2018; Mortensen et al., 2019; Naessens et al., 2020). Using invasive methods, previous studies have detected functional irregularities at the BCSFB locus in the SHR model (Al-Sarraf and Philip, 2003; Castañeyra-Perdomo et al., 2010; Gonzalez-Marrero et al., 2022). Employing a non-invasive standard-ASL and BCSFB-ASL approach, we investigated whether the impairment of BCSFB function is detectable using non-invasive MRI techniques in the SHR model, relative to Wistar Kyoto (WKY) controls. Additionally, we quantified changes in cortical CBF—a conventional biomarker for cerebrovascular health (Hays et al., 2016)—as well as obtaining measures of $T1_{CSF}$ and ventricular volumes to assess CSF homeostasis. We hypothesize that non-invasive measures of BCSFB function will reveal its derangement under systemic hypertension.

Materials and methods

Animal preparation

All animal procedures were performed under the UK Home Office Act (Scientific Procedures, 1986). SHR and WKY normotensive rats (provided by Envigo) were used in our study

(male, $n = 6$ in each group). A pilot study for the optimization of parameters was conducted using the WKY subjects at 10 weeks old. Following parameter optimization, the final data collection was conducted with SHRs and WKYs at 21 weeks old. Body weight measurements at the time of scanning were: WKY 348 ± 5.0 g vs. SHR 369 ± 9.5 g.

Prior to commencing MRI acquisitions, subjects underwent anesthetic induction using 4% isoflurane in 0.8 L/min medical air and 0.2 L/min O_2. Following induction and weighing, rats were placed into the MRI cradle with bite bar, nose cone and ear bars to ensure a well secured position of the rat head to minimize motion during the data acquisition. Eye ointment was also applied to prevent drying.

A scavenger pump was placed inside the magnet bore to prevent isoflurane build-up. Anesthesia was maintained during the acquisition by reducing isoflurane concentration to 2% in 0.4 L/min room air and 0.1 L/min O_2.

Temperature and breathing rate were monitored throughout all the experiments using a rectal probe and a respiration pad (SA Instruments). Rat temperature was maintained at 37 ± 0.5°C using heated water tubing during data acquisition.

Magnetic resonance imaging protocols

MRI protocols were applied to inform on BCSFB function, CSF homeostasis, and cerebrovascular health (**Figure 1**). Images were acquired on a 9.4 T Bruker imaging system (BioSpec 94/20 USR) with a horizontal bore and 440 mT/m gradient set with an outer/ inner diameter of 205 mm/116 mm, respectively (BioSpec B-GA 12S2), 86 mm volume coil and a four-channel array rat brain surface coil (RAPID Biomedical GmbH) for the transmission and the reception of the RF signal, respectively. The center of the volume coil was positioned caudally 3 cm from the iso-center of the magnet to ensure a good labeling efficiency of the global inversion pulse during the flow-alternating inversion recovery (FAIR)-ASL acquisition.

Anatomical reference scans

A T2-TurboRARE sequence (fast-spin echo, Paravision v6.0.1) was used to collect sagittal and coronal anatomical reference images to clearly visualize the location of the major CSF compartments in the rat brain. Sequence parameters were: (field of view (FOV) = 30 mm × 30 mm; matrix size = 256 × 256; RARE factor = 8; effective echo time (TE) = 33 ms; repetition time (TR) = 2,500 ms.

Sagittal anatomical reference images (12 × 1 mm slices) were used to position the axial anatomical reference imaging slice and the ASL imaging slices. Coronal anatomical reference images (12 × 0.4 mm slices, 4.8 mm total) were manually positioned to align with the caudal region of the lateral ventricles. These coronal images were subsequently manually segmented to provide an estimate of lateral ventricular volume for each of the subjects.

Flow-alternating inversion recovery-arterial spin labeling scans using a multi-inflow time approach

Each ASL data set was acquired using a FAIR sequence with a single slice, single shot spin echo—echo planar imaging readout, 20 mm slice-selective width, and a global labeling pulse, across all the experiments.

Parameters for standard-ASL: 2.4 mm slice thickness, matrix size = 32 × 32, FOV = 32 mm × 32 mm, 4 dummy scans, TE = 20 ms. Inflow times (TI) = (200, 500, 1,000, 1,500, 2,000, 3,000, 4,000, 6,000 ms), using TR = 12,000 ms, 5 repetitions per TI.

Parameters for BCSFB-ASL: single slice, 4.8 mm slice thickness, matrix size = 32 × 32, FOV = 32 mm × 32 mm, 6 dummy scans, TE = 220 ms. TI = (200, 750, 1,500, 2,750, 4,000, 5,000, 6,000 ms), using recovery time = 12,000 ms, 10 repetitions per TI.

Importantly, the ASL imaging slice was manually positioned to align with the caudal end of the lateral ventricles, as it has been previously shown to be the predominant region within the lateral ventricles occupied by the CP (Lein et al., 2007). The large slice thickness was chosen to ensure that the slice contained the majority of the lateral ventricles (excluding the more rostral sections which are known to not contain choroid plexus tissue). Therefore, as described in our recent work, our measurements of BCSFB function are concentrated to CP within the lateral ventricles and not the 3rd and 4th ventricles (Evans et al., 2020; Perera et al., 2021).

Image processing and analysis for relative arterial spin labeling quantification

When analyzing standard-ASL images obtained with TE = 20 ms, a single region of interest (ROI) was drawn for each subject across the cortex of the brain using a non-selective (control) FAIR image, and the mean voxel signal was calculated across the ROI. For each ASL image pair, the non-selective mean ROI value (M_c) was subtracted from the slice-selective (labeled) mean ROI value to provide the perfusion-weighted signal ΔM.

For the BCSFB-ASL technique, our approach was to take the sum of the BCSFB—ASL signal in the lateral ventricles (**Supplementary Figure 1**). This would enable the measurement of the total amount of labeled arterial-blood-water delivery to ventricular CSF, thereby yielding an overall measure of total

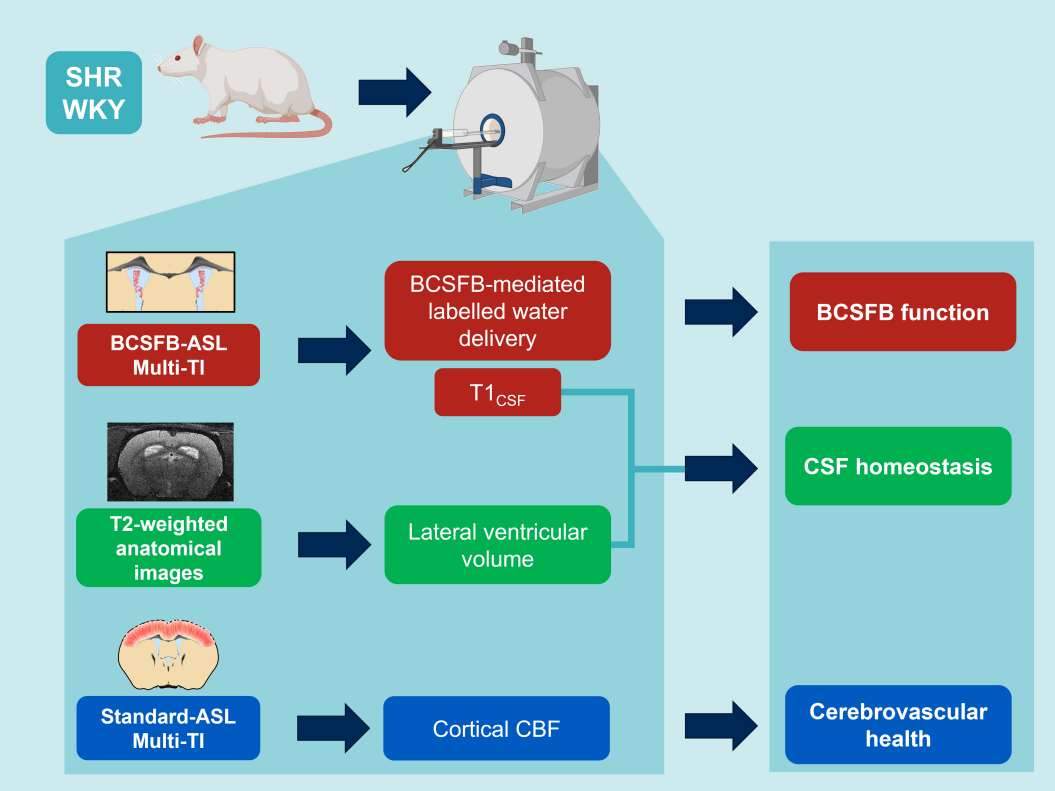

FIGURE 1
MRI protocols: non-invasive multi-inflow time (multi-TI) arterial spin labeling (ASL) and structural, T2-weighted MRI to inform on hypertension-induced impairment of BCSFB function, CSF homeostasis and cerebrovascular health (created with Biorender.com).

BSCFB function in the lateral ventricles. Therefore, for the BCSFB-ASL images, two 3 × 3 voxel ROIs (18 voxels in total, ROI volume = 86.4 mm^3) were positioned on a slice-selective image, overlaid with the position of the lateral ventricles (Perera et al., 2021). As with the standard-ASL analysis, the combined ROI average signals were subtracted in a pairwise fashion to provide ΔM values, with an added step of subject-wise ventricular volume normalisation to provide volume-normalised, equilibrium magnetization ($M0_{corr}$, equation 1). This correction accounts for the total ventricular volume (quantified from T2-weighted anatomical images) and the ventricular ROI volume (i.e., from the 12 voxels used for the ROI from the low resolution functional data) (Evans et al., 2020). This step is critical for the accurate quantification of the total amount of BCSFB-mediated water delivery; the calculated M0 will be highly dependent on ventricle size due to partial volume effects in the low resolution ASL images (Evans et al., 2020).

$$M0_{corr} = M0 \times \frac{Total\ ventricular\ volume}{Ventricular\ ROI\ volume}$$

Equation 1—M0 volume correction for BCSFB-ASL data.

Repeated measures of ΔM and M_c values were averaged for each TI providing [TI, ΔM] and [TI, M_c] datasets. The [TI, M_c] data were fitted to a simple inversion recovery curve, permitting the extraction of T1 and M0 for each subject. The T1 of the CSF and of cortical brain tissue was calculated from the control images acquired at TE = 220 and 20 ms, respectively. The [TI, ΔM] values were then fit to the relevant Buxton model. The subject-wise T1 ($T1_{CSF}$ for BCSFB-ASL or $T1_{cortex}$ for standard ASL) and M0 (or $M0_{corr}$ for BCSFB-ASL) values extracted from the IR fittings were used in the Buxton model as inputs when calculating CBF and BCSFB-mediated water delivery values for each subject (Evans et al., 2020). For the quantification of cortical CBF, a single-compartment Buxton kinetic model approach was used (Buxton et al., 1998), with BCSFB-ASL requiring a 2-compartment adaptation of this model (Alsop and Detre, 1996; Wang et al., 2002; Evans et al., 2020). The latter adaptation aims to more accurately account for transit effects and intraluminal spins, ultimately allowing for the model to be utilized to describe the delivery of labeled blood water into the CSF (compartment), as opposed to extra-vascular brain tissue in standard-ASL.

The outputs of the model fittings provided subject-wise quantitative values for cortical perfusion (standard-ASL images at TE = 20 ms), and rates of BCSFB-mediated water delivery (BCSFB-ASL images at TE = 220 ms). We report the group average of the individually extracted values of BCSFB-mediated water delivery rate, cortical CBF, and $T1_{CSF}$.

Taking the average rate of BCSFB-mediated labeled water delivery to the lateral ventricles and incorporating the total size of the functional voxels (86.4mm^3) returns a total BCSFB-labeled water delivery rate to the lateral ventricles.

For the purpose of visual comparison of the group-averaged kinetic curves (e.g., **Figures 2B,D**), we averaged the values of ΔM/M0 for standard-ASL, or ΔM/M0$_{corr}$ for BCSFB-ASL.

Pilot study for parameter optimization

The pilot study in 10-week-old WKY controls (n = 6) were fit to a 2-compartment Buxton Kinetic model to extract 3 variables: the rate of labeled water delivery, as well as arrival time (Δt) and temporal length (τ) of the tagged bolus of arterial blood water. Based on this pilot dataset, the arrival time (Δt = 1.04 s) and temporal length (τ = 3.66 s) values were fixed when fitting the dataset acquired at 21-weeks to the 2-compartment Buxton kinetic model, in order to extract solely the rate of arterial water delivery with a higher degree of precision (**Supplementary Figure 2**).

Measurements of blood pressure

Following completion of the MRI protocols, confirmation of the subjects' hypertensive state was confirmed through invasive blood pressure measurements in 4 of the subjects within each group (8 in total). Here, an identical anesthesia protocol as used for MRI was employed. Arterial blood pressure was measured through an arterial catheter in the femoral artery and connected to a physiological monitoring system. Data were sampled at 400 Hz for the recording of arterial blood pressure for a baseline reading over 20 min.

Statistical methods

Statistical comparisons between SHR and WKY data were made using unpaired, 2-tailed, Student's t-tests (GraphPad Prism 9 and Microsoft Excel).

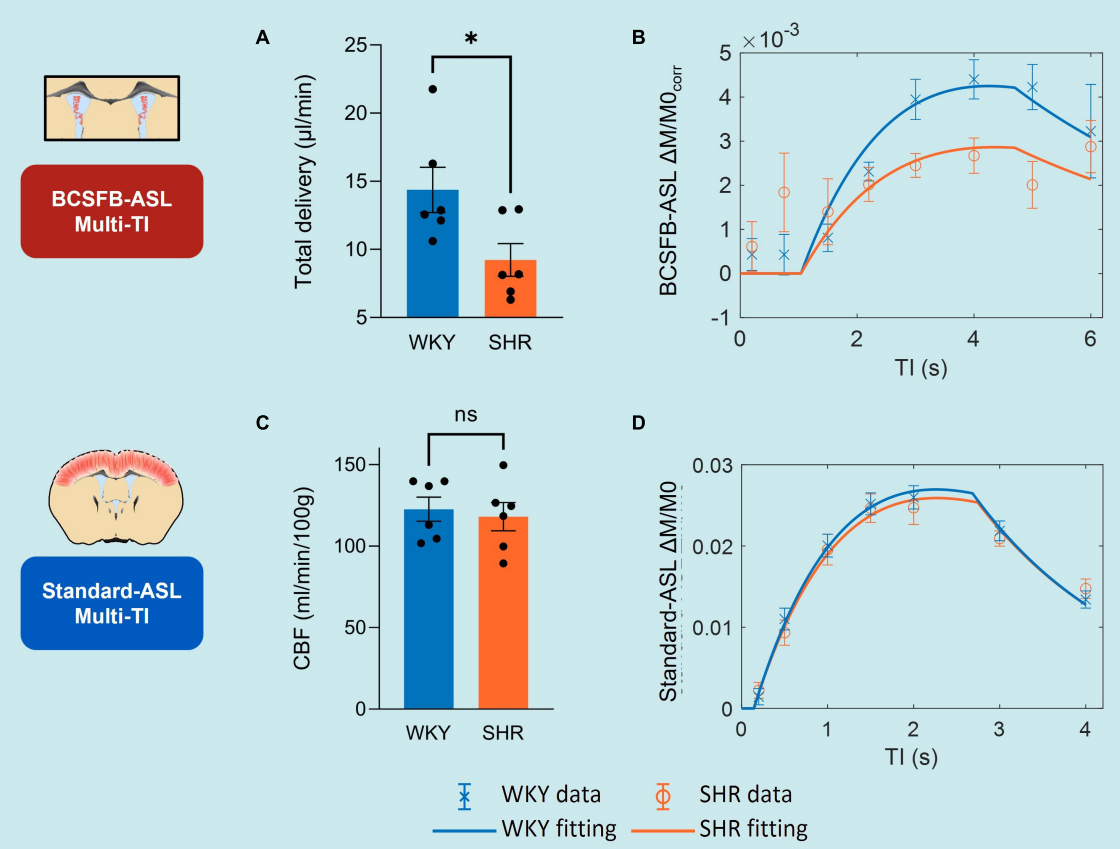

FIGURE 2
Multi-TI kinetic data for BCSFB-ASL and Standard-ASL. **(A)** Extracted BCSFB-mediated total water delivery in WKY and SHR subjects. **(B)** Averaged BCSFB-ASL multi-TI data alongside kinetic curve fits for WKY and SHR subjects. **(C)** Extracted cortical CBF in WKY and SHR subjects. **(D)** Averaged standard-ASL multi-TI data alongside kinetic curve fits for WKY and SHR subjects. Error bars: ± SEM (n = 6 WKY, 6 SHR). Asterisks: 2-tailed t-test significance, *p < 0.05, **p < 0.01, ***p < 0.001, and ****p < 0.0001.

Results

Blood-cerebrospinal fluid barrier-mediated water delivery

Recent evidence indicates that the CP-BCSFB system is notably perturbed by systemic hypertension (Al-Sarraf and Philip, 2003; Castañeyra-Perdomo et al., 2010), as such we applied a multi-inflow time (multi-TI) BCSFB-ASL MRI approach in SHR and WKY subjects (n = 6 in each group, 21-weeks old) to measure the degree a change in BCSFB derangement under hypertension (**Figure 1**).

The total rate of BCSFB-mediated labeled arterial water delivery to ventricular CSF was extracted from multi-TI BCSFB-ASL data (**Figures 2A,B** and **Supplementary Figure 4**). We measured a 35.8%, decrease in the total rate of water delivery in the SHRs compared to WKYs, which can be observed in the extracted water delivery values WKY 14.4 ± 1.92 μl/min vs. SHR 9.22 ± 1.20 μl/min (p = 0.037, 2 -tailed unpaired t-test, **Figure 2A**), as well as from visual inspection of the group-averaged BCSFB-ASL kinetic curves (**Figure 2B**).

Cortical cerebral blood flow

Changes in CBF under chronic hypertension can inform on cerebrovascular health. However, CBF changes under hypertension have shown to be variable (Wardlaw et al., 2003; Beason-Held et al., 2007; Li et al., 2015). Here, we applied a multi-TI standard-ASL approach for the extraction of cortical CBF (**Figure 2D**). Cortical CBF was not significantly different between the WKY normotensive controls and the SHRs, as shown by the group-averaged (n = 6) fitted perfusion values: WKY 123 ± 7.4 ml/min/100 g vs. SHR 118 ± 8.7 ml/min/100 g 100 g (p = 0.70, **Figure 2C**). The group-averaged standard-ASL kinetic curves also demonstrate the strong similarity of the two groups (**Figure 2D**).

Cerebrospinal fluid homeostasis

Previous reports have shown that SHRs display marked changes in brain fluid management, as determined through measuring perturbations in CSF secretory profiles, glymphatic flow, brain water mobility and ventriculomegaly (Al-Sarraf and Philip, 2003; Castañeyra-Perdomo et al., 2010; Mortensen et al., 2019; Naessens et al., 2020). To further probe how hypertension impacts CSF volume and composition, we acquired measures for surrogate markers of CSF management: $T1_{CSF}$ and lateral ventricular volumes.

Single subject examples of data obtained from WKY and SHR groups of the signal (M_c) variation with TI obtained using BCSFB-ASL, alongside the fits to the simple inversion recovery model is depicted in **Figure 3B**. $T1_{CSF}$ was found to be significantly higher in the lateral ventricles of the hypertensive rats: SHR 4.58 ± 0.06 s vs. WKY 4.24 ± 0.04 s (p = 0.0012, **Figure 3A**). Cortical tissue T1 was not significantly different between the two groups: SHR 1.91 ± 0.01 vs. WKY 1.88 ± 0.01 s (p = 0.14, data not shown).

Volumes of the lateral ventricles were quantified for all subjects using T2-weighted anatomical images (**Figures 3C,D**). SHR subjects had a ∼1.5-fold increase in their lateral ventricular volumes relative to normotensive controls: WKY 56 ± 3.0 mm^3 vs. SHR 83 ± 1.0 mm^3 ($p = 6 \times 10^{-6}$, **Figure 3C**). This is supported by visual inspection of the T2-weighted anatomical images (equivalent slices) from SHR and WKY subjects (**Figure 3D**).

Blood pressure measurements

Measurement of blood pressure in our SHR (n = 4) and WKY (n = 4) rats confirmed their respective blood pressure states (**Supplementary Figure 3**). SHRs were shown to have a significantly higher blood pressure compared to WKY controls, which was evident from systolic (SHR 185 ± 6.5 vs. WKY 105 ± 12 mmHg, p = 0.0010), diastolic (SHR 113 ± 7.5 vs. WKY 55 ± 7.4 mmHg, p = 0.0016) and mean blood pressure (SHR 149 ± 6.9 vs. WKY 80 ± 9.5 mmHg, p = 0.0011). Additionally, SHRs were found to have an increased blood pressure range (systolic-diastolic) compared to WKYs (SHR 73 ± 2.5 vs. WKY 50 ± 5.4 mmHg, p = 0.009).

Discussion

Patients suffering from systemic hypertension face an increased risk of cognitive decline later in life (Iadecola et al., 2016). Thus, there is a need for not only an improvement in our understanding of disease etiology, but also for early biomarkers of upstream pathological processes. Addressing the need for non-invasive methodologies, we recently developed BCSFB-ASL—a translatable ASL-MRI approach which provides a surrogate measure of BCSFB function by quantifying the rate of labeled endogenous arterial blood-water delivery, mediated by the BCSFB, into ventricular CSF (Evans et al., 2020). In this work we record a 36% reduction in the rate of BCSFB-mediated water delivery in the SHR model relative to normotensive controls, indicating an impaired BCSFB function under chronic hypertension. We also measure perturbations in CSF homeostasis, as measured by changes in $T1_{CSF}$ and lateral ventricular volume. However, the cortical CBF measurements revealed no changes under hypertension.

To date, the bulk of work investigating the mechanisms underpinning hypertension-driven neurodegeneration have been centered on studying the cerebral vasculature, revealing

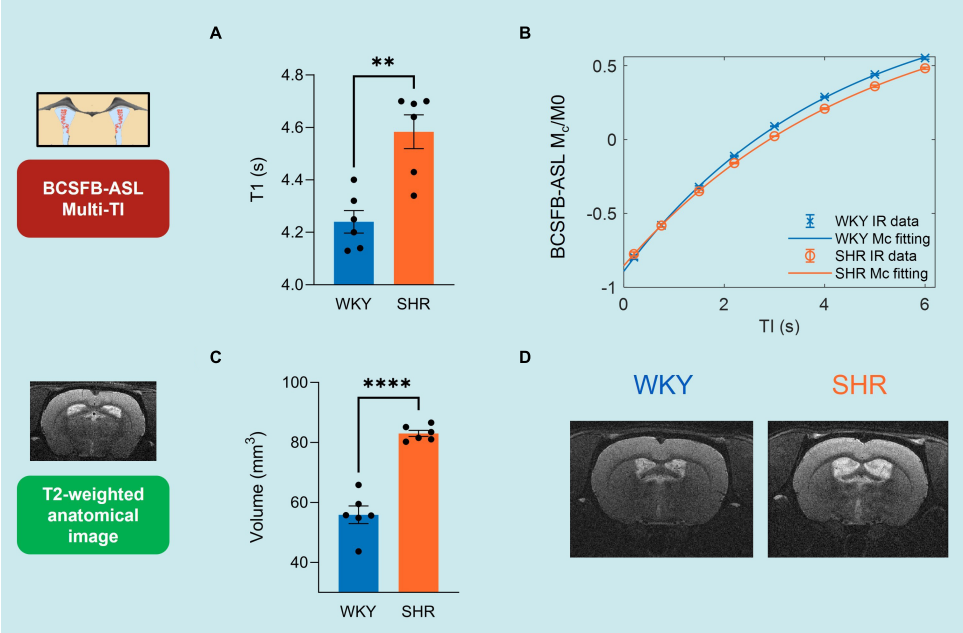

FIGURE 3
CSF homeostasis: $T1_{CSF}$ and lateral ventricular volume. **(A)** $T1_{CSF}$ values from WKY and SHR subjects, extracted from BCSFB-ASL multi-TI data. Error bars: ± SEM (n = 6 WKY, 6 SHR). **(B)** Example of multi-TI inversion recovery fitting (n = 1 WKY, 1 SHR). Error bars: ± stdev (20 repetitions at each TI). **(C)** Lateral ventricular volume values from WKY and SHR subjects, from T2-weighted anatomical images. Error bars: ± SEM (n = 6 WKY, 6 SHR). **(D)** Examples of T2-weighted anatomical images (equivalent slices) displaying ventriculomegaly (n = 1 WKY, 1 SHR). Asterisks: 2-tailed t-test significance, *p < 0.05, **p < 0.01, ***p < 0.001, and ****p < 0.0001.

impairments to the integrity of the cellular network at the BBB and the associated abnormalities in CBF and cerebrovascular reactivity (Wardlaw et al., 2003; Li et al., 2015). These changes are thought to increase the brain's vulnerability toward neurodegenerative diseases (Korte et al., 2020; Nielsen et al., 2020). However, despite serving as an established biomarker for neurovascular pathology, there are inconsistencies in the directionality of change for CBF in hypertension studies. Baseline CBF in SHRs has been shown to increase from elevated mean arterial blood pressures (Heinert et al., 1998), but other studies point to CBF decreasing or remaining similar (Grabowski et al., 1993; Lee et al., 2011) due to autoregulatory mechanisms (Li et al., 2015; Naessens et al., 2018; Yazdani et al., 2020). Our multi-TI conventional ASL data revealed no significant difference in the cortical CBF between hypertensive and normotensive groups, likely due to vasoconstrictive autoregulation previously reported in SHRs of a similar age (Li et al., 2015). Our data, combined with the variability in the literature, suggests that CBF measurements may not be the most sensitive biomarker of functional derangement under hypertension.

The BCSFB-ASL methodology was developed and applied first in the mouse brain (Evans et al., 2020). Here, we present the application of BCSFB-ASL under systemic hypertension to investigate functional impairment, as well as the first application of this methodology in the rat brain. In this study, there is a good fit of the multi-TI data to the 2-compartment Buxton Kinetic model, and similar to the initial characterization in the mouse brain, the BCSFB-ASL kinetic curve has features distinct to that of the standard-ASL dataset, i.e., a delayed arrival time for the tagged bolus, delayed time to peak for the ASL signal, and a reduced rate of ASL-signal decay due to the lengthened T1 of lateral ventricular CSF relative to cortical tissue. The healthy rat brain was found to have a total BCSFB-mediated water delivery rate of 14.4 μl/min, which, as expected, is markedly higher than the rate observed in the mouse brain (2.7 μl/min) (Evans et al., 2020), given that the volume of the rat brain is ∼4.5 times larger (Ma et al., 2008; Yang et al., 2021). By providing an initial reference value for BCSFB-mediated water delivery to ventricular CSF in the healthy (WKY) and hypertensive (SHR) groups, we have demonstrated the feasibility of this measurement in larger animal models. In regards to clinical translation, recent work has captured the delivery of labeled blood water into the CSF in the human brain (Petitclerc et al., 2021) using ultra-long TE ASL, and other studies have applied traditional ASL methods to estimate apparent choroid plexus perfusion, with promising results (Johnson et al., 2020, 2021; Zhao et al., 2020).

We detected a marked reduction in rates of BCSFB-mediated water delivery in the SHR providing evidence that the BCSFB-ASL technique can detect derangement of the CP-BCSFB locus in hypertension. The limited study of the CP-BCSFB system *in-vivo* has been due to the lack of non-invasive methodologies, and has historically necessitated

the use of radioactive tracers or contrast agents alongside terminal surgical methods (Prinzen and Bassingthwaighte, 2000; Hubert et al., 2019). Given this limitation, the role of the BCSFB in hypertension has only been assessed in *ex-vivo* brain tissues (Al-Sarraf and Philip, 2003; Castañeyra-Perdomo et al., 2010). This literature points to the selective vulnerability of the BCSFB to hypertensive damage, with damage manifesting as a disruption in BCSFB integrity, and an alteration in the profile of proteins secreted into the CSF, which will affect CSF homeostasis and subsequent overall CNS function (Al-Sarraf and Philip, 2003; Castañeyra-Perdomo et al., 2010). Furthermore, hypertensive BCSFB damage was reported to resemble the BCSFB impairment observed with Alzheimer's Disease (Castañeyra-Perdomo et al., 2010), thus further implicating the BCSFB in the development of dementia. Together, these previous reports support the existence of marked hypertension-induced BCSFB impairment. However, the invasive nature of these methodologies to determine BCSFB impairment has a limited capacity for studies of *in-vivo* disease progression, which our translatable measures of BCSFB function show the potential to provide.

Previous work aiming to investigate how hypertension may modulate BCSFB permeability in the brain has been relatively limited. A total of 42-week-old SHRs were found to display no change in the permeabilities of both the BBB and BCSFB when quantifying fluorescein leakage (Naessens et al., 2018). In contrast, measurements of barrier integrity using ^{14}C-sucrose in 12–16 week-old SHRs revealed an increased permeability of the BCSFB (Al-Sarraf and Philip, 2003)., with no difference in BBB permeability detected. The BCSFB-ASL signal, measured here, reflects the average rate of perfusion to the CP convolved with the permeability of the BCSFB to water (the "extraction fraction"; Raichle et al., 1974) and the mass of the CP tissue within the lateral ventricles. Therefore, considering the aforementioned report of increased BCSFB-permeability in the SHR brain, this may suggest that the decreased rates of BCSFB-mediated water delivery detected here primarily reflect decreased CP perfusion. It is important to note, however, that changes in the permeability of the BCSFB to larger tracers may not be indicative of changes in permeability to water (where, for example, Aquaporin-1 is thought to play an important role). Despite the limited specificity of the BCSFB-ASL measurement to changes in BCSFB physiology, it may still represent a valuable biomarker of BCSBF derangement given its non-invasive nature and good reproducibility (Evans et al., 2020) to probe the function of this difficult-to-measure structure.

The SHR model exhibits a range of neurodegenerative changes that occur later in life for patients suffering from chronic hypertension: BBB dysfunction with high levels of amyloid-B accumulation (Wang et al., 2018), non-spatial memory deficits, brain atrophy, neuroinflammation, and dysregulated brain fluid (ISF and CSF) homeostasis (Mortensen et al., 2019). Here, our sensitivity to BCSFB dysfunction suggests that obtaining such *in-vivo* measures may be informative for early detection of the changes that occur in the hypertensive brain that may accelerate the progression of neurodegenerative pathways. Importantly, given the minimal changes in CBF observed in this work, investigation into BCSFB function may provide distinct staging of disease processes relative to more conventional biomarkers of cerebrovascular health. Future studies could perform longitudinal measures of BCSFB function together with imaging biomarkers of neurodegeneration to characterize the timeline and possible predictive relationship of such measurements.

The BCSFB-ASL multi-TI approach also permitted an estimation of changes in $T1_{CSF}$ under hypertension, which may arise from alterations in the secretory profile of signaling factors by the CP-BCSFB system that occur concurrently with structural and functional barrier decline (Castañeyra-Perdomo et al., 2010). The changes in CSF management are indicative of brain fluid dysregulation under hypertension which are in line with previous imaging studies, e.g., through abnormalities of glymphatic CSF transport measured with dynamic contrast-enhanced-MRI (DCE-MRI) using the infusion of a gadolinium-based contrast agent into the cisterna magna, in both young (∼8 week-old) and adult (∼20 week-old) SHRs (Mortensen et al., 2019). Imbalance of brain fluid management has also been observed through a reduction in apparent diffusion coefficient (ADC) values in 45-week old SHRs (Naessens et al., 2020), By measuring BCSFB function alongside $T1_{CSF}$ changes, this provides the potential for an increased sensitivity to changes in the early phases of hypertension-driven neurodegeneration in a manner that is more translatable than contrast agent infusion into the cisterna magna for DCE-MRI studies of glymphatic function.

Changes in $T1_{CSF}$ may stem directly from impairments in BCSFB function in the hypertensive cohort, such as alterations in the secretion of proteins into the CSF. For example, transferrin (Tf), the major iron transport protein in the brain, is secreted by the choroid plexus into the interstitial fluid (ISF) to acquire Fe^{3+}, which will then equilibrate with the CSF (Leitner and Connor, 2012; Möller et al., 2019). Relaxivity data obtained from blood serum has shown that Tf and other proteins such as globulins and albumin contribute to the serum T1 relaxation times (Yilmaz et al., 2004). It is likely that the changes in CSF protein composition in hypertensive rats will influence the $T1_{CSF}$ values, i.e., potential reductions in CSF Tf-Fe^{3+} levels would lengthen the measured $T1_{CSF}$.

Ventriculomegaly in the hypertensive subjects in this work is similar to the increases in volume measured previously in rats of a similar age (Naessens et al., 2020), as well as in hypertensive patients (Salerno et al., 1992; Strassburger et al., 1997; Wiseman et al., 2004). The expansion of this region is reported to arise from a combination of factors including: increase in CSF production rates (Al-Sarraf and Philip, 2003); increased CSF reabsorption resistance; or ventricular expansion

due to cerebral atrophy (Naessens et al., 2018). Given that ventriculomegaly is a hallmark of systemic hypertension, this provides an opportunity to investigate the etiology of conditions such as hydrocephalus and dementia, where there is a high degree of clinical overlap and that share hypertension as a common risk factor for their onset.

To conclude, in this work we provide the first application of the BCSFB-ASL technique to the rat brain, providing reference values for rates of BCSFB-mediated water delivery into the lateral ventricles. The decreased rate of BCSFB-mediated arterial water delivery and altered CSF homeostasis in hypertensive subjects demonstrates the potential utility of the method to study the mechanisms that link systemic hypertension to downstream neurodegeneration. The observed functional impairment at the BCSFB suggests that the CP-BCSFB-CSF system may represent a key site of brain vulnerability to systemic hypertension.

Data availability statement

The raw data supporting the conclusions of this article will be made available by the authors, without undue reservation.

Ethics statement

The animal study was reviewed and approved by the United Kingdom Home Office Act (Scientific Procedures, 1986).

Author contributions

CP: conceptualization, data curation, investigation, methodology, formal analysis, and writing—original draft. DT, YO, and RB: methodology and writing—review and editing. AK: data curation and writing—review and editing. ML: conceptualization, resources, and writing—review and editing. DLT: conceptualization, supervision, methodology, and writing—review and editing. JW: conceptualization, supervision, funding acquisition, investigation, methodology, writing—original draft, review and editing, and project administration. All authors contributed to the article and approved the submitted version.

Funding

CP was supported by the Alzheimer's Society (AS-PhD-18-006). ML received funding from: the Rosetrees Trust and the John Black Charitable Foundation (grant no. A2200), the Brain Tumor Charity (grant no. QfC_2018_10387), the Edinburgh-UCL CRUK Brain Tumor Centre of Excellence (grant no. C7893/A27590), the Medical Research Council (grant no. MR/J013110/1), the CRUK and EPSRC Comprehensive Cancer Imaging Centre at KCL and UCL (grant nos. C1519/A16463 and C1519/A10331). JW was supported by the Wellcome Trust/Royal Society (grant no. 204624/Z/16/Z). YO was funded by the EPSRC code EP/S031510/1. RB received funding from the EPSRC-funded UCL Centre for Doctoral Training in Medical Imaging (EP/L016478/1) and the Department of Health's NIHR-funded Biomedical Research Centre at University College London Hospitals.

Acknowledgments

We would like to thank George Martin, Matthew Lawson, Lizzie Steptoe, Yasmin Alphonse, Gabi Sturges, and Jayne Holby for their help in maintaining animal welfare and environmental enrichment.

Conflict of interest

The authors declare that the research was conducted in the absence of any commercial or financial relationships that could be construed as a potential conflict of interest.

Publisher's note

All claims expressed in this article are solely those of the authors and do not necessarily represent those of their affiliated organizations, or those of the publisher, the editors and the reviewers. Any product that may be evaluated in this article, or claim that may be made by its manufacturer, is not guaranteed or endorsed by the publisher.

Supplementary material

The Supplementary Material for this article can be found online at: https://www.frontiersin.org/articles/10.3389/fnmol.2022.964632/full#supplementary-material

SUPPLEMENTARY FIGURE 1
ROI selection for BCSFB-ASL images. Left: examples of WKY **(A)** and SHR **(B)** ROIs (green) are shown on control (M_C, non-selective FAIR) images (TI = 4 s, n = 1 per group). Right: examples of T2-weighted coronal anatomical images for reference (n = 1 per group).

SUPPLEMENTARY FIGURE 2
Pilot data: averaged BCSFB-ASL multi-TI data (WKY, 10-weeks old, n = 6). Error bars: ± SEM.

SUPPLEMENTARY FIGURE 3
Group-averaged arterial pressures from WKY and SHR subjects. Error bars: ± SEM (n = 4 WKY, 4 SHR). Asterisks: 2-tailed t-test significance, *p < 0.05, **p < 0.01, ***p < 0.001, and ****p < 0.0001.

SUPPLEMENTARY FIGURE 4
BCSFB-ASL multi-TI data: individual subject fits to Buxton kinetic model. **(A)** WKY cohort (n = 6). **(B)** SHR cohort (n = 6). Error bars: ± standard deviation across 10 repetitions at each TI.

References

Al-Sarraf, H., and Philip, L. (2003). Effect of hypertension on the integrity of blood brain and blood CSF barriers, cerebral blood flow and CSF secretion in the rat. *Brain Res.* 975, 179–188. doi: 10.1016/S0006-8993(03)02632-5

Alsop, D. C., and Detre, J. A. (1996). Reduced transit-time sensitivity in noninvasive magnetic resonance imaging of human cerebral blood flow. *J. Cerebral Blood Flow Metab.* 16, 1236–1249. doi: 10.1097/00004647-199611000-00019

Beason-Held, L. L., Moghekar, A., Zonderman, A. B., Kraut, M. A., and Resnick, S. M. (2007). Longitudinal changes in cerebral blood flow in the older hypertensive brain. *Stroke* 38, 1766–1773. doi: 10.1161/STROKEAHA.106.477109

Buxton, R. B., Frank, L. R., Wong, E. C., Siewert, B., Warach, S., and Edelman, R. R. (1998). A general kinetic model for quantitative perfusion imaging with arterial spin labeling. *Magnetic Res. Med.* 40, 383–396. doi: 10.1002/MRM.1910400308

Castañeyra-Perdomo, A., Gonzalez-Marrero, I., Castro, R., Castañeyra-Ruiz, A., De Paz-Camona, H., Castañeyra-Ruiz, L., et al. (2010). Long-term effects of arterial hypertension on the choroid plexus, blood to cerebrospinal fluid barrier and CSF proteins and their involved in certain types of dementia. *Cereb. Fluid Res.* 7, 1–2. doi: 10.1186/1743-8454-7-S1-S29

Evans, P. G., Sokolska, M., Alves, A., Harrison, I. F., Ohene, Y., Nahavandi, P., et al. (2020). Non-invasive MRI of blood–cerebrospinal fluid barrier function. *Nat. Commun.* 11, 1–11. doi: 10.1038/s41467-020-16002-4

Gonzalez-Marrero, I., Hernández-Abad, L. G., Castañeyra-Ruiz, L., Carmona-Calero, E. M., and Castañeyra-Perdomo, A. (2022). Changes in the choroid plexuses and brain barriers associated with high blood pressure and ageing. *Neurologia* 37, 371–382. doi: 10.1016/j.nrl.2018.06.001

Grabowski, M., Mattsson, B., Nordborg, C., and Johansson, B. B. (1993). Brain capillary density and cerebral blood flow after occlusion of the middle cerebral artery in normotensive Wistar-Kyoto rats and spontaneously hypertensive rats. *J. Hypert.* 11, 1363–1368. doi: 10.1097/00004872-199312000-00007

Hays, C. C., Zlatar, Z. Z., and Wierenga, C. E. (2016). The utility of cerebral blood flow as a biomarker of preclinical Alzheimer's disease. *Cell. Mol. Neurobiol.* 36:167. doi: 10.1007/S10571-015-0261-Z

Heinert, G., Casadei, B., and Paterson, D. J. (1998). Hypercapnic cerebral blood flow in spontaneously hypertensive rats. *J. Hypert.* 16, 1491–1498. doi: 10.1097/00004872-199816100-00014

Hubert, V., Chauveau, F., Dumot, C., Ong, E., Berner, L.-P., Canet-Soulas, E., et al. (2019). Clinical imaging of choroid plexus in health and in brain disorders: A mini-review. *Front. Mol. Neurosci.* 12:34. doi: 10.3389/fnmol.2019.00034

Iadecola, C., Yaffe, K., Biller, J., Bratzke, L. C., Faraci, F. M., Gorelick, P. B., et al. (2016). Impact of hypertension on cognitive function: A scientific statement from the american heart association. *Hypertension* 68, e67–e94. doi: 10.1161/HYP.0000000000000053

Johnson, S. E., McKnight, C. D., Jordan, L. C., Claassen, D. O., Waddle, S., Lee, C., et al. (2021). Choroid plexus perfusion in sickle cell disease and moyamoya vasculopathy: Implications for glymphatic flow. *J. Cerebral Blood Flow Metab.* 41, 2699–2711. doi: 10.1177/0271678X211010731

Johnson, S. E., McKnight, C. D., Lants, S. K., Juttukonda, M. R., Fusco, M., Chitale, R., et al. (2020). Choroid plexus perfusion and intracranial cerebrospinal fluid changes after angiogenesis. *J. Cereb. Blood Flow Metab.* 40, 1658–1671. doi: 10.1177/0271678X19872563

Kaiser, D., Weise, G., Möller, K., Scheibe, J., Pösel, C., Baasch, S., et al. (2014). Spontaneous white matter damage, cognitive decline and neuroinflammation in middle-aged hypertensive rats: An animal model of early-stage cerebral small vessel disease. *Acta Neuropathol. Commun.* 2, 1–15. doi: 10.1186/S40478-014-0169-8/FIGURES/8

Korte, N., Nortley, R., and Attwell, D. (2020). Cerebral blood flow decrease as an early pathological mechanism in Alzheimer's disease. *Acta Neuropathol.* 140, 793–810. doi: 10.1007/S00401-020-02215-W

Lee, T. H., Liu, H. L., Yang, S. T., Yang, J. T., Yeh, M. Y., and Lin, J. R. (2011). Effects of aging and hypertension on cerebral ischemic susceptibility: Evidenced by MR diffusion-perfusion study in rat. *Exp. Neurol.* 227, 314–321. doi: 10.1016/J.EXPNEUROL.2010.12.003

Lein, E. S., Hawrylycz, M. J., Ao, N., Ayres, M., Bensinger, A., Bernard, A., et al. (2007). Genome-wide atlas of gene expression in the adult mouse brain. *Nature* 445, 168–176. doi: 10.1038/nature05453

Leitner, D. F., and Connor, J. R. (2012). Functional roles of transferrin in the brain. *Biochim. Biophys. Acta General Subjects* 1820, 393–402. doi: 10.1016/J.BBAGEN.2011.10.016

Li, Y., Shen, Q., Huang, S., Li, W., Muir, E. R., Long, J. A., et al. (2015). Cerebral angiography, blood flow and vascular reactivity in progressive hypertension. *NeuroImage* 111:53. doi: 10.1016/J.NEUROIMAGE.2015.02.053

Lun, M. P., Monuki, E. S., and Lehtinen, M. K. (2015). Development and functions of the choroid plexus–cerebrospinal fluid system. *Nat. Rev. Neurosci.* 16, 445–457. doi: 10.1038/nrn3921

Ma, Y., Smith, D., Hof, P. R., Foerster, B., Hamilton, S., Blackband, S. J., et al. (2008). In vivo 3D digital atlas database of the adult C57BL/6J mouse brain by magnetic resonance microscopy. *Front. Neuroanat.* 2:1. doi: 10.3389/NEURO.05.001.2008/BIBTEX

Mestre, H., Tithof, J., Du, T., Song, W., Peng, W., Sweeney, A. M., et al. (2018). Flow of cerebrospinal fluid is driven by arterial pulsations and is reduced in hypertension. *Nat. Commun.* 9, 1–9. doi: 10.1038/s41467-018-07318-3

Möller, H. E., Bossoni, L., Connor, J. R., Crichton, R. R., Does, M. D., Ward, R. J., et al. (2019). Iron, myelin, and the brain: Neuroimaging meets neurobiology. *Trends Neurosci.* 42, 384–401. doi: 10.1016/J.TINS.2019.03.009

Mortensen, K. N., Sanggaard, S., Mestre, H., Lee, H., Kostrikov, S., Xavier, A. L. R., et al. (2019). Impaired glymphatic transport in spontaneously hypertensive rats. *J. Neurosci.* 39, 6365–6377. doi: 10.1523/JNEUROSCI.1974-18.2019

Naessens, D. M. P., Coolen, B. F., De Vos, J., Vanbavel, E., Strijkers, G. J., and Bakker, E. N. T. P. (2020). Altered brain fluid management in a rat model of arterial hypertension. *Fluids and Barriers of the CNS* 17, 1–13. doi: 10.1186/S12987-020-00203-6/FIGURES/6

Naessens, D. M. P., De Vos, J., Vanbavel, E., and Bakker, E. N. T. P. (2018). Blood-brain and blood-cerebrospinal fluid barrier permeability in spontaneously hypertensive rats. *Fluids Barriers CNS* 15, 1–10. doi: 10.1186/S12987-018-0112-7/FIGURES/3

Nielsen, R. B., Parbo, P., Ismail, R., Dalby, R., Tietze, A., Brændgaard, H., et al. (2020). Impaired perfusion and capillary dysfunction in prodromal Alzheimer's disease. *Alzheimer's Dementia Diagn. Assess. Dis. Monit.* 12:e12032. doi: 10.1002/DAD2.12032

Perera, C., Harrison, I. F., Lythgoe, M. F., Thomas, D. L., and Wells, J. A. (2021). Pharmacological MRI with simultaneous measurement of cerebral perfusion and blood-cerebrospinal fluid barrier function using interleaved echo-time arterial spin labelling. *NeuroImage* 238:118270. doi: 10.1016/J.NEUROIMAGE.2021.118270

Petitclerc, L., Hirschler, L., Wells, J. A., Thomas, D. L., van Walderveen, M. A. A., van Buchem, M. A., et al. (2021). Ultra-long-TE arterial spin labeling reveals rapid and brain-wide blood-to-CSF water transport in humans. *NeuroImage* 245:118755. doi: 10.1016/J.NEUROIMAGE.2021.118755

Prinzen, F. W., and Bassingthwaighte, J. B. (2000). Blood flow distributions by microsphere deposition methods. *Cardiovasc. Res.* 45, 13–21. doi: 10.1016/S0008-6363(99)00252-7/2/45-1-11-FIG4.GIF

Raichle, M. E., Eichling, J. O., and Grubb, R. L. (1974). Brain permeability of water. *Arch. Neurol.* 30, 319–321. doi: 10.1001/archneur.1974.00490340047010

Salerno, J. A., Murphy, D. G. M., Horwitz, B., DeCarli, C., Haxby, J. V., Rapoport, S. I., et al. (1992). Brain atrophy in hypertension. a volumetric magnetic resonance imaging study. *Hypertension* 20, 340–348. doi: 10.1161/01.HYP.20.3.340

Strassburger, T. L., Lee, H. C., Daly, E. M., Szczepanik, J., Krasuski, J. S., Mentis, M. J., et al. (1997). Interactive effects of age and hypertension on volumes of brain structures. *Stroke* 28, 1410–1417. doi: 10.1161/01.STR.28.7.1410

Wang, J., Alsop, D. C., Li, L., Listerud, J., Gonzalez-At, J. B., Schnall, M. D., et al. (2002). Comparison of quantitative perfusion imaging using arterial spin labeling at 1.5 and 4.0 Tesla. *Magnetic Res. Med.* 48, 242–254. doi: 10.1002/mrm.10211

Wang, Y., Zhang, R., Tao, C., Xu, Z., Chen, W., Wang, C., et al. (2018). Blood-brain barrier disruption and perivascular beta-amyloid accumulation in the brain of aged rats with spontaneous hypertension: Evaluation with dynamic contrast-enhanced magnetic resonance imaging. *Korean J. Radiol.* 19, 498–507. doi: 10.3348/KJR.2018.19.3.498

Wardlaw, J. M., Sandercock, P. A. G., Dennis, M. S., and Starr, J. (2003). Is breakdown of the blood-brain barrier responsible for lacunar stroke, leukoaraiosis, and dementia? *Stroke* 34, 806–811. doi: 10.1161/01.STR.0000058480.77236.B3

Wiseman, R. M., Saxby, B. K., Burton, E. J., Barber, R., Ford, G. A., and O'Brien, J. T. (2004). Hippocampal atrophy, whole brain volume, and white matter lesions in older hypertensive subjects. *Neurology* 63, 1892–1897. doi: 10.1212/01.WNL.0000144280.59178.78

Yang, Y., Zhang, Q., Ren, J., Zhu, Q., Wang, L., Zhang, Y., et al. (2021). Evolution of brain morphology in spontaneously hypertensive and wistar-kyoto rats from early adulthood to aging: A longitudinal magnetic resonance imaging study. *Front. Aging Neurosci.* 13:849. doi: 10.3389/FNAGI.2021.757808/BIBTEX

Yazdani, N., Kindy, M. S., and Taheri, S. (2020). CBF regulation in hypertension and Alzheimer's disease. *Clin. Exp. Hypert.* 42, 622–639. doi: 10.1080/10641963.2020.1764014

Yilmaz, A., Ulak, F., and Batun, M. S. (2004). Proton T1 and T2 relaxivities of serum proteins. *Magnetic Res. Imag.* 22, 683–688. doi: 10.1016/J.MRI.2004.02.001

Zhao, L., Taso, M., Dai, W., Press, D. Z., and Alsop, D. C. (2020). Non-invasive measurement of choroid plexus apparent blood flow with arterial spin labeling. *Fluids Barr. CNS* 17, 1–11. doi: 10.1186/s12987-020-00218-z

Zhou, B., Carrillo-Larco, R. M., Danaei, G., Riley, L. M., Paciorek, C. J., Stevens, G. A., et al. (2021). Worldwide trends in hypertension prevalence and progress in treatment and control from 1990 to 2019: A pooled analysis of 1201 population-representative studies with 104 million participants. *Lancet* 398, 957–980. doi: 10.1016/S0140-6736(21)01330-1/ATTACHMENT/F57BA96E-DFA3-4B0C-9FD5-188725B928ED/MMC1.PDF

frontiers | Frontiers in Bioengineering and Biotechnology

TYPE Original Research
PUBLISHED 12 September 2022
DOI 10.3389/fbioe.2022.932469

OPEN ACCESS

EDITED BY
Seungik Baek,
Michigan State University, United States

REVIEWED BY
Caterina Guiot,
University of Turin, Italy
Nenad Filipovic,
University of Kragujevac, Serbia

*CORRESPONDENCE
Martin Hornkjøl,
martin.hornkjol@hotmail.com

SPECIALTY SECTION
This article was submitted to Biomechanics, a section of the journal Frontiers in Bioengineering and Biotechnology

RECEIVED 14 May 2022
ACCEPTED 17 August 2022
PUBLISHED 12 September 2022

CITATION
Hornkjøl M, Valnes LM, Ringstad G, Rognes ME, Eide P-K, Mardal K-A and Vinje V (2022), CSF circulation and dispersion yield rapid clearance from intracranial compartments. *Front. Bioeng. Biotechnol.* 10:932469. doi: 10.3389/fbioe.2022.932469

CSF circulation and dispersion yield rapid clearance from intracranial compartments

Martin Hornkjøl[1]*, Lars Magnus Valnes[2], Geir Ringstad[3,4], Marie E. Rognes[5,6], Per-Kristian Eide[2,7], Kent-André Mardal[1,5] and Vegard Vinje[5]

[1]Department of Mathematics, University of Oslo, Blindern, Norway, [2]Department of Neurosurgery, Oslo University Hospital–Rikshospitalet, Oslo, Norway, [3]Department of Radiology, Oslo University Hospital, Oslo, Norway, [4]Department of Geriatrics and Internal Medicine, Sorlandet Hospital, Arendal, Norway, [5]Department of Numerical Analysis and Scientific Computing, Simula Research Laboratory, Oslo, Norway, [6]Department of Mathematics, University of Bergen, Bergen, Norway, [7]Institute of Clinical Medicine, Faculty of Medicine, University of Oslo, Oslo, Norway

In this paper, we used a computational model to estimate the clearance of a tracer driven by the circulation of cerebrospinal fluid (CSF) produced in the choroid plexus (CP) located within the lateral ventricles. CSF was assumed to exit the subarachnoid space (SAS) via different outflow routes such as the parasagittal dura, cribriform plate, and/or meningeal lymphatics. We also modelled a reverse case where fluid was produced within the spinal canal and absorbed in the choroid plexus in line with observations on certain iNPH patients. No directional interstitial fluid flow was assumed within the brain parenchyma. Tracers were injected into the foramen magnum. The models demonstrate that convection in the subarachnoid space yields rapid clearance from both the SAS and the brain interstitial fluid and can speed up intracranial clearance from years, as would be the case for purely diffusive transport, to days.

KEYWORDS

mathematical modelling, CSF dynamics, subarachnoid space, convection-diffusion, clearance, glymphatics

1 Introduction

Cerebrospinal fluid (CSF) flow plays a fundamental role in the clearance of solutes from intracranial compartments (Abbott et al., 2018; Proulx, 2021). Current views postulate that CSF is primarily produced in the choroid plexus (Weed, 1922; Abbott et al., 2018), and flows through the ventricular system (Lindstrøm et al., 2018; Lindstrøm et al., 2019; Eide et al., 2020) and along the subarachnoid space (SAS) (Mestre et al., 2018a;

Abbreviations: CP, choroid plexus; CSF, cerebrospinal fluid; ECS, extracellular space; iNPH, idiopathic normal pressure hydrocephalus; ISF, interstitial fluid; MRI, magnetic resonance imaging; SAS, subarachnoid space; PVS, perivascular space; ROI, region of interest.

Bedussi et al., 2018; Ma et al., 2019a). From there, CSF drains towards the venous system via arachnoid granulations (Vinje et al., 2020), towards lymph nodes via e.g., perineural routes across the cribriform plate (Ma et al., 2017; Ma et al., 2019a; Proulx, 2021), or the meningeal lymphatics (Louveau et al., 2017), or flows through the brain parenchyma itself via glymphatic (perivascular) pathways (Iliff et al., 2012). The relative importance of these pathways, their interplay, and role(s) in physiological as well as pathological solute transport remain unresolved (Hladky and Barrand, 2014; Louveau et al., 2017; Abbott et al., 2018; Bedussi et al., 2018; Ma et al., 2019a; Vinje et al., 2020; Proulx, 2021).

Importantly, CSF circulation characteristics change under physiological transitions, in neurological disorders, and with neurodegenerative disease. In patients diagnosed with idiopathic normal pressure hydrocephalus (iNPH), magnetic resonance imaging (MRI) reveals altered solute influx and clearance rates (Ringstad et al., 2018). In both Alzheimer's and iNPH patients, CSF dynamics in the SAS are altered (Ringstad et al., 2018; Schubert et al., 2019), and CSF production within the choroid plexus may be reduced in iNPH (Eide et al., 2020). On the other hand, changes in glymphatic function may be associated with several types of dementia (Tarasoff-Conway et al., 2015). In Alzheimer's disease, alterations in arterial pulsatility (Thal et al., 2008), aquaporin-4 function (Zeppenfeld et al., 2017) and sleep disturbances (Shokri-Kojori et al., 2018) have been proposed as causes of glymphatic impairment. Lastly, glymphatic transport has been reported to increase during sleep (Xie et al., 2013; Eide et al., 2021a).

A key question is to what extent the CSF circulation induced by CSF production, vascular pulsatility, and CSF efflux contributes to the transport of solutes (both influx and outflux) in the SAS and brain parenchyma. While intraparenchymal transport and glymphatics have received substantial attention over the last decade (Iliff et al., 2012; Xie et al., 2013; Hladky and Barrand, 2014; Asgari et al., 2016; Abbott et al., 2018; Mestre et al., 2018b; Smith and Verkman, 2018; Croci et al., 2019; Ray et al., 2019; Valnes et al., 2020; Eide et al., 2021a; Ray et al., 2021), the clearance interplay between different regions within the intracranial compartment is less understood. To illustrate, while Xie et al. (2013) suggest that the sleep-wake cycle regulates the efficiency of glymphatic solute clearance via changes in the interstitial space volume, the findings of Ma et al. (2019a) offer an alternative interpretation in which increased CSF outflux during wakefulness effectively limits the availability of solutes at the surface and within parenchymal perivascular spaces (PVSs). As the intracranial CSF volume is only 10%–30% of that of the brain (Kohn et al., 1991; Yamada et al., 2016), rapid clearance of substances from the SAS is crucial to sustain diffusive transport from the brain parenchyma to the SAS.

Crucially, CSF flow velocities in the SAS, including in surface PVSs, are substantial. Pulsatile CSF velocities of at least 10–40 μm/s can be inferred from experimental measurements of microsphere movement in rodents (Mestre et al., 2018a; Bedussi et al., 2018). Furthermore, the resulting dispersion effects may dominate diffusion by a factor of 10^4 for the transport of smaller molecules such as the MRI contrast molecule Gadoteridol (Ray et al., 2021). In humans, CSF flow in the SAS varies significantly between patients and diseases (Eide et al., 2021b), with velocities at the foramen magnum induced by pulsatile flow on the order of 5 cm/s (Bradley et al., 2016). Interestingly, CSF bulk flow at a magnitude of μm/s can be induced in the ventricular system and surface PVSs by relatively small intracranial pressure gradients (<1–2 mmHg/m) (Vinje et al., 2019).

In this study, using biophysics-based finite element computational models created from T1-and T2-weighted MR images (Ringstad et al., 2017; Ringstad et al., 2018), we study CSF flow in the ventricular system and SAS and solute transport in these CSF-filled spaces and brain parenchyma. We first simulate flow patterns and magnitude induced by a production of 0.5L CSF per day (Pardridge, 2016) in the choroid plexus and different CSF efflux pathways: across the parasagittal dura, across the cribriform plate, and into meningeal lymphatics, as well as reversed flow scenarios. We next simulate solute transport in the SAS and brain parenchyma resulting from an intrathecal injection of gadobutrol. Our findings indicate that CSF flow in the SAS is a major player in brain clearance. However, no single outflow pathway alone is able to explain *in vivo* observations of brain-wide distribution of tracers combined with fast clearance from the SAS, and we thus propose that a combination of different outflow routes seems more likely.

2 Methods

In this computational study, we quantify and characterize CSF flow patterns and molecular transport in the SAS and parenchyma induced by different clearance pathways. We also consider a choroid plexus-based production of 0.5 L/day of CSF and efflux across the 1) parasagittal dura (Ringstad and Eide, 2020), 2) the cribriform plate (Ma et al., 2017), and 3) meningeal lymphatics (Louveau et al., 2017). We consider a scenario with retrograde flow in the aqueduct (Lindstrøm et al., 2018) by assuming that 0.5 L/day CSF production occurs within the spinal cord and, as such, that there is an influx through the foramen magnum, combined with an efflux route in the choroid plexus. An illustration of a slice of the computational domain is given in Figure 1. Also, for the ease of the reader, Table 1 summarizes all physical constants that will be used in this section.

2.1 Patient data and approvals

We consider baseline T1-and T2-weighted MR images (resolution 1 mm) from an iNPH patient collected in a previous

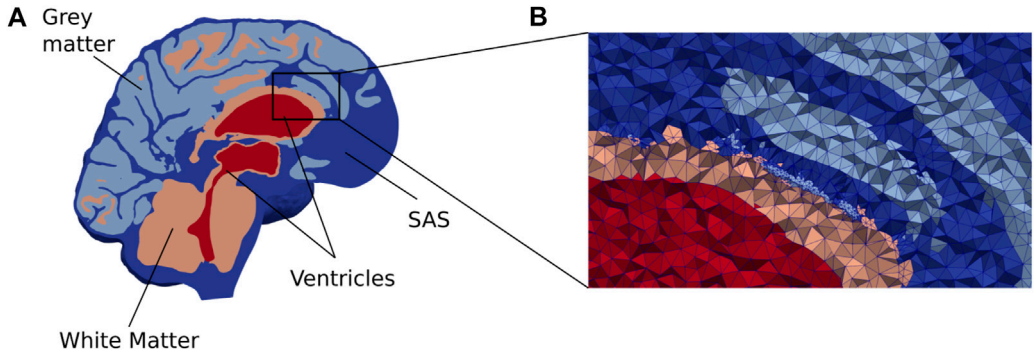

FIGURE 1
(A) A cross section of our brain mesh shows the SAS (dark blue), white matter (orange), gray matter (light blue), and ventricles (red) **(B)** shows a zoom in on a part of the mesh with the edges of the mesh triangles. Note that for visualization purposes, the resolution shown here is coarser than the resolution used in the numerical simulations.

clinical study. This patient then underwent a (0.5 ml, 1 mmol/ml) intrathecal injection of the gadolininium-based tracer gadobutrol, and follow-up MR images were taken at several time points post injection. LookLocker images were also obtained with the T1-weighted MR images. The clinical study was approved by the Regional Committee for Medical and Health Research Ethics (REK) of Health Region South-East, Norway (2015/96), the Institutional Review Board of Oslo University Hospital (2015/1868), and the National Medicines Agency (15/04932-7), and conducted in accordance with the ethical standards of the Declaration of Helsinki of 1975 (and as revised in 1983). All study participants were included after written and oral informed consent.

2.2 *In-vivo* imaging concentration estimates

The baseline MR images were post-processed using FreeSurfer v6.0 (Fischl, 2012) to obtain a segmentation of the brain. To define a choroid plexus (CP) completely enclosed by the lateral ventricles, a CP domain was manually marked in the images. Next, the left and right pial membranes, white matter interface, cerebellum, ventricles, and aqueduct were represented via triangulated surfaces. The segmentation of the SAS was performed by thresholding a registered T2-weighted image, and any clusters not connected to the FreeSurfer segmentation were removed. Subsequently, a surface bounding the SAS was constructed, and expanded by 1 mm in the surface normal direction to ensure that the SAS was represented as a continuous compartment between the pia and dura around the whole brain. The CSF volume before and after expansion was 457 and 602 ml, respectively. The spinal cord was not segmented and was represented as CSF for simplicity. The parenchymal volume was 1,266 ml. Both the CSF and parenchymal volumes are slightly above average values in iNPH patients (Yamada et al., 2016).

The generated surfaces were further post-processed using SVMTK (2021), and finally used to generate a volumetric mesh Ω of the parenchyma Ω_P and surrounding CSF-spaces Ω_F combined (Figure 1). We label the boundary separating Ω_P and Ω_F by $\partial\Omega_P$. The choroid plexus $\Omega_{CP} \subset \Omega_F$ is located within the lateral ventricles and we denote its surface (in contact with the CSF) by $\partial\Omega_{CP}$. The outer boundary of the SAS is split into three parts: $\partial\Omega_S$, $\partial\Omega_{FM}$, and $\partial\Omega_{out}$, representing the arachnoid membrane, foramen magnum, and a chosen efflux route, respectively. We consider and define three different regions Ω_{out} for efflux of CSF: locally across the *parasagittal dura* (Figure 2A), locally across the *cribriform plate* (Figure 2B), or into the meningeal *lymphatics* distributed over the outer (arachnoid) boundary (Figure 2C). Finally, to simulate retrograde net aquaductal flow, we consider flow into the choroid plexus (Figure 2E) from the foramen magnum (Figure 2D).

2.3 Flow in the cerebrospinal fluid spaces

We model the flow of CSF in Ω_F by the incompressible Stokes equations: find the CSF velocity field u and pressure p such that

$$\mu\nabla^2 u - \nabla p = 0 \qquad \text{in } \Omega_F, \tag{1a}$$

$$\nabla \cdot u = g \qquad \text{in } \Omega_F, \tag{1b}$$

where $\mu = 0.7 \times 10^{-3}$ Pas (Daversin-Catty et al., 2020) is the CSF viscosity and g is a given source of fluid. With the low Reynolds numbers (0.001) reported for flow in PVS (Mestre et al., 2018a; Daversin-Catty et al., 2020), we find steady Stokes flow to be a reasonable assumption for the present study. To represent CSF production in the choroid plexus, we let g be a given positive constant in Ω_{CP} and zero elsewhere in Ω_F. Specifically, by default, we set g such that approximately 0.5L of CSF is produced every 24 h. We also consider a scenario with increased CSF production. In humans, CSF production has been reported to increase during

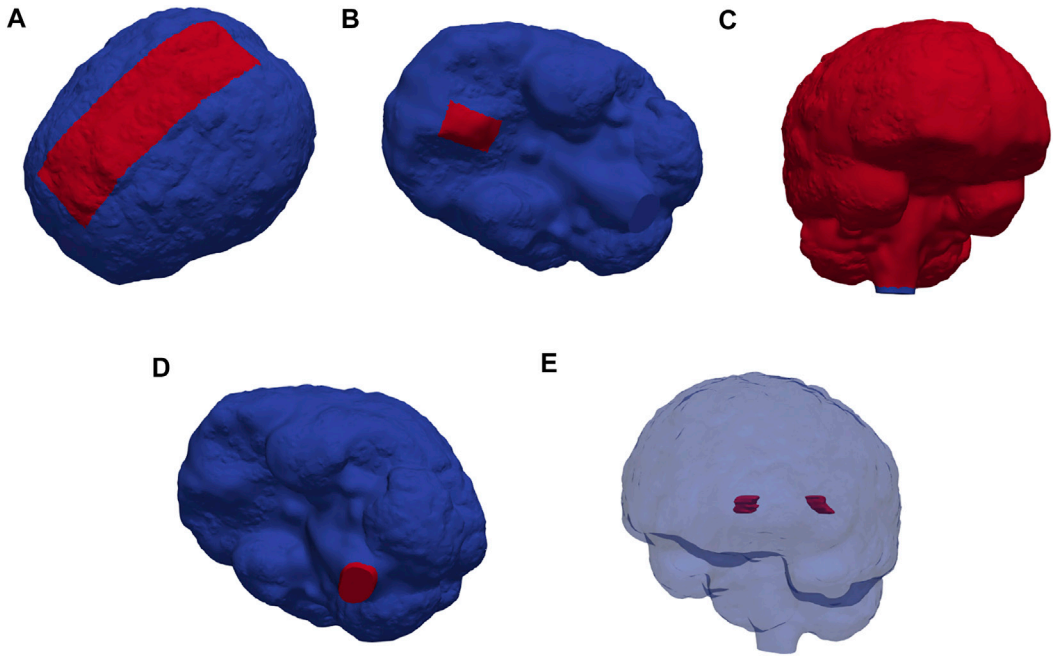

FIGURE 2
Red markers highlight important subregions and boundaries in the computational domain: the **(A)** parasagittal dura, **(B)** cribriform plate, **(C)** meningeal lymphatics, **(D)** foramen magnum, and **(E)** choroid plexus.

sleep (Nilsson et al., 1992), while high CSF turnover through lymphatics has been reported in awake mice (Ma et al., 2019a). We set the parenchymal CSF/brain interstitial fluid (ISF) velocity to be zero (in Ω_P).

We set the CSF velocity at the outer boundary (representing the arachnoid membrane) to be zero, except at specific efflux/absorption sites $\partial\Omega_{\text{out}}$ to be further specified. At these, we set a traction condition:

$$\mu\nabla u \cdot n - pn = -u \cdot nR_0 n \qquad \text{on } \partial\Omega_{\text{out}}, \tag{2}$$

where $R_0 \geq 0$ represents an efflux resistance acting to moderate CSF outflow in these regions, and n denotes the outward-pointing boundary normal. The fluid source, in combination with the zero or low resistance efflux routes, induces a flow of CSF from the CP through the ventricular system, through the SAS, and out across either the parasagittal dura, cribriform plate, or meningeal lymphatics.

We also consider a reversed flow scenario, in which g is set negative with a value corresponding to a sink of 0.5 L/day, a zero traction condition is imposed at the foramen magnum $\partial\Omega_{\text{FM}}$, and zero velocity (no slip) is imposed on the remainder of the boundary.

2.4 Molecular transport in the cerebrospinal fluid and parenchyma

We also model molecular transport within the CSF-spaces and parenchyma resulting from an influx of gadobutrol at the foramen magnum (resulting, e.g., from an intrathecal injection). We model transport of a concentration c in the entire domain Ω via the diffusion-convection equation.

$$\phi\frac{\partial c}{\partial t} + \phi u \cdot \nabla c - \nabla \cdot \left(\phi\alpha D\nabla c\right) = 0 \qquad \text{in } \Omega, \tag{3}$$

where u is a convective velocity field, D denotes an apparent diffusion coefficient, and α is a dispersion factor. We set the apparent diffusion coefficients $D_F = 3.8 \cdot 10^{-4}$ mm^2/s in Ω_F and $D_P = \frac{D_F}{\lambda^2} = 1.2 \cdot 10^{-4}$ mm^2/s in Ω_P (Valnes et al., 2020). Here, $\lambda \approx 1.78$, represents the tortuosity. To represent enhanced diffusion in the CSF due to pulsatile effects, mixing or other forms of dispersion (Asgari et al., 2016; Sharp et al., 2019; Ray et al., 2021), we have introduced the dispersion factor α, and consider a range of $\alpha \in \{1, 10, 100, 1{,}000\}$ in Ω_F. In Ω_P we set $\alpha = 1$. ϕ accounts for the porosity of the extracellular space which occupies 20% of the parenchyma (Nicholson and Phillips, 1981), and we thus set $\phi_P = 0.2$ and $\phi_F = 1$. We consider either $u = 0$ and $\alpha = 1$ (diffusion-only scenarios) or let u be given by solutions of the CSF flow Eq. 1 in combination with all α.

To represent an influx of gadobutrol at the foramen magnum, we set

$$D\nabla c \cdot n - cu \cdot n = F(t) \qquad \text{on } \partial\Omega_{\text{FM}}. \tag{4}$$

Based on tracer enhancement as reported by Eide et al. (2020), $F(t)$ is modeled as a linearly decreasing function until $T_0 \approx 2.24$ h (8,064 s) and zero thereafter, i.e.,

$$F(t) = \begin{cases} 2.395 \cdot 10^{-11}\,(T_0 - t) & \text{if } t < T_0 \\ 0 & \text{otherwise.} \end{cases} \quad (5)$$

The solute influx $F(t)$ (given in mmol/(s mm^2) is chosen such that the total amount of gadobutrol injected is approximately 0.5 mmol. At the efflux sites $\partial\Omega_{\text{out}}$, we let the solute be absorbed via the relation.

$$D\nabla c \cdot n - cu \cdot n = -\beta c \qquad \text{on } \partial\Omega_{\text{out}}, \quad (6)$$

where β is a given membrane permeability. The case $\beta = 0$ corresponds to no absorption, $\beta = \infty$ corresponds to free movement of solutes across the boundary, while $0 < \beta < \infty$ represents a diffusive resistance to molecular outflow. On the remainder of the boundary, we do not allow for solute efflux, by setting $D\nabla c \cdot n - cu \cdot n = 0$. Moreover, we let the initial concentration be $c\,(x, 0) = 0$. Note that to model transport associated with the reversed flow scenario, we let $\partial\Omega_{\text{CP}}$ take the role of $\partial\Omega_{\text{out}}$.

At the interface between Ω_F and Ω_P we conserve mass (enforce conservation of molecules) by setting $\phi D_P \nabla c_P \cdot n = D_F \nabla c_F \cdot n$. Here, D_P and D_F denote D restricted to Ω_P and Ω_F; respectively, n is the normal vector on the interface, pointing from Ω_P to Ω_F and ϕ denotes the extracellular space (ECS) porosity.

2.5 Overview of models

CSF and solutes may have several simultaneous and possibly partially independent outflow routes (Proulx, 2021). We here consider six different flow and transport models separately (Table 2), each with different dispersion factors. This design allows us to systematically examine different pathways and evaluate whether each or combinations thereof could describe *in-vivo* observations of Gadobutrol transport. Model I and II describe flow induced by CSF production in the CP and CSF efflux across the parasagittal dura and cribriform plate, respectively. For these models, we assume free molecular efflux at the absorption sites. Model III is a variant of Model I with a finite molecular efflux permeability at the parasagittal dura absorption site. Model IV reflects a different efflux pathway with CSF production in the CP, CSF efflux in the meningeal lymphatics, and a finite molecular efflux permeability. Model V represents a reversed flow scenario with absorption of CSF in the CP region (and CSF influx at the foramen magnum). Model VI represents a variant of Model II with increased CSF production. CSF production has been reported to vary between subjects and different central nervous system disorders (Eide et al., 2020; Eide et al., 2021b). Furthermore, CSF production has been reported to increase by a factor of up to three during the nighttime compared to the daytime (Nilsson et al., 1992), and increased CSF efflux to the lymphatic system has been reported to limit tracer entry to the brain (Ma et al., 2019b). In this study, we set the CSF production for model VI to be 1.0 L/day (i.e., twice that of all other models).

2.6 Numerical methods, simulation software and verification

The Stokes equations are solved using a finite element method with Taylor-Hood (continuous piecewise quadratic and continuous piecewise linear) elements for the velocity and pressure. The diffusion-convection equation with boundary conditions is solved numerically using the finite element method with continuous linear finite elements for the concentration in space and the backward Euler method in time; all using the FEniCS finite element software (Logg et al., 2012; Alnæs et al., 2015). The brain mesh has 6 691 432 cells and 1 088 640 vertices. The degree of freedom for the diffusion equation is equal to the number of vertices. For the Taylor-Hood case, the number of degrees of freedom is 27 858 018. Moreover, the largest cell size is 2.4 mm and the smallest is 0.07 mm. The largest cells are in the middle of the white matter where there is no stokes flow or sharp gradients.

A time resolution study was performed to ensure that our simulation results were independent of the choice of time step (Supplementary Figure S1). As mesh refinements of the entire geometry are too expensive, a mesh resolution study was performed on a partition of the mesh containing both CSF and brain tissue (Supplementary Figure S2). Refinements from a cell size comparable to the resolution in the full geometry did not change key quantities like flow velocity in the SAS or tracer concentration in the brain (Supplementary Table S2). Including testing and validation, a total of ≈30,000 CPU hours were used to run the simulations on big memory nodes. All simulations were run on the high-performance computing infrastructure Sigma2—the National Infrastructure for High Performance Computing and Data Storage in Norway.

2.7 Concentration estimates from in-vivo MRI

We extract contrast agent concentration estimates from the MR images post injection for comparison with computational predictions. The contrast agent shortens the T1 times as:

$$\frac{1}{T_1(c)} = r_1 c + \frac{1}{T_1(0)}, \quad (7)$$

where c denotes the concentration of the contrast agent, r_1 is known as the T1 relaxivity of the agent, and $T_1(c)$ and T_1 (0) denote the T1 time with and without concentration, respectively. The T1 times can be computed using a T1 mapping (Taylor et al.,

TABLE 1 Overview of parameter values used in the model. Parameters with an asterisk are considered uncertain and were set to vary between different computational models (see Table 2).

Parameter	Description	Value	Unit	Ref
μ	SAS viscosity	0.7×10^{-3}	Pas	Daversin-Catty et al. (2020)
D_F	SAS apparent diffusion coefficient	3.8×10^{-4}	mm^2/s	Valnes et al. (2020)
D_P	Parenchyma apparent diffusion coefficient	1.2×10^{-4}	mm^2/s	Valnes et al. (2020)
ϕ_P	ECS volume fraction	0.2	—	Nicholson and Phillips, (1981)
ϕ_F	SAS volume fraction	1	—	—
α	Dispersion coefficient	1–1,000	—	Asgari et al. (2016); Ray et al. (2021)
R_0^*	Fluid outflow resistance	10^{-5}		
β^*	Molecular outflow resistance	10^{-4}	mm^2/s	—

TABLE 2 Overview of computational models. Production and absorption sites refer to the production sites for CSF and efflux/absorption sites of CSF and the solute concentration, respectively. R_0 is a CSF efflux resistance parameter cf. (2), while β represents a diffusive resistance to molecular efflux cf. (6). The values for R_0 and β were estimated by numerical experimentation.

Model	Production site	Absorption site	R_0 [Pa/(mm s)]	β (mm^2/s)	Production (L/day)
I	Choroid plexus	Parasagittal dura	0	∞	0.5
II	Choroid plexus	Cribriform plate	0	∞	0.5
III	Choroid plexus	Parasagittal dura	0	10^{-4}	0.5
IV	Choroid plexus	meningeal lymphatics	10^{-5}	10^{-4}	0.5
V	Foramen magnum	Choroid plexus	0	∞	0.5
VI	Choroid plexus	Cribriform plate	0	∞	1.0

2016), such as the LookLocker sequence. Through a preliminary phantom study, the relaxivity constant for this LookLocker protocol was found to be 6.5 L mmol^{-1} s^{-1}. The median T1 time over the parenchyma was used in Eq. 7 to estimate the concentration in the parenchyma. The CSF concentration was estimated by manually creating a region of interest (ROI) in the CSF, and using the average T1 time over the ROI with Eq. 7. Finally, to transform the concentration in the parenchyma to be that of the extracellular space, the concentration was multiplied by five.

2.8 Quantities of interest

The total amount of solute in a given region Ω_i ($i = F, P$) at time t was computed as $M_i(t) = \int_{\Omega_i} \phi_i c \, dx$. The total amount within the intracranial compartment $M(t)$ is then the sum $M(t) = M_P(t) + M_F(t)$. The average concentrations per region over time were computed as

$$\overline{c_i} = \frac{M_i(t)}{\phi_i V_i},$$

where V_i refers to the volume of the respective region. To compare parenchymal influx between models, we compute the peak average concentration in the parenchyma and the time to reach this peak. We also compute the relative clearance of tracers after $T_1 = 3$ days as $1 - \frac{M(T_1)}{M(0)}$.

3 Results

All models induce non-trivial CSF flow through the ventricular system and subarachnoid space.

3.1 Different outflow routes induce different cerebrospinal fluid flow patterns and velocities

Models I–IV all reach maximal SAS velocities of 8.9 mm/s in the thinnest part of the aqueduct (Figures 3A–C). Despite their differences in efflux pathways, all of these models predict higher CSF flow velocities in the anterior regions of the SAS compared to the posterior regions. Model II displays the highest velocities in the SAS, reaching 50 μm/s. Models I (and III) reach peak CSF velocities of 40 μm/s. In model IV, CSF flow occurs mainly in the lower regions of the SAS, as CSF can exit the SAS along the entire boundary. Peak velocities in the SAS for model IV reach 20 μm/s.

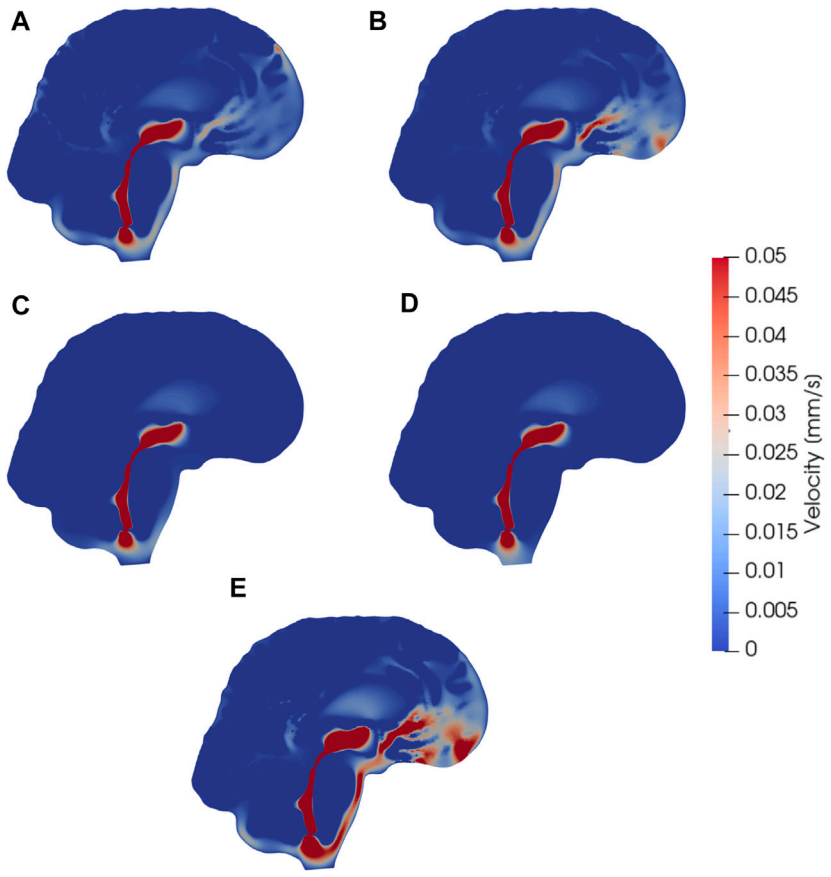

FIGURE 3
Sagittal views (cut through the center of the aqueduct) of CSF velocity magnitudes induced by steady CSF production in the choroid plexus combined with different CSF efflux pathway models, or a reversed flow scenario. Subfigures show velocity fields resulting from CSF efflux through **(A)** the parasagittal dura **(B)** the cribriform plate **(C)** the meningeal lymphatics **(D)** production in the foramen magnum and absorption in the choroid plexus, **(E)** the cribriform plate with double production. The color map is capped at 0.05 mm/s for visualization purposes.

In models where CSF was allowed to exit through outflow routes other than the parasagittal dura (models II and IV), CSF velocity magnitudes were relatively small (<4 μm/s) in the SAS near the upper convexities of the brain.

3.2 Reversed cerebrospinal fluid flow pathways

Model V predicts that, under its assumptions, CSF will predominantly flow from the foramen magnum directly to the CP, limiting CSF flow in other parts of the SAS (Figure 3D). Therefore the flow direction is reversed compared to models I–IV. In the foramen magnum, CSF velocity magnitudes reach 20 μm/s, while the velocity in the aqueduct remains at 8.9 mm/s. In the upper regions of the SAS, not directly associated with the 3rd ventricle, CSF velocities were typically lower than 0.1 μm/s.

3.3 Increased cerebrospinal fluid production increase cerebrospinal fluid velocities

Doubling the CSF production (model VI versus model II) results in a doubling of the CSF velocity field by linearity. Therefore, we observe velocities of approx. 100 μm/s in the CSF space (Figure 3E) and a velocity in the aqueduct of 17.8 mm/s for model VI.

3.4 Diffusion alone yields excessively slow clearance from intracranial compartments

When driven purely by diffusion (without convection or dispersion enhancements), the tracer spreads radially from the foramen magnum and distributes evenly throughout the brain. The distribution is slightly faster in the CSF than in the

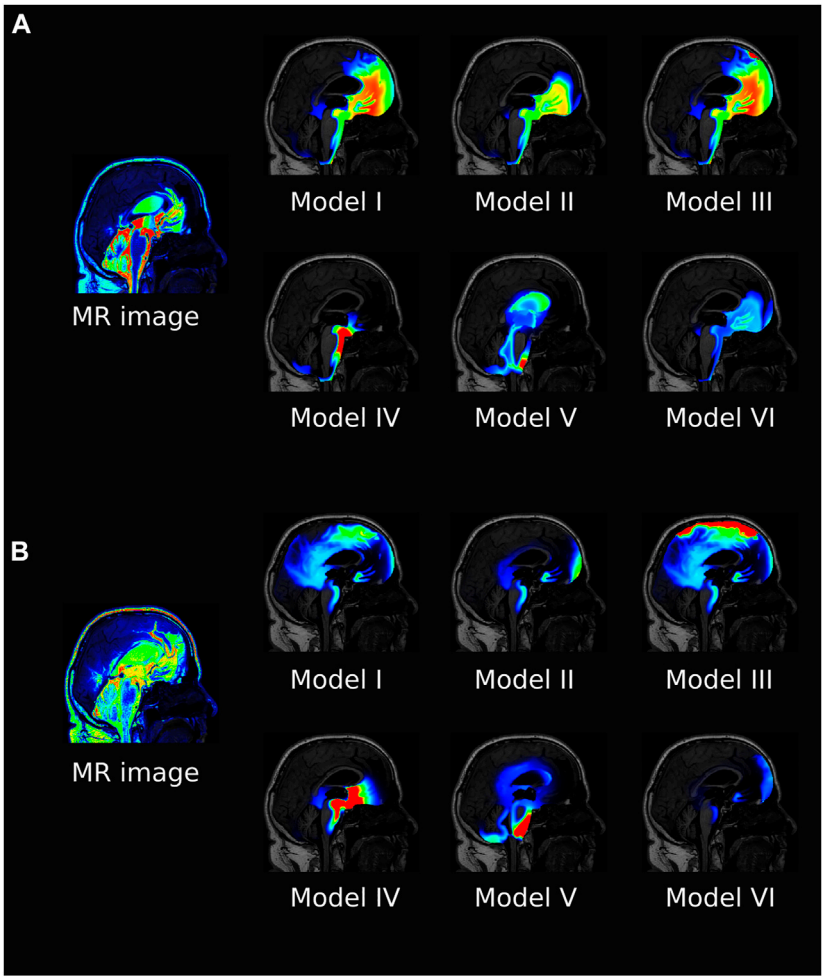

FIGURE 4
The figure shows a sagittal view of all the models at 6 h **(A)** and 24 h **(B)** after intrathecal injection of gadobutrol for α =10. For the simulation data, the colorscale shown is 0.1–5 mmol/L in **(A)** and 0.1–1 mmol/L in **(B)**. For comparison, the T1 contrast enhanced image for the patient at the same time is included. The MR images are scaled separately for picture legibility.

parenchyma, as the free diffusion coefficient in the CSF is larger. However, this effect is not very noticeable. For Models I–III the relative 1 year clearance is only 32.8%, 17.6 %, and 29.9%. Model IV displays faster clearance, clearing 92.5% over 1 week but with a late peak parenchyma concentration occurring after 79 h.

3.5 Tracer distribution patterns induced by cerebrospinal fluid circulation and dispersion

Including the CSF circulation-induced flow as a convective velocity substantially speeds up the clearance rates, both from the SAS and parenchyma.

Tracer distribution is shown for all models after 6 and 24 h and α = 10 in Figure 4, revealing substantial inter-model variations. For Model I, the tracer is mainly confined to the SAS and moves upwards towards the parasagittal dura, showing a clear preference for traveling along the SAS in the right hemisphere (data not shown). As there is no molecular resistance to outflow on the parasagittal dura in Model I, the tracer is instantly transported out when moving into this efflux route. In regions where the tracer concentration in the SAS is high, the tracer also enters the brain due to the large concentration gradient between the SAS and the brain (Figures 4A,B Model I). After 1 week, some traces are still found within the brain, slowly diffusing back towards the pial surface for clearance via convection in the SAS (data not shown). Models I and III (with outflow via the parasagittal dura) are the only models where a tracer reaches the upper convexities of the brain, resulting in a brain-wide distribution of tracers. In Model III, where a

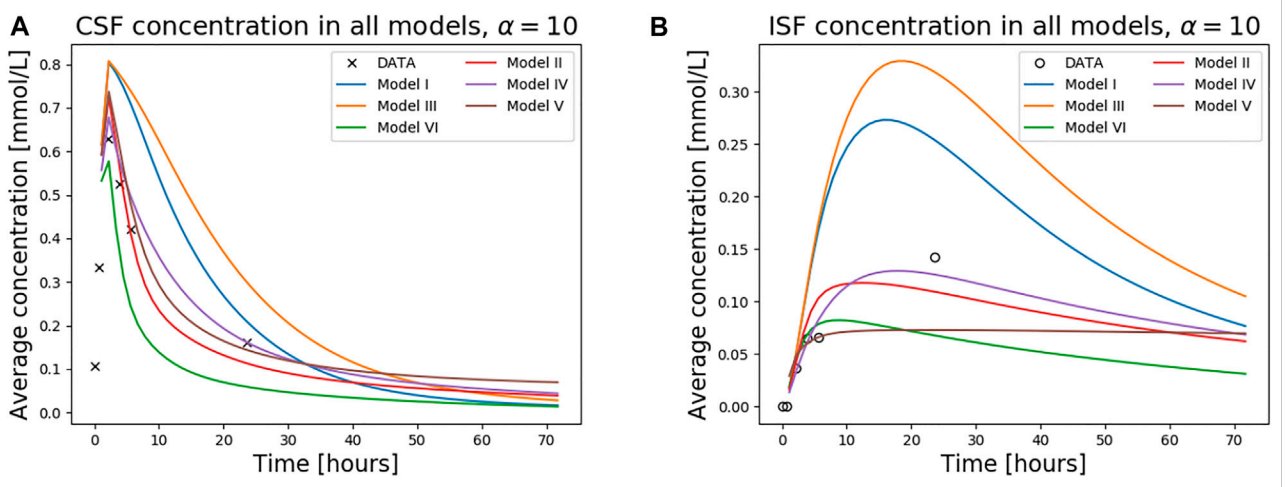

FIGURE 5
The figure shows concentration in the CSF **(A)** and the ISF **(B)** for all models over 1 week. The tracer concentration data from T1 MR images for this patient is also shown.

diffusive molecular resistance is added at the parasagittal dura, tracer accumulates near the outflux region (Figures 4B, Model III).

Model V is the only model where tracer reaches the ventricular system, while Model IV has a localized accumulation of tracers around the brain stem. Model VI, with increased CSF production, shows a generally lower concentration of tracers and some accumulation near the outflux route at the cribriform plate.

The average concentration over time for all models, and α = 10, is compared in Figure 5, both for the ISF and CSF. The figure also contains *in vivo* concentration estimates in both spaces. We observe that a combination of the different outflow routes, i.e., Models I and V, gives a comparable result to that of the MR images. Models I and III both display higher concentrations than the data in both the CSF and parenchyma/ISF (Figure 5). Model II, IV, and V, on the other hand, yield comparable or lower concentrations.

3.6 Clearance rates induced by cerebrospinal fluid circulation and dispersion

Models I and II both display high 3-day clearance rates for all dispersion factors (Figures 6A,B). Specifically, the 3 day clearance rates are between 94.1% and 97.7% for Model I and between 88.9% and 94.9% for Model II (Table 3). The tracer concentration is initially higher in the SAS, allowing for diffusive influx to the brain. At later time points, the SAS has been cleared, mainly via convective flow, and the tracer partly remains inside the parenchyma, delaying the total clearance of tracers from the intracranial compartment. Model I has slightly higher peak average parenchyma concentration values than Model II, reaching 0.30 and 0.24 mmol/L, respectively. The time to peak in the parenchyma occurred after 7.8–19.0 h for Model I and 10.1–16.8 h for Model II.

For the models including a molecular resistance to outflow at the outflow site (i.e., Figures 6C,D, Model III and IV), the 3 day clearance rate is comparable to Models I and II, except for the case when α = 1,000 in Model III (Table 3). The highest 3 day clearance is obtained with α = 1 for both Model III and IV (95.7 and 99.0% clearance, respectively). The lowest 3 day clearance is obtained with α = 1,000 for model III (36.3% clearance) and α = 10 for model IV (89.5% clearance, Table 3). Model III reaches a peak parenchyma concentration of 0.50 mmol/L, while Model IV has a lower peak of 0.23 mmol/L. The time to peak exceeds 19.0 h for all dispersion factors in Model III, which is much later than the other models. Model IV, on the other hand, peaks between 11.2 and 17.9 h.

3.7 Clearance of gadobutrol with reverse pathways

Model V (with reversal of CSF flow in the aqueduct) results in low parenchymal enrichment compared to Models I–IV (Table 3, Figure 6E). The 3 day clearance rate is between 75.1% and 90.0% depending on α and the peak average concentration is 0.18 mmol/L in the parenchyma (Table 3). The time to peak concentration in the parenchyma is long for α = 1, occurring later than after 1 week, but for larger dispersion factors, the peak occurs between 10.8 and 22.4 h.

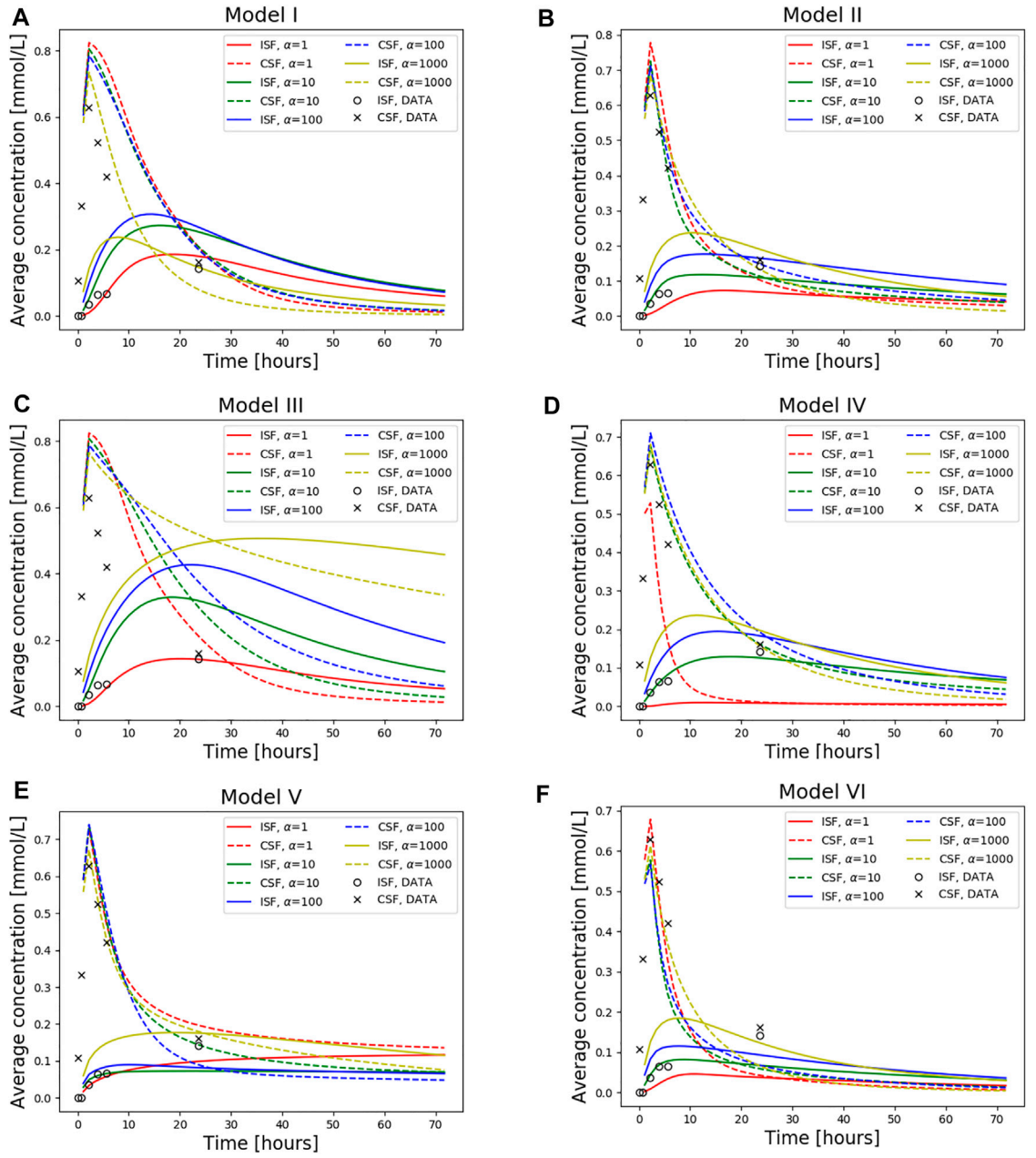

FIGURE 6
Average concentration in the parenchyma (par) and CSF over a period of 72 h. Models I-VI is used with dispersion values α = 1, 10, 100, 1,000. Also plotted is the concentration data taken from T1-weighted images of this specific patient as a ground truth. The tracer injection (present from 0 to 2.24 h) is seen as a sharp increase in CSF concentration at early time points. When the injection is no longer present, the total amount of tracers within the intracranial compartment starts decreasing. The tracer concentration data from T1 contrast enhanced images of the patient is also included. **(A)** Model I **(B)** Model II **(C)** Model III **(D)** Model IV **(E)** Model V and **(F)** Model VI.

3.8 Increased cerebrospinal fluid production results in rapid clearance

Model VI, with double the sCSF production of the other models, displayed rapid clearance from the CSF (Figure 6F). The rapid turnover of CSF limited the influx and facilitated clearance within the parenchyma. The 3 day clearance rate for all dispersion factors ranged between 95.4%–97.9% (Table 3). The peak average parenchyma concentration occurs early, between 7.8 and 11.2 h, and reaches at most 0.15 mmol/L, when α = 1,000.

TABLE 3 The table shows time to peak concentration in the parenchyma (left), total mass clearance in the intracranial compartment after 72 h (middle), and peak average concentration values in the parenchyma (right) for the case of gadobutrol transport. Values are shown for all models and α values. M, Model; α: Dispersion factor, par, parenchyma; conc, concentration; avg, average.

	Time to par peak (hours)				Three day clearance rate (%)				Peak avg par conc (mmol/L)			
M\α	1	10	100	1,000	1	10	100	1,000	1	10	100	1,000
I	19.0	15.7	14.6	7.8	95.6	94.1	94.4	97.7	0.18	0.27	0.30	0.24
II	16.8	12.3	12.3	10.1	94.0	91.2	88.9	94.9	0.07	0.12	0.17	0.24
III	20.2	19.0	22.4	35.8	95.7	91.3	82.8	36.3	0.14	0.32	0.43	0.50
IV	12.3	17.9	15.7	11.2	99.0	89.5	91.5	94.0	0.01	0.13	0.19	0.23
V	>72	22.4	10.8	19.0	75.1	86.9	90.0	82.6	0.12	0.07	0.09	0.18
VI	11.2	9.0	7.8	7.8	97.9	95.5	95.4	97.4	0.05	0.08	0.11	0.18

4 Discussion

In this paper we have simulated molecular transport by diffusion and convection for six different models investigating the distribution of gadobutrol molecules entering the intracranial compartment via the foramen magnum. The different models represent different outflow routes, and CSF flow patterns vary considerably between models. The effects of outflow route and dispersion factor modify the distribution and clearance patterns in a non-linear and unpredictable manner. Outflow through either the parasagittal dura, the cribriform plate, or through meningeal lymphatics, typically clears 80%–99% of injected tracers over a time period of 3 days. These three models, however, display very different spatial distributions of tracers. In Models I and III tracer are distributed more or less throughout the frontal cortex, while when outflow occurs through meningeal lymphatics, tracers are mainly located at the brain stem at the base of the brain.

With a daily production of 0.5 and 1.0 L/day in our models, the velocity reaches 10 and 17.8 mm/s in the aqueduct. Pulsatile aqueductal flow velocities of several cm/s have been measured experimentally (Lee et al., 2004; Tawfik et al., 2017; Spijkerman et al., 2019) in the range of 1–10 cm/s. Average velocities and max velocities were reported at around 5 cm/s, corresponding to a total volume flux of 0.3 ml per cycle, of which 0.01 ml was net (Lindstrøm et al., 2018; Eide et al., 2021b). As the net flow is around 1/30 of the total flux, the corresponding net max velocity can then be estimated as 5/30 cm/s, somewhat below the velocities estimated here. Further, in iNPH patients, it has been reported that phase-contrast MR has reported retrograde net flow in the aqueduct (Lindstrøm et al., 2018). Model V is motivated by retrograde aqueductal flow and we see that this model is distinct from the other models in that there is significant ventricular enrichment, as often seen in iNPH (Ringstad et al., 2018).

On the pial surface of the brain, we observe velocities of up to 20–50 μm/s in models I-IV, and up to 100 μm/s in model VI. These velocities align relatively well with experimentally observed bulk flow velocities of around 20 μm/s observed in mice (Mestre et al., 2018a; Bedussi et al., 2018). Thus, CSF flow observed in these studies may very well be a result of CSF production and absorption driven by small static pressure differences. It should be noted that mice have approximately 3x faster CSF turnover compared to humans (Pardridge, 2016). Given otherwise similar CSF dynamics between the species, one would thus expect CSF production to cause higher velocities at the surface of the mouse brain compared to the human. In comparing model II and model VI, the increased CSF efflux to the cribriform plate limits tracer influx to the brain, in line with the hypothesis of Ma et al. (2019a). We observe that models with a short distance between injection and absorption site (models II, IV, and V) limit the influx of tracers to the parenchyma. In general, tracers will enter the brain if they are present on the surface over a long period of time. For a given tracer, the amount of tracers entering the brain will thus be affected by both the CSF velocity and the distance from the injection site to the absorption site.

Gadobutrol injections have been studied in human subjects in several papers. Eide, Ringstad and colleagues have reported MR intensity increases for a large number of subjects (Ringstad et al., 2017; Ringstad et al., 2018; Eide et al., 2020; Eide et al., 2021a), while Watts et al. (2019) quantified gadobutrol concentrations over time in a single patient. These studies show an initial sharp increase in tracer concentration in the SAS, typically reaching a peak at around 2–6 h. In the parenchyma, peak values occur between 10 and 24 h, depending on the region of interest. Gray matter regions closer to the pial surface typically peak at around 10 h, while for specific white matter regions, peak values may occur closer to 24–40 h post-injection (Ringstad et al., 2018; Watts et al., 2019). In all our models, peak CSF concentration occurs at the time when the gadobutrol influx at the foramen magnum is turned off, i.e., after approximately 2 h. More interestingly, the ISF concentration peaks later, and the time to peak is between

10 and 20 h in 15 out of 24 models tested. ISF concentration is reported to decay relatively slow, with an approximate concentration at 48 h at half its peak value (Eide et al., 2021a). Furthermore, the peak concentration of gadobutrol has been measured as 0.5 mmol/L in the CSF and around 0.12 mmol/L in the ISF (Watts et al., 2019), in line with both the estimates of the concentration in the iNPH patient and the results from our models. Both Model II (outflow through the cribriform plate) and Model IV (outflow via meningeal lymphatics) match all these criteria well when the dispersion in the SAS was modeled by $\alpha = 10$. Model I (outflow through the parasagittal dura) replicates experimentally observed ISF concentration without additional dispersion in the SAS, but clearance from the SAS is delayed in this model compared to experimental data. With a molecular resistance to outflow on the parasagittal dura (Model III), simulations reproduce accumulation of tracers in this region, but clearance kinetics are slower than expected. With a doubling of CSF production (Model VI), the kinetics of ISF and CSF clearance is faster than expected for all dispersion factors tested. In the model with reversed flow in the aqueduct (Model V), we qualitatively reproduce the tracer enhancement in the aqueduct as seen in iNPH patients (Eide et al., 2020). However, rapid flow through the aqueduct and into the choroid plexus prevents the expected brain-wide enhancement of tracers (Ringstad et al., 2018), and in Model V, tracers are confined to the foramen magnum or in the vicinity of the lateral ventricles. Combined, these results suggest that a combination of production and efflux sites may be needed to reproduce the observed tracer distribution (Ringstad et al., 2018; Eide et al., 2020; Eide et al., 2021a).

The role of different outflow routes from the SAS has been debated and challenged over years. In particular, the traditional view of outflow predominately through arachnoid granulations has been criticized recently (Proulx, 2021). Our Model I is conceptually similar to outflow through arachnoid granulations with CSF draining close to the dural sinus. The results from our simulations cannot exclude any of the proposed major outflow routes, as all of them resemble experimental data in at least some measure. A specific weighting between inflow and outflow routes may potentially be sufficient to explain differences between groups (e.g., iNPH vs. control) or differences between individuals. The results do show unequivocally that CSF flow and clearance are major players in CNS clearance. Convective flow in the SAS speeds up intracranial clearance from years to hours and days, an enormous effect compared to the effect of bulk flow of around 1 μm/s within the ECS (Croci et al., 2019). Furthermore, changes in the dispersion factor (increased diffusion due to mixing) only in the SAS changed both peak values and clearance rates within the brain ECS.

In terms of limitations, we only performed the simulations on a single patient. Furthermore, the patient of interest was diagnosed with iNPH, which may alter CSF dynamics (Eide et al., 2021b). Creating one patient-specific mesh with high mesh quality that includes all anatomical regions of interest was time-consuming, and increasing the amount of subjects was not the scope of this study. To resolve all regions of the SAS, the SAS was expanded by 1 mm. This modification increases the volume of which fluid flows, and thus slightly reduces the velocities we find in the SAS. The total CSF volume was increased by around 33%, we thus assume that our reported SAS flow velocities of 20–50 μm/s are lower estimates. In the SAS, we assumed that the dispersion factor was similar in all subregions. In reality, dispersion would be expected to be enhanced close to larger arteries (Ringstad et al., 2017) and in regions where pulsatile CSF flow is substantial (e.g., near the foramen magnum). Furthermore, we did not include ISF velocities in the foramen magnum. There is very little knowledge about how the velocity fields are directed (Croci et al., 2019), especially without a priori knowledge of the location of blood vessels. In addition, the purpose of this study was to assess the effect of SAS convection, independent of potential bulk flow within the brain. Finally, we should note that we assumed that all injected gadobutrol reached the foramen magnum, while around 33% of CSF has been proposed to be drained along the spinal canal (Edsbagge et al., 2004). The latter point may explain the fact that most of the reasonable models tested (Models I, II, and IV) all generally display a slight overestimation of the SAS peak concentration in our models compared to the data.

In conclusion, we have demonstrated that convection in the SAS yields rapid clearance both from the SAS and the ISF, even when pure diffusive transport is assumed in the ECS. Convective fluid flow in the SAS has the potential to speed up clearance from years (as would be the case for purely diffusive transport) to days. As none of the models tested were able to reproduce the observed data perfectly (both qualitatively and quantitatively), a combination of the different outflow routes seems most plausible, and their relative weight may differ between groups (Eide et al., 2020).

Data availability statement

The raw data supporting the conclusion of this article will be made available by the authors without undue reservation.

Ethics statement

The studies involving human participants were reviewed and approved by The study was approved by the Regional Committee for Medical and Health Research Ethics (REK) of Health Region South-East, Norway (2015/96), the Institutional Review Board of Oslo University Hospital (2015/1868), and the National Medicines Agency (15/04932-7), and was registered in the Oslo University Hospital Research Registry (ePhorte 2015/

1868). The conduct of the study was governed by ethical standards according to the Declaration of Helsinki of 1975 (and as revised in 1983). Study participants were included after written and oral informed consent. The patients/participants provided their written informed consent to participate in this study.

Author contributions

MH, VV, LV, PE, GR, MR, and K-AM conceived the simulations; LV and MH segmented and meshed MR images; MH conducted the simulations; VV, MH, and LV did the analysis of the results; and MH made the figures. All authors discussed the simulations and results. MH, VV, LV, MR, and K-AM wrote the first draft. All the authors revised and approved the final manuscript.

Funding

K-AM acknowledges support from the Research Council of Norway, Grant 300305 and 301013, and the national infrastructure for computational science in Norway, Sigma2, Grant NN9279K. MR has received funding from the European Research Council (ERC) under the European Union's Horizon 2020 research and innovation programme under Grant agreement 714892.

Conflict of interest

The authors declare that the research was conducted in the absence of any commercial or financial relationships that could be construed as a potential conflict of interest.

Publisher's note

All claims expressed in this article are solely those of the authors and do not necessarily represent those of their affiliated organizations, or those of the publisher, the editors, and the reviewers. Any product that may be evaluated in this article, or claim that may be made by its manufacturer, is not guaranteed or endorsed by the publisher.

Supplementary material

The Supplementary Material for this article can be found online at: https://www.frontiersin.org/articles/10.3389/fbioe.2022.932469/full#supplementary-material

References

Abbotts, N. J., Pizzo, M. E., Preston, J. E., Janigro, D., and Thorne, R. G. (2018). The role of brain barriers in fluid movement in the cns: Is there a 'glymphatic'system? *Acta Neuropathol.* 135, 387–407. doi:10.1007/s00401-018-1812-4

Alnæs, M., (2015). The fenics project version 1.5. *Archive Numer. Softw.* 3. doi:10.11588/ans.2015.100.20553

Asgari, M., De Zélicourt, D., and Kurtcuoglu, V. (2016). Glymphatic solute transport does not require bulk flow. *Sci. Rep.* 6, 38635–38711. doi:10.1038/srep38635

Bedussi, B., Almasian, M., de Vos, J., VanBavel, E., and Bakker, E. N. (2018). Paravascular spaces at the brain surface: Low resistance pathways for cerebrospinal fluid flow. *J. Cereb. Blood Flow. Metab.* 38, 719–726. doi:10.1177/0271678x17737984

Bradley, W. G., Haughton, V., and Mardal, K.-A. (2016). Cerebrospinal fluid flow in adults. *Handb. Clin. Neurology* 135, 591–601. doi:10.1016/B978-0-444-53485-9.00028-3

Croci, M., Vinje, V., and Rognes, M. E. (2019). Uncertainty quantification of parenchymal tracer distribution using random diffusion and convective velocity fields. *Fluids Barriers CNS* 16, 32–21. doi:10.1186/s12987-019-0152-7

Daversin-Catty, C., Vinje, V., Mardal, K.-A., and Rognes, M. E. (2020). The mechanisms behind perivascular fluid flow. *Plos one* 15, e0244442. doi:10.1371/journal.pone.0244442

Edsbagge, M., Tisell, M., Jacobsson, L., and Wikkelso, C. (2004). Spinal csf absorption in healthy individuals. *Am. J. Physiology-Regulatory, Integr. Comp. Physiology* 287, R1450–R1455. doi:10.1152/ajpregu.00215.2004

Eide, P. K., Valnes, L. M., Pripp, A. H., Mardal, K.-A., and Ringstad, G. (2020). Delayed clearance of cerebrospinal fluid tracer from choroid plexus in idiopathic normal pressure hydrocephalus. *J. Cereb. Blood Flow. Metab.* 40, 1849–1858. doi:10.1177/0271678x19874790

Eide, P. K., Vinje, V., Pripp, A. H., Mardal, K.-A., and Ringstad, G. (2021). Sleep deprivation impairs molecular clearance from the human brain. *Brain* 144, 863–874. doi:10.1093/brain/awaa443

Eide, P. K., Valnes, L. M., Lindstrøm, E. K., Mardal, K.-A., and Ringstad, G. (2021). Direction and magnitude of cerebrospinal fluid flow vary substantially across central nervous system diseases. *Fluids Barriers CNS* 18, 16–18. doi:10.1186/s12987-021-00251-6

Fischl, B. (2012). Freesurfer. *Neuroimage* 62, 774–781. doi:10.1016/j.neuroimage.2012.01.021

Hladky, S. B., and Barrand, M. A. (2014). Mechanisms of fluid movement into, through and out of the brain: Evaluation of the evidence. *Fluids Barriers CNS* 11, 26–32. doi:10.1186/2045-8118-11-26

Iliff, J. J., Wang, M., Liao, Y., Plogg, B. A., Peng, W., Gundersen, G. A., et al. (2012). A paravascular pathway facilitates csf flow through the brain parenchyma and the clearance of interstitial solutes, including amyloid β. *Sci. Transl. Med.* 4, 147ra111. doi:10.1126/scitranslmed.3003748

Kohn, M. I., Tanna, N. K., Herman, G. T., Resnick, S. M., Mozley, P. D., Gur, R. E., et al. (1991). Analysis of brain and cerebrospinal fluid volumes with mr imaging. part i. methods, reliability, and validation. *Radiology* 178, 115–122. doi:10.1148/radiology.178.1.1984289

Lee, J. H., Lee, H. K., Kim, J. K., Kim, H. J., Park, J. K., and Choi, C. G. (2004). Csf flow quantification of the cerebral aqueduct in normal volunteers using phase contrast cine mr imaging. *Korean J. Radiol.* 5, 81–86. doi:10.3348/kjr.2004.5.2.81

Lindstrøm, E. K., Ringstad, G., Mardal, K.-A., and Eide, P. K. (2018). Cerebrospinal fluid volumetric net flow rate and direction in idiopathic normal pressure hydrocephalus. *NeuroImage Clin.* 20, 731–741. doi:10.1016/j.nicl.2018.09.006

Lindstrøm, E. K., Ringstad, G., Sorteberg, A., Sorteberg, W., Mardal, K. A., and Eide, P. K. (2019). Magnitude and direction of aqueductal cerebrospinal fluid flow: Large variations in patients with intracranial aneurysms with or without a previous

subarachnoid hemorrhage. *Acta Neurochir. (Wien).* 161, 247–256. doi:10.1007/s00701-018-3730-6

Logg, A., Mardal, K.-A., and Wells, G. (2012). *Automated solution of differential equations by the finite element method: The FEniCS book*, 84. Berlin: Springer Science & Business Media.

Louveau, A., Plog, B. A., Antila, S., Alitalo, K., Nedergaard, M., and Kipnis, J. (2017). Understanding the functions and relationships of the glymphatic system and meningeal lymphatics. *J. Clin. Invest.* 127, 3210–3219. doi:10.1172/jci90603

Ma, Q., Ineichen, B. V., Detmar, M., and Proulx, S. T. (2017). Outflow of cerebrospinal fluid is predominantly through lymphatic vessels and is reduced in aged mice. *Nat. Commun.* 8, 1434–1513. doi:10.1038/s41467-017-01484-6

Ma, Q., Ries, M., Decker, Y., Muller, A., Riner, C., Bucker, A., et al. (2019). Rapid lymphatic efflux limits cerebrospinal fluid flow to the brain. *Acta Neuropathol.* 137, 151–165. doi:10.1007/s00401-018-1916-x

Ma, Q., Decker, Y., Müller, A., Ineichen, B. V., and Proulx, S. T. (2019). Clearance of cerebrospinal fluid from the sacral spine through lymphatic vessels. *J. Exp. Med.* 216, 2492–2502. doi:10.1084/jem.20190351

Mestre, H., Tithof, J., Du, T., Song, W., Peng, W., Sweeney, A. M., et al. (2018). Flow of cerebrospinal fluid is driven by arterial pulsations and is reduced in hypertension. *Nat. Commun.* 9, 4878–4879. doi:10.1038/s41467-018-07318-3

Mestre, H., Hablitz, L. M., Xavier, A. L., Feng, W., Zou, W., Pu, T., et al. (2018). Aquaporin-4-dependent glymphatic solute transport in the rodent brain. *Elife* 7, e40070. doi:10.7554/elife.40070

Nicholson, C., and Phillips, J. (1981). Ion diffusion modified by tortuosity and volume fraction in the extracellular microenvironment of the rat cerebellum. *J. physiology* 321, 225–257. doi:10.1113/jphysiol.1981.sp013981

Nilsson, C., Stahlberg, F., Thomsen, C., Henriksen, O., Herning, M., and Owman, C. (1992). Circadian variation in human cerebrospinal fluid production measured by magnetic resonance imaging. *Am. J. Physiology-Regulatory, Integr. Comp. Physiology* 262, R20–R24. doi:10.1152/ajpregu.1992.262.1.r20

Pardridge, W. M. (2016). Csf, blood-brain barrier, and brain drug delivery. *Expert Opin. drug Deliv.* 13, 963–975. doi:10.1517/17425247.2016.1171315

Proulx, S. T. (2021). Cerebrospinal fluid outflow: A review of the historical and contemporary evidence for arachnoid villi, perineural routes, and dural lymphatics. *Cell. Mol. Life Sci.* 78, 2429–2457. doi:10.1007/s00018-020-03706-5

Ray, L., Iliff, J. J., and Heys, J. J. (2019). Analysis of convective and diffusive transport in the brain interstitium. *Fluids Barriers CNS* 16, 6–18. doi:10.1186/s12987-019-0126-9

Ray, L. A., Pike, M., Simon, M., Iliff, J. J., and Heys, J. J. (2021). Quantitative analysis of macroscopic solute transport in the murine brain. *Fluids Barriers CNS* 18, 55–19. doi:10.1186/s12987-021-00290-z

Ringstad, G., and Eide, P. K. (2020). Cerebrospinal fluid tracer efflux to parasagittal dura in humans. *Nat. Commun.* 11, 354–359. doi:10.1038/s41467-019-14195-x

Ringstad, G., Vatnehol, S. A. S., and Eide, P. K. (2017). Glymphatic mri in idiopathic normal pressure hydrocephalus. *Brain* 140, 2691–2705. doi:10.1093/brain/awx191

Ringstad, G., Valnes, L. M., Dale, A. M., Pripp, A. H., Vatnehol, S. A. S., Emblem, K. E., et al. (2018). Brain-wide glymphatic enhancement and clearance in humans assessed with mri. *JCI insight* 3, 121537. doi:10.1172/jci.insight.121537

Schubert, J. J., Veronese, M., Marchitelli, L., Bodini, B., Tonietto, M., Stankoff, B., et al. (2019). Dynamic 11c-pib pet shows cerebrospinal fluid flow alterations in alzheimer disease and multiple sclerosis. *J. Nucl. Med.* 60, 1452–1460. doi:10.2967/jnumed.118.223834

Sharp, M. K., Carare, R. O., and Martin, B. A. (2019). Dispersion in porous media in oscillatory flow between flat plates: Applications to intrathecal, periarterial and paraarterial solute transport in the central nervous system. *Fluids Barriers CNS* 16, 13–17. doi:10.1186/s12987-019-0132-y

Shokri-Kojori, E., Wang, G. J., Wiers, C. E., Demiral, S. B., Guo, M., Kim, S. W., et al. (2018). β-amyloid accumulation in the human brain after one night of sleep deprivation. *Proc. Natl. Acad. Sci. U. S. A.* 115, 4483–4488. doi:10.1073/pnas.1721694115

Smith, A. J., and Verkman, A. S. (2018). The "glymphatic" mechanism for solute clearance in alzheimer's disease: Game changer or unproven speculation? *FASEB J.* 32, 543–551. doi:10.1096/fj.201700999

Spijkerman, J. M., Geurts, L. J., Siero, J. C., Hendrikse, J., Luijten, P. R., and Zwanenburg, J. J. (2019). Phase contrast mri measurements of net cerebrospinal fluid flow through the cerebral aqueduct are confounded by respiration. *J. Magn. Reson. Imaging* 49, 433–444. doi:10.1002/jmri.26181

SVMTK (2021). SurfaceVolumeMeshingToolKit. Available at: Original-date: 2017-09-22T15:36:28Z https://github.com/SVMTK/SVMTK.

Tarasoff-Conway, J. M., Carare, R. O., Osorio, R. S., Glodzik, L., Butler, T., Fieremans, E., et al. (2015). Clearance systems in the brain—Implications for alzheimer disease. *Nat. Rev. Neurol.* 11, 457–470. doi:10.1038/nrneurol.2015.119

Tawfik, A. M., Elsorogy, L., Abdelghaffar, R., Naby, A. A., and Elmenshawi, I. (2017). Phase-contrast mri csf flow measurements for the diagnosis of normal-pressure hydrocephalus: Observer agreement of velocity versus volume parameters. *Am. J. Roentgenol.* 208, 838–843. doi:10.2214/ajr.16.16995

Taylor, A. J., Salerno, M., Dharmakumar, R., and Jerosch-Herold, M. (2016). T1 mapping: Basic techniques and clinical applications. *JACC Cardiovasc. Imaging* 9, 67–81. doi:10.1016/j.jcmg.2015.11.005

Thal, D. R., Griffin, W. S. T., de Vos, R. A., and Ghebremedhin, E. (2008). Cerebral amyloid angiopathy and its relationship to alzheimer's disease. *Acta Neuropathol.* 115, 599–609. doi:10.1007/s00401-008-0366-2

Valnes, L. M., Mitusch, S. K., Ringstad, G., Eide, P. K., Funke, S. W., and Mardal, K. A. (2020). Apparent diffusion coefficient estimates based on 24 hours tracer movement support glymphatic transport in human cerebral cortex. *Sci. Rep.* 10, 9176–9212. doi:10.1038/s41598-020-66042-5

Vinje, V., Ringstad, G., Lindstrom, E. K., Valnes, L. M., Rognes, M. E., Eide, P. K., et al. (2019). Respiratory influence on cerebrospinal fluid flow–a computational study based on long-term intracranial pressure measurements. *Sci. Rep.* 9, 9732–9813. doi:10.1038/s41598-019-46055-5

Vinje, V., Eklund, A., Mardal, K.-A., Rognes, M. E., and Støverud, K.-H. (2020). Intracranial pressure elevation alters csf clearance pathways. *Fluids Barriers CNS* 17, 29–19. doi:10.1186/s12987-020-00189-1

Watts, R., Steinklein, J., Waldman, L., Zhou, X., and Filippi, C. (2019). Measuring glymphatic flow in man using quantitative contrast-enhanced mri. *AJNR. Am. J. Neuroradiol.* 40, 648–651. doi:10.3174/ajnr.a5931

Weed, L. H. (1922). The cerebrospinal fluid. *Physiological reviews* 2 (2), 171–203. doi:10.1152/physrev.1922.2.2.171

Xie, L., Kang, H., Xu, Q., Chen, M. J., Liao, Y., Thiyagarajan, M., et al. (2013). Sleep drives metabolite clearance from the adult brain. *science* 342, 373–377. doi:10.1126/science.1241224

Yamada, S., Ishikawa, M., and Yamamoto, K. (2016). Comparison of csf distribution between idiopathic normal pressure hydrocephalus and alzheimer disease. *Am. J. Neuroradiol.* 37, 1249–1255. doi:10.3174/ajnr.a4695

Zeppenfeld, D. M., Simon, M., Haswell, J. D., D'Abreo, D., Murchison, C., Quinn, J. F., et al. (2017). Association of perivascular localization of aquaporin-4 with cognition and alzheimer disease in aging brains. *JAMA Neurol.* 74, 91–99. doi:10.1001/jamaneurol.2016.4370

frontiers | Frontiers in Molecular Neuroscience

TYPE Original Research
PUBLISHED 14 September 2022
DOI 10.3389/fnmol.2022.931091

OPEN ACCESS

EDITED BY
Vegard Vinje,
Simula Research Laboratory, Norway

REVIEWED BY
Marianne Juhler,
Rigshospitalet, University of Copenhagen, Denmark
Hung-Chieh Chen,
National Yang Ming Chiao Tung University, Taiwan
Bruce Arthur Young,
A.T. Still University, United States

*CORRESPONDENCE
Marijan Klarica
mklarica@mef.hr

SPECIALTY SECTION
This article was submitted to Brain Disease Mechanisms, a section of the journal Frontiers in Molecular Neuroscience

RECEIVED 28 April 2022
ACCEPTED 09 August 2022
PUBLISHED 14 September 2022

CITATION
Klarica M, Radoš M, Erceg G, Jurjević I, Petošić A, Virag Z and Orešković D (2022) Cerebrospinal fluid micro-volume changes inside the spinal space affect intracranial pressure in different body positions of animals and phantom.
Front. Mol. Neurosci. 15:931091.
doi: 10.3389/fnmol.2022.931091

Cerebrospinal fluid micro-volume changes inside the spinal space affect intracranial pressure in different body positions of animals and phantom

Marijan Klarica[1]*, Milan Radoš[1], Gorislav Erceg[1], Ivana Jurjević[1], Antonio Petošić[2], Zdravko Virag[3] and Darko Orešković[4]

[1]Department of Pharmacology and Croatian Institute for Brain Research, School of Medicine, University of Zagreb, Zagreb, Croatia, [2]Department of Electroacoustics, Faculty of Electrical Engineering and Computing University of Zagreb, Zagreb, Croatia, [3]Department of Fluid Mechanics, Faculty of Mechanical Engineering and Naval Architecture, University of Zagreb, Zagreb, Croatia, [4]Department of Molecular Biology, Ruder Bošković Institute, Zagreb, Croatia

Interpersonal differences can be observed in the human cerebrospinal fluid pressure (CSFP) in the cranium in an upright body position, varying from positive to subatmospheric values. So far, these changes have been explained by the Monroe–Kellie doctrine according to which CSFP should increase or decrease if a change in at least one of the three intracranial volumes (brain, blood, and CSF) occurs. According to our hypothesis, changes in intracranial CSFP can occur without a change in the volume of intracranial fluids. To test this hypothesis, we alternately added and removed 100 or 200 μl of fluid from the spinal CSF space of four anesthetized cats and from a phantom which, by its dimensions and biophysical characteristics, imitates the cat cerebrospinal system, subsequently comparing CSFP changes in the cranium and spinal space in both horizontal and vertical positions. The phantom was made from a rigid "cranial" part with unchangeable volume, while the "spinal" part was made of elastic material whose modulus of elasticity was in the same order of magnitude as those of spinal dura. When a fluid volume (CSF or artificial CSF) was removed from the spinal space, both lumbar and cranial CSFP pressures decreased by 2.0–2.5 cm H_2O for every extracted 100 μL. On the other hand, adding fluid volume to spinal space causes an increase in both lumbar and cranial CSFP pressures of 2.6–3.0 cm H_2O for every added 100 μL. Results observed in cats and phantoms did not differ significantly. The presented results on cats and a phantom suggest that changes in the spinal CSF volume significantly affect the intracranial CSFP, but regardless of whether we added or removed the CSF volume, the hydrostatic pressure difference between the measuring sites (lateral ventricle and lumbar subarachnoid space)

was always constant. These results suggest that intracranial CSFP can be increased or decreased without significant changes in the volume of intracranial fluids and that intracranial CSFP changes in accordance with the law of fluid mechanics.

KEYWORDS

CSF pressure, CSF volume changes, body position, phantom, subatmospheric CSF pressure

Introduction

It is known that changing the body's position from horizontal to vertical leads to significant changes in the cerebrospinal fluid pressure (CSFP) within the cranium, which varies from positive to negative (subatmospheric) values (Davson et al., 1987; Andresen et al., 2015; Farahmand et al., 2015). This phenomenon is explained by the Monroe–Kellie doctrine and the classical hypothesis of –cerebrospinal fluid physiology. According to the Monroe–Kellie doctrine, intracranial CSFP depends on the interaction of three volumes that fill the cranium: the volumes of blood, brain, and cerebrospinal fluid. After changing the body's position from horizontal to vertical, it is generally accepted that there is a redistribution of venous blood from the cranium to the lower parts of the body, accompanied by the collapse of internal jugular veins (Qvarlander et al., 2013; Holmlund et al., 2018). Inside the cranial space, partial collapse of venous vessels (observed during the cranial opening in neurosurgical operations) might reduce intracranial CSFP (Davson et al., 1987). In addition, it is considered that there is a rapid and short-term movement of part of the intracranial volume of cerebrospinal fluid into the spinal subarachnoid space (Magnaes, 1976a,b; Magnaes, 1989; Alperin et al., 2005a,b). Thus, CSFP decreases due to the simultaneous reduction of the two volumes filling the cranium (blood and CSF), but this change in intracranial CSFP is considered transient. A well-known Davson's equation (Intracranial CSFP = Vf x Ro + Pv, where Vf = rate of secretion; Ro = the resistance to the flow (circulation) of CSF along the CSF system; Pv = the resistance to absorption of the CSF into the venous sinuses/blood circulation) connects CSFP value with the classical concept of CSF secretion, unidirectional circulation, and absorption (Davson et al., 1987). Thus, according to the classical hypothesis of cerebrospinal fluid physiology, due to the constant formation of cerebrospinal fluid within the cerebral ventricles, the decrease in cerebrospinal fluid volume after changing the body's position from horizontal to vertical would be quickly compensated, and intracranial CSFP would take on positive values (Magnaes, 1976a,b; Marmarou et al., 1978; Davson et al., 1987).

In our previous research on cats and phantom (whose biophysical and anatomical characteristics mimic the CSF system of cats), it was observed that CSFP in the vertical position depends on the measuring point, and it varies from about−4 cm H_2O (subatmospheric) in the lateral ventricle (LV) to about +32 cm H_2O in the lumbar subarachnoid space (LSS) (Klarica et al., 2014; Orešković et al., 2017b). However, the negative CSFP value in LV was stable, as well as the hydrostatic gradient value between LV and LSS, while the animal was in the head-up position (Klarica et al., 2014). Furthermore, the measurement of CSFP from animals did not differ from those observed on the phantom, in which there was no change in volume in the "cranial" part when changing position. These findings have led to the development of a new hypothesis that CSFP changes in accordance with the law of fluid mechanics and that the reduction of intracranial CSFP occurs without visible changes in intracranial fluid volume (Klarica et al., 2006, 2014; Orešković et al., 2017a,b, 2018). This hypothesis is further supported by new observations in humans that there are almost no changes in intracranial vessels when changing body position from supine to sitting position (Kosugi et al., 2020).

In the upright position, there is a large interindividual difference in intracranial CSFP values (Magnaes, 1976a,b; Davson et al., 1987; Chapman et al., 1990). As the cerebrospinal fluid volume does not change significantly in the upright position in the cranium, one of the reasons for this CSFP variability could be the existence of a different cerebrospinal fluid volume in the spinal compartment.

We intended to examine whether changes in CSF volume inside the lumbar subarachnoid space (LSS) would lead to changes in intracranial CSFP without significant changes in CSF volume inside the cranium. For this purpose, the same fluid volume will be added or removed from the LSS of cats and the phantom (see Material and methods section), and CSFP will be measured inside the LV and the LSS in horizontal and vertical positions. We expect that the results of this study will demonstrate the dominant role of spinal CSF space in the regulation of intracranial CSFP and compliance of craniospinal space, which is essential for the understanding of the variety of physiological conditions and CSF-related neurological diseases.

Materials and methods

Animal experiments

The study was performed on male and female adult cats (2.2–3.4 kg body weight). The animals were kept in cages with natural light-dark cycles and free access to water and food (SP215 Feline, Hill's Pet Nutrition Inc., Topeka, KS, USA).

Ethics statement

The animals were in quarantine for 30 days, and the experiments were performed in accordance with the Croatian Animal Welfare Act. The protocol was approved by the Ethics Committee of the University of Zagreb Medical School (Approval No. 04-76/2006-18). Experiments shown in the manuscript were performed more than 15 years ago. At that time, the Croatian Animal Welfare Act allowed us to obtain experimental animals from private owners (domestic breeding). However, today in Croatia, we have a new Animal Welfare Act by which it is possible to obtain experimental animals only from official suppliers. The owners were verbally informed about the experimental protocol, which was previously approved by the official ethical committee. All efforts were made to minimize animal suffering, and all surgery, according to the protocol, was performed under anesthesia. The cats were anesthetized with α-chloralose (Fluka; 100 mg/kg i.p.) and fixed in a stereotaxic head holder (David Kopf, Tununga, CA, USA) in the sphinx position. The femoral artery was cannulated, the blood pressure was recorded *via* a T-connector, and blood samples were taken for analysis of the blood gases. No significant changes, either in blood pressure or blood gases, were observed during these experiments on cats, which continued breathing spontaneously under the α-chloralose anesthesia. A stainless steel cannula (0.9 mm ID) was introduced into the left LV at 2 mm lateral and 15 mm anterior to the stereotaxic zero point and 10–12 mm below the dural surface. A second cannula was placed in the right LV at the same position as the cannula in the left LV (Laitinen, 1968). The cannula in the right LV was used to measure intracranial CSFP. In order to measure the spinal CSFP in the lumbar region, a laminectomy (5 x 10 mm) of the L3 vertebra was performed. After the spinal dura and arachnoid incision, a third plastic cannula (0.9 mm ID) was introduced into the subarachnoid space. Leakage of CSF was prevented by applying cyanoacrylate glue to the dura around the cannula. Bone openings in the cranium and vertebra were hermetically closed by the application of a dental acrylate. After setting the measuring cannulas, the cat was removed from the stereotaxic device and then fixed in a prone position on a board (Figure 1A). CSF pressures were recorded using pressure transducers (Gould P23 ID, Gould Instruments, Cleveland, OH, USA) which were connected to a system that transformed analogous to digital data (Quand Bridge and PowerLab/800, ADInstruments, Castle Hill, NSW, Australia), and then entered into a computer (IBM, White Plains, NY, USA) (Figure 1A). Pressure transducers were calibrated using a water column, and the interaural line was taken as zero pressure. Instruments for pressure measurement were fixed on the board in such a way that the membrane of each transducer was at the same hydrostatic level as the corresponding measuring cannula, so there was no need to additionally adjust the transducers during the body position changes (Figure 1A) (Klarica et al., 2014). CSFP changes were recorded at 15-min intervals in horizontal (0°) and head-up (vertical; 90°) positions (Figure 1A).

Experiments on a phantom

A new phantom model of the CSF system is made of two different materials which represent the main biophysical characteristics of the cranial (unchangeable volume) and spinal (changeable volume) parts of the CSF system (Figure 1B) (Klarica et al., 2014). In the construction of the phantom "CSF system," we took into account the anatomical dimensions of the CSF system in cats. The "cranial" part is made of a plastic tube, 6 cm long, with an inner diameter of 0.6 cm and a wall thickness of 2.0 mm (Figures 1, 4). This length of the plastic tube with a rigid wall is chosen because it represents the mean distance from the frontal sinuses to the foramen magnum, as found in 5 cats on x-rays of the animals' skulls (Klarica et al., 2014). The "spinal" part is made of a rubber balloon that is 31 cm in length (Natural Rubber Latex, Gemar, Casalvieri, Italy). This length is similar to the mean distance between the cisterna magna and the LSS at the level L3 vertebra where the pressure in cats was measured. The measuring cannula in the "cranial" part of the phantom was placed 4 cm proximally from the lower end of the plastic tube (Figure 1B), which corresponded to the distance between the cranial cannula in LV and the foramen magnum in cats. The second cannula was placed at the base of the rubber balloon so that the total distance between the two measuring cannulas was 35 cm (Figure 1B). Before measuring the pressures, the phantom was filled with artificial CSF without the presence of air bubbles and fixed on the board. The pressure transducers (Gould P23 ID, Gould Instruments, Cleveland, OH, USA) were fixed at the same level as the measuring cannulas and connected to the computer *via* an amplifier (QUAD Bridge and PowerLab/800, ADInstruments Ltd., Castle Hill, NSW, Australia) (Figure 1B). The pressures were measured in the same positions as in the cats (horizontal and vertical positions). The rubber balloon used to create the "spinal" part of the phantom had two modules of elasticity (Jurjević et al., 2011). Those modules were of the same order of magnitude as dural elasticity modules in big experimental animals (Tunturi, 1977; Kenning et al., 1981; Rosner and Coley, 1986). It was possible to stretch that balloon, especially in the horizontal plane, similar to the

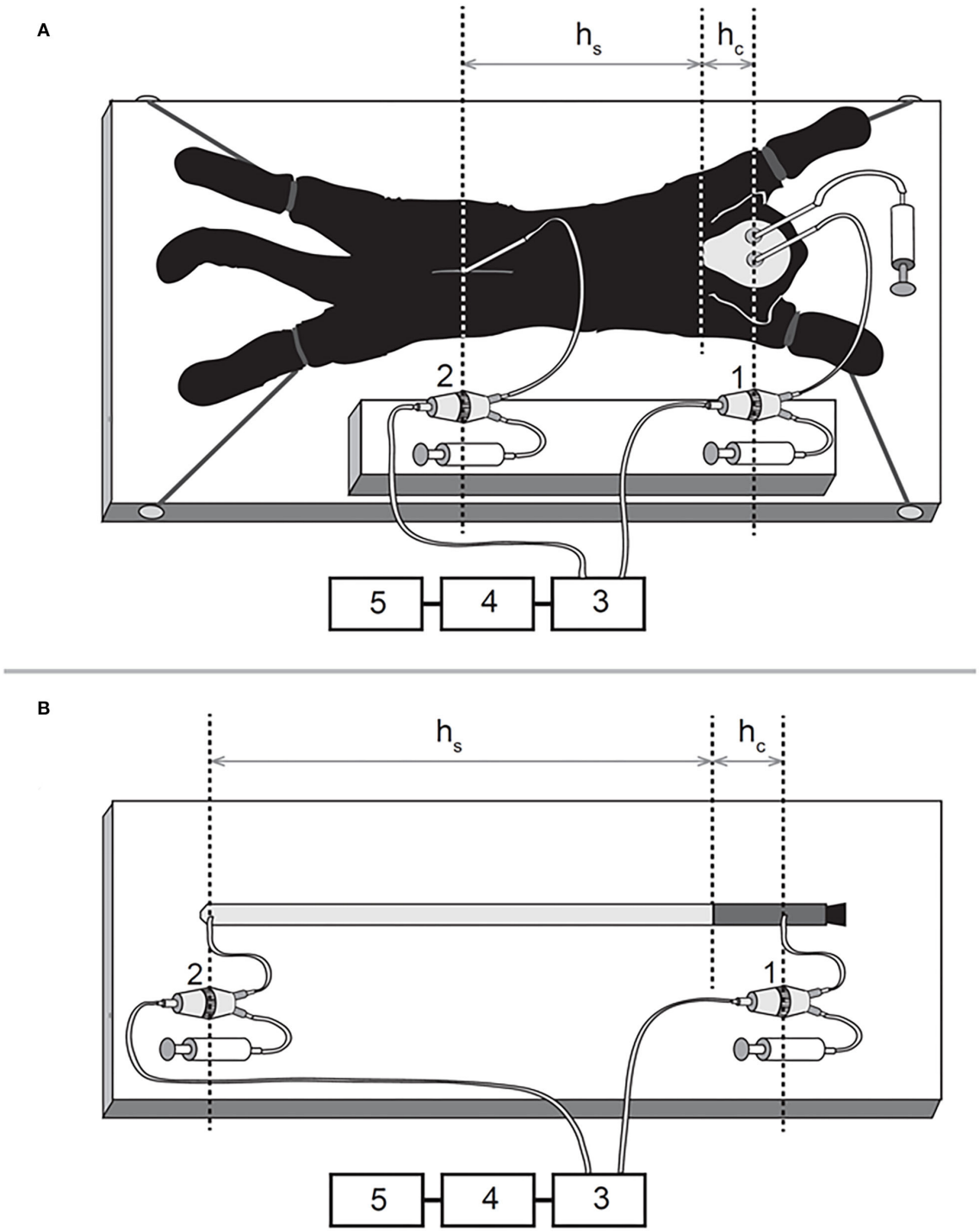

FIGURE 1
Schematic representations of the experimental models on a cat **(A)** and phantom **(B)** in horizontal position 1, pressure transducer connected to the cannula inside the lateral ventricle; 2, pressure transducer connected to the cannula inside the lumbar subarachnoid space; 3, Quand Bridge; 4, PowerLab/800; 5, personal computer; hc, the distance between the cisterna magna and the pressure measuring point inside the lateral ventricle; hs, the distance between the cisterna magna and the pressure measuring point inside the lumbar subarachnoid space.

animal dura mater. Namely, in the craniocaudal direction, the dura mater is almost maximally stretched, while the stretching in the horizontal direction is possible because of the arrangement of collagen fibers (Kenning et al., 1981; Rosner and Coley, 1986). "CSFP" changes were recorded in phantom at 15-min intervals in horizontal (0°) and vertical (90°) positions (Figure 1B).

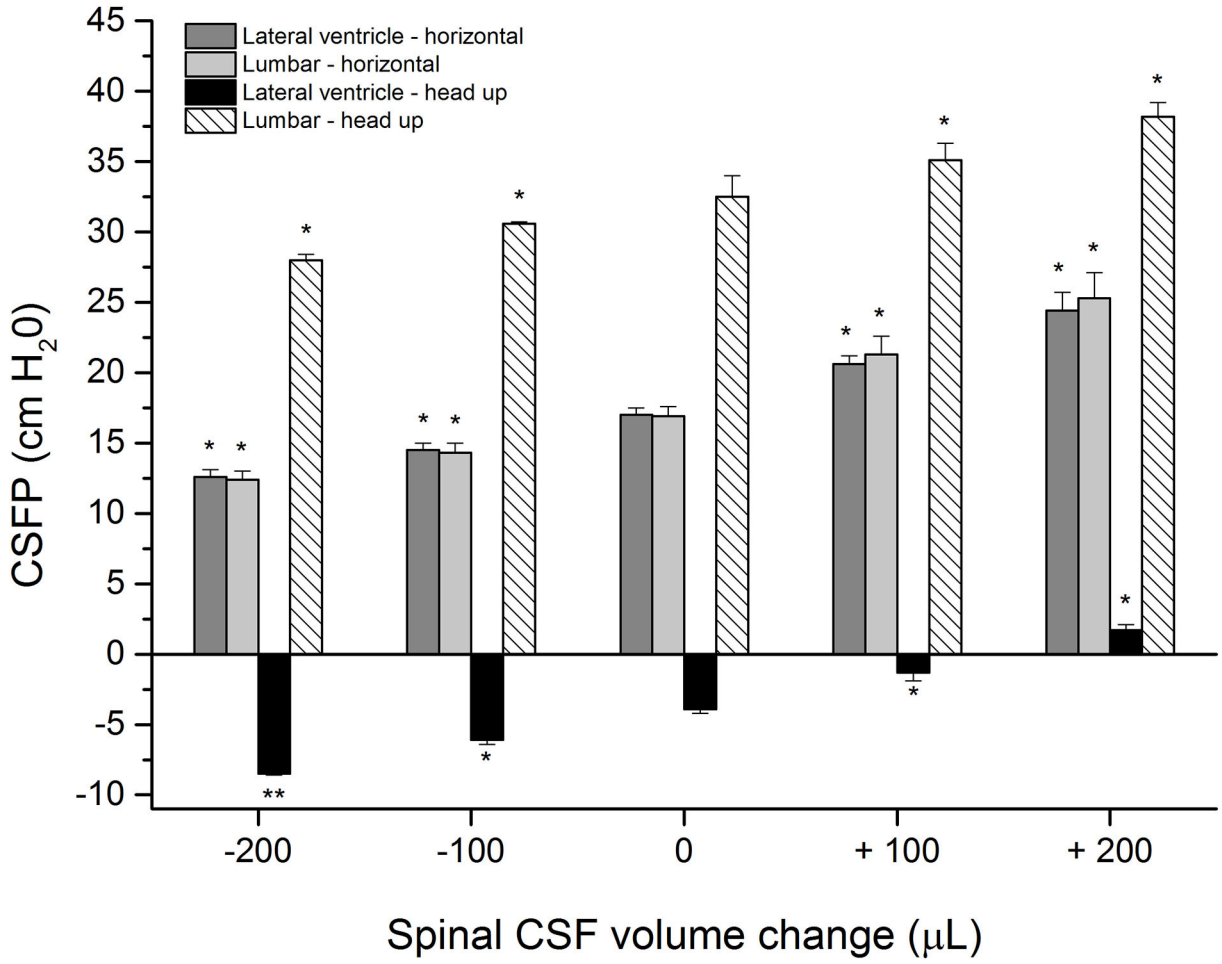

FIGURE 2
CSFP changes (cm H_2O) in anesthetized cats in horizontal-0° (lateral ventricle-horizontal and lumbar-horizontal) and head-up 90° (vertical) body position inside the lateral ventricle (lateral ventricle-head-up) and in the lumbar subarachnoid space at L3 level (lumbar-head-up) in control condition (0 μL; $n = 4$), after addition (+) of 100 and 200 μL of artificial CSF into the lumbar space ($n = 4$) and after extraction (-) of 100 or 200 μL from the lumbar space ($n = 4$). Columns represent mean measurement values, while vertical lines represent standard errors of the mean values. There is a statistically significant difference between CSF pressure in the control condition and after adding/removal of fluid volume, $*p < 0.05$;$**p < 0.001$.

CSFP measurement in experimental animals during lumbar CSF volume changes

In this experimental series, we aimed to verify if an increase or decrease of CSF volume inside the lumbar part of the CSF system leads to an increase or decrease in CSFP inside the cranial part. First, initial pressure values (control) were measured in cats fixed on a measuring board in a horizontal position (0°; Figure 1A). After the initial evaluation, 100 μL of artificial CSF was added to the LSS *via* T-connector, and pressure values were recorded in both the lumbar and cranial parts of the CSF system. When pressure values dropped to initial values, 200 μL of artificial CSF was added into the lumbar space, and the measurement was repeated. After returning to control values, 100 μL of CSF was extracted from the lumbar part and the pressure was measured again. When pressure returned to control values, a volume of 200 μL of CSF was extracted from the same space, and pressure measurement was repeated. The described measurements were then carried out in a head-up (vertical) position (90°; Figure 1A) in the same volume extraction and addition order.

"CSFP" measurement in phantom during "lumbar" CSF volume changes

The experiments on the phantom were done in the same way. Through the cannula positioned in the "lumbar" part of the phantom in a horizontal position (0°; Figure 1B), the volume

of artificial CSF was increased or decreased in the "lumbar" space, and CSFP was measured in the "cranial" and the "spinal" parts of the phantom "CSF system." After the measurement of control values, 100 μL of artificial CSF is added into the "lumbar space" *via* T-connector, and the pressure values are recorded in both the "lumbar" and "cranial" parts of the "CSF system." When the pressure returns to control values by taking out the experimentally added volume of artificial CSF (100 μL), 200 μL of artificial CSF is added into the "lumbar" space, and measurement is repeated. After returning to control values by taking out the experimentally added volume of artificial CSF (200 μL), 100 μL of CSF is extracted from the "lumbar" part, and pressure is measured again. When pressure values return to normal by adding the experimentally removed volume of artificial CSF (100 μL), a volume of 200 μL of CSF is extracted from the same space, and pressure measurement is repeated. The described measurements are then carried out in a "head-up" (vertical) position (90°; Figure 1B) in the same volume extraction and addition order.

Compliance within craniospinal space

Compliance is a ratio between the changes in CSF volume and CSF pressure expressed in mL/cm H_2O. It is calculated in animals and phantom after the addition/removal of a fluid volume from the spinal part of the system. The calculation has been done for both horizontal and vertical positions.

Statistical analysis

Data are shown as a mean value ± standard error of the mean (SEM). A statistical analysis of all of the results was performed using the paired Student's *t*-test and ANOVA for repeated measures, with "condition" (cranial part and lumbar part) and position (0° and 90°) as a within-subject variable. In addition, a 2 x 2 mixed ANOVA was conducted on CSFP in a head-up position (90°), with "condition" (cranial part and lumbar part) manipulated as within-subjects and phantom vs. animal as a between-subjects variable. $P < 0.05$ was considered statistically significant. All statistical analysis was performed using the SPSS 20.0.0 software (IBM Corp., Armonk, NY).

Results

Control measurements with an animal in a horizontal position show CSFP of 17.0 ± 0.5 cm H_2O inside the LV and 16.9 ± 0.7 cm H_2O inside the LSS, while in the head-up position, the pressure was−3.9 ± 0.3 cm H_2O inside the LV and 32.5 ± 1.5 cm H_2O in the LSS ($n = 4$) (Figure 2). After the addition of 100 or 200 μL of artificial CSF into the LSS, the CSFP values in the horizontal position increase proportionally inside the LV and LSS (LV = 20.6 ± 0.6 cm H_2O; LSS = 21.3 ± 1.3 cm H_2O or LV = 24.4 ± 1.3 cm H_2O; LSS = 25.3 ± 1.8 cm H_2O, respectively). Changing of position from horizontal to head-up (vertical) after the addition of 100 μl or 200 μl of a CSF in LSS resulted in a CSFP increase in both LV and LSS (LV = −1.3 ± 0.6 cm H_2O; LSS = 35.1 ± 1.2 cm H_2O or LV = 1.7 ± 0.4 cm H_2O; LSS = 38.2 ± 1.0 cm H_2O, respectively) (Figure 2).

After placing the animals back into the horizontal position until the CSFP returns to control values, volumes of 100 or 200 μL of CSF were extracted from the LSS, which led to a proportional pressure decrease in LV and LSS both in the horizontal and head-up positions (LV = 14.5 ± 0.5 cm H_2O; LSS = 14.3 ± 0.7 cm H_2O or LV = 12.6 ± 0.5 cm H_2O; LSS = 12.4 ± 0.6 cm H_2O in horizontal position, LV = −6.1 ± 0.3 cm H_2O; LSS = 30.6 ± 0.1 cm H_2O or LV = −8.5 ± 0.1 cm H_2O; LSS = 28.0 ± 0.4 cm H_2O in head-up position). Statistically, a significant difference exists between measurements after adding/removal of CSF volume and control values (see Figure 2), which would indicate that CSF pressure both in the cranial and spinal space depends on CSF volume changes in the spinal part.

Figure 3 shows the results of corresponding measurements on a phantom with control pressure values in the horizontal and upright position amounting to 12.3 ± 0.1 cm H_2O and−4.1 ± 0.1 cm H_2O inside the "cranial" part, while they were 12.4 ± 0.1 cm H_2O and 30.1 ± 0.2 cm H_2O in the "spinal" part (five measurements). After the addition of 100 or 200 μL of artificial CSF to the "spinal" part of the phantom, the pressures gradually increase in both parts of the phantom in both positions. The pressure inside the "cranial" part was 15.7 ± 0.3 cm H_2O and 19.5 ± 0.5 cm H_2O in the horizontal position, while it was−2.2 ± 0.2 cm H_2O and 0.7 ± 0.5 cm H_2O in the upright position. The pressure inside the "spinal" part was 15.7 ± 0.3 cm H_2O and then 19.2 ± 0.5 cm H_2O in the horizontal position, while it was 32.1 ± 0.3 cm H_2O and 35.0 ± 0.4 cm H_2O in the upright position.

The phantom is then put back to the horizontal position, and 200 μL of artificial CSF is extracted, which allows the pressure to return to control values. This extraction is followed by the removal of 100 or 200 μL of artificial CSF from the "spinal" part of the phantom, which leads to a corresponding decrease of pressure values inside both parts of the phantom, both in the horizontal and upright positions (the pressure inside the "cranial" part was 9.5 ± 0.1 cm H_2O and 7.7 ± 0.1 cm H_2O in the horizontal position, while it was−5,3 ± 0,1 cm H_2O and−6.3 ± 0.1 cm H_2O in the upright position; the pressure inside the "spinal" part was 9.8 ± 0.1 cm H_2O and 8.3 ±

0.1 cm H_2O in the horizontal position, while it was 28.7 ± 0.3 cm H_2O and 28.0 ± 0.3 cm H_2O in the upright position). A statistically significant difference can be observed between measurements after adding/removal of artificial CSF volume and control values, which would imply that the artificial CSF pressure inside the system depends on volume changes inside the "spinal" part of the phantom, as was also observed in animals (Figure 2).

In a horizontal position, during the removal of 100 or 200 μL, compliance values vary from 0.039 to 0.045 mL/cm H_2O in cats and from 0.036 to 0.049 mL/ cm H_2O in a phantom. On the other hand, after adding 100 or 200 μL of artificial CSF, there is an increase in the CSFP accompanied by a decrease in compliance values. In that case, compliance varied from 0.023 to 0.027 mL/cm H_2O in cats while the values varied from 0.028 to 0.030 mL/cm H_2O in a phantom.

There was a slight statistical difference in compliance values between the cats and the phantom in the vertical position, unlike the horizontal one. After verticalization, a significant hydrostatic pressure gradient forms between the measuring points inside the cranial and the spinal space, unlike the horizontal position in which the gradient is practically non-existent. Thus, the compliance values in the cranial and the spinal part of the cat system during the mentioned volumes extraction vary from 0.044 to 0.052 mL/cm H_2O, and during the addition of the corresponding volumes, they vary from 0.035 to 0.038 mL/ cm H_2O. After volume removal from a phantom in a vertical position, compliance varied from 0.071 to 0.095, and after volume addition, it varied from 0.035 to 0.052 mL/ cm H_2O.

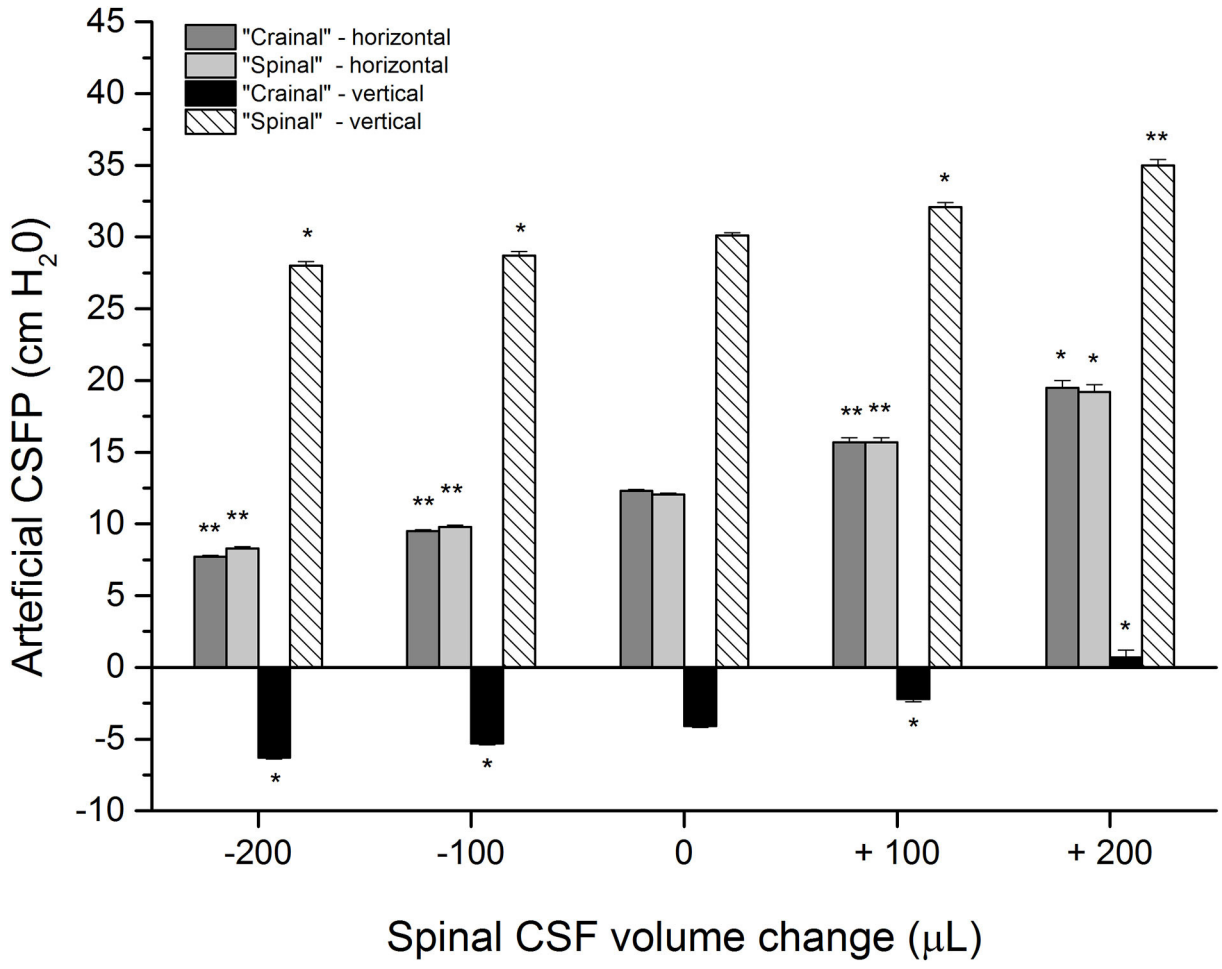

FIGURE 3
Artificial CSFP changes (cm H_2O) in the phantom in different positions: horizontal–0° ("cranial"-horizontal; "spinal"-horizontal) and vertical-90°, inside the "cranial" and the "spinal" part of the phantom in the control condition (0 μL; n=5), after addition (+) of 100 and 200 μL of artificial CSF into the "spinal" part (n=5), and extraction (-) of 100 of 200 μL from the "spinal" part ($n = 5$). Columns represent the mean values of the measurements, and vertical lines represent standard errors of the mean values. There is a statistically significant difference between artificial CSF pressure in the control condition and after adding/removal of artificial CSF volume, $*p < 0.05$;$**p < 0.001$.

Discussion

Physiological values of CSFP within CSF system in horizontal and vertical positions

This study indicates that the increase or decrease in CSFP in the cranium can occur due to small changes in the CSF volume in the spinal part without significant changes in the CSF volume in the cranial part of the CSF system. It is further shown that these changes in intracranial CSFP when changing the body's position from horizontal to upright do not depend on the redistribution of fluid volume from the cranium to the hydrostatically lower parts. In this article (Figures 2, 3) and our previous publications (Klarica et al., 2006, 2014), it was shown in control cats that CSFP in the horizontal position is equal in the cranial and spinal parts of the CSF system. However, CSFP inside the cranium (LV) of the control animal in the vertical position is negative (subatmospheric) (Figure 2), and "zero" CSFP is positioned in the foramen magnum region, while inside the LSS, it is highly positive. The observed huge hydrostatic gradient along the CSF system is stable and permanent for an extended period of time (Klarica et al., 2006, 2014). The observed changes in the CSFP in the horizontal and vertical positions of the phantom (Figure 3), in which there is no visible change in the fluid volume in the "cranial" part, do not differ statistically from those observed in cats.

Since CSF forms a freely communicating fluid column inside the craniospinal space with a huge hydrostatic pressure gradient, a question arises about how to explain the appearance of a stable subatmospheric intracranial CSFP in the head-up position. Previously, this occurrence was explained as a transient phenomenon, since the explanation was sought in light of the classical concept of CSF secretion, unidirectional circulation, and absorption (mainly *via* dural venous sinuses), and the changes in the hydrostatic venous blood column Magnaes, 1976a,b; Davson et al., 1987; Valdueza et al., 2000; Gisoff et al., 2004; Qvarlander et al., 2013; Farahmand et al., 2015; Lawley et al., 2015; Holmlund et al., 2018; Linden et al., 2018). Our experiments were performed on a phantom with no CSF secretion, circulation, or absorption and no influence of venous blood hydrostatic pressure. In addition, it is known that the venous blood column in animals and humans is physically separated from the CSF system. Therefore, obtained results on phantom strongly suggest that the combination of the CSF secretion, circulation, absorption, and venous blood changes do not have a crucial influence on acute CSFP changes during the changes of body position or during the addition and removal of a certain fluid volume from the craniospinal space.

All of the observed results from animals and phantom can be accurately explained using the law of fluid mechanics, i.e., differently for the cranial and spinal space. Since in a healthy organism, there is no interruption of fluid continuity within the CSF system, then in accordance with the law of fluid mechanics, hydrostatic pressure can be calculated anywhere within the

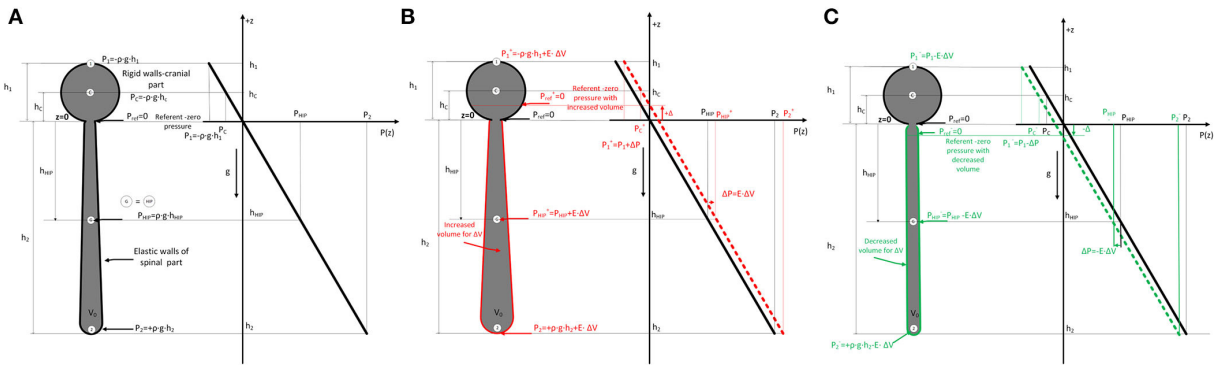

FIGURE 4
(A). Scheme of the cerebrospinal fluid system in cats (left) consisting of two parts (c-cranial with rigid walls and constant volume, bold black line; spinal part with elastic walls and variable volume) which are filled with fluid. The dimensions of the cranial (h_1) and spinal (h_2) parts, as well as the hydrostatic pressure equations, are shown according to the law of fluid mechanics ($P = \rho$ x g x h), where ρ is the fluid density, g is the gravitational force, and h is the distance from the opening of the cranium where the pressure is measured. (P_{ref} - reference pressure or zero hydrostatic pressure equal to atmospheric pressure; P_1 - hydrostatic pressure at the highest point in the cranial part; P_2 - hydrostatic pressure in the spinal part; P_{HIP} – hydrostatic indifferent point defined by Magnes. Change of fluid pressure (ΔP) in the system with effective elasticity (E) of the spinal part and change of volume (ΔV) is described by equation $\Delta P = E \cdot \Delta V$. Therefore, when adding volume **(B)** $P = \rho$ x g x h + $E \cdot \Delta V$ (red), and when removing **(C)** $P = \rho$ x g x h - $E \cdot \Delta V$ (green). According to the law of fluid mechanics, pressure is increased or decreased for this ΔP value everywhere in the system with shown spatial pressure distribution in the z-direction (right part) with referent fluid volume and increased/decreased fluid volumes. ΔP curve describing the spatial pressure dependence is translated for some value ΔP in all considered points in the system (1,C, G=HIP, 2). The position of the referent point (P_{ref}) where the pressure is zero is moved cranially (red arrow) **(B)** or caudally (green arrow) **(C)** ($+\Delta$ and $-\Delta$) when a small volume of fluid is added or removed from the system.

system (as shown in Figure 4) if the distance from the reference point is known ($P = \rho \times g \times h$, where P is the pressure, ρ is the fluid density, g is the gravitational force, and h is the height of fluid column). According to the law of fluid mechanics, inside a space surrounded by rigid walls and an opening at the bottom (like a cranium or a cylindrical "cranial" part of a phantom) (Figure 1), negative pressure appears without changes in fluid volume inside the cranial part (Klarica et al., 2014). Thus, the negative value of the hydrostatic CSFP inside the cranium does not depend on the shape of the volume but only on the distance (h) between the point of measurement and the foramen magnum ($P_1 = -\rho \times g \times h_1$) (Figure 4). Since the distance of the CSFP (h) measuring cannula in the cranial part of the phantom, as well as in the lateral chamber of cats, was about 4 cm (see Material and Methods section) from the opening of the cranial part of the phantom or foramen magnum, the expected CSFP value in LV and the cranial part of the phantom is−4 cm H_2O. This value was generally measured at these locations (Figures 2, 3), entirely in line with the law of fluid mechanics. There was also no difference between expected and measured pressures in the spinal part of the phantom, as well as in the LSS of cats (Figures 2, 3), where measuring cannulas were placed 30 and 32 cm away from the opening of the "cranial" part of the phantom and the cat's magna cistern. However, according to the law of fluid mechanics, the pressure values were positive in the spinal part ($P_2 = \rho \times g \times h_2$) (Figure 4).

If the cerebrospinal fluid pressure behaves in accordance with the law of fluid mechanics, it is to be expected that in the upright position, the pressure in the cranium will be lower than the atmospheric pressure all the time while the body is in the upright position. In our previous studies on cats, we observed that CSFP in the cranium was stable and negative for 75 min while the animal was in the head-up position (Klarica et al., 2014). Clinical studies of CSFP in cranium using telemetric methods in healthy and ill subjects also show such a phenomenon in humans. When changing the position of the body from supine to head-up position (sitting or standing), CSFP in the cranium always falls and takes a long-lasting negative (subatmospheric) value (Andresen et al., 2015; Ertl et al., 2017; Rot et al., 2020).

In contrast to previous observations in the open cranium (Davson et al., 1987) that verticalization leads to a collapse of veins within the cranium, new research on patients with closed cranium using CT has shown that verticalization of patients causes a prominent reduction (collapse) in the volume of neck vein vessels but with almost no change in the volume of intracranial vessels (Kosugi et al., 2020). It seems that described intracranial blood behavior, unlike CSF, has no significant effect on pressure regulation during verticalization. The observed results from animals and humans indicate that subatmospheric CSFP in the cranium in the upright position can be a long-lasting phenomenon, which is the consequence of the influence of gravity predominantly on the CSF system.

CSF micro-volume changes in spinal space affect CSFP in different positions

To explain the changes in CSFP in the head-up position when adding or extracting the volume of artificial CSF from spinal space and moving the zero point of CSFP cranially or caudally, we introduced a simple linear model in accordance with the law of fluid mechanics shown in Figure 4. By using a simplified model of the CSF system (see Figure 4), it is observed that hydrostatic pressure (ΔP) anywhere inside the CSF system is increased/decreased when the mass (Δm)/volume (ΔV) of CSF is added/removed into/from the system. That simplified linear model connects the change of internal pressure (ΔP) in the system with effective elasticity (E) of the spinal part and change of volume (ΔV) by using equation (1) (Landau et al., 2009):

$$\Delta P = E \bullet \Delta V \tag{1}$$

For the cranial part with rigid walls, the elasticity is zero, so the effective elastance (E) is defined with only the elastance of the spinal part (E) because the system can be observed as two coupled systems (rigid+elastic) connected in parallel. If we add or remove a small amount of fluid volume (ΔV), the pressure inside (P) is changed due to increased or decreased tension of spinal walls, and all points in the system are at a higher or lower level (see Figure 4).

The pressure increase, for example, in the reference point G (and at any point in the system) and all other considered points is given with Eqs 2a (fluid added) and 2b (fluid removed) with known effective elastance of spinal part (E) of the system.

$$P_G^+ = P_G + E \bullet \Delta V \tag{2}$$

$$P_G^- = P_G - E \bullet \Delta V \tag{3}$$

The pressure (P) is increased or decreased for this ΔP value everywhere in the system, as shown in Figure 4, according to the hydrostatic pressure law with shown spatial pressure distribution in the z-direction with referent fluid volume and increased/decreased fluid volumes. In the first approximation, the dimension change in the elastic part is negligible in the axial direction, and there is a small increase in radial directions, so there is no change in the z-direction. Due to the change of pressure ΔP, the curve describing the spatial pressure dependence is translated for some value of ΔP at all points in the system. Also, the position of the referent point (P_{ref}) where the pressure is zero is changed to up (red) or down (green) for differential height ($+\Delta$ and $-\Delta$) when a small volume of fluid is added or removed from the system. This is shown for all

considered points (1,C,G=HIP, 2), and increased or decreased values of the pressure are shown with superscript + or -.

The measured CSFP changes in cats and phantoms are consistent with the previously presented theoretical analysis and equations for calculating CSFP changes when adding/removing fluid volume in the spinal space (see Supplementary material). It is important to emphasize that in our research, CSFP changes inside the cat or phantom cranial and spinal space during the addition and extraction of 100 or 200 μL of fluid do not differ significantly and that the hydrostatic gradient between the measuring points in the cranium and the spinal part was constant. For example, when we take off a certain CSF volume from the LSS in cats, both lumbar and cranial CSFP decreased, and zero CSFP point descended for approximately 2.0–2.5 cm for each extracted 100 μL (Figures 2, 4). On the other hand, adding the same CSF volume causes both lumbar and cranial CSFP to increase, and the zero CSFP point moves cranially for 2.6–3.0 cm.

The experiments on a phantom (Figure 3) showed that the addition of 200 μL leads to a pressure increase inside the "cranial" and "spinal" parts and moves the zero pressure value for about 4.8 cm cranially. Conversely, extraction of 200 μL leads to a pressure decrease in the "cranial" and "spinal" parts, which implies that zero pressure point moved from the opening of the "cranial" part of the phantom for 2.2 cm caudally. Thus, the experiments on a phantom and animals support our hypothesis that the observed variability of the zero CSFP value in vertical body position could depend on the fullness of the CSF system in its spinal part.

The ability of craniospinal space to adjust to the volume changes is usually described as spatial compensation (translocation of CSF from the cranial to the spinal space and increase of CSF absorption according to classical hypothesis) and craniospinal compliance (reflects acute volume–pressure relationship, Δ volume/Δ pressure) (Davson et al., 1987; Portella et al., 2005; Lawley et al., 2015; Ocamoto et al., 2021; Löfgren and Zwetnow, 1973). Craniospinal compliance and spatial capacity determine the slope of the volume–pressure curve. There is an exponential relationship between the CSFP changes and craniospinal compliance. According to the well-known phenomena, the value of compliance decreases with CSFP increase, which can also be observed in our research on cats. That is, in those experiments, compliance calculated during the volume removal and pressure decrease (about 0.042 mL/cm H_2O) was bigger than the compliance calculated in the case of volume addition and subsequent pressure increase (about 0.025 mL/ cm H_2O). Since the addition or removal of a certain fluid volume from the spinal CSF space leads to the same pressure changes both cranially and spinally, together with preserved hydrostatic gradient, it is clear that during those pressure changes, the same compliance value will be obtained both inside the cranium and inside the spinal space. Thus, pressure changes inside the cranium enable us to calculate only the compliance of total craniospinal space (Ocamoto et al., 2021). This is generally true for all the experiments done on animals and humans if there is normal communication between the cranial and the spinal space. It is generally accepted that CSF physiology is not different between animal species and humans.

A slight difference in obtained compliance values in an upright position between the model and the animals, especially in the case of volume extraction, could be due to a somewhat better elasticity of the spinal part of the phantom, which is made of rubber compared to the spinal dura mater. Very small differences in pressure could also be the consequences of the certain possibilities of spatial adjustment of brain and blood (e.g., vasoconstriction and vasodilatation) volume within the animal cranium. However, the results of our study done on cats and phantoms in which there is no intracranial compliance, nor the possibility of spatial compensation, suggest that the spinal space plays a crucial role in the regulation of the intracranial CSFP.

Implications in neurological disease

According to our new concept, the cranium seems to play a significant role in body uprightness and position changes (important from an evolutionary point of view) because it prevents sudden changes in the volume of intracranial fluids. Thus, in a study on patients with idiopathic intracranial hypertension (IIH) using automated MRI measurements of the craniospinal CSF volume, it was observed that after the lumbar CSF withdrawal drop in intracranial pressure is primarily related to the increase in spinal compliance and not cranial compliance due to the reduced spinal CSF volume and the nearly unchanged cranial CSF volume (Alperin et al., 2016). Furthermore, the same phenomenon (preservation of intracranial cerebrospinal fluid volume with large changes in the spinal cerebrospinal fluid volume) was observed in a patient with IIH whose LP shunt was replaced by a VP shunt due to severe headaches and over drainage (Nikić et al., 2016). These clinical observations in which significant changes in the spinal cerebrospinal fluid volume occur without significant cranial CSF volume changes strongly support our understanding of intracranial fluid behavior and CSFP regulation, as shown in Figures 2, 3.

In human physiological conditions, such experimentally induced changes of the spinal CSF volume could happen due to abdominal straining during defecation, lifting weight, sneezing, crying of a baby, etc., which can cause pressure to increase inside the abdominal and thoracic veins, and subsequently increase of the CSFP (Davson et al., 1987). Therefore, this could lead to a disruption of blood flow in epidural venous plexuses, an increase in blood volume inside the epidural space, and additional force which influences CSF volume inside the lumbar part of the system, which, as we have shown (Figures 2, 3), should lead to

an increase of the CSFP inside the cranium and consequently cause a shift of the zero pressure position.

Our proposed hypothesis and results shown in Figures 2, 3 could help us understand why patients with spinal liquorrhea have worse clinical status in upright positions than those with cranial liquorrhea (Levine and Rapalino, 2001). According to our hypothesis, in the case of cranial liquorrhea, during body verticalization, the cerebrospinal fluid pressure inside the cranium reaches even subatmospheric values, which stops liquorrhea from the cranium. However, such patients poorly tolerate supine positions because the cerebrospinal fluid pressure in the cranium becomes positive. In the case of spinal liquorrhea, CSF leakage during supine position is less pronounced than in upright position. In an upright position, CSF pressure becomes more positive inside the spinal subarachnoid space. Our proposed hypothesis could explain why lumboperiotneal shunting has common complications, such as over drainage, intracranial hypotension, and postural headache.

It seems that negative intracranial CSFP in the upright position is a long-lasting phenomenon (Klarica et al., 2014). This indicates that cerebral perfusion pressure should be significantly higher than previously believed during two-thirds of the day while people are in the upright or sitting position. According to our concept, it seems that in people in an upright position, the blood supply to the brain is much better, and thus evolutionarily adapted for verticalization and bipedal walking.

Since cranial intradural volume cannot change significantly, unlike the spinal one (Davson et al., 1987), it is to be expected that a tendency to decrease CSF volume inside the cranium (e.g., extraction of cerebrospinal fluid from LV or cortical subarachnoid space), that volume has to be compensated instantly, because the vacuum inside the space, such as the cranial cavity, cannot be created. Therefore, it is most likely that redistribution of CSF volume from the spinal into the cranial space occurs (Orešković et al., 2018). It is necessary to stress that this shift of CSF volume inside the CSF system finally leads to a decrease in the CSF volume inside the spinal part with an instant decrease of CSFP in the cranium (explained by our new concept, Figure 4). The described phenomenon may explain how the reduction of CSFP occurs when applying iv. hyperosmolar mannitol solutions (Orešković et al., 2018), because in the first 30 min after application, there is a decrease in CSFP without changes in the percentage of water in the brain, cerebral blood volume, or intracanal fluid. As mortality in humans caused by high CSFP is a serious/major health problem, new insights into the regulation of CSFP should be very important in preventing and treating this pathological condition.

The presented results strongly support our hypothesis of CSF physiology where CSF/interstitial fluid volume depends on osmotic and hydrostatic force gradient between capillaries and interstitial space inside cranial and spinal CNS tissues (Orešković and Klarica, 2010; Orešković and Klarica, 2011; Bulat and Klarica, 2011; Orešković et al., 2017a,b; Klarica et al., 2019; Radoš et al., 2021). Until today, the regulation of CSFP was explained by the classic hypothesis of CSF physiology, e.g., secretion, circulation, and absorption of CSF. A famous equation that links the classical concept of CSF physiology and intracranial CSFP is CSFP = Vf x Ro + Pv, which suggests that intracranial CSFP has to be positive because the CSF secretes, flows unidirectionally, and absorbs all the time.

Since under the same experimental conditions, changes in CSFP obtained in phantom (Figure 3) reflect the results of CSFP obtained in cats (Figure 2), it is obvious that the classical hypothesis cannot explain CSFP regulation and long-lasting negative CSFP. Therefore, there is neither secretion, circulation, nor absorption in the phantom, and the regulation of "CSFP" could be explained only by the law of fluid mechanics. Thus, "CSFP" behavior in the phantom, compared with its behavior in anesthetized cats, offers us the opportunity to propose that the law of fluid mechanics is a unique explanation of CSFP regulation in different body positions. The use of phantom as a model that faithfully reflects the craniospinal system of cats is therefore of vital importance because the comparison of experimental results allows us to gain new insights into the behavior of CSF volume in the CSF space.

The results of this work, as well as our previous research (Klarica et al., 2006, 2014, 2019; Orešković et al., 2018), suggest that the role of spinal subarachnoid space in the regulation of CSFP is crucial and is consistent with research results that give a significantly greater role in compensation of intracranial hypertension by spinal rather than intracranial space (Löfgren and Zwetnow, 1973; Magnæs, 1989; Alperin et al., 2021). In addition, the existence of craniospinal communication within the cerebrospinal fluid space appears to be important not only to compensate for the increase in cranial pressure but also to enable therapeutic reduction of CSFP within the entire CSF system. That is, the obstruction of craniospinal communication would prevent the reduction of CSFP in the cranium, which, according to our results, would occur due to the reduction of the volume in the spinal space.

Limitations

There are some limitations to this study. In cats, cerebrospinal fluid volumes in the cranial and spinal parts of the CSF system were not determined by adequate volumetric methods. We expect that the combination of neuroradiological research with the help of MR, which allows recording in the head-up position, and the method of long-term measurement of CSFP in various diseases and body positions will confirm our results in the future. This study measured pressure changes in the cranial and spinal spaces that had normal communication. Therefore, from the obtained results, it is impossible to precisely determine the

value of compliance and elastance separately for the cranial and spinal spaces.

Conclusion

The matching results of the CSFP measurements obtained under the same experimental conditions in cat and phantom suggest that the spinal space contributing to the compliance of the total craniospinal space is significantly more than the cranial space, since the results obtained on a phantom without the possibility of the cranial compliance existence can approximate the system very well. The change of the micro-CSF volume in the spinal CSF region also causes a significant CSFP change inside the cranium, i.e., even a minor spinal volume change substantially changes the cranial CSFP. The observed clinical phenomenon of moving the zero (atmospheric) point of the CSFP in the human vertical position could be explained mainly by changes in the CSF volume in the spinal part of the CSF system and a simultaneous increase or decrease of the added volume (CSF, blood, tissue edema, etc.) in the spinal area. The obtained phenomenon is possible to explain only in accordance with the new hypothesis of CSF physiology.

Data availability statement

The raw data supporting the conclusions of this article will be made available by the authors, without undue reservation.

Ethics statement

The animal study was reviewed and approved by Ethics Committee of the University of Zagreb Medical School. Written informed consent for participation was not obtained from the owners because the owners were verbally informed about the experimental protocol, which was previously approved by the official Ethical Committee.

Author contributions

MK and DO designed and conceptualized the study. MK, MR, GE, and IJ performed experiments on animals and phantom. AP and ZV introduced a theoretical model to explain the results. MR, MK, and DO prepared the figures, drafted the initial version of the manuscript, and explained the presented results according to their new hypothesis of CSF physiology. All authors have read and approved the final draft of the manuscript.

Funding

This work has been supported by the Croatian Science Foundation and the Ministry of Science and Education of the Republic of Croatia (Projects: 1. Pathophysiology of cerebrospinal fluid and intracranial pressure: No. 108-1080231-0023; and 2. Serotonergic modulation of obesity: cross-talk between regulatory molecules and pathways: No. IP-2014-09-7827). The research was co-financed by the Scientific Centre of Excellence for Basic, Clinical, and Translational Neuroscience (project Experimental and clinical research of hypoxic-ischemic damage in perinatal and adult brain; GA KK01.1.1.01.0007 funded by the European Union through Europe).

Acknowledgments

Thanks to Mrs. Ljiljana Krznar for technical assistance in performing the experiments.

Conflict of interest

The authors declare that the research was conducted in the absence of any commercial or financial relationships that could be construed as a potential conflict of interest.

Publisher's note

Supplementary material

The Supplementary Material for this article can be found online at: https://www.frontiersin.org/articles/10.3389/fnmol.2022.931091/full#supplementary-material

References

Alperin, N., Bagci, A. M., Lee, S. H., and Lam, B. L. (2016). Automated quantitation of spinal CSF volume and measurement of craniospinal CSF redistribution following lumbar withdrawal in idiopathic intracranial hypertension. *Am. J. Neuroradiol.* 37, 1957–1963. doi: 10.3174/ajnr.A4837

Alperin, N., Burman, R., and Lee, S. H. (2021). Role of the spinal canal compliance in regulating posture-related cerebrospinal fluid hydrodynamics in humans. *J. Magn. Reson. Imaging* 54, 206–214. doi: 10.1002/jmri.27505

Alperin, N., Hushek, S. G., Lee, S. H., Sivaramakrishnan, A., and Lichtor, T. (2005a). MRI study of cerebral blood flow and CSF flow dynamics in an upright posture: the effect of posture on the intracranial compliance and pressure. *Acta. Neurochirurgica* 95, 177–181. doi: 10.1007/3-211-32318-X_38

Alperin, N., Lee, S. H., Sivaramakrishnan, A., and Hushek, S. G. (2005b). Quantifying the effect of posture on intracranial physiology in humans by MRI flow studies. *J. Magn. Reson. Imaging* 22, 591–596. doi: 10.1002/jmri.20427

Andresen, M., Hadi, A., Petersen, L. G., and Juhler, M. (2015). Effect of postural changes on ICP in healthy and ill subjects. *Acta Neurochirurgica* 157, 109–113. doi: 10.1007/s00701-014-2250-2

Bulat, M., and Klarica, M. (2011). Recent insights into a new hydrodynamics of the cerebrospinal fluid. *Brain Res. Rev*. 65, 99–112. doi: 10.1016/j.brainresrev.2010.08.002

Chapman, P. H., Cosman, E. R., and Arnold, M. A. (1990). The relationship between ventricular fluid pressure and body position in normal subjects and subjects with shunts: a telemetric study. *Neurosurgery* 26, 181. doi: 10.1227/00006123-199002000-00001

Davson, H., Welch, K., Segal, M. B., Malcolm B., and Davson, H. (1987). *Physiology and Pathophysiology of the Cerebrospinal Fluid*. Churchill Livingstone.

Ertl, P., Hermann, E. J., Heissler, H. E., and Krauss, J. K. (2017). Telemetric Intracranial Pressure Recording via a Shunt System Integrated Sensor: A Safety and Feasibility Study. *J. Neurol. Surg. A Cent. Eur. Neurosurg.* 78, 572–575. doi: 10.1055/s-0037-1603632

Farahmand, D., Qvarlander, S., Malm, J., Wikkelso, C., Eklund, A., and Tisell, M. (2015). Intracranial pressure in hydrocephalus: impact of shunt adjustment and body positions. *J. Neurol. Neurosurg. Psychiatry* 86, 222–228. doi: 10.1136/jnnp-2014-307873

Gisoff, J., van Lieshout, J. J., van Heusden, K., Pott, F., Stok, W. J., and Karemaker, J. M. (2004). Human cerebral venous outflow pathway depends on posture and central venous pressure. *J. Physiol.* 560, 317–327. doi: 10.1113/jphysiol.2004.070409

Holmlund, P., Eklund, A., Koskinen, L. O. D., Johansson, E., Sundstrom, N., and Malm, J. (2018).Venous collapse regulates intracranial pressure in upright body positions. *Am. J. Physiol. Regul. Integr. Comp. Physiol.* 314, R377–R385. doi: 10.1152/ajpregu.00291.2017

Jurjević, I., Radoš, M., Orešković, J., Priji,ć, R., Tvrdeić, A., and Klarica, M. (2011). Physical characteristics in the new model of the cerebrospinal fluid system. *Coll. Antropol*. 35, 51-6.

Kenning, J. A., Toutant, S. M., and Saunders, R. L. (1981). Upright patient positioning in the management of intracranial hypertension. *Surg. Neurol.* 15, 148–152. doi: 10.1016/0090-3019(81)90037-9

Klarica, M., Rados, M., Draganic, P., Erceg, G., Oreskovic, D., Maraković, J., et al. (2006). Effect of head position on cerebrospinal fluid pressure in cats: comparison with artificial model. *Croat. Med. J.* 47, 233–238.

Klarica, M., Radoš, M., Erceg, G., Petošić, A., Jurjević, I., and Oreškovi,ć, D. (2014). The influence of body position on cerebrospinal fluid pressure gradient and movement in cats with normal and impaired craniospinal communication. *PLoS ONE* 9:e0095229. doi: 10.1371/journal.pone.0095229

Klarica, M., Radoš, M., and Orešković, D. (2019). The movement of cerebrospinal fluid and its relationship with substances behavior in cerebrospinal and interstitial fluid. *Neuroscience* 414, 28–48. doi: 10.1016/j.neuroscience.2019.06.032

Kosugi, K., Yamada, Y., Yamada, M., Yokoyama, Y., Fujiwara, H., Yoshida, K., et al. (2020). Posture-induced changes in the vessels of the head and neck: evaluation using conventional supine CT and upright CT. *Sci. Rep*. 10:16623. doi: 10.1038/s41598-020-73658-0

Laitinen, L. (1968). Origin of arterial pulsation of cerebrospinal fluid. *Acta. Neurol. Scand.* 44, 168–176. doi: 10.1111/j.1600-0404.1968.tb05563.x

Landau, L. D., Lifshitz, E. M., Sykes, J. B., Reid, W. H., and Dill, E. H. (2009). Theory of elasticity: vol. 7 of course of theoretical physics. *Physics Today,* 13, 44. doi: 10.1063/1.3057037

Lawley, J. S., Levine, B. D., Williams, M. A., Malm, J., Eklund, A., Polaner, D. M., et al. (2015). Cerebral spinal fluid dynamics: effect of hypoxia and implications for high-altitude illness. *J. Appl. Physiol.* 120, 251–262. doi: 10.1152/japplphysiol.00370.2015

Levine, D. N., and Rapalino, O. (2001). The pathophysiology of lumbar puncture headache. *J. Neurol. Sci.* 192, 1–8. doi: 10.1016/S0022-510X(01)00601-3

Linden, C., Qvarlander, S., Johannesson, G., Johansson, E., Ostlund, F., Malm, J., et al. (2018). Normal-tension glaucoma has normal intracranial pressure: a prospective study of intracranial pressure and intraocular pressure in different body positions. *Ophtalmology* 125, 361–368. doi: 10.1016/j.ophtha.2017.09.022

Löfgren, J., and Zwetnow, N. N. (1973). Cranial and spinal components of the cerebrospinal fluid pressure-volume curve. *Acta. Neurol. Scand.* 49, 575–585. doi: 10.1111/j.1600-0404.1973.tb01331.x

Magnæs, B. (1989). Clinical studies of cranial and spinal compliance and the craniospinal flow of cerebrospinal fluid. *Br. J. Neurosurg.* 3, 659–668. doi: 10.3109/02688698908992689

Magnaes, B. (1976a). Body position and cerebrospinal fluid pressure. part 1: clinical studies on the effect of rapid postural changes. *J. Neurosurg.* 44, 687–697. doi: 10.3171/jns.1976.44.6.0687

Magnaes, B. (1976b). Body position and cerebrospinal fluid pressure. part 2: clinical studies on orthostatic pressure and the hydrostatic indifferent point. *J. Neurosurg.* 44, 698–705. doi: 10.3171/jns.1976.44.6.0698

Marmarou, A., Shulman, K., and Rosende, R. M. (1978). A nonlinear analysis of the cerebrospinal fluid system and intracranial pressure dynamics. *J. Neurosurg.* 48, 332–344. doi: 10.3171/jns.1978.48.3.0332

Nikić, I., Rado,š, M., Frobe, A., Vuki,ć, M., Oreškovi,ć, D., and Klarica, M. (2016). The effects of lumboperitoneal and ventriculoperitoneal shunts on the cranial and spinal cerebrospinal fluid volume in a patient with idiopathic intracranial hypertension. *Croat. Med. J.* 57, 293–297. doi: 10.3325/cmj.2016.57.293

Ocamoto, G. N., Russo, T. L., Zambetta, R. M., Frigeri, G., Hayashi, C. Y., Brasil, S., et al. (2021). Intracranial compliance concepts and assessment: a scoping review. *Front. Neurol.* 12:756112. doi: 10.3389/fneur.2021.756112

Orešković, D., and Klarica, M. (2010). The formation of cerebrospinal fluid: Nearly a hundred years of interpretations and misinterpretations. *Brain Res. Rev.* 64, 241–262. doi: 10.1016/j.brainresrev.2010.04.006

Orešković, D., Maraković, J., Varda, R., Radoš, M., Jurjević, I., and Klarica, M. (2018). New insight into the mechanism of mannitol effects on cerebrospinal fluid pressure decrease and craniospinal fluid redistribution. *Neuroscience* 392, 164–171. doi: 10.1016/j.neuroscience.2018.09.029

Orešković, D., Radoš, M., and Klarica, M. (2017a). Role of choroid plexus in cerebrospinal fluid hydrodynamics. Neuroscience, 354, 69–87. doi: 10.1016/j.neuroscience.2017.04.025

Orešković, D., Radoš, M., and Klarica, M. (2017b). New concepts of cerebrospinal fluid physiology and development of hydrocephalus. *Pediatric. Neurosurg.* 52, 417–425. doi: 10.1159/000452169

Portella, G., Cormio, M., Citerio, G., Contant, C., Kiening, K., Enbland, P., et al. (2005). Continuous cerebral compliance monitoring in severe head injury: its relationship with intracranial pressure and cerebral perfusion pressure. *Acta Neurochir.* 147, 707–713, doi: 10.1007/s00701-005-0537-z

Qvarlander, S., Sundstrom, N., Malm, J., and Eklund, A. (2013). Postural effects on intracranial pressure: modeling and clinical evaluation. *J. Appl. Physiol.* 115, 1474–1480. doi: 10.1152/japplphysiol.00711.2013

Radoš, M., Živko, M., Periša, A., Orešković, D., and Klarica, M. (2021). No arachnoid granulations-no problems: number, size, and distribution of arachnoid granulations from birth to 80 years of age. *Front. Aging Neurosci.* 13:698865. doi: 10.3389/fnagi.2021.698865

Rosner, M. J., and Coley, I. B. (1986). Cerebral perfusion pressure, intracranial pressure, and head elevation. *J. Neurosurg.* 65, 636–641. doi: 10.3171/jns.1986.65.5.0636

Rot, S., Dweek, M., Gutowski, P., Goelz, L., Meier, U., and Lemcke, J. (2020). Comparative investigation of different telemetric methods for measuring intracranial pressure: a prospective pilot study. *Fluids Barriers CNS,* 17, 63. doi: 10.1186/s12987-020-00225-0

Tunturi, A. R. (1977). Elasticity of the spinal cord dura in the dog. *J. Neurosurg.* 47, 391–396. doi: 10.3171/jns.1977.47.3.0391

Valdueza, J. M., von Munster, T., Hoffman, O., Schreiber, S., and Einhaupl, K. M. (2000). Postural dependency of the cerebral venous outflow. *Lancet* 355, 200–201. doi: 10.1016/S0140-6736(99)04804-7

frontiers | Frontiers in Molecular Neuroscience

TYPE Review
PUBLISHED 20 September 2022
DOI 10.3389/fnmol.2022.952036

OPEN ACCESS

EDITED BY
Adjanie Patabendige,
Edge Hill University, United Kingdom

REVIEWED BY
Yu-Feng Wang,
Harbin Medical University, China
Andrea Quattrone,
University Magna Graecia, Italy
Nobutaka Hattori,
Juntendo University, Japan
Ville Leinonen,
Kuopio University Hospital, Finland

*CORRESPONDENCE
Gelei Xiao
xiaogelei@csu.edu.cn

†These authors have contributed equally to this work and share first authorship

SPECIALTY SECTION
This article was submitted to Brain Disease Mechanisms, a section of the journal Frontiers in Molecular Neuroscience

RECEIVED 24 May 2022
ACCEPTED 12 August 2022
PUBLISHED 20 September 2022

CITATION
Zhao Z, He J, Chen Y, Wang Y, Wang C, Tan C, Liao J and Xiao G (2022) The pathogenesis of idiopathic normal pressure hydrocephalus based on the understanding of AQP1 and AQP4. *Front. Mol. Neurosci.* 15:952036. doi: 10.3389/fnmol.2022.952036

The pathogenesis of idiopathic normal pressure hydrocephalus based on the understanding of AQP1 and AQP4

Zitong Zhao[1,2,3†], Jian He[4†], Yibing Chen[1,2,3], Yuchang Wang[1,2,3], Chuansen Wang[1,2,3], Changwu Tan[1,2,3], Junbo Liao[1,2,3] and Gelei Xiao[1,2,3*]

[1]Department of Neurosurgery, Xiangya Hospital, Central South University, Changsha, China, [2]Diagnosis and Treatment Center for Hydrocephalus, Xiangya Hospital, Central South University, Changsha, China, [3]National Clinical Research Center for Geriatric Disorders, Xiangya Hospital, Central South University, Changsha, China, [4]Department of Pediatrics, Xiangya Hospital, Central South University, Changsha, China

Idiopathic normal pressure hydrocephalus (iNPH) is a neurological disorder without a recognized cause. Aquaporins (AQPs) are transmembrane channels that carry water through cell membranes and are critical for cerebrospinal fluid circulation and cerebral water balance. The function of AQPs in developing and maintaining hydrocephalus should be studied in greater detail as a possible diagnostic and therapeutic tool. Recent research indicates that patients with iNPH exhibited high levels of aquaporin 1 and low levels of aquaporin 4 expression, suggesting that these AQPs are essential in iNPH pathogenesis. To determine the source of iNPH and diagnose and treat it, it is necessary to examine and appreciate their function in the genesis and maintenance of hydrocephalus. The expression, function, and regulation of AQPs in iNPH are reviewed in this article, in order to provide fresh targets and suggestions for future research.

KEYWORDS

iNPH, AQP1, AQP4, hydrocephalus, pathogenesis

Introduction

Normal pressure hydrocephalus (NPH) is a clinical condition characterized by gait abnormalities, cognitive impairment, and urinary incontinence. Clinically, it is often divided into two categories: secondary NPH (sNPH), often secondary to diseases with clear causes, such as craniocerebral trauma, subarachnoid hemorrhage, intracranial infection, encephalitis; and idiopathic NPH (iNPH), which has no definite etiology, mainly occurs in adults, and has a high incidence among the elderly. Misdiagnosis with Alzheimer's, Parkinson's syndrome, or a combination of these is common. The pathophysiology of iNPH is currently unclear. The basic theory of intracranial intravenous system compliance reduction is demonstrated by decreased cerebrospinal fluid (CSF) pulsation and impaired cobweb particle function, influencing CSF flow and absorption. The pathogenesis of iNPH is linked to irregular CSF circulatory dynamics

based on circulation theory, inflammatory responses, osmosis abnormalities, and lymphatic drainage disorders based on penetration theory. Aquaporins (AQPs), which are responsible for CSF penetration and lymphatic outflow, are also involved in creating iNPH (Leinonen et al., 2021; Wang Y. et al., 2021).

AQPs are transmembrane channels that specifically transport water through their formation of an integral membrane protein. Totally, 13 AQP members (AQP0 to AQP12) have been found in mammals and amphibians. These proteins are tiny and intact membrane molecules with a molecular weight of about 30 kDa/monomer. There are currently 13 water-channel proteins that can be cloned, and they are found in every organ and gland in the body. The central nervous system contains five AQPs: AQP1, AQP4, AQP7, AQP9, and AQP11, with AQP1 and AQP4 having the greater concentration and AQP4 having the greatest concentration. The role of AQPs in CSF circulation, formation, and absorption of CSF, along with related mechanisms in cerebral edema and hydrocephalus, is being investigated.

Water is transported across primary ventricular fluids *via* AQPs: between CSF (containing ventricles and subarachnoid space), brain material (intracellular and extracellular), and intra-brain. CSF is a fluid found in the subarachnoid space and ventricles with a total volume of around 150 ml, of which 125 ml is in the substrate (Hodler et al., 2020). Net filtration and adsorption of water and solute in the interstitial space maintains CSF content (Papadopoulos and Verkman, 2013; Iliff et al., 2015; Nakada and Kwee, 2019). CSF enters the brain in the Virchow–Robin space of the para-arterial space and then is absorbed into the venous blood flow in the para-venous space (Iliff et al., 2013; Rasmussen et al., 2018). Whereas, water channels regulate water exchange, AQPs passively allow two-way water transport based on static water pressure and osmotic pressure (Papadopoulos and Verkman, 2013; Rasmussen et al., 2018).

AQP1 and AQP4 are the most abundant proteins in the mammalian central nervous system.

AQP1 is a 28 kD channel-forming integral protein widely distributed in the cell's plasma membrane in the form of tetramers, with each monomer (one AQP molecule) capable of generating a separate functional water channel. Because of its structural characteristics, AQP1 is highly permeable to water molecules, allowing 3,109 water molecules to flow through every second through a single AQP1 molecule. On the CSF side of the choroid plexus (CP), AQP1 is mainly expressed in epithelial cells and, together with carbonic anhydrase and the sodium pump on the basal side, plays a role in the production of CSF.

The most abundant aquaporin in the brain, spinal cord, and the optic nerves is AQP4, which regulates the brain's distribution and balance of water. It is found primarily in the astrocyte end-feet in the blood–brain barrier CSF–astrocyte boundary membranes, and ventricular membranes. As the most abundant water channel, AQP4 governs the water steady state. The AQP4 monomer is 30 kDa in molecular weight and consists of six cross-film spirals and two incomplete cross-film spirals. Each monomer contains a central water hole. AQP4 is expressed as a tetramer in the cell membrane. AQP4 is classified into two subtypes, M1 and M23, and its translation begins earlier than that of methionine M1 (323 amino acids) or methionine M23 (301 amino acids). A quadrangle composed of M23 forms a higher order structure known as an orthogonal array of particles, a crystal-like supermolecular component of a mass membrane (Wang et al., 2022). Although the biological significance of orthogonal arrays of particles has not been determined, it has been hypothesized to increase water permeability, alter cell–cell adhesion, and induce AQP4 polarization. Its highly efficient transmembrane and transcellular water transport channels contribute to the formation and removal of cerebral edema, as well as the generation and absorption of CSF. AQP1 and AQP4 are water channels located in the areas above and are associated with eliminating cerebral edema and hydrocephalus (Castañeyra-Ruiz et al., 2013).

In the current study, patients with iNPH had higher levels of AQP1 expression and lower levels of AQP4 expression, while AQP4 expression has grown with little polarization in chronic and age-related experimental models (de Laurentis et al., 2020).

AQPs may prove to be a useful diagnostic tool. The sole treatment option for hydrocephalus is treatment with a CSF shunt, but there is a risk of fatal complications (Raneri et al., 2017; Hodler et al., 2020). Thus, they are critical for diagnosing hydrocephalus. Diagnosis of iNPH remains challenging. However, detecting AQPs in CSF as biomarkers for identifying iNPH and separating these individuals from those with Alzheimer's disease is impossible, according to recent studies, at least given the detection levels afforded by commercial ELISA kits. AQP1 and AQP4 shedding into the CSF does not appear to occur in any of these illnesses, at least not at measurable quantities by ELISA (Hiraldo-González et al., 2021). A potentially useful method is to provide quantitative CSF samples during aspiration tests (de Laurentis et al., 2020). Although there are no extremely sensitive and specific CSF biomarkers that may predict the efficacy of a CSF shunt intervention, several studies have shown the potential of A42, p-tau, total tau, NfL, and LRG (Nakajima et al., 2021; Thavarajasingam et al., 2022). Additionally, AQPs may be used as therapeutic targets (Rizwan Siddiqui et al., 2018; Ding et al., 2019). Their exact activity enables alternating inhibition and activation of medicines, administered intrauterine or orally. Early intervention in the prodromal phase of iNPH was shown to aid strong cognitive and mobility function as well as social involvement capacity in the long-term experimental investigations. Its ability to maintain long-term cognitive function implies that it can help prevent dementia. Establishing an early diagnosis method for iNPH is desirable in order to provide early intervention for iNPH (Kajimoto et al., 2022).

It is critical to investigate and understand the role of aquaporin in the formation and maintenance of hydrocephalus

to ascertain the causes of iNPH, leading to diagnosis and treatment. This article summarizes the current state of research on iNPH and findings on AQPs to identify future targets and research directions.

The pathogenesis of iNPH

The exact cause of iNPH is still unknown, despite the fact that various mechanisms have been theorized to contribute to its development. Previously, it was believed that ventriculomegaly and other neurological abnormalities in iNPH were first caused by a change in the dynamics of the CSF. A proxy for CSF pulsatility may be the aqueduct stroke volume, which is measured using phase-contrast magnetic resonance imaging (PC-MRI) and is defined as the average of the flow volume *via* the aqueduct during diastole and systole. Aqueduct stroke volume levels in patients with iNPH are higher than in healthy controls (Qvarlander et al., 2017; Yin et al., 2017). Reduced arterial pulsatility and decreased intracranial compliance may be related to increased CSF pulsatility. Under normal circumstances, pressure gradients cause the CSF in the subarachnoid space to be reabsorbed through the arachnoid granulations and brought up into the superior sagittal sinus (Bothwell et al., 2019). In individuals with iNPH, the normal CSF drainage is disturbed. The resistance to CSF outflow (Rout), which has been widely utilized to diagnose iNPH and identify candidates for shunt operations, is pathologically high in these individuals (Malm et al., 2011).

The bulk flow of CSF into the brain is facilitated by the recently discovered glial–lymphatic (glymphatic) pathway along the para-arterial space, the interstitial space, and ultimately into the paravenous space. Intact AQP4 channels, proper arterial pulsation, and proper sleep are all necessary for the glymphatic system to operate normally (Rasmussen et al., 2018). Individuals with iNPH have a compromised glymphatic system. Reduced clearance of neurotoxic chemicals like beta amyloid and hyperphosphorylated tau is a direct result of the glymphatic system disruption (HP tau) (Eide and Ringstad, 2019). Accumulation of these neurotoxic chemicals may cause astrogliosis and neuroinflammation in addition to impairing the physiological functioning of neurons (Angelucci et al., 2019).

In addition, aberrant CSF dynamics cause ventricular hypertrophy, which increases mechanical stress on the parenchyma and blood vessels, leading to hypoperfusion and subsequent hypoxia. Hypoperfusion may also cause a number of pathological abnormalities to brain tissue, such as gliosis, neuroinflammation, and impairments to the blood–brain barrier. They are each acknowledged for their contributions to INPH. In the sections that follow, we'll analyze it in view of CSF overproduction and discharge disorder and investigate how AQP1 and AQP4 may be involved.

AQP1 and hydrocephalus

The polarized expression of AQP1 in humans has also been demonstrated to play a role in CSF secretion. Existing experimental research has demonstrated a strong correlation between the development of hydrocephalus and the overexpression of AQP1. There is still a need for additional research despite evidence in iNPH patients, but numerous investigations have consistently shown that AQP1 controls water molecule distribution. The apical membrane of choroid plexus epithelial cells displays a significant amount of AQP1 expression. CSF production can be decreased by down-regulating AQP1 in the apical membrane. Therefore, specific AQP1 inhibition or down-regulation and strengthening of this beneficial negative feedback can further limit CSF secretion, reduce intracranial pressure, and postpone the pathological progression of hydrocephalus, which may also be a promising therapeutic target.

Regulation of AQP1 on CSF circulation

AQP1 is predominantly present on the apical membrane of plexus epithelial cells (on the CSF side), with a tiny amount on the outside (near the side of the blood vessel). CSF is produced and secreted by CP epithelial cells. Some cells of the chamber membrane can also exude CSF in trace amounts, although the majority is produced by the CP epithelial cells. Regarding its transcellular transport of water molecules during CSF formation, the apical AQP1 has a relatively wide distribution. The synergy between Na, K-ATPase and AQP1 in the CP is presently the critical molecular pathway for water transfer in the ventricle and CSF creation model. Because AQP1 in the apical membrane allows water to flow in the direction of the permeation gradient, it is vital to maintain the permeability of the apical membrane. Reduced AQP1 expression on the CP's surface may account for how water molecules pass through the membrane of transmembrane CP cells and into the ventricle where they create CSF and cause hydrocephalus. According to the study, AQP1's polarized expression pattern is also involved in human CSF generation. AQP1 has been found in astrocytes surrounding cerebral arteries in various neurological disorders, including multiple sclerosis, traumatic brain injury, cerebral infarction, epilepsy, viral infections, and Alzheimer's disease. Healthy CSF contains AQP1, whereas patients with neuro-inflammatory diseases such as bacterial meningitis have elevated AQP1 levels (Blocher et al., 2011). Additionally, AQP1 is located in the blood–brain barrier, which may explain why AQPs are implicated in cerebral edema clearance.

Verkman (2008a) found that *AQP1* knockout animals had a 20% decrease in CSF fluid production and a 56% decrease in intracranial pressure compared to wild-type mice. The study discovered that when the *AQP1* gene was deleted, aquaporin

expression in choroid plexus epithelial cells and CSF secretion decreased in mice, AQP expression in the nephropathic tube decreased, because AQP1 relies on decreased cross-cell reabsorption of primary urine, which results in decreased blood volume, sinus pressure, and CSF reflux. Smith et al. (2007) described an instance of communicating hydrocephalus. CP immunohistochemistry showed that the expression of AQP1 on the apical membrane of the choroid plexus epithelial cells of the ill choroid plexus was lower than that of normal children of the same age.

In conclusion, when hydrocephalus occurs, AQP1 on the to apical membrane of the choroid plexus epithelial cell enters the cytoplasm *via* endocytosis, decreasing CSF production and secretion and compensating for the decreased CSF secretion to maintain relative intracranial pressure stability, which may be a protective mechanism of the body.

However, the efficacy of this stabilizing mechanism is not without defects, as demonstrated by Jeon et al. (2017), who found (Rasmussen et al., 2018) protein in the CP of acute hydrocephalus rats using a kaolin-induced hydrocephalus paradigm. They reported abrupt reduction of AQP 1 protein expression in the CP of rats with acute hydrocephalus, increasing at later stages, following the same trend as AQP1 mRNA expression. The quick decline in AQP1 expression during the early stages of hydrocephalus is consistent with a decrease in CSF compensatory production, corroborating our theory. On the other hand, later expression levels in the experimental group were considerably higher than in the control group. The researchers believed that this was related to additional mechanisms of CSF secretion, such as neuroendocrine function (AQP1 expression may be enhanced in response to stress-induced neuroendocrine regulators) (Paul et al., 2011). Additionally, this late upregulation of expression must be confirmed. Increased expression of CP AQP1 may increase the number of water channels activated by an atrial natriuretic factor or other cGMP-producing factors in late hydrocephalus, hence decreasing CSF generation. Alternatively, cGMP-producing substances may impede the choroidal Na, K-ATPase action, resulting in decreased fluid secretion (Eide and Ringstad, 2019).

The failure of the stabilizing mechanism, which causes an increase in cerebral fluid and further aggravates stagnant fluid, may be the cause of the later increase in expression. When Wang et al. (2011) examined the brain tissue of kaolin-injected mice to create an animal model of hydrocephalus, they revealed that a substantial number of AQP1 immune granules were present in the apical membrane of CP epithelial cells in the control group. This immunological granule is normally only found in the mitochondria in the cytoplasm, whereas in the experimental group, AQP1 was abundant in both the cytoplasm and the cell membrane. Apart from mitochondria, the cytoplasm contained AQP1 immune gold granules such as vesicles and lysosomes, and almost half of AQP1 entered the cytoplasm *via* the cytomembrane. Simultaneously, when AQP1 gene knockout animals were compared to wild-type mice, it was revealed that the *AQP1* gene knockout mice's baseline ventricular area was much lower than that of wild-type mice. When lateral ventricle injection of kaolin was used to induce hydrocephalus formation, AQP1 mice in the gene deletion group exhibited a 30% reduction in ventricle dilation, a faster weight recovery following surgery, and significantly fewer side effects such as aberrant behavior.

AQP1 in iNPH

There is a dearth of studies on AQP1 markers in patients with iNPH, and Castañeyra-Ruiz et al. (2016) found no significant increase in AQP1 levels in CSF compared to a control group. However, there were fewer cases, and in four of the six cases studied, these levels were significantly higher than those of ten control subjects, and all samples in the first quartile were controls, indicating a significant relationship between controls and low AQP1 values.

The apical membrane of choroid plexus epithelial cells expresses a high level of AQP1, and down-regulation of AQP1 in the apical membrane can result in decreased CSF production. Additionally, AQP1 can decrease blood volume and intracranial pressure by inhibiting primary urine reabsorption in the proximal convoluted tubule. These factors justify further investigation of AQP1 as a potential novel target for the treatment of hydrocephalus. Thus, selective inhibition or down-regulation of AQP1 expression, combined with enhancement of this protective negative feedback loop, can further reduce CSF secretion and intracranial pressure and delay the pathological process of hydrocephalus (Figure 1).

The expression and regulation mechanism of AQP1

The nervous system contains a high concentration of AQP1, and various variables regulate its expression, including hormones, osmotic pressure, hypoxia, ischemia, and medications. Similar to the regulation of other proteins, cell signal transduction plays a critical role in the regulation of AQP1 expression. Numerous influencing factors can modulate AQP1 expression by activating or inhibiting the appropriate transduction pathway (Wang C. et al., 2021).

Activity regulation of AQP1

Phosphorylation is the most common approach for altering the function of proteins at the protein level. This also applies to AQP1, as protein phosphorylation affects AQP transport, control, and redistribution. As a result, phosphorylation is a critical strategy for modulating AQP1 function. The structural

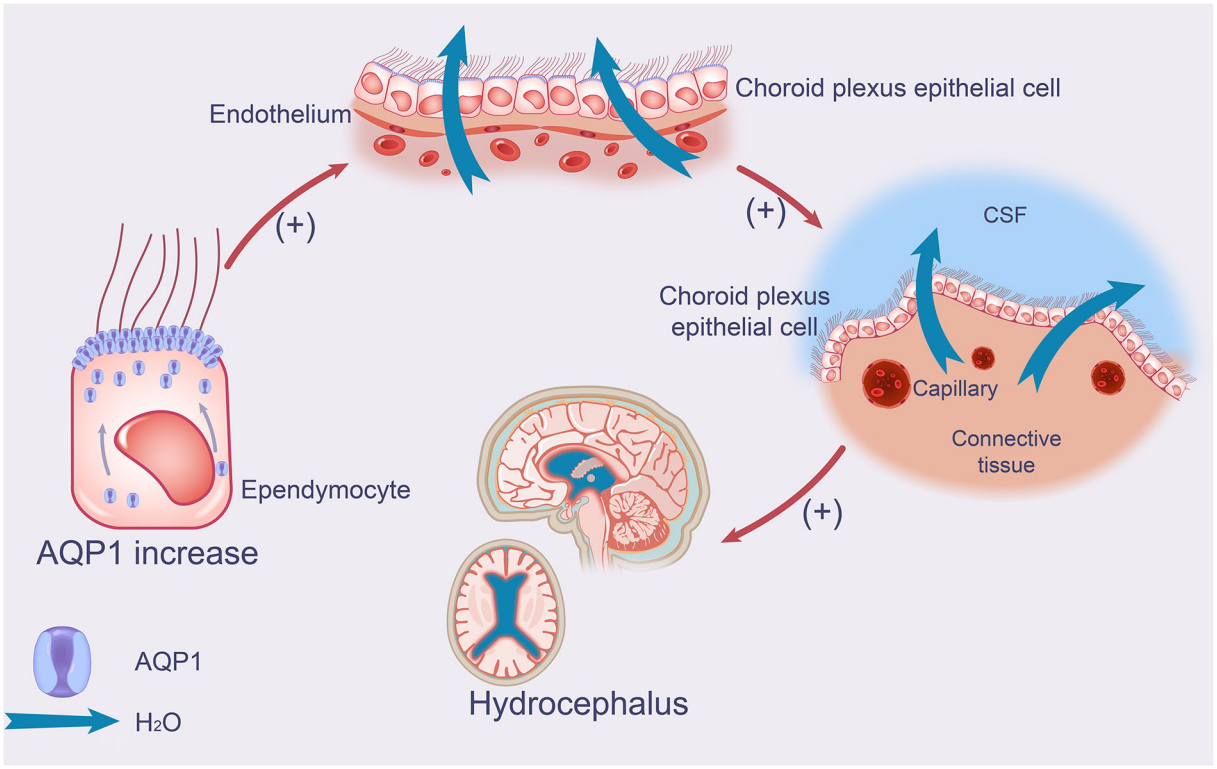

FIGURE 1
Effect of AQP1 on production of CSF in iNPH. The schematic drawing demonstrates increases in AQP1 and its function in iNPH, which leads to increased CSF production. AQP1 increases the production and secretion of CSF in the apical membrane of choroid plexus epithelial cells by accumulating in the ependymal membrane of ependymal cells. AQP1, aquaporin 1; iNPH, idiopathic normal pressure hydrocephalus; CSF, cerebrospinal fluid.

properties of AQP1 demonstrate that the nap structure, ar/R region, and sections of amino acid sequence or domain segments in the center hole all contribute to the protein's transport function; changes to these structures can directly or indirectly modify its permeability. AQP1 comprises four potential phosphorylation sites in humans and mice: S236-PKA phosphate sites, T159/T239-PKC phosphorylation sites, and S262-CKII phosphorylation sites (Zelenina, 2010). There is an additional PKC phosphorylation site in the human AQP1 amino acid sequence that CKI can phosphorylate. Additionally, Cys189 in AQP1 is a Hg^{2+} binding site, whereas Tyr186 is a TAE binding site, with the former limiting AQP1's water and ion permeability and the latter inhibiting its water permeability.

Several studies have demonstrated that PKA can phosphorylate AQP1 *in vitro* and that activators of PKA, such as cAMP and forskolin, can increase AQP1's water permeability (Smith et al., 2007). Vasopressin can enhance the water permeability of AQP1-transfected oocytes, and co-incubation and injection of 8-Bromo-cAMP into cells can also increase water permeability, which is hypothesized to occur *via* the cAMP pathway (Zelenina, 2010). Sakurada et al. (2004) demonstrated that 5% glucose enhanced AQP1 membrane transfer *via* the PKA pathway, which PKA-specific inhibitors could inhibit. However, several investigations have indicated that PKA does not promote AQP1 permeability *in vitro* (Wang et al., 2011). Sakurada et al. (2004) and Oshio et al. (2005) found that forskolin may increase CSF in wild-type mice and $AQP1^{-/-}$ mice. It has not been established conclusively that PKA-regulated AQP1 phosphorylation occurs in the brain.

For PKC pathways, Zhang et al. (2007) showed that the water and ion permeability of AQP1 is regulated by PKC's short-term activity, involving two phosphorylation sites, T159 and T239. The most recent study discovered that, in addition to phosphorylation regulation, AQP1 could also be regulated by ubiquitin.

Chemical blockers of AQP1 that are permeable to water are constantly being developed, Hg^{2+} and TAE are constrained by their toxic effects, and recent studies have demonstrated that the Na+-K+-Cl-co-transport blocker and medullary loop diuretic Bumetanide has a slight inhibitory effect on the water permeability of AQP4. Furthermore, the body can tolerate a high amount (100 mg/kg). This finding paved the way for the development of further molecular compounds based on the structure of Bumetanide. According to Kim et al. (2010),

the aryl-sulfonamide AqB013 significantly reduced the water permeability of AQP1 and AQP4, although its therapeutic potential remains unknown.

Gene regulation of AQP1

Changes in the external environment can affect the expression of the AQP1 gene (e.g., high seepage, low oxygen, etc.). AQP1 mRNA expression increased 2 fold in a high seepage environment (220 mM NaCl) but decreased in a low seepage environment (90 mM NaCl) (Bouley et al., 2009). Wang Feng et al. used primary culture of adult rabbit lumbar myelin nuclear cells, immunohistochemistry, and real-time quantitative PCR detection, and found significantly increased AQP1 expression in cells, which may be attributed to the increased expression of AQP1 to enhance oxygen delivery. 2-methoxyestradiol can inhibit hypoxia inducible factor-1α (HIF-1α) and vascular endothelial growth factor, hence influencing the expression of AQP-1.

This signal transduction pathway is critical for the regulation of AQP1 expression. In one study, Schwann cells inflated and AQP1 expression increased in response to hypoxia and HIF-1α may play a role in this process (Zhang et al., 2013), implying that the cGMP pathway regulates AQP1 expression. Ding et al. (2013) mimicked cardiopulmonary reflux using the guanosine cyclase inhibitor ODQ as a control. Compared to the control group, AQP1 mRNA expression fell by 39.7%, indicating that the cGMP pathway regulates AQP1 expression. McCoy and Sontheimer (2010) studied the expression of AQP1 following injury to active astrocytes using epidermal sting tests and discovered that the MEK1/2 pathway inhibitor U0126 might inhibit AQP1 expression. It was further demonstrated that cytokinin activates the protein kinase signaling pathway, inducing AQP expression. Experiments have also verified regulatory effects of JNK (Tie et al., 2012) and related pathways.

In both flanks of the *AQP1* gene, a substantial number of cis-regulatory elements have been identified. Although they do not encode any proteins themselves, they are critical for gene regulation. In conjunction with trans-acting factors, these cis-regulatory elements govern the transcription and translation of *AQP1* at the gene level. In the promoter region of *AQP1*, Moon et al. (1997) identified two glucocorticoid response elements. Steroid hormones can activate this response element and increase *AQP1* expression in murine leukemia cells.

Additionally, Stoenoiu et al. (2003) discovered that a high dose of corticosteroid (1.5 mg/kg) could stimulate AQP1 mRNA and protein expression in the peritoneum of rats. Simultaneously, the glucocorticoid receptor inhibitor Ru-486 worked on the glucocorticoid receptor and inhibited corticosteroid production. de Arteaga et al. (2011) discovered that high-dose corticosteroid therapy could increase the water level in patients undergoing peritoneal dialysis. These corresponding changes indicate that the glucocorticoid receptor and glucocorticoid response elements in the *AQP1* promoter region are intimately related to *AQP1* expression.

Translocation of AQP1

Owler et al. (2010) induced hydrocephalus in adult mice by injecting kaolin into the medullary cistern. In the experimental group, AQP1 was detected in the cytoplasm of CP epithelial cells, indicating a shift in the translocation of AQP1. Caveolin is a subunit of the membrane lipid cutting architecture that selectively transfers membrane proteins. It has been suggested that it is closely related to AQP1 translocation (Tie et al., 2012). Kobayashi et al. (2006) extended Western blotting findings to establish co-expression of AQP1 and caveolin in lipid cutting, and AQP1 localization indicated that AQP1 translocation might be associated with caveolin. Tietz et al. (2006) cultured bile duct epithelial cells *in vitro*, demonstrating that actin and microtubules may be involved in AQP1 translocation.

AQP4 in hydrocephalus

It has been gradually understood that AQP4, a crucial component of CSF transport and interstitial fluid clearance, plays a role in iNPH in the impairment of CSF circulation, astrocyte hyperplasia, and impaired lymphatic circulation in the perivascular space and brain parenchyma. This leads to CSF accumulation, an inability to efficiently remove metabolic waste, and neurodegenerative changes. A promising prospective therapeutic target, AQP4 plays a variety of roles in iNPH. Contrary to other types of hydrocephalus, the expression of *AQP4* shows a decrease in iNPH, which may allow treatment routes that affect AQP4 activation to have a more noticeable effect in iNPH than in other types of hydrocephalus (Table 1).

Regulation of AQP4 on CSF circulation

As another vital member of the water channel family, AQP4 is the most abundant aquaporin subtype in the central nervous system. It is primarily found in the protrusion membrane, glial boundary membrane, and ependyma of the foot processes of astrocytes surrounding capillaries, where it regulates the flow of water into and out of the brain *via* the CSF and blood. It exerts a considerable regulatory influence on CSF production and absorption (Hara-Chikuma and Verkman, 2008a,b; Verkman, 2008b). In cytotoxic cerebral edema caused by injuries such as water poisoning, cerebral infarction, or meningitis, AQP4-deficient mice had a better prognosis than wild-type mice (Verkman, 2008b). AQP4 deficiency bypasses the whole blood-brain barrier, hence lowering cytotoxic brain edema. In vascular cerebral edema mouse models such as cortical freezing, brain tumors, and intracranial rehydration fluid, AQP4-deficient

TABLE 1 Main studies investigating AQP1 and AQP4 in humans.

AQP	Author (years)	Research object	Result
AQP1	Verkman (2008a)	AQP1 gene knockout animals	20% decrease in CSF fluid production and a 56% decrease in intracranial pressure
	Smith et al. (2007)	Communicating hydrocephalus	Lower expression of AQP1 on the apical membrane of the CPEpiC* of the ill choroid plexus
	Jeon et al. (2017)	Kaolin-injected hydrocephalus mice	AQP 1 protein expression reduced abruptly in the choroid plexus of rats with acute hydrocephalus and increased at later stages
	Wang et al. (2011)	Kaolin-injected hydrocephalus mice	A substantial number of AQP1 immune granules are present in the apical membrane of CPEpiC*
	Castañeyra-Ruiz et al. (2016)	iNPH patient	No significant increase in AQP1 levels in cerebrospinal fluid compared to the control group
AQP4	Ismail et al. (2009)	SAH mouse model	
	Papadopoulos and Verkman (2007)	AQP4 gene knockout mice	Increase in intracranial pressure and the moisture content of brain tissue
	Mao et al. (2006)	Kaolin-injected hydrocephalus mice	AQP-4mRNA expression increased significantly in the parietal lobe and hippocampus
	Bloch et al. (2006)	Congenital AQP4 protein deficiency rats	AQP4 protein can exacerbate hydrocephalus in kaolin-induced H-t gene deletion rats
	Tourdias et al. (2009)	Hemolytic lecithin-induced traffic hydrocephalus	AQP4 expression increased significantly in the foot process of astrocytes
	Shen et al. (2006)	Congenital hydrocephalus model in rats	Increased AQP4 expression in the blood-brain barrier, ependyma, and subpial astrocytes
	Eide and Hansson (2020)	iNPH	Decrease in AQP4 expression at the LM and EM levels of perivascular astrocyte terminals, which were inversely proportional
	Hasan-Olive et al. (2019b)	iNPH	Reduced density of AQP4 water channels in astrocytic endfoot membranes along cortical microvessels in patients with iNPH

AQP1, aquaporin 1; AQP4, aquaporin 4; iNPH, idiopathic normal pressure hydrocephalus; CPEpiC, choroid plexus epithelial cell.

animals demonstrated significantly more brain swelling than wild-type mice, most likely because AQP4 in wild mice expedited the outflow of water from edema tissue. Additionally, in hydrocephalus, AQP4 regulates CSF absorption (Kusayama et al., 2011). Matthew et al. established the first mouse model of subarachnoid hemorrhage by injecting autologous blood into the basal cistern, simulating how high-pressure blood enters the CSF in human subarachnoid hemorrhage. The results indicated that AQP negative mice had more evident brain swelling and a poorer clinical prognosis than controls, primarily because AQP4 encouraged the evacuation of excess water in brain tissue *via* the compromised blood–brain barrier (Ismail et al., 2009).

Additional evidence linking AQP4 protein to CSF production and absorption has been revealed. Papadopoulos and Verkman (2007) observed an increase in intracranial pressure and the moisture content of brain tissue in gene knockout mice. When *AQP4* knockout mice were compared to wild-type mice, they had significantly reduced water penetration and a larger ventricular volume, implying that AQP4 is required for cross-substantive absorption of CSF. AQP4 demonstrates its impact on the occurrence and progression of hydrocephalus in a number of animal models of the condition. Mao et al. (2006) discovered that AQP4 mRNA expression increased significantly in the parietal lobe and hippocampus when kaolin-induced hydrocephalus was studied in mice. This could be because peripheral AQP4 expression is more easily activated in the brain's parietal lobe, and the parietal lobe and hippocampal regions have a lower water content than other regions. Bloch et al. (2006) also discovered that AQP4 can exacerbate hydrocephalus in kaolin-induced *H-t* gene deletion rats (congenital AQP4 protein deficiency rats) by decreasing the rate of extracellular fluid clearance across the blood-brain barrier, indicating that AQP4 plays a beneficial role in increasing the blood-brain barrier clearance rate and preventing the accumulation of excess water in the ventricles. Tourdias et al. (2009) calculated the apparent diffusion coefficient in rats with hemolytic lecithin-induced traffic hydrocephalus. After 2 weeks, it was discovered that AQP4 expression increased

significantly in the foot processes of astrocytes and that there was a significant correlation between AQP4 levels, apparent diffusion coefficient, and ventricular volume. Shen et al. (2006) used the congenital hydrocephalus model in rats and discovered that 8-week-old rats had increased AQP4 expression in the blood–brain barrier, ependyma, and subpial astrocytes. Additionally, it was hypothesized that increased AQP4 expression might be a compensatory response to CSF absorption in static hydrocephalus. In normal circumstances, CSF circulation is hampered after hydrocephalus. AQP4 expression rises as a result of compensatory trans-parenchymal absorption of CSF, and accumulating CSF is absorbed into the circulation *via* an AQP4-dependent transcellular pathway.

AQP4 in iNPH

In iNPH, the situation is substantially different, possibly due to a failure of the compensating process or a weakness in specific CSF linkages. Although it is commonly believed that AQP4 levels are elevated in patients with hydrocephalus, it was found that they decreased in iNPH (Eide and Hansson, 2018, 2020; Arighi et al., 2019; Hasan-Olive et al., 2019a,b). Eide and Hansson (2020) found a significant increase in the percentage of fibrin (fibrinogen) areas in iNPH cerebral cortex exosmosis. At the same time, AQP4 expression was decreased in the vicinity of blood vessels. Immunohistochemistry revealed a decrease in AQP4 expression at the light and electron microscopy levels of perivascular astrocyte terminals, which were inversely proportional.

In the research of Hasan-Olive et al. (2019b), AQP4 immunogold cytochemistry study of cortical brain samples from 30 patients with iNPH and 12 control participants revealed lower AQP4 density in the perivascular astroglial end-feet of patients. In brains from individuals with aneurysms, epilepsy, and cancer, astroglial AQP4 density facing the neuropil remained unaltered, as did perivascular AQP4 density. This link could point to a role for inflammation-induced AQP4 depolarization in iNPH pathogenesis, in which reduced perivascular AQP4 expression limits glymphatic fluid flux, increasing beta amyloid buildup and ventriculomegaly. In iNPH, the expression of AQP4 is decreased in the vicinity of blood vessels, resulting in issues with lymphatic circulation, waste disposal, and neurodegeneration (Hasan-Olive et al., 2019b).

There is no apparent explanation for why AQP4 expression differs so much between common hydrocephalus and iNPH. Recent research suggests that this phenomenon may be linked to inflammation. It was related to lymphatic malfunction in the early stages of inflammation by Reeves et al. (2020). In fact, investigations in both humans (Sosvorova et al., 2015) and animals (Sosvorova et al., 2015; Chaudhry et al., 2017) have identified a connection between perivascular space inflammation and the development of iNPH. In iNPH, the neuroinflammatory response is highly noticeable (Lolansen et al., 2021), and the level of inflammatory cytokines indicated by TNF in the CSF fluid is dramatically altered (Wang et al., 2020). However, we can demonstrate that AQP4 plays a role in CSF transport and interstitial fluid clearance, and that its reduction in iNPH has an effect on CSF circulation and lymphatic metabolic abnormalities.

Effect of AQP4 on the hyperplasia of astrocytes

The AQP4 protein is favorably linked with astrocyte development. Tomas-Camardiel et al. (2005) described an intracerebroventricular injection of lipopolysaccharide as a model of hemorrhagic brain edema. It was revealed that activated astrocytes expressed a high quantity of AQP4. Saadoun et al. (2009) discovered that pricking the cortex decreased astrocyte growth in AQP4 rats with congenital gene deficits, indicating that AQP4 promoted astrocyte proliferation. Zhou et al. (2008) also discovered that the absence of AQP4 caused a significant decrease in the expression of GFAP in the surrounding brain microvessels when examining rats with congenital AQP4 deficits, and GFAP was positively linked with the degree of astrocyte proliferation.

GFAP interacts closely with membrane anchoring proteins, allowing GFAP fibers to pull the membrane back when they retract in response to changes in signaling molecules. That is, as GFAP fibers retract, squeezing water out of the cytoplasm of the processes, the interactions between the anchor proteins and GFAP fibers cause volemic reduction (Wang and Hatton, 2009). The expression of volume-regulating proteins and their interactions with membrane anchoring proteins determine the volemic influence on GFAP's guiding role. AQP4 expression is synchronized with the levels and spatial distribution of GFAP, as expected for a volume-regulating protein (Wang and Hatton, 2009; Li et al., 2020). Furthermore, Wang X. et al. (2021) found TGN-020's ability to prevent GFAP retraction surrounding vasopressin neurons during hyposmotic challenge (20 min) and hyperosmotic stress suggesting that AQP4 plays a role in GFAP retraction. AQP4 is functionally connected with several ion channels and transporters, and its opening for water flux is accompanied by changes in ion concentration in astrocytes, which might affect GFAP metabolism and assembly, as previously discussed. By coupling with transient receptor potential vanilloid 4, Benfenati et al. (2011) and Stokum et al. (2018) discovered that AQP4 can increase intracellular Ca^{2+}; however this coupling is not required (Mola et al., 2016). Increased intracellular Ca^{2+} levels are required for GFAP depolymerization *via* protein kinase A and other signaling pathways (Petković et al., 2017), suggesting that AQP4 might reduce GFAP filament extension.

However, astrocyte growth also contributes to alterations in brain tissue function after hydrocephalus. When hydrocephalus occurs, the ventricle system extends the ventricular wall due to the accumulation of CSF. Astrocyte proliferation also occurs surrounding the ventricle, creating compensatory enlargement of the ventricle, causing CSF extravasation into the brain tissue around the ventricle, causing brain white matter edema and white matter tissue deterioration. When the CSF content is further increased, the elasticity of the brain tissue reduces due to compression, the cerebral cortex gets thinner, leading to brain atrophy, and these pathological changes result in neurological dysfunction, indicating that AQP4 stimulates GFAP and astrocyte proliferation, which may be the source of the changes in neurological function following hydrocephalus.

In patients with iNPH, Eide and Hansson (2018, 2020) detected nerve cell degeneration, astrocyte proliferation, and decreased expression of AQP4 and Dp71. In comparison to reference patients, cortical biopsies of individuals with iNPH revealed increased astrocyte proliferation and lower expression of AQP4 and Dp71 in astrocyte perivascular terminals in the foot and certain surrounding neural canals. The degree of astrocyte proliferation was substantially linked with a decrease in AQP4 and Dp71 levels in the astrocytes' perivascular terminal feet. Additionally, all patients with iNPH have bulging nerve cell bodies and neurodegeneration. While astrocytosis is associated with activated macrophages and microglia, the inflammatory marker CD68 did not differ between iNPH and REF. Dp71 is the major dystrophin subtype in the brain, connecting the cytoskeleton, cell membrane, and extracellular matrix dystrophin-related protein complex (DAPC) to anchor AQP4 and ion channels, with a preference for the lipid raft surrounding the astrocytes' terminal foot. It is required for adequate fluid transport between the cerebrovascular system, the interstitial fluid space, and astrocytes. AQP4 appears to be polarized toward the terminal foot of perivascular astrocytes in response to the components of the DAPC (Nicchia et al., 2008; Enger et al., 2012; Camassa et al., 2015). As Eide and Hansson (2018) previously established, dystrophin deficiency causes instability in the interface between the cytoskeleton and the mass membrane, impairing signal transduction. Experiments causing the loss or displacement of AQP4 or DAPC can result in aberrant brain water flux and disruption of intermediate metabolism, which can eventually result in the slow development of neurodegeneration (Nagelhus and Ottersen, 2013; Pavlin et al., 2017). Patients with iNPH who reacted to CSF fluid shunts had aberrant intracranial throbbing pressure, indicating impaired compliance. The primary histopathological findings were the proliferation of astrocytes and the subsequent drop of AQP4 and Dp71 at the astrocytes' perivascular terminal foot. According to Eide, alterations in the AQP4 and Dp71 complexes are related to sub-ischemia, often in tissue (Eide and Hansson, 2018).

Astrocytosis may contribute to the decreased intracranial compliance (pressure-volume reserve capacity) observed in patients with iNPH, as indicated by higher pulse wave intracranial pressure (Eide and Sorteberg, 2010, 2016; Eidsvaag et al., 2017). Mechanical resistance and hardness are known to be significantly increased by iNPH (Lu et al., 2011). Glia, including astrocytes, account for more than half of the total number of cells and brain volume in adults (Zhan et al., 2020). Fibrin (fibrinogen) has been shown to excite astrocytes and small astrocytes, implying that they may contribute to the progression of neurodegenerative changes and cognitive deficiencies (Figure 2) (Cortes-Canteli et al., 2010; Schachtrup et al., 2010; Merlini et al., 2019).

Effect of AQP4 on lymphatic system drainage disorder

In contrast to other types of hydrocephalus, the decrease in AQP4 in iNPH and Alzheimer's disease is related to the progressive loss of perivascular units responsible for water exchange (Reeves et al., 2020). This finding may indicate a different sort of hydrocephalus, which would account for the normal intracranial pressure and low AQP4 levels. Indeed, there may be no loss of brain parenchyma in traffic hypertension hydrocephalus but rather an accumulation of CSF due to constriction of the perivascular space (Blasco et al., 2014; Schmidt et al., 2016). As a result, as intracranial pressure increases, AQP4 levels may rise, first in the blood, then in the CSF (Castañeyra-Ruiz et al., 2013; Blasco et al., 2014). On the other hand, iNPH does not result in an increase in intracranial pressure despite the increasing buildup of amyloid beta, loss of brain parenchyma, and progressive lymphatic system dysfunction. Brain atrophy could be the cause. Hence, patients with iNPH may have low AQP4 concentrations in their CSF due to a lack of AQP4 expression and the loss of functional vascular units (Eide and Hansson, 2018, 2020; Arighi et al., 2019; Hasan-Olive et al., 2019a,b).

In rodents, AQP4 deficiency results in water build-up in the brain parenchyma (Haj-Yasein et al., 2011; Vindedal et al., 2016), decreased perivascular cerebrospinal and interstitial fluid circulation, and poor amyloid beta clearance (Iliff et al., 2012). These findings are equally perplexing as those regarding the blood–brain barrier, as AQP4 defective mice demonstrate normal blood–brain barrier integrity (Saadoun et al., 2009; Eilert-Olsen et al., 2012). As a result, a decrease in AQP4 surrounding blood vessels may directly affect the flow of fluid around blood vessels and the brain's steady state.

According to MRI studies, individuals with iNPH showed decreased lymphatic function, higher accumulation, and a reduced clearance rate for the intrauterine injectable contrast agent gadobutrol (Ringstad et al., 2017; Eide and Ringstad, 2019). MRI revealed reduced vascular side gaps and lymphatic circulation in patients with iNPH (Eide and Ringstad, 2019).

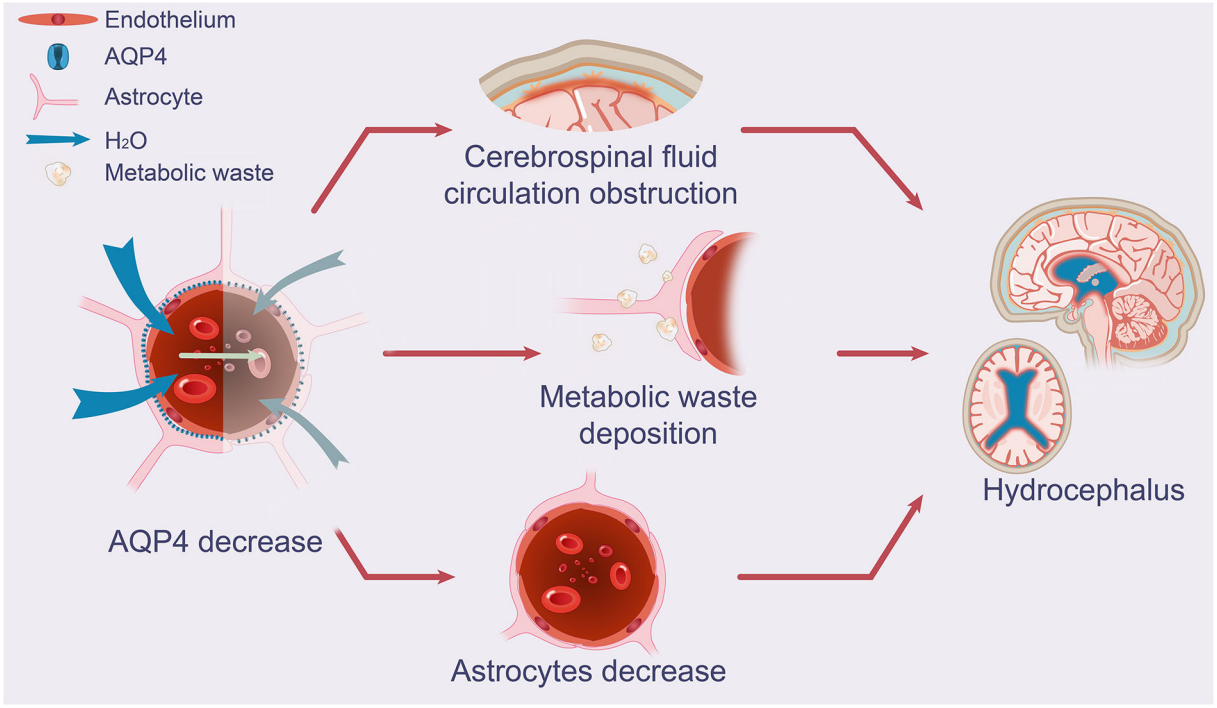

FIGURE 2
Effect of AQP4 on potential glymphatic dysfunction and growth of astrocytes in iNPH. The schematic drawing demonstrates decreases in AQP4 and its function in iNPH, which leads to diminished CSF periarterial inflow, CSF-ISF exchange, and perivenous outflow of CSF mediated by AQP4 depolarization, as seen in patients with iNPH. Increased concentrations of neuronal metabolic waste products in the brain interstitial space result from the decreased exchange of CSF and ISF. A decrease in AQP4 in the end-feet of astrocytes near arteries was substantially associated with astrocyte growth and CSF circulation obstruction. AQP4, aquaporin 4; iNPH, idiopathic normal pressure hydrocephalus; CSF, cerebrospinal fluid; ISF, interstitial fluid.

Gadobutrol circulates through the brain's large soft meningeal arteries. In individuals with iNPH, cerebral blood flow perfusion and brain metabolic levels were decreased (Eide and Stanisic, 2010; Calcagni et al., 2013; Ziegelitz et al., 2016).

Hasan-Olive et al. (2019b) confirmed for the first time that AQP4 expression in patients with iNPH dropped dramatically in astrocytic end-foot membranes facing capillary endothelial cells than in end-foot membranes facing neuropil. Reduced AQP4 around blood vessels may impair fluid and lymphatic circulation in the brains of patients with iNPH. Given the strategic location of the AQP4 water channel between the blood and the interstitial fluid, it is fair to assume that a CSF shunt will improve liquid flow through the AQP4 water channel. This increases the availability of nutrients and oxygen, as well as waste elimination, in the brains of patients with iNPH (Tan et al., 2021).

The expression and regulation mechanism of AQP4

Numerous studies have been conducted to elucidate the numerous endogenous mechanisms of AQP4 control, as well as the potential for pharmacological modulation. Four distinct regulation mechanisms have been extensively studied: microRNA (miRNA)-mediated regulation of gene expression, phosphorylation-mediated regulation of AQP4 channel gating/transport, heavy metal-ion-mediated regulation of water permeability, and small molecular inhibitor-mediated regulation of water permeability.

MiRNA targeting of AQP4 has become an area of research and development in AQP4 regulation (Gomes et al., 2018). The miRNA is an endogenous single-stranded RNA sequence obtained from most of its inclusions that function primarily in the degradation or inhibition of mRNA translation (Eide and Sorteberg, 2010, 2016). Recently, numerous studies have established a relationship between specific miRNAs and therapeutic AQP4s (miR-224/miR-19a, miR-29b, miRNA-145, miRNA-320a, miRNA-130a, and miRNA-130b).

Phosphorylation is an effective post-translational modification method. It can modulate protein function or expression by influencing protein structure, protein-protein interaction, and protein transport labels (Nesverova and Tornroth-Horsefield, 2019). Phosphorylation of AQP4 is required for its transport and subcellular localization and may be involved in channel gating (Kadohira et al., 2008; Nesverova and Tornroth-Horsefield, 2019). While the majority of recent research has been on S111, S180, and S276, there are still more putative phosphorylation sites, including S285,

S315, S316, S321, and S322, whose function is unknown (Lundby et al., 2012; Nesverova and Tornroth-Horsefield, 2019). However, tests in oocytes utilizing mutant rAQP4 protein showed that phosphorylation of the COOH terminal serine residues S315, S316, S321, and S322 did not affect transport or channel gating (Assentoft et al., 2014). The S315 phosphorylation location discovered in rats is not conserved in human AQP4 (Lundby et al., 2012) as serine is converted to glutamine. The effect of phosphorylation on AQP4 remains an intriguing area of research, with numerous processes and routes yet unknown.

The Kidins220–SNX27–retromer–AQP4 pathway was discovered as a regulatory mechanism for brain AQP4 expression and its participation in brain ventricular enlargement and hydrocephalus by Puerto et al. We detected an unexpected relationship between SNX27-retromer downregulation and AQP4 lysosomal degradation caused by the loss of Kidins220, as well as a dramatic drop in Kidins220 and AQP4 expression at the ependymal barrier in patients with iNPH (Del Puerto et al., 2021).

Mercury is at least one of the metals that regulates the majority of AQPs (Ximenes-da-Silva, 2016; Abir-Awan et al., 2019). It inhibits practically all AQPs except AQP6 and acts predominantly on AQPs (Yasui et al., 1999). Experiments with protein liposomes demonstrated that the Hg^{2+} binding site on AQP4 is located within the cell, which means that Hg^{2+} cannot reach its direct binding site on AQP4 in oocytes or most cell models and, thus, cannot regulate its activity (Yukutake et al., 2008; Yukutake and Yasui, 2010). On the other hand, the mercury ion can covalently attach to the C178 residue of the D ring of rAQP4's intracellular domain, exposing the Hg^{2+} binding site to the external solution and perhaps causing AQP4's conformational change (Yukutake et al., 2008; Ximenes-da-Silva, 2016). *In vivo*, however, the effect was not inhibition but a significant increase in AQP4 protein production, most seen in reactive astrocytes.

Additionally, zinc and copper were found to be inhibitors of rAQP4 in protein liposomes (Yukutake et al., 2009). Not all metal ions that affect AQP4 activity operate directly; some act indirectly by initiating phosphorylation pathways, leading to AQP4 expression or water permeability changes. These characteristics are shared by other materials such as lead (Gunnarson et al., 2005), manganese (Rao et al., 2010), and copper (Qing et al., 2009).

A small-molecule inhibitor is a compound that inhibits AQP4 without the need for metal ions. It is critical to identify small molecule AQP4 antagonists as AQP4 activity or expression is associated with various illnesses, and small molecule inhibitors can inhibit AQP4 without generating metal ion toxicity. Experimental verification tests have been performed on acetazolamide, validic acid, topiramate, ethoxzolamide, zonisamide, phenytoin, lamotrigine, and sumatriptan, among other drugs.

The methodological diversity is one of the most perplexing features of AQP4 regulation. Although *in vitro* techniques vary considerably, various miRNAs, heavy metal ions, and two small molecule inhibitors, acetazolamide and TGN-020, all demonstrate promise in regulating AQP4.

Conclusions

While the pathogenesis of iNPH remains a complicated subject, AQPs appear to be a feasible avenue for treatment. As AQP4 and AQP1, which have been studied for over a decade, are highly expressed in brain tissue and participate in the pathophysiological processes underlying related brain diseases, their critical role in maintaining the balance of brain tissue water in the nervous system and CSF circulation is undisputed. Numerous experimental studies have corroborated the pattern of increased AQP1 and decreased AQP4 protein expression in iNPH (Table 2).

AQP1, through its polar distribution, mainly plays a role in promoting CSF production, maintaining the balance of hydrocephalus, and participating in pathological processes. When CSF levels are elevated in iNPH, defective internal protective mechanisms permit AQP1 to continue to play a role in boosting generation, suggesting that we can govern linked brain illnesses by regulating AQP1. In the three levels of AQP1 regulation, the most effective control is the translation level of transcription adjustment and AQP1 itself. Transposing during the pathologic process complicates its management. Thus, in the future, we will require a more accurate understanding and in-depth investigations of the regulation mechanisms of AQP1 expression to develop a more effective method for AQP1 regulation. At the same time, the mechanisms causing changes in its polar distribution requires further investigation; the causes of abnormalities in AQP1-related protection mechanisms—the mechanism of iNPH occurrence—from a more comprehensive perspective are necessary for a deeper level understanding essential for the diagnosis and treatment.

AQP4 contributes to the development of many neurological illnesses through various biological effects, including an increase in the pace of blood-brain barrier clearance and a decrease in excess water storage in ventricles. AQP4 expression is increased in other types of hydrocephaly to drain extra CSF. However, its expression is frequently reduced in patients with iNPH, resulting in poor lymphatic circulation, waste clearance, and consequent neurodegeneration. As a result, AQP4 may be a critical therapeutic target in the treatment of neurological disorders, and with the advancement of research, the study of AQP4 gene polymorphisms and a range of neurological diseases is also advancing.

The role of AQPs in iNPH has gradually come to the attention of more researchers, with the majority of research focusing on AQP4 and AQP1, and the mechanisms of damage

TABLE 2 AQP1 and AQP4 in iNPH.

	AQP1	AQP4
Positional distribution in the nervous system	The top and outer parts of the vein epithelial cells	Plasma membrane, glial boundary membrane and ependyma of foot process of astrocytes around capillaries
Effects on cerebrospinal fluid circulation	The positional distribution of the top AQP1 facilitates cross-cell transport of water molecules during the development of cerebrospinal fluid	Accumulated cerebrospinal fluid be absorbed into the bloodstream through AQP4-dependent transcellular pathway
In the genetic knockout animal model	Cerebrospinal fluid production is reduced and intracranial pressure is reduced	The cerebrospinal fluid increases, intracranial pressure increases, and the permeability of water in brain tissue is greatly reduced
In iNPH patients	Abnormally elevated	Abnormally decreased
Mechanisms that act in brain tissue in iNPH patients	Mostly like other types of hydrocephalus, the polarity distribution of AQP1 is protected from extinction	Mostly unlike other types of hydrocephalus patients, may be blocked lymphatic circulation and hyperplication of glial cells
Expression and adjustment	Multi-level adjustment	MicroRNAs, phosphorylation, heavy metal ions, small molecule inhibitors

AQP1, aquaporin 1; AQP4, aquaporin 4.

in iNPH have been gradually revealed, although there is still a need for further exploration. Applications in the diagnosis and treatment of iNPH have also received an increasing amount of interest. However, as evidenced by recent studies, it appears to be impossible to detect AQP1 and AQP4 in CSF to serve as diagnostic markers. As far as enzyme-linked immunodetection assays are concerned, it appears that AQP1 and AQP4 will not enter CSF. Additional opportunities, such as targeted imaging enhancement, are also worth investigating. Following acetazolamide, the AQP4 activator EPO has emerged as a potential therapy option and has so far shown promising results in animal models. Despite the fact that AQP1 inhibitors have been cited in a few publications, there has been no advancement in their use at this time. In subsequent stages of this research, there are numerous points to consider as well. The distribution of AQP1 and AQP4 in the brain is not confined to a single location. While AQP4 was discovered in the CP, AQP1 was also discovered in capillary astrocytes. The issue remains of how to direct medications to the precise locations where they will be most beneficial. The usefulness of using AQPs in targeted treatments for neurological illnesses has been made more evident.

Author contributions

ZZ and JH collected the related manuscript. ZT, JH, YC, YW, CW, CT, and JL drafted and revised the manuscript. GX participated in the design of the review, helped to draft, and revised the manuscript. All authors read and approved the final manuscript.

Funding

This work was supported by National Natural Science Foundation of China (No. 82171347), Hunan Provincial Natural Science Foundation of China (No. 2019JJ50949), the Scientific Research Project of Hunan Provincial Health Commission of China (No. 202204040024), and the Students Innovations in Central South University of China (No. S2022105330687).

Acknowledgments

I would like to express my gratitude to all those who helped us during the writing of this manuscript and thanks to all the peer reviewers for their opinions and suggestions.

Conflict of interest

The authors declare that the research was conducted in the absence of any commercial or financial relationships that could be construed as a potential conflict of interest.

Publisher's note

References

Abir-Awan, M., Kitchen, P., Salman, M. M., Conner, M. T., Conner, A. C., and Bill, R. M. (2019). Inhibitors of mammalian aquaporin water channels. *Int. J. Mol. Sci.* 20. doi: 10.3390/ijms20071589

Angelucci, F., Cechová, K., and Pruša, R., Hort, J. (2019). Amyloid beta soluble forms and plasminogen activation system in alzheimer's disease: consequences on extracellular maturation of brain-derived neurotrophic factor and therapeutic implications. *CNS Neurosci. Ther.* 25, 303–313. doi: 10.1111/cns.13082

Arighi, A., Di Cristofori, A., Fenoglio, C., Borsa, S., D'Anca, M., Fumagalli, G. G., et al. (2019). Cerebrospinal fluid level of aquaporin4: a new window on glymphatic system involvement in neurodegenerative disease? *J. Alzheimers. Dis.* 69, 663–669. doi: 10.3233/JAD-190119

Assentoft, M., Larsen, B. R., Olesen, E. T. B., Fenton, R. A., and MacAulay, N. (2014). Aqp4 plasma membrane trafficking or channel gating is not significantly modulated by phosphorylation at cooh-terminal serine residues. *Am. J. Physiol,. Cell Physiol.* 307, C957–C965. doi: 10.1152/ajpcell.00182.2014

Benfenati, V., Caprini, M., Dovizio, M., Mylonakou, M. N., Ferroni, S., Ottersen, O. P., et al. (2011). An aquaporin-4/transient receptor potential vanilloid 4 (aqp4/trpv4) complex is essential for cell-volume control in astrocytes. *P. Natl. Acad. Sci. U. S. A.* 108, 2563–2568. doi: 10.1073/pnas.1012867108

Blasco, E., Martorell, J., De la Fuente, C., and Pumarola, M. (2014). Immunohistochemical study of aquaporins in an african grey parrot (psittacus erithacus) with hydrocephalus. *J. Avian Med. Surg.* 28, 309–315. doi: 10.1647/2013-059

Bloch, O., Auguste, K. I., Manley, G. T., and Verkman, A. S. (2006). Accelerated progression of kaolin-induced hydrocephalus in aquaporin-4-deficient mice. *J. Cereb. Blood Flow Metab.* 26, 1527–1537. doi: 10.1038/sj.jcbfm.9600306

Blocher, J., Eckert, I., Elster, J., Wiefek, J., Eiffert, H., and Schmidt, H. (2011). Aquaporins aqp1 and aqp4 in the cerebrospinal fluid of bacterial meningitis patients. *Neurosci. Lett.* 504, 23–27. doi: 10.1016/j.neulet.2011.08.049

Bothwell, S. W., Janigro, D., and Patabendige, A. (2019). Cerebrospinal fluid dynamics and intracranial pressure elevation in neurological diseases. *Fluids Barriers CNS* 16, 9. doi: 10.1186/s12987-019-0129-6

Bouley, R., Palomino, Z., Tang, S. S., Nunes, P., Kobori, H., Lu, H. A., et al. (2009). Angiotensin ii and hypertonicity modulate proximal tubular aquaporin 1 expression. *Am. J. Physiol. Renal Physiol.* 297, F1575–F1586. doi: 10.1152/ajprenal.90762.2008

Calcagni, M. L., Taralli, S., Mangiola, A., Indovina, L., Lavalle, M., De Bonis, P., et al. (2013). Regional cerebral metabolic rate of glucose evaluation and clinical assessment in patients with idiopathic normal-pressure hydrocephalus before and after ventricular shunt placement: a prospective analysis. *Clin. Nucl. Med.* 38, 426–431. doi: 10.1097/RLU.0b013e31828e949b

Camassa, L., Lunde, L. K., Hoddevik, E. H., Stensland, M., Boldt, H. B., De Souza, G. A., et al. (2015). Mechanisms underlying aqp4 accumulation in astrocyte endfeet. *Glia*. 63, 2073–2091. doi: 10.1002/glia.22878

Castañeyra-Ruiz, L., González-Marrero, I., Carmona-Calero, E. M., Abreu-Gonzalez, P., Lecuona, M., Brage, L., et al. (2016). Cerebrospinal fluid levels of tumor necrosis factor alpha and aquaporin 1 in patients with mild cognitive impairment and idiopathic normal pressure hydrocephalus. *Clin. Neurol. Neurosurg.* 146, 76–81. doi: 10.1016/j.clineuro.2016.04.025

Castañeyra-Ruiz, L., González-Marrero, I., González-Toledo, J. M., Castañeyra-Ruiz, A., de Paz-Carmona, H., Castañeyra-Perdomo, A., et al. (2013). Aquaporin-4 expression in the cerebrospinal fluid in congenital human hydrocephalus. *Fluids Barriers CNS* 10, 18. doi: 10.1186/2045-8118-10-18

Chaudhry, S. R., Stoffel-Wagner, B., Kinfe, T. M., Guresir, E., Vatter, H., Dietrich, D., et al. (2017). Elevated systemic il-6 levels in patients with aneurysmal subarachnoid hemorrhage is an unspecific marker for post-sah complications. *Int. J. Mol. Sci.* 18. doi: 10.3390/ijms18122580

Cortes-Canteli, M., Paul, J., Norris, E. H., Bronstein, R., Ahn, H. J., Zamolodchikov, D., et al. (2010). Fibrinogen and β-amyloid association alters thrombosis and fibrinolysis: a possible contributing factor to alzheimer's disease. *Neuron* 66, 695–709. doi: 10.1016/j.neuron.2010.05.014

de Arteaga, J., Ledesma, F., Garay, G., Chiurchiu, C., de la Fuente, J., Douthat, W., et al. (2011). High-dose steroid treatment increases free water transport in peritoneal dialysis patients. *Nephrol. Dial. Transplant.* 26, 4142–4145. doi: 10.1093/ndt/gfr533

de Laurentis, C., Cristaldi, P., Arighi, A., Cavandoli, C., Trezza, A., Sganzerla, E. P., et al. (2020). Role of aquaporins in hydrocephalus: what do we know and where do we stand? A systematic review. *J. Neurol.* 268, 4078–4094. doi: 10.1007/s00415-020-10122-z

Del Puerto, A., Pose-Utrilla, J., Simón-García, A., López-Menéndez, C., Jiménez, A. J., Porlan, E., et al. (2021). Kidins220 deficiency causes ventriculomegaly via snx27-retromer-dependent aqp4 degradation. *Mol. Psychiatr.* 26, 6411–6426. doi: 10.1038/s41380-021-01127-9

Ding, F. B., Yan, Y. M., Bao, C. R., Huang, J. B., Mei, J., Liu, H., et al. (2013). The role of aquaporin 1 activated by cgmp in myocardial edema caused by cardiopulmonary bypass in sheep. *Cell. Physiol. Biochem.* 32, 1320–1330. doi: 10.1159/000354530

Ding, Y., Zhang, T., Wu, G., McBride, D. W., Xu, N., Klebe, D. W., et al. (2019). Astrogliosis inhibition attenuates hydrocephalus by increasing cerebrospinal fluid reabsorption through the glymphatic system after germinal matrix hemorrhage. *Exp. Neurol.* 320, 113003. doi: 10.1016/j.expneurol.2019.113003

Eide, P. K., and Hansson, H. (2018). Astrogliosis and impaired aquaporin-4 and dystrophin systems in idiopathic normal pressure hydrocephalus. *Neuropath. Appl. Neuro.* 44, 474–490. doi: 10.1111/nan.12420

Eide, P. K., and Hansson, H. A. (2020). Blood-brain barrier leakage of blood proteins in idiopathic normal pressure hydrocephalus. *Brain Res.* 1727, 146547. doi: 10.1016/j.brainres.2019.146547

Eide, P. K., and Ringstad, G. (2019). Delayed clearance of cerebrospinal fluid tracer from entorhinal cortex in idiopathic normal pressure hydrocephalus: a glymphatic magnetic resonance imaging study. *J. Cereb. Blood Flow Metab.* 39, 1355–1368. doi: 10.1177/0271678X18760974

Eide, P. K., and Sorteberg, W. (2010). Diagnostic intracranial pressure monitoring and surgical management in idiopathic normal pressure hydrocephalus: a 6-year review of 214 patients. *Neurosurgery.* 66, 80–91. doi: 10.1227/01.NEU.0000363408.69856.B8

Eide, P. K., and Sorteberg, W. (2016). Outcome of surgery for idiopathic normal pressure hydrocephalus: role of preoperative static and pulsatile intracranial pressure. *World Neurosurg.* 86, 186–193. doi: 10.1016/j.wneu.2015.09.067

Eide, P. K., and Stanisic, M. (2010). Cerebral microdialysis and intracranial pressure monitoring in patients with idiopathic normal-pressure hydrocephalus: association with clinical response to extended lumbar drainage and shunt surgery. *J. Neurosurg.* 112, 414–424. doi: 10.3171/2009.5.JNS09122

Eidsvaag, V. A., Hansson, H., Heuser, K., Nagelhus, E. A., and Eide, P. K. (2017). Brain capillary ultrastructure in idiopathic normal pressure hydrocephalus: relationship with static and pulsatile intracranial pressure. *J. Neuropath. Exp. Neur.* 76, 1034–1045. doi: 10.1093/jnen/nlx091

Eilert-Olsen, M., Haj-Yasein, N. N., Vindedal, G. F., Enger, R., Gundersen, G. A., Hoddevik, E. H., et al. (2012). Deletion of aquaporin-4 changes the perivascular glial protein scaffold without disrupting the brain endothelial barrier. *Glia* 60, 432–440. doi: 10.1002/glia.22277

Enger, R., Gundersen, G. A., Haj-Yasein, N. N., Eilert-Olsen, M., Thoren, A. E., Vindedal, G. F., et al. (2012). Molecular scaffolds underpinning macroglial polarization: an analysis of retinal muller cells and brain astrocytes in mouse. *Glia* 60, 2018–2026. doi: 10.1002/glia.22416

Gomes, A., Da, S. I., Rodrigues, C., Castro, R. E., and Soveral, G. (2018). The emerging role of micrornas in aquaporin regulation. *Front Chem.* 6, 238. doi: 10.3389/fchem.2018.00238

Gunnarson, E., Axehult, G., Baturina, G., Zelenin, S., Zelenina, M., and Aperia, A. (2005). Lead induces increased water permeability in astrocytes expressing aquaporin 4. *Neuroscience* 136, 105–114. doi: 10.1016/j.neuroscience.2005.07.027

Haj-Yasein, N. N., Vindedal, G. F., Eilert-Olsen, M., Gundersen, G. A., Skare, O., Laake, P., et al. (2011). Glial-conditional deletion of aquaporin-4 (aqp4) reduces blood-brain water uptake and confers barrier function on perivascular astrocyte endfeet. *Proc. Natl. Acad. Sci. U. S. A.* 108, 17815–17820. doi: 10.1073/pnas.1110655108

Hara-Chikuma, M., and Verkman, A. S. (2008a). Prevention of skin tumorigenesis and impairment of epidermal cell proliferation by targeted aquaporin-3 gene disruption. *Mol. Cell. Biol.* 28, 326–332. doi: 10.1128/MCB.01482-07

Hara-Chikuma, M., and Verkman, A. S. (2008b). Aquaporin-3 facilitates epidermal cell migration and proliferation during wound healing. *J. Mol. Med.* 86, 221–231. doi: 10.1007/s00109-007-0272-4

Hasan-Olive, M. M., Enger, R., Hansson, H. A., Nagelhus, E. A., and Eide, P. K. (2019a). Pathological mitochondria in neurons and perivascular astrocytic endfeet of idiopathic normal pressure hydrocephalus patients. *Fluids Barriers CNS* 16, 39. doi: 10.1186/s12987-019-0160-7

Hasan-Olive, M. M., Enger, R., Hansson, H. A., Nagelhus, E. A., and Eide, P. K. (2019b). Loss of perivascular aquaporin-4 in idiopathic normal pressure hydrocephalus. *Glia* 67, 91–100. doi: 10.1002/glia.23528

Hiraldo-González, L., Trillo-Contreras, J. L., García-Miranda, P., Pineda-Sánchez, R., Ramírez-Lorca, R., Rodrigo-Herrero, S., et al. (2021). Evaluation of aquaporins in the cerebrospinal fluid in patients with idiopathic normal pressure hydrocephalus. *PLoS ONE* 16, e258165. doi: 10.1371/journal.pone.0258165

Hodler, J., Kubik-Huch, R. A., and von Schulthess, G. K. (2020). *Diseases of the Brain, Head and Neck, Spine 2020-2023: Diagnostic Imaging*. Cham: Springer International Publishing AG. doi: 10.1007/978-3-030-38490-6

Iliff, J. J., Goldman, S. A., and Nedergaard, M. (2015). Implications of the discovery of brain lymphatic pathways. *Lancet Neurol.* 14, 977–979. doi: 10.1016/S1474-4422(15)00221-5

Iliff, J. J., Lee, H., Yu, M., Feng, T., Logan, J., Nedergaard, M., et al. (2013). Brain-wide pathway for waste clearance captured by contrast-enhanced mri. *J. Clin. Invest*. 123, 1299–1309. doi: 10.1172/JCI67677

Iliff, J. J., Wang, M., Liao, Y., Plogg, B. A., Peng, W., Gundersen, G. A., et al. (2012). A paravascular pathway facilitates csf flow through the brain parenchyma and the clearance of interstitial solutes, including amyloid beta. *Sci. Transl. Med.* 4, 111r−147r. doi: 10.1126/scitranslmed.3003748

Ismail, M., Bokaee, S., Morgan, R., Davies, J., Harrington, K. J., and Pandha, H. (2009). Inhibition of the aquaporin 3 water channel increases the sensitivity of prostate cancer cells to cryotherapy. *Br. J. Cancer* 100, 1889–1895. doi: 10.1038/sj.bjc.6605093

Jeon, T., Park, K., Park, S., Hwang, J., and Hwang, S. K. (2017). Expression of aquaporin 1 and 4 in the choroid plexus and brain parenchyma of kaolin-induced hydrocephalic rats. *Korean J. Neurotrauma* 13, 68–75. doi: 10.13004/kjnt.2017.13.2.68

Kadohira, I., Abe, Y., Nuriya, M., Sano, K., Tsuji, S., Arimitsu, T., et al. (2008). Phosphorylation in the c-terminal domain of aquaporin-4 is required for golgi transition in primary cultured astrocytes. *Biochem. Biophys. Res. Commun*. 377, 463–468. doi: 10.1016/j.bbrc.2008.09.155

Kajimoto, Y., Kameda, M., Kambara, A., Kuroda, K., Tsuji, S., Nikaido, Y., et al. (2022). Impact of early intervention for idiopathic normal pressure hydrocephalus on long-term prognosis in prodromal phase. *Front. Neurol*. 13, 866352. doi: 10.3389/fneur.2022.866352

Kim, J. H., Lee, Y. W., Park, K. A., Lee, W. T., and Lee, J. E. (2010). Agmatine attenuates brain edema through reducing the expression of aquaporin-1 after cerebral ischemia. *J. Cereb. Blood Flow Metab*. 30, 943–949. doi: 10.1038/jcbfm.2009.260

Kobayashi, H., Yokoo, H., Yanagita, T., Satoh, S., Kis, B., Deli, M., et al. (2006). Induction of aquaporin 1 by dexamethasone in lipid rafts in immortalized brain microvascular endothelial cells. *Brain Res.* 1123, 12–19. doi: 10.1016/j.brainres.2006.09.066

Kusayama, M., Wada, K., Nagata, M., Ishimoto, S., Takahashi, H., Yoneda, M., et al. (2011). Critical role of aquaporin 3 on growth of human esophageal and oral squamous cell carcinoma. *Cancer Sci*. 102, 1128–1136. doi: 10.1111/j.1349-7006.2011.01927.x

Leinonen, V., Kuulasmaa, T., and Hiltunen, M. (2021). Inph-the mystery resolving. *EMBO Mol. Med.* 13, e13720. doi: 10.15252/emmm.202013720

Li, D., Liu, X., Liu, T., Liu, H., Tong, L., Jia, S., et al. (2020). Neurochemical regulation of the expression and function of glial fibrillary acidic protein in astrocytes. *Glia* 68, 878–897. doi: 10.1002/glia.23734

Lolansen, S. D., Rostgaard, N., Oernbo, E. K., Juhler, M., Simonsen, A. H., and MacAulay, N. (2021). Inflammatory markers in cerebrospinal fluid from patients with hydrocephalus: a systematic literature review. *Dis. Markers* 2021, 8834822. doi: 10.1155/2021/8834822

Lu, Y., Iandiev, I., Hollborn, M., Körber, N., Ulbricht, E., Hirrlinger, P. G., et al. (2011). Reactive glial cells: increased stiffness correlates with increased intermediate filament expression. *FASEB J.* 25, 624–631. doi: 10.1096/fj.10-163790

Lundby, A., Secher, A., Lage, K., Nordsborg, N. B., Dmytriyev, A., Lundby, C., et al. (2012). Quantitative maps of protein phosphorylation sites across 14 different rat organs and tissues. *Nat. Commun.* 3, 876. doi: 10.1038/ncomms1871

Malm, J., Jacobsson, J., Birgander, R., and Eklund, A. (2011). Reference values for csf outflow resistance and intracranial pressure in healthy elderly. *Neurology* 76, 903–909. doi: 10.1212/WNL.0b013e31820f2dd0

Mao, X., Enno, T. L., and Del, B. M. (2006). Aquaporin 4 changes in rat brain with severe hydrocephalus. *Eur. J. Neurosci.* 23, 2929–2936. doi: 10.1111/j.1460-9568.2006.04829.x

McCoy, E., and Sontheimer, H. (2010). Mapk induces aqp1 expression in astrocytes following injury. *Glia* 58, 209–217. doi: 10.1002/glia.20916

Merlini, M., Rafalski, V. A., Rios Coronado, P. E., Gill, T. M., Ellisman, M., Muthukumar, G., et al. (2019). Fibrinogen induces microglia-mediated spine elimination and cognitive impairment in an alzheimer's disease model. *Neuron* 101, 1099–1108. doi: 10.1016/j.neuron.2019.01.014

Mola, M. G., Sparaneo, A., Gargano, C. D., Spray, D. C., Svelto, M., Frigeri, A., et al. (2016). The speed of swelling kinetics modulates cell volume regulation and calcium signaling in astrocytes: a different point of view on the role of aquaporins. *Glia* 64, 139–154. doi: 10.1002/glia.22921

Moon, C., King, L. S., and Agre, P. (1997). Aqp1 expression in erythroleukemia cells: genetic regulation of glucocorticoid and chemical induction. *Am. J. Physiol.* 273, C1562–C1570. doi: 10.1152/ajpcell.1997.273.5.C1562

Nagelhus, E. A., and Ottersen, O. P. (2013). Physiological roles of aquaporin-4 in brain. *Physiol. Rev.* 93, 1543–1562. doi: 10.1152/physrev.00011.2013

Nakada, T., and Kwee, I. L. (2019). Fluid dynamics inside the brain barrier: current concept of interstitial flow, glymphatic flow, and cerebrospinal fluid circulation in the brain. *Neuroscientist* 25, 155–166. doi: 10.1177/1073858418775027

Nakajima, M., Kawamura, K., Akiba, C., Sakamoto, K., Xu, H., Kamohara, C., et al. (2021). Differentiating comorbidities and predicting prognosis in idiopathic normal pressure hydrocephalus using cerebrospinal fluid biomarkers: a review. *Croat. Med. J.* 62, 387–398. doi: 10.3325/cmj.2021.62.387

Nesverova, V., and Tornroth-Horsefield, S. (2019). Phosphorylation-dependent regulation of mammalian aquaporins. *Cells* 8, 82. doi: 10.3390/cells8020082

Nicchia, G. P., Rossi, A., Nudel, U., Svelto, M., and Frigeri, A. (2008). Dystrophin-dependent and -independent aqp4 pools are expressed in the mouse brain. *Glia* 56, 869–876. doi: 10.1002/glia.20661

Oshio, K., Watanabe, H., Song, Y., Verkman, A. S., and Manley, G. T. (2005). Reduced cerebrospinal fluid production and intracranial pressure in mice lacking choroid plexus water channel aquaporin-1. *FASEB J.* 19, 76–78. doi: 10.1096/fj.04-1711fje

Owler, B. K., Pitham, T., and Wang, D. (2010). Aquaporins: relevance to cerebrospinal fluid physiology and therapeutic potential in hydrocephalus. *Cerebrospinal Fluid Res.* 7, 15. doi: 10.1186/1743-8454-7-15

Papadopoulos, M. C., and Verkman, A. S. (2007). Aquaporin-4 and brain edema. *Pediatr. Nephrol.* 22, 778–784. doi: 10.1007/s00467-006-0411-0

Papadopoulos, M. C., and Verkman, A. S. (2013). Aquaporin water channels in the nervous system. *Nat. Rev. Neurosci.* 14, 265–277. doi: 10.1038/nrn3468

Paul, L., Madan, M., Rammling, M., Chigurupati, S., Chan, S. L., and Pattisapu, J. V. (2011). Expression of aquaporin 1 and 4 in a congenital hydrocephalus rat model. *Neurosurgery* 68, 462–473. doi: 10.1227/NEU.0b013e3182011860

Pavlin, T., Nagelhus, E. A., Brekken, C., Eyjolfsson, E. M., Thoren, A., Haraldseth, O., et al. (2017). Loss or mislocalization of aquaporin-4 affects diffusion properties and intermediary metabolism in gray matter of mice. *Neurochem. Res.* 42, 77–91. doi: 10.1007/s11064-016-2139-y

Petković, F., Campbell, I. L., Gonzalez, B., and Castellano, B. (2017). Reduced cuprizone-induced cerebellar demyelination in mice with astrocyte-targeted production of il-6 is associated with chronically activated, but less responsive microglia. *J. Neuroimmunol.* 310, 97–102. doi: 10.1016/j.jneuroim.2017.07.003

Qing, W. G., Dong, Y. Q., Ping, T. Q., Lai, L. G., Fang, L. D., Min, H. W., et al. (2009). Brain edema after intracerebral hemorrhage in rats: the role of iron overload and aquaporin 4. *J. Neurosurg.* 110, 462–468. doi: 10.3171/2008.4.JNS17512

Qvarlander, S., Ambarki, K., Wåhlin, A., Jacobsson, J., Birgander, R., Malm, J., et al. (2017). Cerebrospinal fluid and blood flow patterns in idiopathic normal pressure hydrocephalus. *Acta Neurol. Scand.* 135, 576–584. doi: 10.1111/ane.12636

Raneri, F., Zella, M. A. S., Di Cristofori, A., Zarino, B., Pluderi, M., and Spagnoli, D. (2017). Supplementary tests in idiopathic normal pressure hydrocephalus: a single-center experience with a combined lumbar infusion test and tap test. *World Neurosurg.* 100, 567–574. doi: 10.1016/j.wneu.2017.01.003

Rao, K. V. R., Jayakumar, A. R., Reddy, P. V. B., Tong, X., Curtis, K. M., and Norenberg, M. D. (2010). Aquaporin-4 in manganese-treated cultured astrocytes. *Glia* 58, 1490–1499. doi: 10.1002/glia.21023

Rasmussen, M. K., Mestre, H., and Nedergaard, M. (2018). The glymphatic pathway in neurological disorders. *Lancet Neurol.* 17, 1016–1024. doi: 10.1016/S1474-4422(18)30318-1

Reeves, B. C., Karimy, J. K., Kundishora, A. J., Mestre, H., Cerci, H. M., Matouk, C., et al. (2020). Glymphatic system impairment in alzheimer's disease and idiopathic normal pressure hydrocephalus. *Trends Mol. Med.* 26, 285–295. doi: 10.1016/j.molmed.2019.11.008

Ringstad, G., Vatnehol, S., and Eide, P. K. (2017). Glymphatic mri in idiopathic normal pressure hydrocephalus. *Brain* 140, 2691–2705. doi: 10.1093/brain/awx191

Rizwan Siddiqui, M., Attar, F., Mohanty, V., Kim, K. S., Shekhar Mayanil, C., and Tomita, T. (2018). Erythropoietin-mediated activation of aquaporin-4 channel for the treatment of experimental hydrocephalus. *Childs Nervous Syst. ChNS* 34, 2195–2202. doi: 10.1007/s00381-018-3865-z

Saadoun, S., Tait, M. J., Reza, A., Davies, D. C., Bell, B. A., Verkman, A. S., et al. (2009). Aqp4 gene deletion in mice does not alter blood-brain barrier integrity or brain morphology. *Neuroscience* 161, 764–772. doi: 10.1016/j.neuroscience.2009.03.069

Sakurada, T., Kuboshima, S., Ogimoto, G., Fujino, T., Sato, T., Maeba, T., et al. (2004). Aquaporin-1 is recruited to the plasma membrane by hyperosmotic stimuli via a protein kinase a-dependent pathway in rat peritoneal mesothelial cells. *Adv. Perit. Dial.* 20, 37–42.

Schachtrup, C., Ryu, J. K., Helmrick, M. J., Vagena, E., Galanakis, D. K., Degen, J. L., et al. (2010). Fibrinogen triggers astrocyte scar formation by promoting the availability of active tgf-beta after vascular damage. *J. Neurosci.* 30, 5843–5854. doi: 10.1523/JNEUROSCI.0137-10.2010

Schmidt, M. J., Rummel, C., Hauer, J., Kolecka, M., Ondreka, N., McClure, V., et al. (2016). Increased csf aquaporin-4, and interleukin-6 levels in dogs with idiopathic communicating internal hydrocephalus and a decrease after ventriculo-peritoneal shunting. *Fluids Barriers CNS* 13, 12. doi: 10.1186/s12987-016-0034-1

Shen, X. Q., Miyajima, M., Ogino, I., and Arai, H. (2006). Expression of the water-channel protein aquaporin 4 in the h-tx rat: possible compensatory role in spontaneously arrested hydrocephalus. *J. Neurosurg* 105, 459–464. doi: 10.3171/ped.2006.105.6.459

Smith, Z. A., Moftakhar, P., Malkasian, D., Xiong, Z., Vinters, H. V., and Lazareff, J. A. (2007). Choroid plexus hyperplasia: surgical treatment and immunohistochemical results. *Case Rep*. 107, 255–262. doi: 10.3171/PED-07/09/255

Sosvorova, L., Mohapl, M., Vcelak, J., Hill, M., Vitku, J., and Hampl, R. (2015). The impact of selected cytokines in the follow-up of normal pressure hydrocephalus. *Physiol. Res.* 64, S283–S290. doi: 10.33549/physiolres.933069

Stoenoiu, M. S., Ni, J., Verkaeren, C., Debaix, H., Jonas, J. C., Lameire, N., et al. (2003). Corticosteroids induce expression of aquaporin-1 and increase transcellular water transport in rat peritoneum. *J. Am. Soc. Nephrol.* 14, 555–565. doi: 10.1097/01.ASN.0000053420.37216.9E

Stokum, J. A., Kwon, M. S., Woo, S. K., Tsymbalyuk, O., Vennekens, R., Gerzanich, V., et al. (2018). Sur1-trpm4 and aqp4 form a heteromultimeric complex that amplifies ion/water osmotic coupling and drives astrocyte swelling. *Glia* 66, 108–125. doi: 10.1002/glia.23231

Tan, C., Wang, X., Wang, Y., Wang, C., Tang, Z., Zhang, Z., et al. (2021). The pathogenesis based on the glymphatic system, diagnosis, and treatment of idiopathic normal pressure hydrocephalus. *Clin. Interv. Aging* 16, 139–153. doi: 10.2147/CIA.S290709

Thavarajasingam, S. G., El-Khatib, M., Vemulapalli, K. V., Iradukunda, H. A. S., Laleye, J., Russo, S., et al. (2022). Cerebrospinal fluid and venous biomarkers of shunt-responsive idiopathic normal pressure hydrocephalus: a systematic review and meta-analysis. *Acta Neurochir.* 164, 1719–1746. doi: 10.1007/s00701-022-05154-5

Tie, L., Lu, N., Pan, X. Y., Pan, Y., An, Y., Gao, J. W., et al. (2012). Hypoxia-induced up-regulation of aquaporin-1 protein in prostate cancer cells in a p38-dependent manner. *Cell. Physiol. Biochem.* 29, 269–280. doi: 10.1159/000337608

Tietz, P. S., McNiven, M. A., Splinter, P. L., Huang, B. Q., and Larusso, N. F. (2006). Cytoskeletal and motor proteins facilitate trafficking of aqp1-containing vesicles in cholangiocytes. *Biol. Cell.* 98, 43–52. doi: 10.1042/BC20040089

Tomas-Camardiel, M., Venero, J. L., Herrera, A. J., De Pablos, R. M., Pintor-Toro, J. A., Machado, A., et al. (2005). Blood-brain barrier disruption highly induces aquaporin-4 mrna and protein in perivascular and parenchymal astrocytes: protective effect by estradiol treatment in ovariectomized animals. *J. Neurosci. Res.* 80, 235–246. doi: 10.1002/jnr.20443

Tourdias, T., Dragonu, I., Fushimi, Y., Deloire, M. S., Boiziau, C., Brochet, B., et al. (2009). Aquaporin 4 correlates with apparent diffusion coefficient and hydrocephalus severity in the rat brain: a combined mri-histological study. *Neuroimage* 47, 659–666. doi: 10.1016/j.neuroimage.2009.04.070

Verkman, A. S. (2008a). Mammalian aquaporins: diverse physiological roles and potential clinical significance. *Expert Rev. Mol. Med.* 10, e13. doi: 10.1017/S1462399408000690

Verkman, A. S. (2008b). A cautionary note on cosmetics containing ingredients that increase aquaporin-3 expression. *Exp. Dermatol.* 17, 871–872. doi: 10.1111/j.1600-0625.2008.00698.x

Vindedal, G. F., Thoren, A. E., Jensen, V., Klungland, A., Zhang, Y., Holtzman, M. J., et al. (2016). Removal of aquaporin-4 from glial and ependymal membranes causes brain water accumulation. *Mol. Cell. Neurosci.* 77, 47–52. doi: 10.1016/j.mcn.2016.10.004

Wang, C., Wang, X., Tan, C., Wang, Y., Tang, Z., Zhang, Z., et al. (2021). Novel therapeutics for hydrocephalus: insights from animal models. *CNS Neurosci. Ther.* 27, 1012–1022. doi: 10.1111/cns.13695

Wang, D., Nykanen, M., Yang, N., Winlaw, D., North, K., Verkman, A. S., et al. (2011). Altered cellular localization of aquaporin-1 in experimental hydrocephalus in mice and reduced ventriculomegaly in aquaporin-1 deficiency. *Mol. Cell. Neurosci.* 46, 318–324. doi: 10.1016/j.mcn.2010.10.003

Wang, X., Li, T., Liu, Y., Jia, S., Liu, X., Jiang, Y., et al. (2021). Aquaporin 4 differentially modulates osmotic effects on vasopressin neurons in rat supraoptic nucleus. *Acta physiologica* 232, e13672. doi: 10.1111/apha.13672

Wang, Y., Chen, R., Wa, Y., Ding, S., Yang, Y., Liao, J., et al. (2022). Tumor immune microenvironment and immunotherapy in brain metastasis from non-small cell lung cancer. *Front. Immunol.* 13, 829451. doi: 10.3389/fimmu.2022.829451

Wang, Y., and Hatton, G. I. (2009). Astrocytic plasticity and patterned oxytocin neuronal activity: dynamic interactions. *J. Neurosci.* 29, 1743–1754. doi: 10.1523/JNEUROSCI.4669-08.2009

Wang, Y., Wang, X., Tan, C., Wang, C., Tang, Z., Zhang, Z., et al. (2021). Hydrocephalus after aneurysmal subarachnoid hemorrhage: epidemiology, pathogenesis, diagnosis, and management. *Signa Vitae* 17, 4–17. doi: 10.22514/sv.2021.021

Wang, Z., Zhang, Y., Hu, F., Ding, J., and Wang, X. (2020). Pathogenesis and pathophysiology of idiopathic normal pressure hydrocephalus. *CNS Neurosci. Ther.* 26, 1230–1240. doi: 10.1111/cns.13526

Ximenes-da-Silva, A. (2016). Metal ion toxins and brain aquaporin-4 expression: an overview. *Front. Neurosci.* 10, 233. doi: 10.3389/fnins.2016.00233

Yasui, M., Hazama, A., Kwon, T. H., Nielsen, S., Guggino, W. B., and Agre, P. (1999). Rapid gating and anion permeability of an intracellular aquaporin. *Nature.* 402, 184–187. doi: 10.1038/46045

Yin, L. K., Zheng, J. J., Zhao, L., Hao, X. Z., Zhang, X. X., Tian, J. Q., et al. (2017). Reversed aqueductal cerebrospinal fluid net flow in idiopathic normal pressure hydrocephalus. *Acta Neurol. Scand.* 136, 434–439. doi: 10.1111/ane.12750

Yukutake, Y., Hirano, Y., Suematsu, M., and Yasui, M. (2009). Rapid and reversible inhibition of aquaporin-4 by zinc. *Biochemistry* 48, 12059–12061. doi: 10.1021/bi901762y

Yukutake, Y., Tsuji, S., Hirano, Y., Adachi, T., Takahashi, T., Fujihara, K., et al. (2008). Mercury chloride decreases the water permeability of aquaporin-4-reconstituted proteoliposomes. *Biol. Cell* 100, 355–363. doi: 10.1042/BC20070132

Yukutake, Y., and Yasui, M. (2010). Regulation of water permeability through aquaporin-4. *Neuroscience* 168, 885–891. doi: 10.1016/j.neuroscience.2009.10.029

Zelenina, M. (2010). Regulation of brain aquaporins. *Neurochem. Int.* 57, 468–488. doi: 10.1016/j.neuint.2010.03.022

Zhan, C., Xiao, G., Zhang, X., Chen, X., Zhang, Z., and Liu, J. (2020). Decreased mir-30a promotes tgf-beta1-mediated arachnoid fibrosis in post-hemorrhagic hydrocephalus. *Transl. Neurosci.* 11, 60–74. doi: 10.1515/tnsci-2020-0010

Zhang, J., Xiong, Y., Lu, L. X., Wang, H., Zhang, Y. F., Fang, F., et al. (2013). Aqp1 expression alterations affect morphology and water transport in schwann cells and hypoxia-induced up-regulation of aqp1 occurs in a hif-1alpha-dependent manner. *Neuroscience* 252, 68–79. doi: 10.1016/j.neuroscience.2013.08.006

Zhang, W., Zitron, E., Homme, M., Kihm, L., Morath, C., Scherer, D., et al. (2007). Aquaporin-1 channel function is positively regulated by protein kinase c. *J. Biol. Chem.* 282, 20933–20940. doi: 10.1074/jbc.M703858200

Zhou, J., Kong, H., Hua, X., Xiao, M., Ding, J., and Hu, G. (2008). Altered blood-brain barrier integrity in adult aquaporin-4 knockout mice. *Neuroreport* 19, 1–5. doi: 10.1097/WNR.0b013e3282f2b4eb

Ziegelitz, D., Arvidsson, J., Hellstrom, P., Tullberg, M., Wikkelso, C., and Starck, G. (2016). Pre-and postoperative cerebral blood flow changes in patients with idiopathic normal pressure hydrocephalus measured by computed tomography (ct)-perfusion. *J. Cereb. Blood Flow Metab.* 36, 1755–1766. doi: 10.1177/0271678X15608521

frontiers | Frontiers in Molecular Neuroscience

TYPE Review
PUBLISHED 26 September 2022
DOI 10.3389/fnmol.2022.932955

OPEN ACCESS

EDITED BY
Vegard Vinje,
Simula Research Laboratory, Norway

REVIEWED BY
Edward Haig Beamer,
Nottingham Trent University,
United Kingdom
Chandler L. Walker,
Indiana University–Purdue University
Indianapolis (IUPUI), United States

*CORRESPONDENCE
Qinghua Zhang
doctorzhanghua@163.com
Gelei Xiao
xiaogelei@csu.edu.cn

†These authors have contributed equally to this work

SPECIALTY SECTION
This article was submitted to Brain Disease Mechanisms, a section of the journal Frontiers in Molecular Neuroscience

RECEIVED 30 April 2022
ACCEPTED 06 September 2022
PUBLISHED 26 September 2022

CITATION
Yang Y, Wang C, Chen R, Wang Y, Tan C, Liu J, Zhang Q and Xiao G (2022) Novel therapeutic modulators of astrocytes for hydrocephalus. *Front. Mol. Neurosci.* 15:932955. doi: 10.3389/fnmol.2022.932955

Novel therapeutic modulators of astrocytes for hydrocephalus

Yijian Yang[1,2,3,4†], Chuansen Wang[2,3,4†], Rui Chen[1†], Yuchang Wang[2,3,4], Changwu Tan[2,3,4], Jingping Liu[2,3,4], Qinghua Zhang[5,6*] and Gelei Xiao[2,3,4*]

[1]Department of Neurosurgery, Affiliated Nanhua Hospital, Hengyang Medical School, University of South China, Hengyang, China, [2]Department of Neurosurgery, Xiangya Hospital, Central South University, Changsha, China, [3]Diagnosis and Treatment Center for Hydrocephalus, Xiangya Hospital, Central South University, Changsha, China, [4]National Clinical Research Center for Geriatric Disorders, Xiangya Hospital, Central South University, Changsha, China, [5]Department of Neurosurgery, Huazhong University of Science and Technology Union Shenzhen Hospital, Shenzhen, China, [6]The 6th Affiliated Hospital of Shenzhen University Health Science Center, Shenzhen, China

Hydrocephalus is mainly characterized by excessive production or impaired absorption of cerebrospinal fluid that causes ventricular dilation and intracranial hypertension. Astrocytes are the key response cells to inflammation in the central nervous system. In hydrocephalus, astrocytes are activated and show dual characteristics depending on the period of development of the disease. They can suppress the disease in the early stage and may aggravate it in the late stage. More evidence suggests that therapeutics targeting astrocytes may be promising for hydrocephalus. In this review, based on previous studies, we summarize different forms of hydrocephalus-induced astrocyte reactivity and the corresponding function of these responses in hydrocephalus. We also discuss the therapeutic effects of astrocyte regulation on hydrocephalus in experimental studies.

KEYWORDS

astrocytes, hydrocephalus, cerebrospinal fluid, pathogenesis, neuroinflammation

Highlights

- Astrocytes are understudied in hydrocephalus but plays an essential role in the condition.
- Their specific pathologic contributions and targeting astrocytes as a therapy for hydrocephalus are summarized for the first time.

Introduction

Hydrocephalus is a cerebrospinal fluid (CSF) functional disorder that causes ventricular dilation and intracranial hypertension (sometimes, it may not be associated with it). Hydrocephalus is commonly caused by craniocerebral trauma, intracranial space-occupying lesions, or intracranial infection. Periventricular gliosis, including

astrocytes, microglia hypertrophy, and hyperplasia, has been reported in human and animal models of hydrocephalus (Del Bigio, 2001; Deren et al., 2010; Eskandari et al., 2011; Zhan et al., 2020); this suggests that gliosis is a significant neuropathological feature of hydrocephalus. Changes in glial cells, especially astrocytes, may play an essential role in the pathogenesis of hydrocephalus.

Astrocytes are the most widely distributed type of cells in the mammalian brain and the most numerous type of glial cells (Zhou et al., 2019). They play an important role in various physiological activities, such as maintaining ion homeostasis and participating in cerebrospinal fluid circulation (Volterra et al., 2014; Plog and Nedergaard, 2018; Lafrenaye and Simard, 2019). They can regulate their own metabolic activities and control the synthesis and reuptake of neurotransmitters and neurotrophic factors through the transduction of various receptors and signaling pathways (Pekny and Pekna, 2014; Li-Na et al., 2017; Durkee and Araque, 2019). Moreover, their ability to regulate inflammatory cytokines and free radical release play an important role in the pathological process of central nervous system (CNS) diseases (Sofroniew, 2015; González-Reyes et al., 2017; Cabezas et al., 2019). Research showed extensive gliosis in communicating hydrocephalus, which is related to the pro-inflammatory role of astrocytes (Xu et al., 2012b; Xu et al., 2015). Reactive astrocyte proliferation is a repair and healing response to brain tissue injury, mainly manifested as fibrous astrocyte proliferation, which eventually becomes a glial scar with strong positive staining for glial fibrillary acidic protein (GFAP). Moreover, the CNS responds to different injury situations by causing different changes in astrocytes, suggesting that astrocytes are important response cells in CNS injury. Therefore, targeting astrocytes for the treatment of hydrocephalus may show some promise.

In this manuscript, based on prior experimental studies, we first described the morphological characteristics of astrocytes under physiological conditions and their changes in hydrocephalus. We then focused on the astrocyte responses to hydrocephalus and the consecutive functions of these responses in hydrocephalus development. They finally briefly discussed the therapeutic effects of regulating astrocytes on hydrocephalus in animal model studies.

Astrocytes in the central nervous system

Astrocytes are distributed throughout the CNS and are involved in structural support, blood–brain barrier (BBB) formation, extracellular environment maintenance, anti-oxidative stress, and many other activities (Pekny and Nilsson, 2005). Astrocytes give off many long, branching processes from the cell body, which extend and fill the space between the cell body and its processes. Astrocytes can be divided into two types: fibrous astrocytes and protoplasmic astrocytes (Borggrewe et al., 2021). Fibrous astrocytes are mostly distributed in the cortex of the spinal cord with elongated protrusions and few branches. Protoplasmic astrocytes are mainly distributed in gray matter, with stubby cell projections and many branches (Miller and Raff, 1984).

The ends of the protuberance are often enlarged to form the end feet and attach to the adjacent capillary wall or the inferior membrane of the ependyma. Three-dimensional electron microscopy reconstruction of the endings of vessels in the rat hippocampus revealed that the end feet interdigitated without leaving any slits between them (Mathiisen et al., 2010). Astrocytes have extensive gap junctions composed mainly of connexins (CXs). These gap junctions are enriched in the endfeet of astrocytes, which enwrap the blood vessels' walls and provide a perivascular route (Liu and Chopp, 2016). Small molecules can pass through gap junctions and participate in cell-to-cell communication.

The mitochondria in endfeet differ markedly in size and shape. The 3D reconstructions found two main types of mitochondria: small/ovoid and elongated (Mathiisen et al., 2010). Others show very complex shapes. Different mitochondria intertwine and form large bundles that fit tightly into the endfoot membranes around the blood vessels.

Astrocytes are the key response cells in CNS injuries since they respond to inflammatory stimuli by releasing pro-inflammatory molecules. Therefore, they are greatly involved in the development of hydrocephalus. They are associated with neuroinflammation by producing various pro-inflammatory molecules (Cekanaviciute et al., 2014b; Pekny and Pekna, 2014). They are also involved in fluid regulation because over-expressing aquaporin 4 (AQP4) can regulate cell swelling or reduce volume (Petzold et al., 2006). Besides, they can provide antioxidant protection by secreting neurotrophic factors and antioxidants (Sofroniew, 2015).

The above briefly describes the main functions of astrocytes, which are closely related to the pathogenesis of hydrocephalus and are the focus of our research and will be described in detail below.

Abnormal astrocytes in hydrocephalus

In hydrocephalus, factors such as hypoxia promote the activation of astrocytes. In patients with hydrocephalus, the astrocytes show significant edema and phagocytic activity (Castejon, 1994; Castejón, 2010). Furthermore, active astrocytes express more intermediate filament proteins, including glial fibrillary acidic protein (GFAP), vimentin, nestin, and many other altered molecules (Petzold et al., 2006; Liu and Chopp, 2016; Eide and Hansson, 2018). Reactive astrocytes were

mainly found in periventricular white matter and cortical gray matter (Del Bigio, 2010). Activated astrocytes can recruit other astrocytes to migrate to the site, forming a glial scar (Pekny and Nilsson, 2005). The number of reactive astrocytes may be reduced after shunt, but they cannot return to normal conditions for a long time (Eskandari et al., 2011). Therefore, surgical treatment cannot completely reverse the reaction even in the long term (**Figure 1**).

Interestingly, neuroinflammation-induced reactive astrocytes exhibit the property of secreting neurotoxins that promote the death of neurons and oligodendrocytes (Liddelow et al., 2017). In contrast, ischemia-induced reactive astrocytes increased neurotrophic factor expression and exhibited more neuroprotective properties (Zamanian et al., 2012).

The functional role of the glial scar is also controversial. On the one hand, it can secrete molecules such as chondroitin sulfate proteoglycans that inhibit axon regeneration (McKeon et al., 1991). On the other hand, it acts as a barrier to prevent the spread of inflammatory cells and factors into healthy tissue (Burda et al., 2016). Loss of proliferating astrocytes leads to significantly increased levels of amyloid-β, indicating that reactive astrocytes are involved in the clearance of amyloid peptides (Katsouri et al., 2020).

Endoependymal exfoliation in hyh mutant mice caused adjacent astrocytic proliferation. These astrocytes expressed specific glial markers and formed a layer of surface cells to replace the lost ependyma (Roales-Buján et al., 2012). Reactive astrocytes on the removed ependymal surface showed a small but significant increase in AQP4 compared with the ependymal of wild-type mice (Roales-Buján et al., 2012). This may be an adaptive change in response to ependymal damage. Whether this change is due to the direct effect of ependymal damage

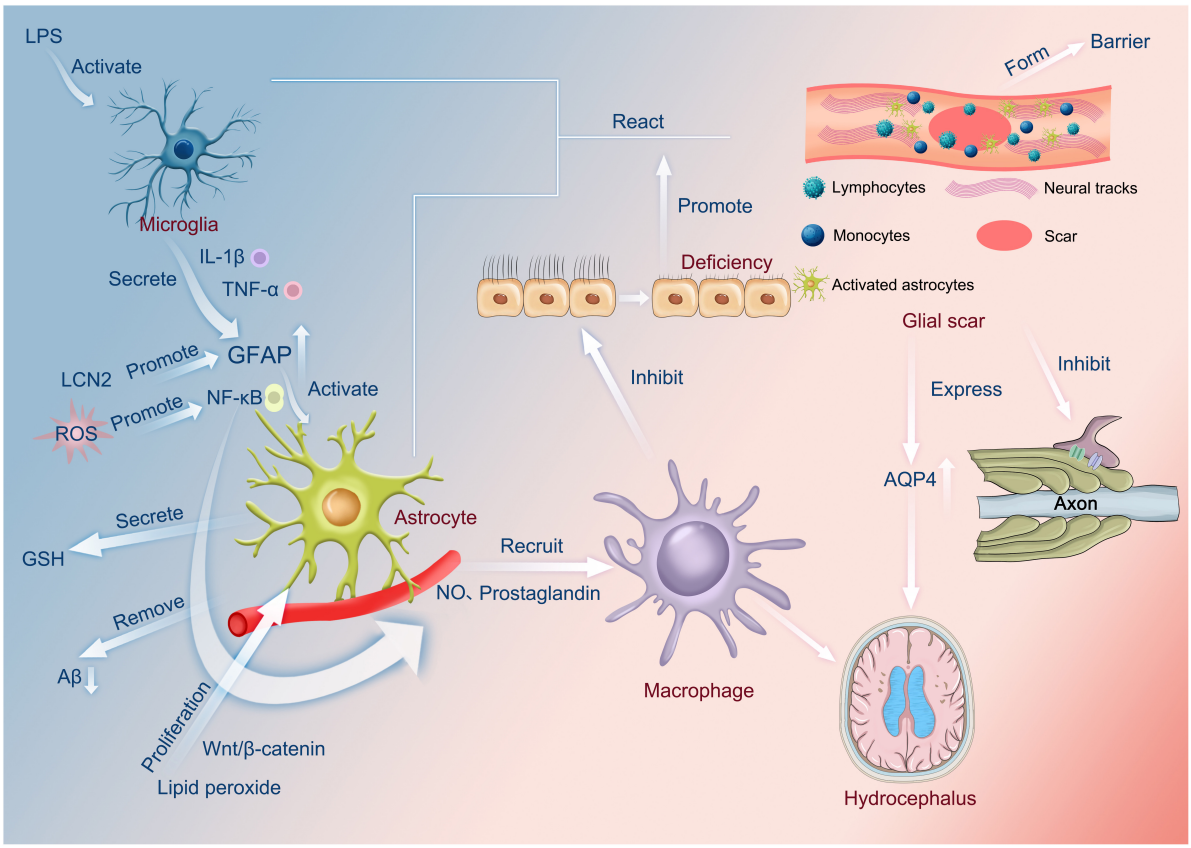

FIGURE 1
Functions of astrocytes. LPS activates microglia to secrete cytokines, such as IL-1β and TNF-α, which increase the amount of GFAP. In addition, LCN2 also promotes the increase in GFAP. The increased GFAP activates astrocytes *via* NF-κB, which, in turn, recruits macrophages through the release of nitric oxide or prostaglandins. Lipid peroxide can also affect macrophages *via* Wnt/β-catenin in this process, and reactive oxygen species can also influence the production of nitric oxide and prostaglandin by promoting NF-κB and then affecting macrophages. Macrophages can inhibit normal cilia, and cilia abnormalities can occur, encouraging the interaction of microglia and astrocytes and the appearance of glial scars. On the one hand, this can produce a barrier. On the other hand, it can inhibit axonal neurotransmission and, most importantly, contribute to the overexpression of AQP4, causing hydrocephalus. In addition, astrocytes have the function of secreting glutathione and scavenging amyloid. LPS, Lipopolysaccharide; IL-1β, Interleukin-1β; TNF-α, Tumor necrosis factor-α; GFAP, glial fibrillary acidic protein; LCN2, Lipoprotein 2; ROS, Reactive oxygen species; GSH, glutathione; Aβ, amyloid protein; NO, nitric oxide; AQP4, aquaporin 4.

or the mechanical compression of hydrocephalus needs to be studied.

Electron microscopy was used to analyze cerebral cortex slices from 30 idiopathic normal pressure hydrocephalus (iNPH) patients. The results showed that the number of normal mitochondria decreased significantly in the astrocytic endfeet of iNPH patients compared to normal individuals, accompanied by a significant increase in the number of pathological mitochondria (Hasan-Olive et al., 2019a). These changes were obviously related to the degree of astrogliosis. This indicates an energy metabolism disorder in the astrocytes of patients with iNPH (Wang et al., 2020). Also, pathological mitochondria were significantly and negatively correlated with the perivascular expression of AQP4 and dystrophin-71 (Hasan-Olive et al., 2019a).

Astrocytes regulate neuroinflammation in hydrocephalus

Many neurological diseases, including hydrocephalus, are associated with neuroinflammation, but the exact mechanisms are not fully understood. In the CNS, astrocytes play a major role in inflammation (Sun et al., 2021). In animal models, significant inflammatory responses have been demonstrated in all stages of hydrocephalus, in which reactive astrocytes may play a central role (Lopes Lda et al., 2009; Deren et al., 2010; Olopade et al., 2012). After intraperitoneal injection of lipopolysaccharide (LPS), the expression of pro-inflammatory cytokines in microglia was found to peak 2–4 h after injection, but the peak of pro-inflammatory cytokine expression in astrocytes occurred 12–24 h after injection (Norden et al., 2016). This might indicate that microglia are involved in activating astrocytes by secreting pro-inflammatory factors in the inflammatory response of the CNS. Astrocytes can be activated by various pro-inflammatory mediators, such as IL-1β (John et al., 2004). Microglia are the main source of IL-1β, mainly expressed in astrocytes and perivascular macrophages 4 weeks after hydrocephalus induction (Olopade et al., 2019). At the same time, astrocytes can produce a variety of pro-inflammatory molecules, such as prostaglandins and nitric oxide (NO), to amplify neuroinflammation (Sofroniew, 2015; Michinaga and Koyama, 2019).

Astrocyte signaling pathways appear to be regulated by common downstream transcriptional regulators during inflammation (Linnerbauer et al., 2020). Nuclear factor-κB (NF-κB) is greatly involved in the response of astrocytes to inflammatory stimuli and other injuries. NF-κB is a major regulator of cell survival, differentiation, and proliferation, as well as innate and adaptive immunity. The NF-κB signal of astrocytes can be directly activated by various pro-inflammatory factors such as TNF-α, IL-1β, and TLR signals (Kawai and Akira, 2007; Shih et al., 2015). Activation of NF-κB in astrocytes induces the expression of pro-inflammatory mediators, leading to the recruitment of macrophages, thereby inhibiting ependymal cilia formation and, ultimately, hydrocephalus formation (Lattke et al., 2012). However, in this study, activation of NF-κB caused hydrocephalus only in the developing brain and did not show significant lateral ventricular dilation in mature rats. However, NF-κB may promote hydrocephalus through mechanisms other than inhibiting ependymal cilia formation, such as promoting the secretion of other pro-inflammatory factors.

A study has shown that neuroinflammation is found in ventricular dilation in rats with hydrocephalus and suggests that it is involved in the upregulation of IL-1β secreted by astrocytes in the early stages of the disease (Olopade et al., 2019). In this study, IL-1β was significantly increased at weeks 1 and 4, followed by downregulation at week eight, which seems to be consistent with the clinical characteristics of posthemorrhagic hydrocephalus in premature infants (Schmitz et al., 2007). It suggests that neuroinflammation in the later stage of hydrocephalus is relieved. In some disease models, astrocytes secrete transforming growth factor-β to reduce disease-associated inflammatory responses (Cekanaviciute et al., 2014a,b). However, transforming growth factor-β is closely related to subarachnoid fibrosis in the development of hydrocephalus (Cherian et al., 2004; Zhan et al., 2020; Wang et al., 2021). In subarachnoid hemorrhage, the body responds to the injury by releasing various factors through many different pathways to activate astrocytes, which, in turn, repair the BBB.

Lipoprotein 2 (LCN2) is an iron-carrier binding protein that plays a role in endogenous iron chelation. It is an acute-phase protein expressed by astrocytes after ischemic stroke, cerebral hemorrhage, and neuroinflammation (Dong et al., 2013; Ni et al., 2015). It is reported that LCN2 knock-out mice injected with hemoglobin showed less ventricular dilation and fewer activated astrocytes and amoeba microglia compared with control mice (Shishido et al., 2016). Another recent study has demonstrated that LCN2 deficiency reduces neuroinflammation by reducing glial and microglial cell activation in a model of systemic inflammation (Jin et al., 2014). Previous studies have also shown that LCN2 increases glial fibrillary acid protein (GFAP) expression and promotes activation of astrocytes and microglia (Xing et al., 2014).

Astrocytes regulate abnormal expression of aquaporins in hydrocephalus

Aquaporins (AQPs) are non-selective bidirectional channel proteins that allow water to diffuse passively and thus allow

net fluxes of water driven by concentration gradients. There are three main types of AQPs in the CNS: AQP1, AQP4, and AQP9 (Potokar et al., 2016). AQP4 is mainly located in the endfeet of astrocytes, with a severalfold higher density of the membrane domains facing capillaries than membranes facing the neuropil (Nielsen et al., 1997). This polarization depends on the α-syntrophin, an intracellular component of the dystroglycan complex (Neely et al., 2001). This spatial distribution may be beneficial in improving the efficiency of CSF-interstitial fluid exchange. Astrocytes overexpressing AQP4 have a greater ability to regulate cell swelling or reduce volume (Lisjak et al., 2017). Also, basal brain water content was increased in mice with a complete loss of AQP4 water channels (Vindedal et al., 2016). These suggest that AQP4 in astrocytes may be involved in fluid regulation in the brain. AQP4 may also be involved in astrocyte migration. The leading edge of AQP4 expression was increased in migrating astrocytes, and the ability of AQP4-null migration was significantly reduced compared to wild-type astrocytes (Saadoun et al., 2005). Inhibition of glial scarring was also observed in AQP4-null mice, which may be related to the inhibition of astrocyte migration by AQP4 reduction (Auguste et al., 2007).

Moreover, AQP4 may be involved in the regulation of inflammation. Astrocyte cultures from wild-type mice released more tumor necrosis factor-α (TNF-α) and interleukin-6 (IL-6) than those from AQP4-null mice. In animal models, lipopolysaccharide (LPS)-treated AQP4-inactivated mice also showed a smaller inflammatory response (Li et al., 2011). It is also reported that deletion of AQP4 is associated with a distinct inflammatory response of the retina (Pannicke et al., 2010). Thus, AQP4 may play different roles in the regulation of inflammation under different pathological conditions.

The expression of AQP4 by the endfeet of astrocytes changes dynamically in hydrocephalus. In kaolin-induced hydrocephalus rats, the abundance of AQP4 in the periventricular area and cortex was significantly decreased on day two after treatment with kaolin on day one but increased significantly after week 2 (Skjolding et al., 2010). On the other hand, Mao et al. investigated the effect of obstructive hydrocephalus on the expression of AQP4 in rats and found that the mRNA levels of the AQP4 channel were changed (Mao et al., 2006). But surprisingly, this was not accompanied by an increase in protein levels. The most likely explanation is that a major redistribution of AQP4 occurs in hydrocephalus rather than an increase in overall abundance. This redistribution may be a protective mechanism against the accumulation of CSF.

Normally, AQP4 is expressed primarily in the terminal foot of astrocytes. However, in the case of hydrocephalus, this polarization may change. Immunogold cytochemical analysis of AQP4 in cortical brain biopsies from 30 iNPH patients and 12 reference individuals showed that AQP4 density was reduced in astrocytic endfoot membranes along cortical microvessels of the iNPH brain compared to the control group (Hasan-Olive et al., 2019b). As β-dystroglycan-immunopositivity in brain vessels coincides with the reactive glial reaction; this depolarization may be due to the activation of astrocytes (Szabó and Kálmán, 2008; Kálmán et al., 2011). This may indicate an obstruction of perivascular CSF-interstitial fluid circulation.

Interestingly, the expression profile of AQP4 in rat brain tissue seems to differ from that in human tissue. In human hydrocephalus samples, AQP4 fluorescence signals were present throughout the astrocyte membrane. In rats with hydrocephalus, the fluorescence signal of AQP4 was strongly polarized to the perivascular foot of astrocytes (Skjolding et al., 2013). One possible explanation is that this may be due to diseases having different characteristics in different species. Therefore, AQP4 depolarization occurs in the mouse model of iNPH (Kress et al., 2014). Moreover, because progressive AQP4 depolarization occurs throughout the physiological aging process of mice, further age-matched human studies are needed to determine whether the AQP4 pathological depolarization is a characteristic response of iNPH rather than a feature of aging (Kress et al., 2014).

Overexpression of AQP4 in CSF may also be present in patients with congenital hydrocephalus. CSF samples were collected from the lateral ventricles of 13 full-term t infants. Western-blot analysis showed that AQP4 expression was higher in traffic hydrocephalus than in the control group but was not significant in obstructive hydrocephalus (Castañeyra-Ruiz et al., 2013). This AQP4 movement may be a consequence of ependyma denudation. Loss of communication between ependymal cells leads to ependymal dissection and entry of AQP4 into the CSF. The ependymal deletion was accompanied by microglia and astrocyte reactions. Subependymal astrocytes proliferate to form a glial scar covering the ventricle surface, and the replacement of the ependymal reduces the chance of AQP4 entering CSF (Páez et al., 2007; Roales-Buján et al., 2012).

Astrocytes regulate oxidative stress in hydrocephalus

As the brain consumes more energy than any other organ in the body, it produces large amounts of free radicals, such as reactive oxygen species (ROS) or reactive nitrogen. However, oxidative damage can occur when the production of free radicals outstrips the brain's ability to clear them. Although the role of oxidative stress in hydrocephalus has not been clearly understood, more studies suggest that oxidative stress may be one of the causes of hydrocephalus (Socci et al., 1999; Li et al., 2014; Guzelcicek et al., 2020). Oxidative stress produces large amounts of ROS and lipid peroxidation products, which may cause great damage to proteins, lipids, and DNA. ROS have also been found to be involved in crosstalk with NF-κB

signaling, which links neuroinflammation to oxidative stress (Morgan and Liu, 2011). Lipid peroxidation products may also induce reactive astrocyte proliferation in hydrocephalus by activating the Wnt/β-catenin pathway (Xu et al., 2015; Suryaningtyas et al., 2020). Wnt/β-catenin signaling also plays an important anti-inflammatory and pro-inflammatory role. The regulation of the NF-κB pathway may be involved in this effect (Ma and Hottiger, 2016).

There is also evidence that the overproduction of NO may be involved in the pathological process of hydrocephalus (Del Bigio et al., 2012). In the CNS, NO is mainly produced by neuronal NO synthase, inducible NO synthase produced by activated microglia, and endothelial NO synthase (Barnham et al., 2004). Although NO can alleviate hypoxia by dilating blood vessels, NO may also be oxidized into peroxynitrite ONOO, causing serious damage to cells. Furthermore, the increase of ROS during neuroinflammation may lead to the activation of NF-κB, which, in turn, induces the overexpression of NO synthase in astrocytes and microglia, especially inducible NO synthase, leading to the production of superoxide (González-Reyes et al., 2017).

A sustained increase in ventricular volume was observed in rat pups reared under chronic sublethal hypoxia (Ment et al., 1998). Nerve cell-specific hypoxia-inducible factor-1α deficient mice showed severe hydrocephalus with memory loss (Tomita et al., 2003), suggesting that hypoxia may contribute to the development of hydrocephalus. Cortical compression caused by ventricular enlargement may cause local tissue ischemia and hypoxia, producing free radicals. The detection of hypoxia and free radical production markers in hydrocephalus rats also suggests that hypoxia mechanisms play a role in hydrocephalus brain injury (Del Bigio et al., 2012). However, no upregulation of antioxidant enzymes was detected in this model. The protective effect of antioxidant enzymes in hydrocephalus after hypoxia seems negligible. However, there was an increased vascular endothelial growth factor (VEGF) immune response in reactive astrocytes (Del Bigio et al., 2012). Increased expression of VEGF has also been reported in CSF of posthemorrhagic hydrocephalus in premature infants (Ballabh et al., 2007). Thus, VEGF-induced angiogenesis may be an alternative mechanism for hypoxic tissue protection. VEGF has been proposed as a treatment for hypoxia. However, in animal models, injections of VEGF have been shown to cause ventricular enlargement (Harrigan et al., 2002; Shim et al., 2013).

In the case of brain injury, astrocytes provide antioxidant protection, such as the secretion of neurotrophic factors, antioxidants, and so on (Cabezas et al., 2019). Astrocytes contain high concentrations of antioxidants such as glutathione(GSH), which can remove excess ROS (Dringen, 2000). There is also evidence that astrocytes release glutathione precursors, which neurons use for glutathione synthesis (Dringen et al., 1999). IL-1β may stimulate the production of GSH in astrocytes through a process dependent on NF-κB, thereby enhancing the antioxidant capacity of tissues (He et al., 2015). When GSH depletion occurs, astrocytes and neurons are affected, with the latter being greatly influenced (González-Reyes et al., 2017). This neurotoxicity reflects the antioxidant dependence of neurons on astrocytes.

In iNPH, Aβ deposition appears in the cerebral cortex (Tan et al., 2021). Recent studies on astrocytes have shown that astrocytes can also secrete Aβ (Frost and Li, 2017; Sanchez-Mico et al., 2021). Increases in pro-inflammatory cytokines seem to gradually lead to significant increases in post-translational levels of amyloid precursor protein and secreted Aβ (Zhao et al., 2011). This suggests that the persistent presence of inflammatory mediators may lead to dysfunction in astrocyte metabolism and production of Aβ, thereby aggravating oxidative stress (**Figure 2**).

Therapeutic targeting of astrocytes for the treatment of hydrocephalus

At present, the mainstay of hydrocephalus treatment is surgery, and the research on non-surgical treatment has not achieved good results (Del Bigio and Di Curzio, 2016). Astrocytes can be involved in the pathological process of hydrocephalus in various ways, but there are still few studies targeting astrocytes. Current studies on astrocytes have mainly focused on the regulation of astrocyte-mediated neuroinflammation, abnormal expression of water channels, and oxidative stress.

Astrocyte-mediated neuroinflammation plays a role in the development of hydrocephalus, and some anti-inflammatory drugs seem to have a certain therapeutic effect. Minocycline is the second-generation tetracyclines. Minocycline is a highly lipophilic compound that can easily penetrate the BBB (Yong et al., 2004). Minocycline as a neuroprotective agent has been widely studied (Garrido-Mesa et al., 2013). Minocycline is reported to inhibit reactive gliosis and ventricular dilation in rat models of hydrocephalus (Xu et al., 2012a; Guo et al., 2015; Gu et al., 2019) and may provide additional benefits when used as a supplement for the ventricular shunt. However, considering that the studies on minocycline mainly focus on its inhibition of microglia activation and thus inhibit inflammation and other responses (Garrido-Mesa et al., 2013), the inhibitory effect of minocycline on reactive astrocytes in hydrocephalus might be caused by the regulation of expression of the pro-inflammatory factor of microglia.

Increasing AQP4 expression to accelerate CSF clearance appears to slow the development of hydrocephalus. Erythropoietin (EPO) treatment upregulated AQP4 expression and reduced ventricular dilation in kaolin-induced rat models of obstructive hydrocephalus (Rizwan Siddiqui et al., 2018;

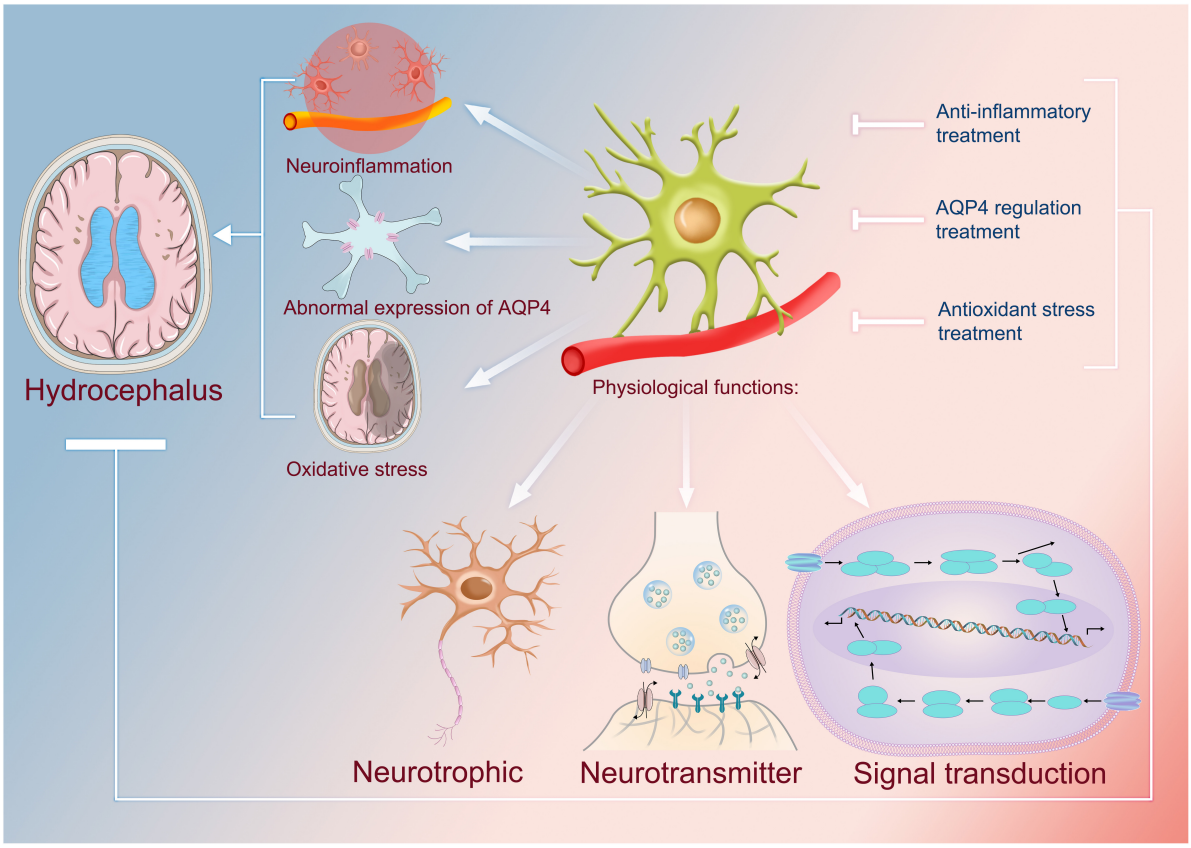

FIGURE 2
Physiological functions of astrocytes and their uses as targets in the treatment of hydrocephalus. The physiological functions of astrocytes include neurotrophic, neurotransmitter, and cellular signal transduction. It has been found that abnormal astrocytes are closely associated with the formation of hydrocephalus, and for some of the mechanisms identified so far, they can be involved in the development of neuroinflammation; therefore, anti-inflammatory therapies that use astrocytes as targets can be one of the means by which we treat hydrocephalus. Astrocytes are capable of causing abnormal overexpression of AQP4, which in turn leads to excessive accumulation of cerebrospinal fluid and causes hydrocephalus. Therefore, using astrocytes as a target to regulate the expression of AQP4 can also regulate the production of cerebrospinal fluid, which in turn can be used to treat hydrocephalus. In addition, astrocytes are also associated with oxidation, which contributes to hydrocephalus. Thus, it is safe to say that antioxidant therapy associated with them may be an effective treatment. AQP4, aquaporin 4.

Suryaningtyas et al., 2019). EPO might decrease the expression of miR-130a and increase the expression of miR-668 (Rizwan Siddiqui et al., 2018). Upregulation of AQP4 may be a way to accelerate CSF clearance to treat hydrocephalus. However, maintaining AQP4 polarization in the endfeet of astrocytes may also be as therapeutic as simply increasing the abundance of AQP4.

The duality of astrocytes in oxidative stress makes them a good target for regulating the oxidative stress response. Edaravone is an excellent antioxidant that inhibits the production of free radicals, thereby preventing cell death caused by oxidative stress (Wang et al., 2011; Kikuchi et al., 2017). It is reported that treatment with edaravone for 14 days after hydrocephalus induction can reduce the activity of astrocytes on the corpus callosum and germinal matrix (Garcia et al., 2017). However, the dose of the drug used did not show antioxidant ability. There is also evidence that edaravone can inhibit the development of hydrocephalus by activating the Nrf2/HO-1 signaling pathway to protect ependymal cilia and neurons from oxidative stress damage (Zhang et al., 2018). Some natural extracts with antioxidant properties have conflicting therapeutic benefits (Catalão et al., 2014; Sampaio et al., 2019). Interestingly, the oral antioxidant mixture α-tocopherol, L-ascorbic acid, coenzyme Q10, reduced glutathione, and reduced lipoic acid showed no therapeutic benefits for juvenile rats with kaolin-induced hydrocephalus (Di Curzio et al., 2014). Further, there was no evidence in this study suggesting that the antioxidant treatment reduced the astrocyte response. This may be due to lower peak levels of oral therapy than after parenteral administration. In other studies, hydrocephalic young rats treated with hyperbaric oxygen therapy performed better on behavioral tests than untreated rats, although there was no

significant effect on ventricular dilation (da Silva et al., 2018). Silva et al. suggested that hyperbaric oxygen therapy may promote functional recovery of the CNS by inhibiting the activation of astrocytes and forming an extensive fibrillar network, in addition to its own antioxidant stress effect (da Silva et al., 2018; **Supplementary Table 1**).

In addition to the known therapeutic measures mentioned above, based on the analytical elaboration of the role of astrocytes above, we can use this as a target to consider the choice of therapeutic measures in future studies. For example, developing drugs to act on astrocytes to clear neuroinflammation, targeting astrocyte AQP4 expression to address cerebrospinal fluid problems, and using certain antioxidants to clear free radicals may be possible. These could be the focus of research into new measures for the astrocyte-based treatment of hydrocephalus.

Conclusion

Astrocytes play a key role in maintaining the normal function of the CNS. Astrocytes maintain the normal metabolism of the brain, regulate synaptic transmission and plasticity, and prevent neurons from producing toxic compounds. Recent studies have shown that the response of astrocytes in hydrocephalus is twofold and depends on its appearance period and specific signaling mechanisms. In the early stage of hydrocephalus, astrocytes can inhibit the spread of inflammation, show adaptive changes to the accumulation of CSF to enhance absorption, and release antioxidant substances to fight oxidative stress. However, as the disease progresses, reactive astrocytes release inflammatory mediators and promote oxidative stress. The abnormal expression of AQPs is also gradually harmful. Therefore, reactive astrocytes may be a potential target of therapeutic strategies for hydrocephalus. Despite that, the dual role of astrocytes complicates the study of their therapeutic effects. Stimulating glial activity in the early stages may yield good results. Notwithstanding, this activation in the late stages may worsen the disease. Therefore, grasping the right time window is the key to achieving its optimal effects.

Although we have searched for new astrocyte-based treatments for hydrocephalus and explored new approaches based on existing measures, we still do not know anything about the molecular mechanisms behind them, which may limit our thinking and thus require us to study them in depth.

In conclusion, we have discovered the important role of astrocytes in three aspects: participation in neuroinflammation, regulation of water molecule proteins, and antioxidation, which are also factors in the pathogenesis of hydrocephalus; thus, astrocytes can be used as targets for us to investigate new methods of drug treatment for hydrocephalus, and as a result, numerous highly effective drugs can be developed.

Author contributions

YJY, CSW, and RC collected the related manuscript.YJY, RC, YCW, CWT, CSW, and JPL drafted and revised the manuscript. QHZ and GLX participated in the review design and helped draft and revise the manuscript. All authors have read and approved the final manuscript.

Funding

This work was supported by the National Natural Science Foundation of China (No. 82171347), Shenzhen Municipal Science and Technology Innovation Commission (No. Z2021N059), Hunan Provincial Natural Science Foundation of China (No. 2022JJ30971), the Scientific Research Project of Hunan Provincial Health Commission of China (No. 202204040024), and the Students Innovations in Central South University of China (Nos. 20210033020055, 20210033020036, 20210033020044, and 2022105330190).

Acknowledgments

We would like to express my gratitude to all those who helped us while writing this manuscript. We are equally grateful to all the peer reviewers for their opinions and suggestions.

Conflict of interest

The authors declare that the research was conducted in the absence of any commercial or financial relationships that could be construed as a potential conflict of interest.

Publisher's note

Supplementary material

The Supplementary Material for this article can be found online at: https://www.frontiersin.org/articles/10.3389/fnmol.2022.932955/full#supplementary-material

References

Auguste, K. I., Jin, S., Uchida, K., Yan, D., Manley, G. T., Papadopoulos, M. C., et al. (2007). Greatly impaired migration of implanted aquaporin-4-deficient astroglial cells in mouse brain toward a site of injury. *FASEB J.* 21, 108–116. doi: 10.1096/fj.06-6848com

Ballabh, P., Xu, H., Hu, F., Braun, A., Smith, K., Rivera, A., et al. (2007). Angiogenic inhibition reduces germinal matrix hemorrhage. *Nat. Med.* 13, 477–485. doi: 10.1038/nm1558

Barnham, K. J., Masters, C. L., and Bush, A. I. (2004). Neurodegenerative diseases and oxidative stress. *Nat. Rev. Drug. Discov.* 3, 205–214. doi: 10.1038/nrd1330

Borggrewe, M., Grit, C., Vainchtein, I. D., Brouwer, N., Wesseling, E. M., Laman, J. D., et al. (2021). Regionally diverse astrocyte subtypes and their heterogeneous response to EAE. *Glia* 69, 1140–1154. doi: 10.1002/glia.23954

Burda, J. E., Bernstein, A. M., and Sofroniew, M. V. (2016). Astrocyte roles in traumatic brain injury. *Exp. Neurol.* 275(Pt 3), 305–315. doi: 10.1016/j.expneurol.2015.03.020

Cabezas, R., Baez-Jurado, E., Hidalgo-Lanussa, O., Echeverria, V., Ashrad, G. M., Sahebkar, A., et al. (2019). Growth factors and neuroglobin in astrocyte protection against neurodegeneration and oxidative stress. *Mol. Neurobiol.* 56, 2339–2351. doi: 10.1007/s12035-018-1203-9

Castañeyra-Ruiz, L., González-Marrero, I., González-Toledo, J. M., Castañeyra-Ruiz, A., de Paz-Carmona, H., Castañeyra-Perdomo, A., et al. (2013). Aquaporin-4 expression in the cerebrospinal fluid in congenital human hydrocephalus. *Fluids Barriers CNS.* 10:18. doi: 10.1186/2045-8118-10-18

Castejon, O. J. (1994). Transmission electron microscope study of human hydrocephalic cerebral cortex. *J. Submicrosc. Cytol. Pathol.* 26, 29–39.

Castejón, O. J. (2010). Submicroscopic pathology of human and experimental hydrocephalic cerebral cortex. *Folia. Neuropathol.* 48, 159–174.

Catalão, C. H., Correa, D. A., Saito, S. T., and Lopes Lda, S. (2014). Camellia sinensis neuroprotective role in experimentally induced hydrocephalus in Wistar rats. *Childs Nerv. Syst.* 30, 591–597. doi: 10.1007/s00381-013-2262-x

Cekanaviciute, E., Dietrich, H. K., Axtell, R. C., Williams, A. M., Egusquiza, R., Wai, K. M., et al. (2014b). Astrocytic TGF-β signaling limits inflammation and reduces neuronal damage during central nervous system Toxoplasma infection. *J. Immunol.* 193, 139–149. doi: 10.4049/jimmunol.1303284

Cekanaviciute, E., Fathali, N., Doyle, K. P., Williams, A. M., Han, J., and Buckwalter, M. S. (2014a). Astrocytic transforming growth factor-beta signaling reduces subacute neuroinflammation after stroke in mice. *Glia* 62, 1227–1240. doi: 10.1002/glia.22675

Cherian, S., Whitelaw, A., Thoresen, M., and Love, S. (2004). The pathogenesis of neonatal post-hemorrhagic hydrocephalus. *Brain Pathol.* 14, 305–311. doi: 10.1111/j.1750-3639.2004.tb00069.x

da Silva, S. C., Feres, O., da Silva Beggiora, P., Machado, H. R., Menezes-Reis, R., Araújo, J. E., et al. (2018). Hyperbaric oxygen therapy reduces astrogliosis and helps to recovery brain damage in hydrocephalic young rats. *Childs Nerv. Syst.* 34, 1125–1134. doi: 10.1007/s00381-018-3803-0

Del Bigio, M. R. (2001). Pathophysiologic consequences of hydrocephalus. *Neurosurg. Clin. N. Am.* 12, 639–49,vii. doi: 10.1016/S1042-3680(18)30022-6

Del Bigio, M. R. (2010). Neuropathology and structural changes in hydrocephalus. *Dev. Disabil. Res. Rev.* 16, 16–22. doi: 10.1002/ddrr.94

Del Bigio, M. R., and Di Curzio, D. L. (2016). Nonsurgical therapy for hydrocephalus: a comprehensive and critical review. *Fluids Barriers CNS.* 13:3. doi: 10.1186/s12987-016-0025-2

Del Bigio, M. R., Khan, O. H., da Silva Lopes, L., and Juliet, P. A. (2012). Cerebral white matter oxidation and nitrosylation in young rodents with kaolin-induced hydrocephalus. *J. Neuropathol. Exp. Neurol.* 71, 274–288. doi: 10.1097/NEN.0b013e31824c1b44

Deren, K. E., Packer, M., Forsyth, J., Milash, B., Abdullah, O. M., Hsu, E. W., et al. (2010). Reactive astrocytosis, microgliosis and inflammation in rats with neonatal hydrocephalus. *Exp. Neurol.* 226, 110–119. doi: 10.1016/j.expneurol.2010.08.010

Di Curzio, D. L., Turner-Brannen, E., and Del Bigio, M. R. (2014). Oral antioxidant therapy for juvenile rats with kaolin-induced hydrocephalus. *Fluids Barriers CNS.* 11:23. doi: 10.1186/2045-8118-11-23

Dong, M., Xi, G., Keep, R. F., and Hua, Y. (2013). Role of iron in brain lipocalin 2 upregulation after intracerebral hemorrhage in rats. *Brain Res.* 1505, 86–92.

Dringen, R. (2000). Metabolism and functions of glutathione in brain. *Prog. Neurobiol.* 62, 649–671.

Dringen, R., Pfeiffer, B., and Hamprecht, B. (1999). Synthesis of the antioxidant glutathione in neurons: supply by astrocytes of CysGly as precursor for neuronal glutathione. *J. Neurosci.* 19, 562–569. doi: 10.1523/JNEUROSCI.19-02-00562.1999

Durkee, C. A., and Araque, A. (2019). Diversity and specificity of astrocyte-neuron communication. *Neuroscience* 396, 73–78.

Eide, P. K., and Hansson, H. A. (2018). Astrogliosis and impaired aquaporin-4 and dystrophin systems in idiopathic normal pressure hydrocephalus. *Neuropathol. Appl. Neurobiol.* 44, 474–490. doi: 10.1111/nan.12420

Eskandari, R., Harris, C. A., and McAllister, J. P. II (2011). Reactive astrocytosis in feline neonatal hydrocephalus: acute, chronic, and shunt-induced changes. *Childs Nerv. Syst.* 27, 2067–2076. doi: 10.1007/s00381-011-1552-4

Frost, G. R., and Li, Y. M. (2017). The role of astrocytes in amyloid production and Alzheimer's disease. *Open Biol.* 7:170228. doi: 10.1098/rsob.170228

Garcia, C. A. B., Catalão, C. H. R., Machado, H. R., Júnior, I. M., Romeiro, T. H., Peixoto-Santos, J. E., et al. (2017). Edaravone reduces astrogliosis and apoptosis in young rats with kaolin-induced hydrocephalus. *Childs Nerv. Syst.* 33, 419–428. doi: 10.1007/s00381-016-3313-x

Garrido-Mesa, N., Zarzuelo, A., and Gálvez, J. (2013). Minocycline: far beyond an antibiotic. *Br. J. Pharmacol.* 169, 337–352.

González-Reyes, R. E., Nava-Mesa, M. O., Vargas-Sánchez, K., Ariza-Salamanca, D., and Mora-Muñoz, L. (2017). Involvement of Astrocytes in Alzheimer's Disease from a Neuroinflammatory and Oxidative Stress Perspective. *Front. Mol. Neurosci.* 10:427. doi: 10.3389/fnmol.2017.00427

Gu, C., Hao, X., Li, J., Hua, Y., Keep, R. F., and Xi, G. (2019). Effects of minocycline on epiplexus macrophage activation, choroid plexus injury and hydrocephalus development in spontaneous hypertensive rats. *J. Cereb. Blood Flow Metab.* 39, 1936–1948. doi: 10.1177/0271678X19836117

Guo, J., Chen, Q., Tang, J., Zhang, J., Tao, Y., Li, L., et al. (2015). Minocycline-induced attenuation of iron overload and brain injury after experimental germinal matrix hemorrhage. *Brain Res.* 1594, 115–124. doi: 10.1016/j.brainres.2014.10.046

Guzelcicek, A., Koyuncu, I., Gönel, A., Cigdem, G., and Karadag, M. (2020). Relationship Between Oxidative Stress, Tau Level and Antioxidant Mechanisms of the KEAP-1/NRF-2/HO-1 in Children with Hydrocephalus. *Antiinflamm Antiallergy Agents Med. Chem.* 20, 282–289. doi: 10.2174/1871523019666201228111713

Harrigan, M. R., Ennis, S. R., Masada, T., and Keep, R. F. (2002). Intraventricular infusion of vascular endothelial growth factor promotes cerebral angiogenesis with minimal brain edema. *Neurosurgery* 50, 589–598. doi: 10.1097/00006123-200203000-00030

Hasan-Olive, M. M., Enger, R., Hansson, H. A., Nagelhus, E. A., and Eide, P. K. (2019a). Pathological mitochondria in neurons and perivascular astrocytic endfeet of idiopathic normal pressure hydrocephalus patients. *Fluids Barriers CNS.* 16:39. doi: 10.1186/s12987-019-0160-7

Hasan-Olive, M. M., Enger, R., Hansson, H. A., Nagelhus, E. A., and Eide, P. K. (2019b). Loss of perivascular aquaporin-4 in idiopathic normal pressure hydrocephalus. *Glia* 67, 91–100. doi: 10.1002/glia.23528

He, Y., Jackman, N. A., Thorn, T. L., Vought, V. E., and Hewett, S. J. (2015). Interleukin-1β protects astrocytes against oxidant-induced injury via an NF-κB-dependent upregulation of glutathione synthesis. *Glia* 63, 1568–1580. doi: 10.1002/glia.22828

Jin, M., Jang, E., and Suk, K. (2014). Lipocalin-2 Acts as a Neuroinflammatogen in Lipopolysaccharide-injected Mice. *Exp. Neurobiol.* 23, 155–162. doi: 10.5607/en.2014.23.2.155

John, G. R., Chen, L., Rivieccio, M. A., Melendez-Vasquez, C. V., Hartley, A., and Brosnan, C. F. (2004). Interleukin-1beta induces a reactive astroglial phenotype via deactivation of the Rho GTPase-Rock axis. *J. Neurosci.* 24, 2837–2845. doi: 10.1523/JNEUROSCI.4789-03.2004

Kálmán, M., Mahalek, J., Adorján, A., Adorján, I., Pócsai, K., Bagyura, Z., et al. (2011). Alterations of the perivascular dystrophin-dystroglycan complex following brain lesions: an immunohistochemical study in rats. *Histol. Histopathol.* 26, 1435–1452. doi: 10.14670/HH-26.1435

Katsouri, L., Birch, A. M., Renziehausen, A. W. J., Zach, C., Aman, Y., Steeds, H., et al. (2020). Ablation of reactive astrocytes exacerbates disease pathology in a model of Alzheimer's disease. *Glia* 68, 1017–1030. doi: 10.1002/glia.23759

Kawai, T., and Akira, S. (2007). Signaling to NF-kappaB by Toll-like receptors. *Trends Mol. Med.* 13, 460–469. doi: 10.1016/j.molmed.2007.09.002

Kikuchi, K., Setoyama, K., Kawahara, K. I., Nagasato, T., Terashi, T., Ueda, K., et al. (2017). Edaravone, a Synthetic Free Radical Scavenger, Enhances Alteplase-Mediated Thrombolysis. *Oxid. Med. Cell Longev.* 2017:6873281. doi: 10.1155/2017/6873281

Kress, B. T., Iliff, J. J., Xia, M., Wang, M., Wei, H. S., Zeppenfeld, D., et al. (2014). Impairment of paravascular clearance pathways in the aging brain. *Ann. Neurol.* 76, 845–861. doi: 10.1002/ana.24271

Lafrenaye, A. D., and Simard, J. M. (2019). Bursting at the seams: molecular mechanisms mediating astrocyte swelling. *Int. J. Mol. Sci.* 20:330. doi: 10.3390/ijms20020330

Lattke, M., Magnutzki, A., Walther, P., Wirth, T., and Baumann, B. (2012). Nuclear factor κB activation impairs ependymal ciliogenesis and links neuroinflammation to hydrocephalus formation. *J. Neurosci.* 32, 11511–11523. doi: 10.1523/JNEUROSCI.0182-12.2012

Li, L., Zhang, H., Varrin-Doyer, M., Zamvil, S. S., and Verkman, A. S. (2011). Proinflammatory role of aquaporin-4 in autoimmune neuroinflammation. *FASEB J.* 25, 1556–1566.

Li, X., Li, L., Li, J., Sipple, J., Schick, J., Mehta, P. A., et al. (2014). Concomitant inactivation of foxo3a and fancc or fancd2 reveals a two-tier protection from oxidative stress-induced hydrocephalus. *Antioxid Redox Signal.* 21, 1675–1692. doi: 10.1089/ars.2013.5597

Liddelow, S. A., Guttenplan, K. A., Clarke, L. E., Bennett, F. C., Bohlen, C. J., Schirmer, L., et al. (2017). Neurotoxic reactive astrocytes are induced by activated microglia. *Nature* 541, 481–487.

Li-Na, Z., Deng, C., Da, X., Si-Han, C., Hai-Jiao, W., and Ling, L. (2017). Mesencephalic astrocyte-derived neurotrophic factor and its role in nervous system disease. *Neurol. Sci.* 38, 1741–1746. doi: 10.1007/s10072-017-3042-2

Linnerbauer, M., Wheeler, M. A., and Quintana, F. J. (2020). Astrocyte Crosstalk in CNS Inflammation. *Neuron* 108, 608–622. doi: 10.1016/j.neuron.2020.08.012

Lisjak, M., Potokar, M., Rituper, B., Jorgačevski, J., and Zorec, R. (2017). AQP4e-Based Orthogonal Arrays Regulate Rapid Cell Volume Changes in Astrocytes. *J. Neurosci.* 37, 10748–10756. doi: 10.1523/JNEUROSCI.0776-17.2017

Liu, Z., and Chopp, M. (2016). Astrocytes, therapeutic targets for neuroprotection and neurorestoration in ischemic stroke. *Prog. Neurobiol.* 144, 103–120.

Lopes Lda, S., Slobodian, I., and Del Bigio, M. R. (2009). Characterization of juvenile and young adult mice following induction of hydrocephalus with kaolin. *Exp. Neurol.* 219, 187–196. doi: 10.1016/j.expneurol.2009.05.015

Ma, B., and Hottiger, M. O. (2016). Crosstalk between Wnt/β-Catenin and NF-κB Signaling Pathway during Inflammation. *Front. Immunol.* 7:378. doi: 10.3389/fimmu.2016.00378

Mao, X., Enno, T. L., and Del Bigio, M. R. (2006). Aquaporin 4 changes in rat brain with severe hydrocephalus. *Eur. J. Neurosci.* 23, 2929–2936.

Mathiisen, T. M., Lehre, K. P., Danbolt, N. C., and Ottersen, O. P. (2010). The perivascular astroglial sheath provides a complete covering of the brain microvessels: an electron microscopic 3D reconstruction. *Glia* 58, 1094–1103. doi: 10.1002/glia.20990

McKeon, R. J., Schreiber, R. C., Rudge, J. S., and Silver, J. (1991). Reduction of neurite outgrowth in a model of glial scarring following CNS injury is correlated with the expression of inhibitory molecules on reactive astrocytes. *J. Neurosci.* 11, 3398–3411. doi: 10.1523/JNEUROSCI.11-11-03398.1991

Ment, L. R., Schwartz, M., Makuch, R. W., and Stewart, W. B. (1998). Association of chronic sublethal hypoxia with ventriculomegaly in the developing rat brain. *Brain Res. Dev. Brain Res.* 111, 197–203.

Michinaga, S., and Koyama, Y. (2019). Dual roles of astrocyte-derived factors in regulation of blood-brain barrier function after brain damage. *Int. J. Mol. Sci.* 20:571. doi: 10.3390/ijms20030571

Miller, R. H., and Raff, M. C. (1984). Fibrous and protoplasmic astrocytes are biochemically and developmentally distinct. *J. Neurosci.* 4, 585–592. doi: 10.1523/JNEUROSCI.04-02-00585.1984

Morgan, M. J., and Liu, Z. G. (2011). Crosstalk of reactive oxygen species and NF-κB signaling. *Cell Res.* 21, 103–115.

Neely, J. D., Amiry-Moghaddam, M., Ottersen, O. P., Froehner, S. C., Agre, P., and Adams, M. E. (2001). Syntrophin-dependent expression and localization of Aquaporin-4 water channel protein. *Proc. Natl. Acad. Sci. U.S.A.* 98, 14108–14113. doi: 10.1073/pnas.241508198

Ni, W., Zheng, M., Xi, G., Keep, R. F., and Hua, Y. (2015). Role of lipocalin-2 in brain injury after intracerebral hemorrhage. *J. Cereb. Blood Flow Metab.* 35, 1454–1461.

Nielsen, S., Nagelhus, E. A., Amiry-Moghaddam, M., Bourque, C., Agre, P., and Ottersen, O. P. (1997). Specialized membrane domains for water transport in glial cells: high-resolution immunogold cytochemistry of aquaporin-4 in rat brain. *J. Neurosci.* 17, 171–180. doi: 10.1523/JNEUROSCI.17-01-00171.1997

Norden, D. M., Trojanowski, P. J., Villanueva, E., Navarro, E., and Godbout, J. P. (2016). Sequential activation of microglia and astrocyte cytokine expression precedes increased Iba-1 or GFAP immunoreactivity following systemic immune challenge. *Glia* 64, 300–316.

Olopade, F. E., Shokunbi, M. T., and Sirén, A. L. (2012). The relationship between ventricular dilatation, neuropathological and neurobehavioural changes in hydrocephalic rats. *Fluids Barriers CNS.* 9:19. doi: 10.1186/2045-8118-9-19

Olopade, F. E., Shokunbi, M. T., Azeez, I. A., Andrioli, A., Scambi, I., and Bentivoglio, M. (2019). Neuroinflammatory response in chronic hydrocephalus in juvenile rats. *Neuroscience* 419, 14–22. doi: 10.1016/j.neuroscience.2019.08.049

Páez, P., Bátiz, L. F., Roales-Buján, R., Rodríguez-Pérez, L. M., Rodríguez, S., Jiménez, A. J., et al. (2007). Patterned neuropathologic events occurring in hyh congenital hydrocephalic mutant mice. *J. Neuropathol. Exp. Neurol.* 66, 1082–1092. doi: 10.1097/nen.0b013e31815c1952

Pannicke, T., Wurm, A., Iandiev, I., Hollborn, M., Linnertz, R., Binder, D. K., et al. (2010). Deletion of aquaporin-4 renders retinal glial cells more susceptible to osmotic stress. *J. Neurosci. Res.* 88, 2877–2888. doi: 10.1002/jnr.22437

Pekny, M., and Nilsson, M. (2005). Astrocyte activation and reactive gliosis. *Glia* 50, 427–434.

Pekny, M., and Pekna, M. (2014). Astrocyte reactivity and reactive astrogliosis: costs and benefits. *Physiol. Rev.* 94, 1077–1098. doi: 10.1152/physrev.00041.2013

Petzold, A., Keir, G., Kerr, M., Kay, A., Kitchen, N., Smith, M., et al. (2006). Early identification of secondary brain damage in subarachnoid hemorrhage: a role for glial fibrillary acidic protein. *J. Neurotrauma.* 23, 1179–1184. doi: 10.1089/neu.2006.23.1179

Plog, B. A., and Nedergaard, M. (2018). The glymphatic system in central nervous system health and disease: past. present, and future. *Annu. Rev. Pathol.* 13, 379–394. doi: 10.1146/annurev-pathol-051217-111018

Potokar, M., Jorgačevski, J., and Zorec, R. (2016). Astrocyte aquaporin dynamics in health and disease. *Int. J. Mol. Sci.* 17:1121.

Rizwan Siddiqui, M., Attar, F., Mohanty, V., Kim, K. S., Shekhar Mayanil, C., and Tomita, T. (2018). Erythropoietin-mediated activation of aquaporin-4 channel for the treatment of experimental hydrocephalus. *Childs Nerv. Syst.* 34, 2195–2202. doi: 10.1007/s00381-018-3865-z

Roales-Buján, R., Páez, P., Guerra, M., Rodríguez, S., Vío, K., Ho-Plagaro, A., et al. (2012). Astrocytes acquire morphological and functional characteristics of ependymal cells following disruption of ependyma in hydrocephalus. *Acta Neuropathol.* 124, 531–546. doi: 10.1007/s00401-012-0992-6

Saadoun, S., Papadopoulos, M. C., Watanabe, H., Yan, D., Manley, G. T., and Verkman, A. S. (2005). Involvement of aquaporin-4 in astroglial cell migration and glial scar formation. *J. Cell Sci.* 118(Pt 24), 5691–5698.

Sampaio, G. B., Da Silva, S. C., Romeiro, T. H., Beggiora, P. D. S., Machado, H. R., and Lopes, L. D. S. (2019). Evaluation of the effects of quercetin on brain lesions secondary to experimental hydrocephalus in rats. *Childs Nerv. Syst.* 35, 2299–2306. doi: 10.1007/s00381-019-04184-2

Sanchez-Mico, M. V., Jimenez, S., Gomez-Arboledas, A., Munoz-Castro, C., Romero-Molina, C., Navarro, V., et al. (2021). Amyloid-beta impairs the phagocytosis of dystrophic synapses by astrocytes in Alzheimer's disease. *Glia* 69, 997–1011.

Schmitz, T., Heep, A., Groenendaal, F., Hüseman, D., Kie, S., Bartmann, P., et al. (2007). Interleukin-1beta, interleukin-18, and interferon-gamma expression in the cerebrospinal fluid of premature infants with posthemorrhagic hydrocephalus–markers of white matter damage? *Pediatr. Res.* 61, 722–726. doi: 10.1203/pdr.0b013e31805341f1

Shih, R. H., Wang, C. Y., and Yang, C. M. (2015). NF-kappaB signaling pathways in neurological inflammation: A Mini Review. *Front. Mol. Neurosci.* 8:77. doi: 10.3389/fnmol.2015.00077

Shim, J. W., Sandlund, J., Han, C. H., Hameed, M. Q., Connors, S., Klagsbrun, M., et al. (2013). VEGF, which is elevated in the CSF of patients with hydrocephalus, causes ventriculomegaly and ependymal changes in rats. *Exp. Neurol.* 247, 703–709. doi: 10.1016/j.expneurol.2013.03.011

Shishido, H., Toyota, Y., Hua, Y., Keep, R. F., and Xi, G. (2016). Role of lipocalin 2 in intraventricular haemoglobin-induced brain injury. *Stroke Vasc. Neurol.* 1, 37–43. doi: 10.1136/svn-2016-000009

Skjolding, A. D., Holst, A. V., Broholm, H., Laursen, H., and Juhler, M. (2013). Differences in distribution and regulation of astrocytic aquaporin-4 in human and rat hydrocephalic brain. *Neuropathol. Appl. Neurobiol.* 39, 179–191. doi: 10.1111/j.1365-2990.2012.01275.x

Skjolding, A. D., Rowland, I. J., Søgaard, L. V., Praetorius, J., Penkowa, M., and Juhler, M. (2010). Hydrocephalus induces dynamic spatiotemporal regulation

of aquaporin-4 expression in the rat brain. *Cerebrospinal Fluid Res.* 7:20. doi: 10.1186/1743-8454-7-20

Socci, D. J., Bjugstad, K. B., Jones, H. C., Pattisapu, J. V., and Arendash, G. W. (1999). Evidence that oxidative stress is associated with the pathophysiology of inherited hydrocephalus in the H-Tx rat model. *Exp. Neurol.* 155, 109–117. doi: 10.1006/exnr.1998.6969

Sofroniew, M. V. (2015). Astrocyte barriers to neurotoxic inflammation. *Nat. Rev. Neurosci.* 16, 249–263.

Sun, C., An, Q., Li, R., Chen, S., Gu, X., An, S., et al. (2021). Calcitonin gene-related peptide induces the histone H3 lysine 9 acetylation in astrocytes associated with neuroinflammation in rats with neuropathic pain. *CNS Neurosci. Ther.* 27, 1409–1424. doi: 10.1111/cns.13720

Suryaningtyas, W., Arifin, M., Rantam, F. A., Bajamal, A. H., Dahlan, Y. P., Dewa Gede Ugrasena, I., et al. (2019). Erythropoietin protects the subventricular zone and inhibits reactive astrogliosis in kaolin-induced hydrocephalic rats. *Childs Nerv. Syst.* 35, 469–476. doi: 10.1007/s00381-019-04063-w

Suryaningtyas, W., Parenrengi, M. A., Bajamal, A. H., and Rantam, F. A. (2020). Lipid Peroxidation Induces Reactive Astrogliosis by Activating WNT/β-Catenin Pathway in Hydrocephalus. *Malays J. Med. Sci.* 27, 34–42. doi: 10.21315/mjms2020.27.3.4

Szabó, A., and Kálmán, M. (2008). Post traumatic lesion absence of beta-dystroglycan-immunopositivity in brain vessels coincides with the glial reaction and the immunoreactivity of vascular laminin. *Curr. Neurovasc. Res.* 5, 206–213. doi: 10.2174/156720208785425657

Tan, C., Wang, X., Wang, Y., Wang, C., Tang, Z., Zhang, Z., et al. (2021). The Pathogenesis Based on the Glymphatic System, Diagnosis, and Treatment of Idiopathic Normal Pressure Hydrocephalus. *Clin. Interv. Aging.* 16, 139–153. doi: 10.2147/CIA.S290709

Tomita, S., Ueno, M., Sakamoto, M., Kitahama, Y., Ueki, M., Maekawa, N., et al. (2003). Defective brain development in mice lacking the Hif-1alpha gene in neural cells. *Mol. Cell Biol.* 23, 6739–6749. doi: 10.1128/MCB.23.19.6739-6749.2003

Vindedal, G. F., Thoren, A. E., Jensen, V., Klungland, A., Zhang, Y., Holtzman, M. J., et al. (2016). Removal of aquaporin-4 from glial and ependymal membranes causes brain water accumulation. *Mol. Cell Neurosci.* 77, 47–52. doi: 10.1016/j.mcn.2016.10.004

Volterra, A., Liaudet, N., and Savtchouk, I. (2014). Astrocyte Ca^{2+} signalling: an unexpected complexity. *Nat. Rev. Neurosci.* 15, 327–335.

Wang, G. H., Jiang, Z. L., Li, Y. C., Li, X., Shi, H., Gao, Y. Q., et al. (2011). Free-radical scavenger edaravone treatment confers neuroprotection against traumatic brain injury in rats. *J. Neurotrauma.* 28, 2123–2134. doi: 10.1089/neu.2011.1939

Wang, Y., Wang, X., Tan, C., Wang, C., Tang, Z., Zhang, Z., et al. (2021). Hydrocephalus after aneurysmal subarachnoid hemorrhage: Epidemiology, Pathogenesis, Diagnosis, and Management. *Signa Vitae* 17, 4–17. doi: 10.22514/sv.2021.021

Wang, Z., Zhang, Y., Hu, F., Ding, J., and Wang, X. (2020). Pathogenesis and pathophysiology of idiopathic normal pressure hydrocephalus. *CNS Neurosci. Ther.* 26, 1230–1240.

Xing, C., Wang, X., Cheng, C., Montaner, J., Mandeville, E., Leung, W., et al. (2014). Neuronal production of lipocalin-2 as a help-me signal for glial activation. *Stroke* 45, 2085–2092. doi: 10.1161/STROKEAHA.114.005733

Xu, H., Tan, G., Zhang, S., Zhu, H., Liu, F., Huang, C., et al. (2012a). Minocycline reduces reactive gliosis in the rat model of hydrocephalus. *BMC Neurosci.* 13:148. doi: 10.1186/1471-2202-13-148

Xu, H., Xu, B., Wang, Z., Tan, G., and Shen, S. (2015). Inhibition of Wnt/β-catenin signal is alleviated reactive gliosis in rats with hydrocephalus. *Childs Nerv Syst.* 31, 227–234. doi: 10.1007/s00381-014-2613-2

Xu, H., Zhang, S. L., Tan, G. W., Zhu, H. W., Huang, C. Q., Zhang, F. F., et al. (2012b). Reactive gliosis and neuroinflammation in rats with communicating hydrocephalus. *Neuroscience* 218, 317–325. doi: 10.1016/j.neuroscience.2012.05.004

Yong, V. W., Wells, J., Giuliani, F., Casha, S., Power, C., and Metz, L. M. (2004). The promise of minocycline in neurology. *Lancet Neurol.* 3, 744–751. doi: 10.1016/S1474-4422(04)00937-8

Zamanian, J. L., Xu, L., Foo, L. C., Nouri, N., Zhou, L., Giffard, R. G., et al. (2012). Genomic analysis of reactive astrogliosis. *J. Neurosci.* 32, 6391–6410.

Zhan, C., Xiao, G., Zhang, X., Chen, X., Zhang, Z., and Liu, J. (2020). Decreased MiR-30a promotes TGF-beta1-mediated arachnoid fibrosis in post-hemorrhagic hydrocephalus. *Transl. Neurosci.* 11, 60–74. doi: 10.1515/tnsci-2020-0010

Zhang, J., Shi, X., Chen, Z., Geng, J., Wang, Y., Feng, H., et al. (2018). Edaravone Reduces Iron-Mediated Hydrocephalus and Behavioral Disorder in Rat by Activating the Nrf2/HO-1 Pathway. *J. Stroke Cerebrovasc. Dis.* 27, 3511–3520. doi: 10.1016/j.jstrokecerebrovasdis.2018.08.019

Zhao, J., O'Connor, T., and Vassar, R. (2011). The contribution of activated astrocytes to Aβ production: implications for Alzheimer's disease pathogenesis. *J. Neuroinflammation.* 8:150. doi: 10.1186/1742-2094-8-150

Zhou, B., Zuo, Y. X., and Jiang, R. T. (2019). Astrocyte morphology: Diversity, plasticity, and role in neurological diseases. *CNS Neurosci. Ther.* 25, 665–673. doi: 10.1111/cns.13123

frontiers | Frontiers in Molecular Neuroscience

TYPE Review
PUBLISHED 21 October 2022
DOI 10.3389/fnmol.2022.949231

OPEN ACCESS

EDITED BY
Marcus Stoodley,
Macquarie University, Australia

REVIEWED BY
Jinwei Zhang,
University of Exeter, United Kingdom
Qianwei Chen,
Army Medical University, China

*CORRESPONDENCE
Zhixiong Lin
linzx@ccmu.edu.cn
Gelei Xiao
xiaogelei@csu.edu.cn

†These authors have contributed equally to this work and share first authorship

SPECIALTY SECTION
This article was submitted to Brain Disease Mechanisms, a section of the journal Frontiers in Molecular Neuroscience

RECEIVED 20 May 2022
ACCEPTED 15 August 2022
PUBLISHED 21 October 2022

CITATION
Liu R, Zhang Z, Chen Y, Liao J, Wang Y, Liu J, Lin Z and Xiao G (2022) Choroid plexus epithelium and its role in neurological diseases. *Front. Mol. Neurosci.* 15:949231. doi: 10.3389/fnmol.2022.949231

Choroid plexus epithelium and its role in neurological diseases

Ruizhen Liu[1,2,3†], Zhiping Zhang[1,2,3†], Yibing Chen[1,2,3], Junbo Liao[1,2,3], Yuchang Wang[1,2,3], Jingping Liu[1,2,3], Zhixiong Lin[4*] and Gelei Xiao[1,2,3*]

[1]Department of Neurosurgery, Xiangya Hospital, Central South University, Changsha, China, [2]Diagnosis and Treatment Center for Hydrocephalus, Xiangya Hospital, Central South University, Changsha, China, [3]National Clinical Research Center for Geriatric Disorders, Xiangya Hospital, Central South University, Changsha, China, [4]Department of Neurosurgery, Sanbo Brain Hospital, Capital Medical University, Beijing, China

Choroid plexus epithelial cells can secrete cerebrospinal fluid into the ventricles, serving as the major structural basis of the selective barrier between the neurological system and blood in the brain. In fact, choroid plexus epithelial cells release the majority of cerebrospinal fluid, which is connected with particular ion channels in choroid plexus epithelial cells. Choroid plexus epithelial cells also produce and secrete a number of essential growth factors and peptides that help the injured cerebrovascular system heal. The pathophysiology of major neurodegenerative disorders like Alzheimer's disease, Parkinson's disease, as well as minor brain damage diseases like hydrocephalus and stroke is still unknown. Few studies have previously connected choroid plexus epithelial cells to the etiology of these serious brain disorders. Therefore, in the hopes of discovering novel treatment options for linked conditions, this review extensively analyzes the association between choroid plexus epithelial cells and the etiology of neurological diseases such as Alzheimer's disease and hydrocephalus. Finally, we review CPE based immunotherapy, choroid plexus cauterization, choroid plexus transplantation, and gene therapy.

KEYWORDS

choroid plexus epithelium, Alzheimer's disease, Parkinson's disease, hydrocephalus, stroke, treatment

Introduction

The choroid plexus epithelium (CPE), a specialized compartmental membrane cell at the choroid plexus created by the ventricle wall, is a glial cell of the central nervous system (CNS). The blood-cerebrospinal fluid barrier (BCSFB) is maintained by the apical tight junctions of the CPE, which are made up of a layer of cuboidal to low cylindrical epithelial cells joined by contact complexes. Scientists have long been concerned about the CPE being the primary source of secreted cerebrospinal fluid (CSF). Despite a substantial amount of research on the CPE's robust ability to secrete CSF, the potential link between the CPE and diseases caused by a disrupted or dysregulated CSF ion balance, as well as the pathophysiology of these disorders, remains unknown (Redzic and Segal, 2004; Chodobski et al., 2019). At the same time, several of the active chemicals it produces, such

as Insulin-like growth factor, suggest that it has a role in brain repair and inflammation (Ghersi-Egea et al., 2018). It's worth noting that the distribution of several chemicals in the CPE differs significantly from that of other epithelial cells, and it has a particularly appealing reverse polarity (Damkier et al., 2018).

CPE anomalies have been linked to the development of numerous neurological illnesses, including hydrocephalus and Alzheimer's disease (AD), according to recent research. Damage to the CPE will result in a lethal blow to the blood-brain barrier, which will have a significant impact on brain fluid circulation and may potentially lead to the development of hydrocephalus (Yamada et al., 2021). CPE failure is present in AD, and changes in cerebrospinal fluid production and CPE converging effects, as well as the lack of CPE-mediated macrophage recruitment, all contribute to AD pathogenesis (Mesquita et al., 2012).

This review summarizes recent research on choroid plexus epithelial cell malfunction and neurological illnesses, as well as the involvement of epithelial cell venation in neurological diseases. The relationship between the mechanism of these connected brain disorders and the aberrations of the CPE is thoroughly studied in this work, which describes numerous types of typical brain diseases such as neurodegenerative diseases. We want to encourage more research into choroid plexus epithelial cells as a target for neurological disease therapy and innovative targeted medicines.

Choroid plexus epithelium

Structure

Through a thin layer of connective tissue and fenestrated capillaries in the equivalent bottom layer, blood equilibrates with the CPE. The CPE features a tight junction (TJ) nearest to the luminal membrane, which divides the ventricular lumen from the lateral intercellular and basal gaps, similar to other epithelia. Desmosomes appear to be more inferior to the adherens junction, which is positioned below the TJ. The surface of the CPE has many microvilli and many different kinds of motor cilia. Except for the transition zone between the lateral and basal zones, the membranes of the lateral and basal zones do not expand through surface extension. Adjacent cells create multiple interdigitating protrusions that form a basolateral maze at this location, resulting in a 10-fold increase in surface area (Cserr, 1971; Mortazavi et al., 2014; Spector et al., 2015; Praetorius and Damkier, 2017; Ghersi-Egea et al., 2018). Interestingly, there have been numerous reports on the heterogeneity of the CPE (Hirano et al., 2002; Lobas et al., 2012; Wang et al., 2019; Perin et al., 2021). For example, choroid plexus epithelial cells not only highly express most members of the Pcdh-γ gene family (γ-Pcdh) of cell adhesion molecules, but also γ-Pcdh expression is strictly restricted to the apical membrane and is not expressed in tight junctions, basolateral adherens junctions, and apical ciliary clusters (Lobas et al., 2012) (Figure 1).

Function

Previous studies have revealed that the CPE, as an important structure in the brain, plays an important role in cerebrospinal fluid homeostasis balance (Husted and Reed, 1977; Kazemi and Choma, 1977; Lindsey et al., 1990; Bouzinova et al., 2005; Praetorius and Nielsen, 2006; Millar and Brown, 2008; Damkier et al., 2009, 2013, 2018; Christensen et al., 2017), neurogenesis (Baruch et al., 2014; Silva-Vargas et al., 2016), and inflammation regulation (Baruch and Schwartz, 2013; Baruch et al., 2013; Schwartz and Baruch, 2014).

The composition and acidity and alkalinity of cerebrospinal fluid maintain a dynamic balance under normal physiological conditions and play a unique role in regulating important life activities such as inflammation regulation. This maintenance of homeostasis is inextricably linked to some important ion transporters or anion transport channels on the CPE (Damkier et al., 2018), such as acid-base transporters Cl^{--}/H^{+}, NHE6 and CLC-7 on the CPE (Kazemi and Choma, 1977; Damkier et al., 2018). The distribution of these transporters on the CPE can be remarkably heterogeneous (Lobas et al., 2012; Ghersi-Egea et al., 2018), which correlates with their function. There are also many microvilli and active cilia on the surface of the CPE, which play an important role in cerebrospinal fluid dynamics and can ensure the normal transport and circulation of cerebrospinal fluid (Cserr, 1971). If the cilia are damaged, retention of CSF may lead to hydrocephalus and other diseases (Oi et al., 2011; Kumar et al., 2021).

The first report of cation channel gene disruption leading to CPE dysfunction was published in 2013 (Roepke et al., 2011), and suggests that KCNE2 regulates KCNQ1 and KCNA3 in

Abbreviations: CPE, choroid plexus epithelium; CNS, central nervous system; BCSFB, blood-cerebrospinal fluid barrier; CSF, cerebrospinal fluid; AD, Alzheimer's disease; TJ, tight junction; γ-Pcdh, Pcdh-γ gene family; CP, choroid plexus; SCN, suprachiasmatic nucleus; Aβ, amyloid-β; PHH, posthemorrhagic hydrocephalus; TLR4, toll-like receptor 4; IVH, intraventricular hemorrhage; ZT-1A, 5-chloro-N-(5-chloro-4-((4-chlorophenyl)(cyano)methyl)-2-methylphenyl)-2-hydroxybenzamide; CCC, cation-Cl^{-} cotransporters; LRP-1 and 2, lipoprotein receptor-related proteins 1 and 2; MMP, matrix metalloproteinases; PD, Parkinson's disease; DA, dopamine; Cp, ceruloplasmin; CPEC-CM, choroid plexus epithelial cell conditioned medium; KS, knockout serum; hADSCs, human adipose-derived stem cells; PACRG, parkin co-regulated gene; MS, multiple sclerosis; IFN-α, interferon-α; IFN-γ, interferon-γ; MRI, magnetic resonance imaging; IFN-β, interferon-β; EVA, epithelial v-like antigen; AAV, adeno-associated virus; AAV5, adeno-associated virus type 5; TLR9, toll-like receptor 9; CPC, choroid plexus cauterization; ETV/CPC, endoscopic third ventriculostomy with CPC; TH, tyrosine hydroxylase; CT, computed tomography.

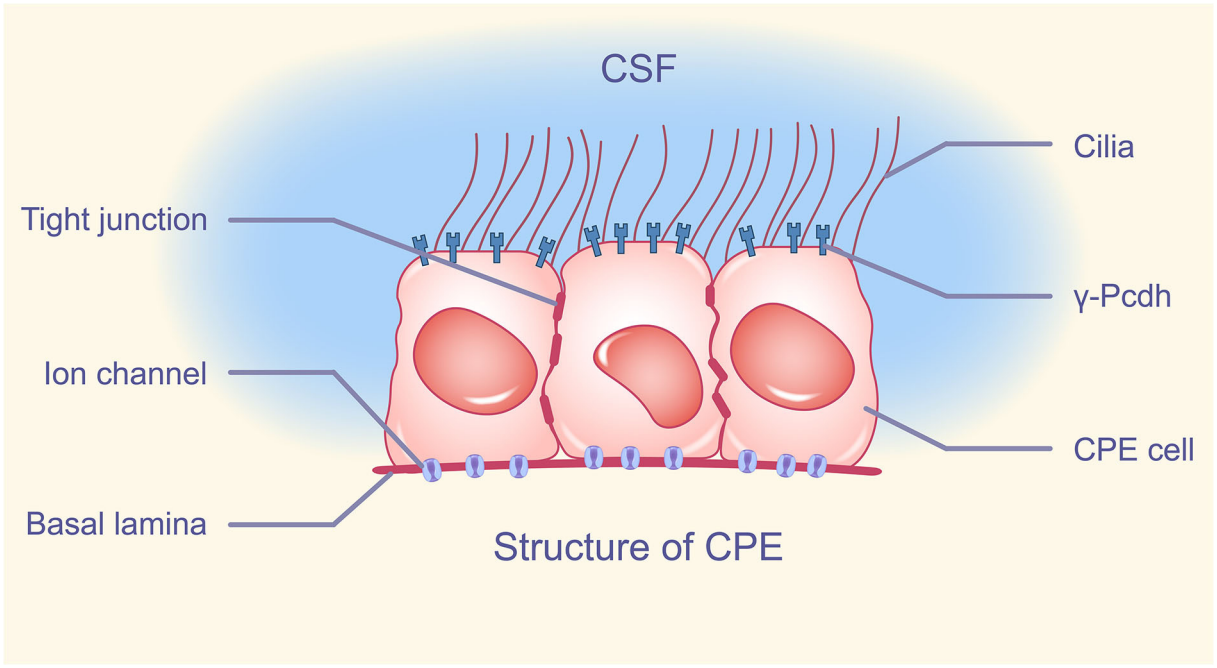

FIGURE 1
Structure of CPE. The apical membrane of CPE has a variable number of cilia, intercalated between cells, tight junctions composing BCSFB, and cell adhesion molecule γ-Pcdh distributed on the apical membrane except cilia. A large number of ion channels are distributed in the basement membrane of CPE. CPE, choroid plexus epithelium; BCSFB, blood-cerebrospinal fluid barrier; γ-Pcdh, Pcdh-γ gene family.

the CPE to influence blood-CSF anion flow. In the choroid plexus epithelium, KCNE2 forms potassium channels with KCNA3 and KCNQ1. In addition to transporters and channel proteins for diverse solutes and water, glucose, fructose, and uric acid transporters have been discovered in choroid plexus epithelial cells, which could serve as neuroprotective energy and antioxidation substrates.

Choroid plexus epithelial cells in the lateral ventricle not only directly contact adult neural stem cells in the ventricular-subventricular zone in the CSF, but also secrete cellular activation and proliferation factors that promote the development of adult neural stem cells in the ventricular-subventricular zone in the lateral ventricle choroid plexus epithelial cells, and these brain microecological factors play an important role in the neural development of adult neural stem cells in the ventricular-subventricular zone throughout the life cycle (Silva-Vargas et al., 2016). The CPE separates CSF from tissues within the choroid plexus (CP) such as capillaries. Under normal physiological conditions, the CPE maintains CSF homeostasis by secreting neurotrophins and regulating pH. When chronic neuroinflammation occurs, leukocytes need to be recruited from peripheral tissue vessels and enter the central nervous system through the "gate". Recent studies have confirmed that the blood-cerebrospinal fluid barrier is a selective channel for leukocyte entry during inflammation (Schwartz and Baruch, 2014). The CPE promotes leukocyte recruitment and trafficking by expressing chemokines and adhesion molecules that support transepithelial leukocyte migration (Kunis et al., 2013; Schwartz and Baruch, 2014). Direct evidence of migration of leukocytes such as T cells, neutrophils, etc., has also been found in the CPE during inflammation (Carrithers et al., 2000; Szmydynger-Chodobska et al., 2012). The CPE is also involved in the accumulation of inflammatory cells in the brain following stroke, which will be detailed in Section Stroke below.

Neurological diseases related with the choroid plexus epithelium

In today's world, neurological problems are extremely common, especially among the elderly (Chan et al., 2013). Most chronic neurological illnesses have a complex etiology that has yet to be determined. However, central nervous system inflammation is linked to dysregulation as people age (Skaper et al., 2018). The CPE plays an essential role in the regulation of brain homeostasis as the main organ secreting CSF in the brain, and current studies suggest that the CPE is a portal for leukocytes to enter the brain (Schwartz and Baruch, 2014). The CPE also plays an important role in the pathogenesis of the central nervous system (Bolos et al., 2013; Barbariga et al.,

2020). Accelerated CPE atrophy has been reported in stroke, multiple sclerosis, schizophrenia, and other central nervous system illnesses (Silverberg et al., 2003; Redzic et al., 2005; Schmidt et al., 2005), indicating that CPE atrophy is linked to CNS disease aggravation and that ciliary abnormalities on the CPE are linked to hydrocephalus (Narita et al., 2010). In the central nervous system, there is only one main thyroid hormone carrier partitioning protein: CP-derived transthyretin. As a result, a lack of thyroid hormone in the central nervous system is linked to aberrant brain development, adult dementia, depression, and other cognitive issues (Davis et al., 2003). The pathogenesis of AD is linked to three major methods of amyloid-β (Aβ) peptide clearance: cerebrospinal fluid-mediated A clearance, direct Aβ absorption, and synthesis of Aβ partners and proteases, all of which may contribute to impaired Aβ clearance in our brains. Alzheimer's disease is also linked to CPE atrophy (Serot et al., 2003; Silverberg et al., 2003). As previously stated, the CPE serves as a conduit for the recruitment of leukocytes from distant places into the brain, and the incidence and treatment of many CNS inflammations are inextricably linked to the CPE's effect on inflammatory cells. Based on the important role of the CPE in CSF secretion, regulation of brain homeostasis, development of the central nervous system, and regulation of chronic inflammation in the central nervous system, the possible mechanism by which CPE abnormalities lead to neurological diseases will be discussed later.

Hydrocephalus

Hydrocephalus is a common brain disease in which the amount of intracranial CSF increases, the ventricular system enlarges, or the arachnoid membrane enlarges due to excessive CSF secretion or circulation and malabsorption caused by craniocerebral diseases. The mainstream classification divides hydrocephalus into obstructive hydrocephalus and communicating hydrocephalus. Obstructive hydrocephalus, also known as non-communicating hydrocephalus or intraventricular obstructive hydrocephalus, which refers to the formation of lesions located in or near the ventricular system and the blocking the cerebrospinal fluid circulation in the ventricular system. Hydrocephalus caused by obstruction above the exit site of the fourth ventricle is the most common form of hydrocephalus. It is common in arachnoid cysts, aqueductal atresia or stenosis, and dysplasia of the median or interventricular foramen. Communicating hydrocephalus, on the other hand, is hydrocephalus due to an obstruction of the extraventricular cerebrospinal fluid circulation pathway or CSF malabsorption and can also be caused by excessive cerebrospinal fluid secretion such as choroid plexus papilloma (Oi et al., 2011; Li et al., 2021).

The basic causes of hydrocephalus are divided into three types: Obstruction, CSF malabsorption, and excessive CSF production. Hydrocephalus may occur if obstruction occurs in any part associated with normal CSF flow. CSF malabsorption is usually caused by inflammation of the brain tissue, and of course CPE ciliary abnormalities can also cause congenital hydrocephalus (Oi et al., 2011). Excessive CSF production may manifest as diffuse villous hyperplasia of the choroid plexus (Smith et al., 2007; Kumar et al., 2021). In addition, central nervous system infection and cerebral hemorrhage can be the origin of hydrocephalus (Karimy et al., 2017).

As a common type of hydrocephalus, posthemorrhagic hydrocephalus (PHH) is a condition that occurs frequently in premature infants. The current understanding of PHH is still in its early stages, and CSF drainage is also basically used to treat PHH, but the optimal timing of intervention is not clear. Recent studies have revealed a potential link between PHH and the CPE that has attracted our attention. In a rat model established with PHH, the investigators demonstrated that intraventricular hemorrhage (IVH) leads to toll-like receptor 4 (TLR4) and nf-kb-dependent inflammatory responses in the CPE. The IVH-induced CSF hypersecretion is mediated by TLR4-dependent activation of the ste20-type stress kinase SPAK, which binds, phosphorylates, and stimulates NKCC1 co-transporters on the apical membrane of the CPE. Genetic deletion of TLR4 or SPAK can normalize the rate of hyperactive cerebrospinal fluid secretion and reduce PHH symptoms (Karimy et al., 2017). Similarly, 5-chloro-N-(5-chloro-4-((4-chlorophenyl)(cyano)methyl)-2-methylphenyl)-2-hydroxybenzamide (ZT-1a) administration has been found to reduce inflammation-induced cation-Cl^- cotransporters (CCC) phosphorylation of CP and CSF oversecretion in a model of PHH (Zhang et al., 2020). This reveals a direct association between CSF hypersecretion due to altered ion transport mechanisms in CPE and hemorrhagic hydrocephalus. At the same time, more and more recent studies have shown that there is an inseparable link between cerebrospinal fluid composition and the occurrence of PHH. Cerebrospinal fluid NCAM-1 concentration was shown to be associated with neurodevelopmental outcomes in premature infants with hemorrhagic hydrocephalus (Limbrick et al., 2021), and cerebrospinal fluid amyloid levels in premature infants with hemorrhagic hydrocephalus were also shown to be associated with ventricular size (Morales et al., 2015).

Choroid plexus papilloma is a rare central nervous system tumor more common in children, accounting for <1% of brain tumors. After surgical treatment, the mortality rate is <1%. Even so, choroid plexus papillomas are associated with hydrocephalus. Many case reports have been recorded (Sahar et al., 1980; Kuyama et al., 1987; Miyagi et al., 2006). However, whether choroid plexus papillomas can cause hydrocephalus or whether there is a causal relationship between the two is still unsatisfactory. Tumor-induced hydrocephalus may result from excessive CSF secretion or ventricular blockage. Studies have shown that AQP1 expression is strong and diffuse in

low-grade choroid plexus papillomas, but not in high-grade choroid plexus papillomas, which may be associated with the disappearance of papillary structures in high-grade tumors. And in low-grade choroid plexus papillomas, AQP1 expression had no significant polarity, no clear expression pattern, and each patient had a significant difference, and AQP1 expression on the normal choroid plexus had a significant polarity completely opposite, but this study was unattended (Longatti et al., 2006). Alternately, studies have concluded that CSF secretion is not significantly increased in choroid plexus papillomas (Sahar et al., 1980). These studies suggest that choroid plexus tumors may not be associated with CSF hypersecretion. Perhaps it is only the tumor that blocks the ventricles that leads to hydrocephalus. We expect future studies to overturn or prove this view.

In brief, when there are CPE tumors in the brain, changes in the CPE ion transport mechanism, CPE ciliary malformation, CP hyperplasia, abnormal CSF composition, etc., it will have a great impact on the normal absorption and excretion of CSF, CSF circulation, and finally lead to the occurrence of hydrocephalus.

Stroke

Stroke is a collective term for acute cerebrovascular diseases in traditional Chinese medicine. Stroke is a common brain disease in which brain tissue injury is caused by sudden rupture of blood vessels in the brain or by ischemia of the brain due to blockage of blood vessels. Many times, stroke is the result of cerebral ischemia and it is more common in the elderly. For children, arterial infection is the main cause of stroke (Fullerton et al., 2015, 2017). Irreversible damage to brain tissue by stroke can lead to the death of a large number of brain cells within a few minutes, which is a great damage to neurological function, and leads to disability (Hornung and Sievert, 2021). Stroke is currently one of the diseases of high concern all over the world. Since stroke is an acutely developing serious brain disease, patients must be sent to the hospital as soon as possible. For stroke patients, time is life (Davies and Delcourt, 2021).

At present, the etiology of stroke is mainly about cerebrovascular artery occlusion or cerebrovascular, thrombotic bleeding. For the generation of cerebral thrombosis, the most important and direct factor is cerebrovascular lesions such as atherosclerosis. Poor life habits such as smoking, obesity, and hypertension are important inducers of cerebral thrombosis and are positively correlated with the production of cerebral thrombosis (Ozturk, 2014). The CPE does not have direct contact with blood, abnormalities in the CPE do not appear to be directly related to thrombus, and abnormalities in the CPE do not appear to directly contribute to stroke. However, cases of an abnormal CPE are often present in hypertensive patients (Ruchoux et al., 1992) and hypertension is an important potential factor for stroke. At the same time, the CPE plays an important role in the mechanism of brain cell injury after stroke (Llovera et al., 2017). A profound understanding of these two points will greatly promote the treatment of stroke.

Hypertension is the most common chronic disease among the elderly, primarily essential hypertension. Studies have found that in spontaneously hypertensive mice, the CPE nuclei show heterogeneous chromatin. The number of Golgi apparatus of an abnormal CPE was higher, mitochondria were also more prevalent, microvilli were significantly lost, and basement membrane infoldings were reduced (Ruchoux et al., 1992). It was then found that the expression of the natriuretic peptide A receptor and cGMP production were reduced in the choroid plexus of spontaneously hypertensive rats (Zorad et al., 1998). Later studies of the CP in the brain of stroke-prone spontaneously hypertensive rats showed that activation of the MR/ENaCS pathway of the CP in stroke-prone spontaneously hypertensive rats is involved in the development of hypertension through elevation of CSF (Nakano et al., 2013). These results suggest that there should be similar changes in the CPE in hypertensive patients.

Although brain cell injury obviously occurs after stroke, in addition to ischemia itself, neuro inflammatory brain injury is more studied. There are many studies on the convening of inflammatory cells and the invasion of brain cells after stroke, but the role of the CPE as a BCSFB in this process is not particularly clear. Some studies have reported the specific accumulation of T cells in the peri-infarct cortex and detected T cells as the major population in the ipsilateral CP in mice as well as in post-stroke autopsy samples in humans (Llovera et al., 2017). *In vivo* cell tracking of photo activated T cells confirmed the migration of T cells from the CP to the peri-infarct cortex (Llovera et al., 2017). Neonatal stroke and TLR1/2 ligands have also been found to recruit myeloid cells through the choroid plexus *via* CX3CR1-CCR2 and context-specific manners (Rayasam et al., 2020). And the response of the CP to cortical stroke was achieved by up-regulating the gene expression of monocyte-derived macrophage transport mediators, as shown by the increase of monocyte-derived macrophages in the CP and CSF (Ge et al., 2017). A full understanding of the invasion of brain cells by neuro-inflammatory cells after stroke by the CPE can facilitate the development of corresponding therapeutic measures for the CPE in the future to reduce the damage to brain cells after stroke and greatly increase the sense of accomplishment of stroke treatment.

In conclusion, an abnormal CPE and hypertension often appear together, and hypertensive patients with an abnormal CPE are prone to stroke, and the causal relationship between an abnormal CPE and hypertension needs to be further demonstrated. Secondly, the CPE plays an important role in the mechanism of brain destruction by post-stroke inflammation. The CPE is involved in the accumulation of inflammatory cells in the post-stroke brain

and is a potential therapeutic target to reduce post-stroke brain injury.

Alzheimer's disease

Alzheimer's disease (AD) is the most common neurodegenerative disease of the central nervous system in elderly or pre-elderly patients. The language, emotion, cognition, and calculation of the elderly with AD can be devastated. At present, there is basically no possibility of cure, treatment is only to delay the disease; Alzheimer's disease is as irreversible as aging itself. The most striking abnormality in the patient's brain tissue is amyloid plaques with fibrillar tangles in neurons, mainly due to the deposition of amyloid beta and microtubule-associated tau. The current understanding of the etiology of AD is that protein polymers formed by excessive production or decreased clearance of beta-amyloid disrupt brain function. And hyperphosphorylation of tau affects the stabilization of neuronal skeleton microtubules and disrupts the normal function of neurons. But the understanding of why amyloid beta deposition with microtubule-associated tau occurs is not clear. Protein deposition and fibrillary tangles cannot be simply attributed to aging, because although the elderly have senile plaques, many of the elderly will not suffer from AD in their whole life. In recent years, the world has invested a lot in AD research, but still an effective means of cure has not been found. These results indicate that the pathogenesis of AD is complex and cannot be produced by impaired function of just one gene mutation. Recently, it was found that there is also β-like deposition in the CPE of AD patients, which may be associated with neuro inflammatory signals (Bolos et al., 2013). At the same time many have proposed that AD is associated with a decreased ability of the CPE to clear Aβ-like deposits (Serot et al., 2012). This indicates that there is a potential relationship between the occurrence of AD and the abnormality of the CP and aging (Serot et al., 2003; Bergen et al., 2015), but this aspect is often under appreciated.

The CPE acts as the main cell secreting CSF, but also secretes a variety of cytokines such as neurotrophic factors, which are also components in the CSF. Recently, a large number of studies have shown that aging and abnormalities in the CPE manifested as reduced tight junctions, reduced CSF secretion, and decreased ability to remove waste products (Brkic et al., 2015). Altered expression of several transporters such as lipoprotein receptor-related proteins 1 and 2 (LRP-1 and 2) are closely linked to AD (Balusu et al., 2016). Specifically, the expression of LRP-1 was down-regulated in AD patients compared with non-AD patients, and LRP-1 could promote the clearance of Aβ in AD patients (Serot et al., 1997).

Recently, it was found that choroid plexus annexin A5 levels were decreased in AD patients in the late stage of the disease, accompanied by increased Aβ levels and cell death, and that CSF annexin A5 levels were increased, indicating that annexin A5 is able to protect choroid plexus cells from Aβ-induced autophagic injury and apoptosis (Bartolome et al., 2020). It has also been proposed that the accumulation of tau and ApoE within the choroid plexus can increase the oligomerization rate of Aβ, which will impair the trafficking of tau, leading to pathological changes in AD (Raha-Chowdhury et al., 2019). These results indicate that Aβ deposition in the CPE of AD patients has a promoting effect on AD. According to the latest theory, AD is thought to be caused by chronic neuroinflammation. Recently, the CSF levels of the inflammatory cytokine TNF-α have been found to be significantly higher in AD patients than in non-AD patients, which may lead to the activation of matrix metalloproteinases (MMP) and lead to opening of the blood-cerebrospinal fluid barrier (Tarkowski et al., 2003). The above shows that the role of neuroinflammation on AD is not negligible.

In summary, several possible mechanisms of CPE abnormalities and AD are proposed: (1) Factors such as increased Aβ deposition in the CPE block the secretion of CSF, and the small flow of CSF substantially reduces the clearance of Aβ protein deposition in AD (Serot et al., 2012; Raha-Chowdhury et al., 2019). (2) The tight junctions of the CPE are greatly reduced, which increases the permeability of blood cerebrospinal fluid, allows inflammatory cells to enter, and causes an increase in the degree of chronic neuritis (Brkic et al., 2015). (3) Certain proteins (LRP-1) in the CPE can protect the CPE from harmful substances such as Aβ, but the reduced expression of this "beneficial protein" predicts the irreversible period (late) arrival of AD (Serot et al., 1997).

Parkinson's disease

Parkinson's disease (PD) is a common neurodegenerative disease. The main pathological findings are resting tremor and muscle rigidity, and slow movement. It is more common in the elderly, and there are rare cases in adolescents. The causes of PD are not well understood, and current research tends to include multiple factors of genetics and aging contributing to the pathogenesis (Elbaz et al., 2016). The current mainstream understanding of its pathogenesis is that reduced DA synthesis in PD patients leads to reduced striatal dopamine (DA) content causing a series of symptoms including resting tremor, so the most classical drug for the treatment of PD is DA itself (Starkstein et al., 2012; Fernandez-Sotos et al., 2019).

Although the cause of PD is unknown, there are many factors that have been studied in relation to the pathogenesis of PD, and the CPE is a relatively clear target. In Parkinson's disease, the ferroxidase ceruloplasmin (Cp) is oxidized and deaminated by pathological CSF (Barbariga et al., 2020). In studies of human primary choroid plexus epithelial cells, the oxidized/deamidated-Cp was found to be an *in vivo* target

for pathological CSF production, which mediates cell adhesion through isoDGR/integrin binding, transduces intracellular signals, and inhibits cell proliferation (Barbariga et al., 2020). There are also studies that have examined the ability of choroid plexus epithelial cell conditioned medium (CPEC-CM) alone or in combination with knockout serum (KS) to induce dopaminergic differentiation of human adipose-derived stem cells (hADSCs). The experimental results show that CPEC-CM and KS can act synergistically and significantly enhance the dopaminergic induction of hADSCs, which is exciting for the study of PD (Boroujeni et al., 2017).

The study of Parkinson-related gene Parkin co-regulated gene (PACRG) showed that PACRG was strongly expressed in the choroid plexus of the lateral ventricle, third ventricle, and fourth ventricle in mouse brains. Immunohistochemical analysis showed that PACRG is a component of ependymal cells and intraventricular cilia, and the results showed that PACRG is a component of ependymal cilia and plays an important role in the stability of the central nervous system (Wilson et al., 2009), This study showed a profound relationship between the CPE and PD. The CPE plays an irreplaceable role in the stabilization of the central nervous system. When an abnormal CPE occurs, it leads to a variety of serious diseases including PD. In the treatment of diseases such as PD, it is inevitable to think of whether the replacement of the CPE in patients will improve the disease, that is, choroid plexus transplantation. The experimental study of microencapsulated neonatal porcine choroid plexus cells in a non-human primate model of Parkinson's disease has emerged (Luo et al., 2013). However, in a recent follow-up study of PD patients for up to 104 weeks, no significant improvement in neurological function was observed in advanced PD patients treated with xenografted immune protective (sodium alginate-encapsulated) porcine choroid plexus cells (Mulroy et al., 2021). Although this result of is somewhat disappointing, it also reflects a problem that, for patients with advanced PD, it is not a simple change in the CPE function, but also accompanied by some irreversible changes in brain components (such as CSF components) and functions or mutations in genes, showing the complexity of PD.

In conclusion, the potential link between PD and the CPE has been confirmed by many studies so far (Wilson et al., 2009; Mulroy et al., 2021), but there is no clear answer. Alterations in CSF protein composition, possibly due to alterations in the CPE, contribute to the development of PD (Mulroy et al., 2021), but the causal relationship between the two needs to be further confirmed.

Multiple sclerosis

Multiple sclerosis (MS) is a disease in which the myelin sheath of central nervous cells is damaged resulting in a series of adverse consequences including visual problems, sensory disturbances, and muscle weakness, which occurs frequently in whites, and is more common in women than in men (Wilson et al., 2009). It is not fully understood for the etiology of MS, but there have been related theories proposed such as destruction of the immune system and invasion of inflammatory cells into the brain leading to demyelination of nerve cells (Baecher-Allan et al., 2018).

Certain parenchymal changes in the CPE in the brains of MS patients, including reduced expression of claudin-3, a tight junction selectively expressed by the CPE, which increases the permeability of BCSFB, which may be an important channel for MS inflammatory cells to invade into the brain (Ricigliano et al., 2021). Studies have shown that in the brains of patients with multiple sclerosis, there are a large number of HLA-DR immune stained T lymphocytes and surface myocytes in the CPE, indicating that the CPE is actively involved in antigen presentation (Baecher-Allan et al., 2018). Memory B cells present in the CSF can enter the brain through the blood-brain barrier and BCSFB. Recently, a team has illustrated the important barrier role of BCSFB as a harmful activated B cell into the brain by screening the transcriptome of intrathecal B cells from MS patients through a series of cytokines/chemokines that mediate B cell diapedesis including qRT-PCR (Haas et al., 2020), while the permeability change of BCSFB is due to a series of changes including changes in the CPE. More hypoxia of CPE in the brains of MS patients than in normal subjects illustrates that the secretion of CPE undergoes non-negligible changes under MS pathological conditions (Rodriguez-Lorenzo et al., 2020).

To conclude, under the influence of peripheral neuro inflammation, the CPE undergoes changes including reduced expression of claudin-3, which leads to increased BCSFB permeability, resulting in accelerated entry of inflammatory cells such as leukocytes into the brain to accelerate their damage, and the CPE is also involved in the process of these immune responses including antigen presentation (Ricigliano et al., 2021). The above is sufficient to illustrate that the CPE plays a non-negligible role in MS (Figure 2).

Treatment

Through the above description, we can understand the key role of the CPE on the occurrence of neurological diseases. Nowadays, there are also many therapeutic measures targeting the CPE to treat neurological diseases. Some popular related therapeutic measures will be summarized below, in hopes of bringing us some inspiration.

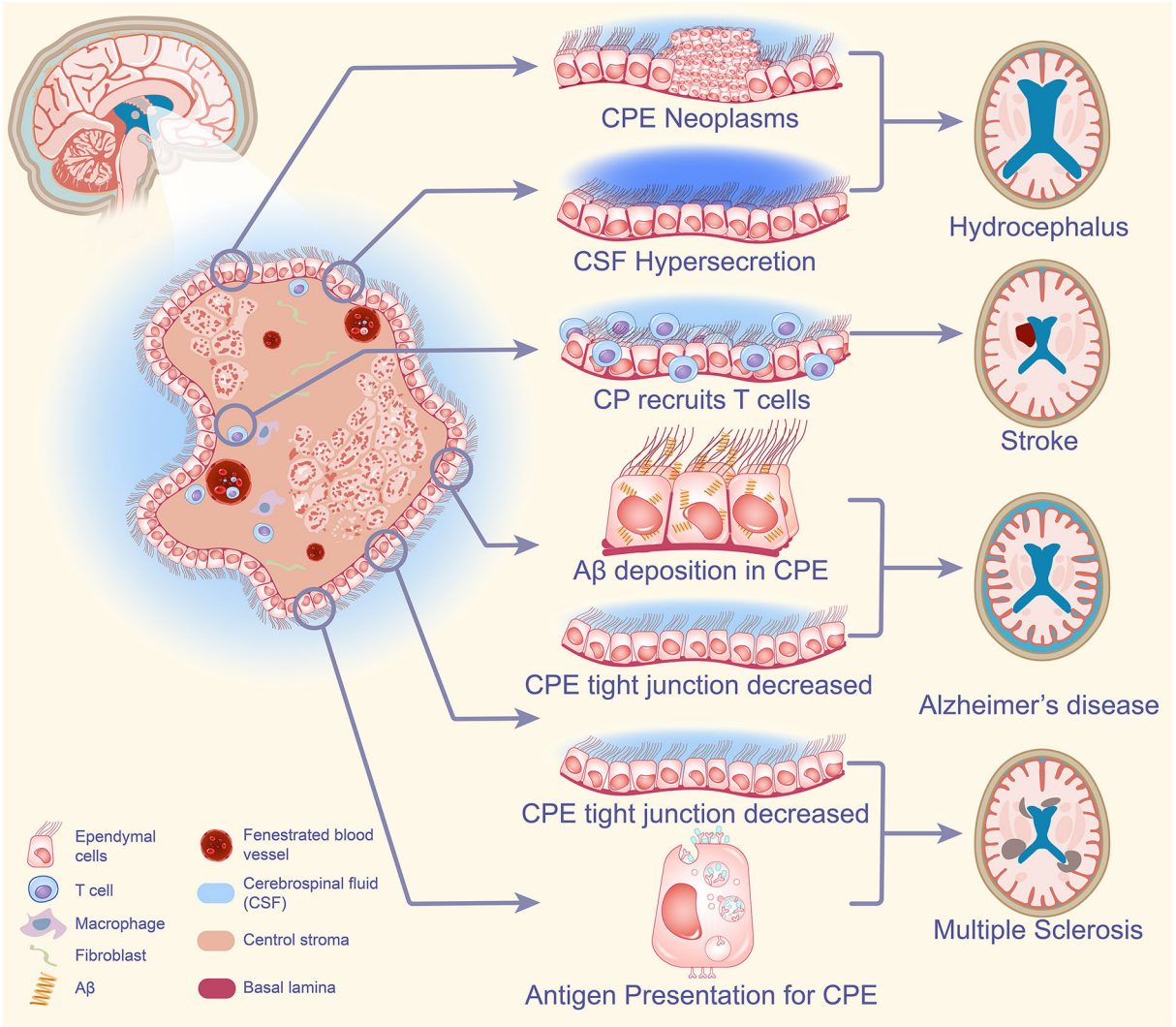

FIGURE 2
CPE-based neurological pathogenesis. When CPE tumors are present in the brain, excessive CSF secretion can have a great impact on the normal absorption and excretion of CSF, CSF circulation, and ultimately the development of hydrocephalus. The CPE is involved in the accumulation of inflammatory cells in the brain after stroke and plays an important role in the destruction of brain mechanisms by post-stroke inflammation. Increased Aβ deposition in CPE blocks the secretion of CSF, and the small flow of CSF significantly reduces the clearance of Aβ protein deposition in AD, while the reduction of tight junctions in CPE increases the permeability of blood cerebrospinal fluid, causing an increase in the degree of chronic neuritis, leading to the development of AD. Under the influence of peripheral neuroinflammation, the CPE changes and cellular tight junctions decrease, resulting in increased permeability of BCSFB and accelerated entry of inflammatory cells such as leukocytes into the brain to accelerate their injury. The CPE is also involved in the immune response process including antigen presentation and plays an important role in the pathogenesis of MS. CPE, choroid plexus epithelium; CSF, cerebrospinal fluid; Aβ, amyloid-β; AD, Alzheimer's disease; BCSFB, blood-cerebrospinal fluid barrier; MS, multiple sclerosis.

Immune therapy

In neurological diseases, the purpose of implementing immunotherapy is to intervene in certain immune links so as to prevent disease progression in autoimmune diseases such as MS. Interferon, the earliest discovered cytokine, is a glycoprotein produced by monocytes and lymphocytes and has a wide range of antiviral effects. At the same time, as the most first-line drug for the treatment of MS, its immunomodulatory effect is gradually moving toward the center. Interferon-α (IFN-α) and interferon-γ (IFN-γ) were used to treat MS in the earliest clinical trials, which significantly reduced the recurrence rate of patients and achieved preliminary results. But it was eliminated due to its serious side effects (Knobler

et al., 1984; Camenga et al., 1986; Panitch, 1987; Durelli et al., 1994).

Finally, the low side effects and significant efficacy of IFN-β make it the most popular drug for the treatment of MS. As the first immune modulator approved for the treatment of relapsing remitting MS, it is divided into three different IFN-β formulations for its use, including "low-dose" IFN-β1a (Avonex) and "high-dose" IFN-β1a (Rebif22/44) or IFN-β1b (Betaferon, Betaseron). These agents are considered first-line disease modifiers for the treatment of MS (Kieseier, 2011). IFN-β treatment results in reduced magnetic resonance imaging (MRI) lesion activity, reduced relapse rates, reduced odds of brain atrophy and progression of persistent disability in MS patients. The beneficial effect of interferon-β (IFN-β) is thought to stem from its change in the environment from inflammatory regulation to regulation at several levels of immune cell activation, while preventing immune cell migration through the blood-brain barrier to the central nervous system. The pleiotropic effects of IFN-β on the peripheral immune system mainly include the reduction of pathogenic Th1 and Th17 cells and the increase of IL-10-producing Tregs *via* the JAK-STAT signaling pathway (Furber et al., 2017; Maimaitijiang et al., 2019; Ayatollahi et al., 2020). In addition, IFN-β reduces $CD27^+$ memory B cells and increases IL-10-producing B cells, and IFN-β may downregulate the ability of adhesion molecules to inhibit pro-inflammatory cell entry into the CNS. These are sufficient to show that the therapeutic effect of IFN-β on the disease is multifaceted and effective.

As a CSF-producing organ, the immune monitoring of the CP on the brain and the repair after injury have also been studied a lot recently. Epithelial v-like antigen (EVA) found in mouse models is expressed in the CPE and $CD4^+$ T lymphocytes and regulates $CD4^+$ T lymphocyte adhesion to the CPE *in vitro* (Wojcik et al., 2011). Detecting the migration of T lymphocytes into the brain and the CP after enterotoxin-induced systemic immune activation showed that T lymphocytes preferentially migrated to the CP rather than to the brain (Petito and Adkins, 2005), showing a portal effect of the CP on T cells, which has been discussed above. Moreover, immune cells in the CP appear to communicate with epithelial cells through pannexin-1 channels expressed by epithelial cells in the CP, and excitedly, *in vitro* studies have shown that the expression of immune cell trafficking determinants in choroid plexus epithelium is specifically induced by IFN-γ (Kunis et al., 2013). *In vivo*, IFN-γ-dependent signaling controls transport mechanisms through the choroid plexus; IFN-γ receptor knockout mice have reduced levels of T cells and monocytes in the cerebrospinal fluid, and recovery after spinal cord injury is also impaired in mice. Moreover, reduced expression of choroid plexus trafficking molecules positively correlated with decreased $CD4^+$ T cells in the choroid plexus and cerebrospinal fluid of IFN-γ receptor knockout mice. Similar effects were found in bone marrow chimeric mice lacking IFN-γ receptors in the central nervous system. Moreover, the experimental results also showed that the expression of TNF-α and IFN-γ receptors was mutually controlled by both through the CP (Kunis et al., 2013). This shows that for immunotherapy of MS, the exertion of a part of the effect of interferon depends on the CP. In other words, if the CP has some problems, it may affect the efficacy of interferon.

Therefore, for MS, an autoimmune disease, specific blockade of IFN-γ signaling pathway in the CP (add IFN-γ receptor antagonist or anti-IFN-γ antibody) may improve the development process of MS (Kunis et al., 2013). However, blocking signaling will lead to impaired recruitment of immune cells in the brain, which may lead to difficult recovery of inflammation in patients with CNS inflammation, so the indications for the disease require further study.

Gene therapy

Gene therapy can treat diseases by exogenous input of genes (DNA, RNA) or intervention of genes resulting in their inability to translate and delete this gene normally, or manual editing of genes to delete the wrong gene and introduce normal genes. It has potential therapeutic value for congenital diseases. How to deliver gene modification-related small molecules or genes themselves for gene therapy is one of the major problems that plague gene therapy. There are now modes of viral delivery, non-viral delivery as well as cell delivery. Direct delivery was also often used early in the study, but this approach is clearly difficult to apply to humans. For targeted CP for gene therapy, the mode of its delivery has excitedly seen great possibilities in the current study.

Six different serotypes of adeno-associated virus (AAV) vectors (AAV2/1, AAV2/5, AAV2/8, AAV2/9, AAV2-BR1, and AAV2-PHP.EB) and lentiviruses have been injected into adult mice, respectively. It was found that AAV2/5 and AAV2/8 were significantly infected in the CP, and AAV2/1 was co-infected with ependymal cells in the CP. Transthyretin immunohistochemical staining indicates that AAV2/5 has a strong infectious capacity for the CPE and can act as a specific viral vector for the CP (Chen et al., 2020). While phages target epidermal growth factor, they are able to enter choroidal epithelial cells cultured *in vitro*, as tissue explants, or into viable choroidal epithelial cells by intraventricular injection. Gene expression in the choroid plexus and ependymal epithelium was detected by immunohistochemistry and non-invasive imaging when the phage genome was reconstituted into genes containing green fluorescent protein under the control of the cytomegalovirus promoter. Experiments have shown that recombinant ligand-mediated gene delivery is a feasible strategy that can improve the specificity of gene delivery to the central nervous system, and the CP is an important vector for this process (Gonzalez et al., 2010). Studies in which recombinant

AAV serotype 5-green fluorescent protein was injected into the ventricles of pregnant mice also demonstrated that the CPE could act as a specific receptor for AAV5, with a sustained role (Haddad et al., 2013). At present, not many gene therapy studies have been conducted in the CP. Intracerebroventricular injection of adeno-associated virus type 5 (AAV5) containing reduced-size human ATP7A and copper chloride into neonatal mottled-brindled mice successfully rescued mice and greatly improved mouse survival. This demonstrates the important clinical value of gene therapy *via* the CP in the treatment of Menkes' disease (Donsante et al., 2011).

For the methods of virus administration in gene therapy, some articles have reviewed this (Jang and Lehtinen, 2022), and several methods of intravenous administration such as ultrasound-guided intrauterine vena cava administration have been proposed. The hazards of adenovirus use are also described in this article. In order to avoid the immune response produced by AAV, we can design a short DNA oligonucleotide that antagonizes toll-like receptor 9 (TLR9) activation and inserts it into the vector genome. We know that in AAVs, the vector genome can activate TLR9, TLR9 can recognize exogenous DNA (Chan et al., 2021), so the design can reduce innate immunity and T cell response.

In summary, targeting the CP for gene therapy is feasible. We can target and transmit certain effective therapeutic genes through the specific recognition of the CP by AAV5, which has very important clinical significance for neurodegenerative diseases of the brain or some refractory diseases. Of course, whether gene therapy by targeting the CP with AAV5 has significant side effects remains to be examined. Further research is needed on the injection of AAV5 into the brain itself. And what brain diseases do this gene therapy work? Which do not? These questions need to be studied more deeply.

Choroid plexus cauterization

As the primary site of CSF production, the role of the CP is evident. However, for some conditions, such as communicating hydrocephalus, the balance between CSF secretion and absorption is broken so that CSF retention in the ventricles results in hydrocephalus. For its treatment, it is natural to start from the source, that is, to destroy the choroid plexus. However, as an important organ of the human body, there are indeed many unknown factors for directly burning or removing it. In 1910, when urologist Victor Darwin Lespinasse performed the first choroidectomy, the history of choroid plexus cauterization (CPC) began (Grant, 1996).

Theoretically, hydrocephalus should be relieved after CPC, however the clinical results of single CPC are not consistent with the theory. The largest single series of endoscopic CPC in history served as 82 patients in a stand-alone procedure, of which only 29 had a successful procedure (Pople and Ettles, 1995). The therapeutic effect of CPC alone is not as good as first thought, thus, the treatment of hydrocephalus with CPC alone has been basically eliminated. Recently, with the rise of endoscopic third ventriculostomy with CPC (ETV/CPC), CPC has been better applied in clinical treatment. Of course this is only 20 years (Warf, 2005). Therefore, it should be noted that the CPC in this paper is all part of ETV/CPC, rather than CPC alone. The probability of success of the ETV/CPC procedure was not inferior to that of ETV alone or CPC alone (Warf, 2005). The obvious benefit of ETV/CPC is that it does not depend on the shunt, which is one of the reasons for choosing ETV/CPC. For the selection of surgical subjects, it mainly depends on the age of the patient and the etiology. Patients younger than 1 year of age, patients with post-infectious hydrocephalus, and patients with partial or incomplete CPC were considered not eligible for ETV/CPC (Dewan and Naftel, 2017). Scar predicted ETV/CPC failure (Warf and Kulkarni, 2010; Stone and Warf, 2014), which suggests that CPC may not play a full role in the presence of a scar, is not effective in reducing CSF secretion but highlights the important role-played by ETV in ETV/CPC. For the question of the degree of CPC in ETV/CPC, there are studies indicating that the CP must be completely inactivated to achieve the best surgical results (Dewan and Naftel, 2017; Fallah et al., 2017). This may be due to the presence of compensatory CSF output in the CP; that is, a partially inactivated CP may lead to more CSF secretion by the remaining CP, resulting in poor surgical results. As an important part of the brain, whether a devastating blow to the CP can affect the patient's cognitive ability and other abilities after surgery has not been described, and further follow-up studies are needed to prove the utility of ETV/CPC and whether there are long-term side effects.

Overall, CPC now has a place in the treatment of hydrocephalus, and future functional studies that may be more precise for the CP may elicit the potential dangers of ETV/CPC surgery. The CP is an important part of CSF secretion by the brain and an important part in the pathogenesis of neurodegenerative diseases, yet it is incredible if the CP is directly burned so that it loses all relevant functions without minor side effects or even significant side effects. Choroid plexus cauterization inevitably results in abnormal recruitment of leukocytes by the brain, which will have an impact on the recovery of brain inflammation. As CSF-producing organs, the composition of CSF will change after inactivation of the choroid plexus, which will have a serious impact on the brain microenvironment, and will this increase the risk of other brain diseases such as AD in patients after choroid plexus burn surgery? It is hoped that future studies will answer if we have underestimated the compensatory function of the brain or not.

Choroid plexus transplantation

Neurotrophic factors have shown good therapeutic effects for CNS diseases, but intravenous injection cannot be achieved due to the blood-brain barrier. In clinical practice, the supply of neurotrophic factors can only be used for intraventricular infusion using the instrument. This means that repeated injections are needed to maintain efficacy, and the implementation process is not convenient and simple, and there is even a risk of infection. Another idea is to implant genetically engineered cells to produce specific trophic factors. Although the use of this immortalized cell line can avoid many limitations with the form of mechanical delivery, the applicability of the vector, the stability of protein expression, and potential safety issues make the use of transgenic cells theoretically challenging. The CP, as an important component of CSF secretion, has a protective effect on neurons (Borlongan et al., 2004a). If a normal CP can be transplanted into the damaged brain site to allow the CP to secrete neurotrophic factors normally, it theoretically would have a certain therapeutic effect on the disease. Excitingly, the relevant studies conducted so far fully support the view. Choroid plexus transplantation has yielded exciting results in stroke, PD, and ischemic brain injury (Borlongan et al., 2004b; Emerich et al., 2004; Luo et al., 2013; Eslami et al., 2021).

The transplantation experiment of porcine choroid plexus brain has satisfactorily illustrated that choroid plexus transplantation has a significant protective effect on the structure and function of the brain in stroke animals, which coincides with our expectations (Borlongan et al., 2004b). In this study, the CP from neonatal pigs was artificially encapsulated in alginate microcapsules for neuroprotective studies *in vitro* and *in vivo*. Parallel *in vivo* studies have shown that CP transplantation improves behavioral performance, reduces infarct volume, and encapsulates microcapsules more significantly, even if neurotrophic factors produced by an encapsulated CP need to cross obstacles to play an important role. This is closely related to the ability of microcapsules to effectively prevent rejection of an encapsulated CP (Borlongan et al., 2004b). Future applications of choroid plexus transplantation in stroke patients should pay more attention to the choice of transplantation site and the mode of choroid plexus transplantation, and we can do more research to find if there is a more effective treatment than encapsulation in alginate microcapsules.

Some studies have used neonatal porcine choroid plexus to transplant into PD rhesus monkeys, and because the cerebrospinal fluid secreted by the CP contains various neurotrophic and neuroprotective factors, the researchers hope that choroid plexus transplantation can improve parkinsonian symptoms in immunosuppressed rhesus monkeys treated with MPTP (1-methyl-4-phenyl-1,2,3,6-tetrahydropyridine). The findings were unequivocal, with a significant improvement in neurological function in MPTP-treated monkeys within 6 months after transplantation compared to monkeys implanted with empty capsules or subjected to sham surgery. Improvements in neurological scores were accompanied by a corresponding improvement in apomorphine-induced circling behavior and increased striatal tyrosine hydroxylase (TH) staining, all of which indicate that choroid plexus transplantation plays an important role in the treatment of PD monkeys. Because the caudate nucleus of the striatum is close to the ventricles and can be easily identified from computed tomography (CT) cross-sectional images, the caudate nucleus of the striatum was selected as the transplantation site (Luo et al., 2013). Experiments demonstrated that implanting a CP known to secrete many neuroprotective and neuro repair factors into the injured site of a primate model of PD restored striatal nerve fiber networks and improved neuro behavior in animals. The results are consistent with previous studies demonstrating the neuro repair function exhibited by a porcine CP in various animal models of neurodegenerative diseases. This showed a potential value of choroid plexus transplantation for the treatment of PD in primates.

Researchers examined the ability of a cultured CPE to protect against ischemic brain injury when transplanted into rat CSF. In the experiment, the rat's middle cerebral artery was transiently occluded, and then the researchers injected an artificially cultured CPE into the fourth ventricle. Injection significantly reduced the neurological deficit and infarct volume within 24 h. These included reduced numbers of apoptotic and inflammatory cells in the brain, upregulated mRNA expression of the anti-apoptotic effector camp response element-binding protein, and downregulated production of proinflammatory factors such as interleukin-1β and inducible nitric oxide lyase (Matsumoto et al., 2010). It is worth noting that the injected CPEs in the experiment were located in the ventricle and on the surface of the brain and were not ischemic foci, which indeed indicates that they can play their role in the CSF by releasing diffusible neuroprotective factors. It directly illustrates that transplantation of CPEs *via* CSF is a potential new approach to protect against ischemic brain injury.

In conclusion, choroid plexus transplantation has demonstrated good therapeutic effects in many models of inflammatory diseases or neurodegenerative diseases of the brain (Borlongan et al., 2004b; Luo et al., 2013). Transplantation of porcine choroid plexus encapsulated with special containers such as alginate microcapsules into the affected brain does improve pre-existing neuroinflammation (Borlongan et al., 2004b; Emerich et al., 2004). However, the target object and mode of transplantation can be more perfect, and the indications of transplantation need further study (Figure 3).

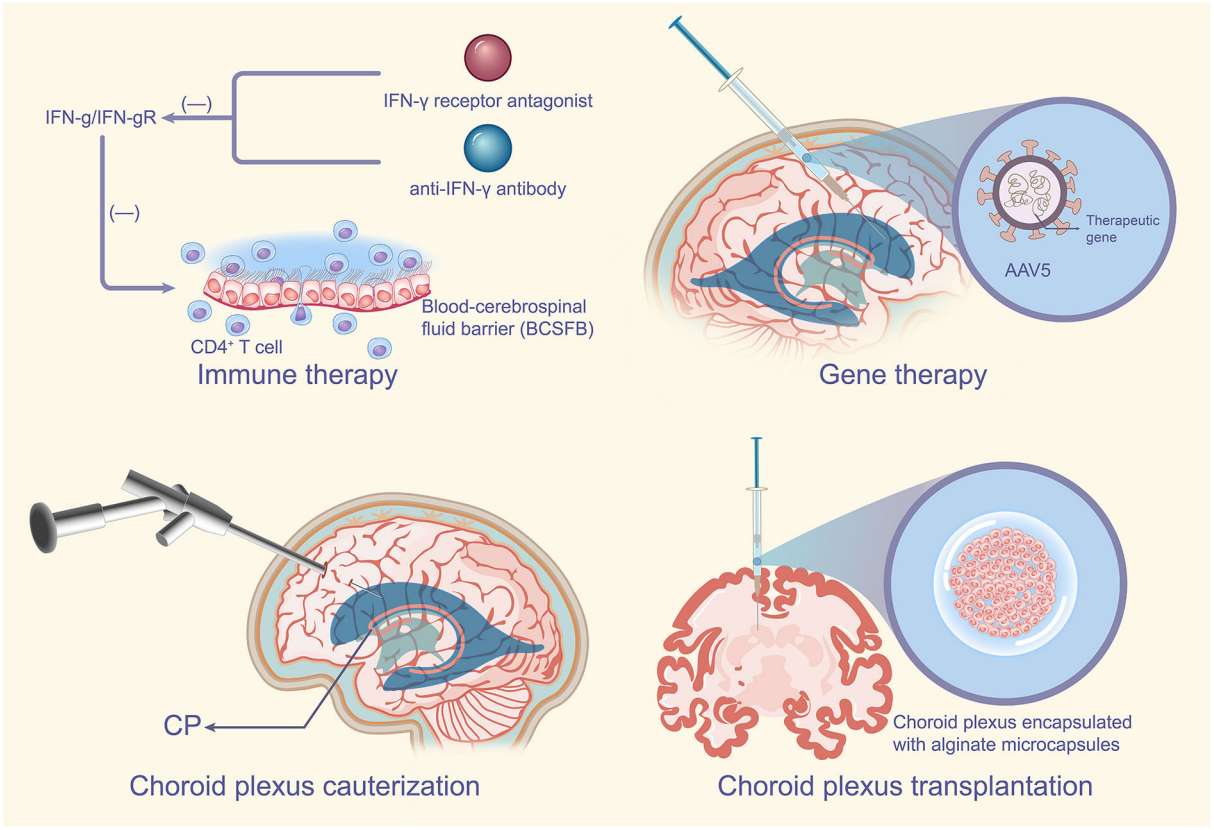

FIGURE 3
CPE-based therapeutic measures. For autoimmune disease MS, specific blockade of the IFN-γ signaling pathway in the CP such as the addition of IFN-γ receptor antagonists or anti-IFN-γ antibodies may improve the development of MS. Targeted delivery of certain effective therapeutic genes through the specific recognition of the CP by AAV5 has very important therapeutic implications for neurodegenerative diseases of the brain or some refractory diseases. CPC can reduce CSF secretion by the CP, which has no doubts about the therapeutic significance for the CP, of course CPC is usually used in combination with ETV. Transplantation of the choroid plexus encapsulated in special containers such as alginate microcapsules into the affected brain can improve pre-existing neuroinflammation with potential implications for the treatment of PD. MS, multiple sclerosis; IFN-γ, interferon-γ; CP, choroid plexus; AAV5, adeno-associated virus type 5; CPC, choroid plexus cauterization; CSF, cerebrospinal fluid; ETV, endoscopic third ventriculostomy; PD, Parkinson's disease.

Conclusions

As the main site of CSF secretion in the brain, the CP is also involved in the regulation of the neurogenesis circadian clock, the transmission of inflammatory signals and the important role in atypical neurodevelopmental processes. The function of the CP has been described by many studies, and the tight junctions on it are important structures that constitute the blood-cerebrospinal fluid barrier.

CSF secreted by the CP plays a role in regulating neurodevelopment and nourishing nerves, and CSF can provide a stable environment for the brain. The description of accelerated atrophy of the CP in stroke, multiple sclerosis, schizophrenia, and other central nervous system diseases illustrates that atrophy of the CP is associated with CNS diseases, and the relationship between ciliary abnormalities on the CPE and hydrocephalus is also illustrated. There must be a close link between CP pathology and cognitive and neurodegenerative diseases. The role of the CP in preventing neurological diseases includes maintaining tight junctions in the CPE to maintain the blood-cerebrospinal fluid barrier, promoting CSF circulation as well as promoting the excretion of waste products from CSF.

Therapeutic modalities with the CP as a therapeutic target include immunotherapy, gene therapy, choroid plexus cauterization, as well as choroid plexus transplantation. The above treatment modalities have shown great value for the treatment of neurological diseases and are worthy of further study. The author believes that the CP can be used as a good viral vector for the purpose of gene therapy. Due to its great advantages of crossing the blood-brain barrier, the author believes that if this is used rationally, it may bring unexpected breakthroughs in the treatment of neurological diseases.

The profound understanding of the CP enables us to view neurological diseases from a new perspective that is CP-centered, even if the etiology of these diseases is not single. As a CP that produces the ecological environment in the brain, it is not too much to pay attention to how it is actually.

Author contributions

YC participated in the drawing of the figure of the article. ZZ, YC, JL, and YW participated in the collection and revision of the article. ZL participated in the polishing of the article. All authors read and approved the final manuscript.

Funding

This work was supported by National Natural Science Foundation of China (No. 82171347) and the Students Innovations in Central South University of China (Nos. 20210033020055, 20210033020036, and 20210033020044).

Acknowledgments

I would like to express my gratitude to all those who helped us during the writing of this manuscript and thanks to all the peer reviewers for their opinions and suggestions.

Conflict of interest

The authors declare that the research was conducted in the absence of any commercial or financial relationships that could be construed as a potential conflict of interest.

The reviewer QC declared a past co-authorship with the author GX to the handling editor.

Publisher's note

References

Ayatollahi, S. A., Ghafouri-Fard, S., Taheri, M., and Noroozi, R. (2020). The efficacy of interferon-beta therapy in multiple sclerosis patients: investigation of the RORA gene as a predictive biomarker. *Pharmacogenom. J.* 20, 271–276. doi: 10.1038/s41397-019-0114-0

Baecher-Allan, C., Kaskow, B. J., and Weiner, H. L. (2018). Multiple Sclerosis: mechanisms and immunotherapy. *Neuron*. 97, 742–768. doi: 10.1016/j.neuron.2018.01.021

Balusu, S., Brkic, M., Libert, C., and Vandenbroucke, R. E. (2016). The choroid plexus-cerebrospinal fluid interface in Alzheimer's disease: more than just a barrier. *Neural. Regen. Res.* 11, 534–537. doi: 10.4103/1673-5374.180372

Barbariga, M., Zanardi, A., Curnis, F., Conti, A., Boselli, D., and et al. (2020). S, et al. Ceruloplasmin oxidized and deamidated by Parkinson's disease cerebrospinal fluid induces epithelial cells proliferation arrest and apoptosis. *Sci. Rep*. 10, 15507. doi: 10.1038/s41598-020-72447-z

Bartolome, F., Krzyzanowska, A., de la Cueva, M., Pascual, C., Antequera, D., Spuch, C., et al. (2020). Annexin A5 prevents amyloid-beta-induced toxicity in choroid plexus: implication for Alzheimer's disease. *Sci. Rep*. 10, 9391. doi: 10.1038/s41598-020-66177-5

Baruch, K., Deczkowska, A., David, E., Castellano, J. M., Miller, O., Kertser, A., et al. (2014). Aging-induced type I interferon response at the choroid plexus negatively affects brain function. *Science*. 346, 89–93. doi: 10.1126/science.1252945

Baruch, K., Ron-Harel, N., Gal, H., Deczkowska, A., Shifrut, E., Ndifon, W., et al. (2013). CNS-specific immunity at the choroid plexus shifts toward destructive Th2 inflammation in brain aging. *Proc. Natl. Acad. Sci. USA*. 110, 2264–2269. doi: 10.1073/pnas.1211270110

Baruch, K., and Schwartz, M. (2013). CNS-specific T cells shape brain function *via* the choroid plexus. *Brain Behav. Immun*. 34, 11–16. doi: 10.1016/j.bbi.2013.04.002

Bergen, A. A., Kaing, S., Ten Brink, J. B., Gorgels, T. G., and Janssen, S. F. (2015). Gene expression and functional annotation of human choroid plexus epithelium failure in Alzheimer's disease. *BMC Genom*. 16, 956. doi: 10.1186/s12864-015-2159-z

Bolos, M., Spuch, C., Ordonez-Gutierrez, L., Wandosell, F., Ferrer, I., Carro, E., et al. (2013). Neurogenic effects of beta-amyloid in the choroid plexus epithelial cells in Alzheimer's disease. *Cell. Mol. Life. Sci*. 70, 2787–2797. doi: 10.1007/s00018-013-1300-x

Borlongan, C. V., Skinner, S. J., Geaney, M., Vasconcellos, A. V., Elliott, R. B., Emerich, D. F., et al. (2004a). CNS grafts of rat choroid plexus protect against cerebral ischemia in adult rats. *Neuroreport*. 15, 1543–1547. doi: 10.1097/01.wnr.0000133298.84901.cf

Borlongan, C. V., Skinner, S. J., Geaney, M., Vasconcellos, A. V., Elliott, R. B., Emerich, D. F., et al. (2004b). Intracerebral transplantation of porcine choroid plexus provides structural and functional neuroprotection in a rodent model of stroke. *Stroke*. 35, 2206–2210. doi: 10.1161/01.STR.0000138954.25825.0b

Boroujeni, M. E., Gardaneh, M., Shahriari, M. H., Aliaghaei, A., and Hasani, S. (2017). Synergy between choroid plexus epithelial cell-conditioned medium and knockout serum replacement converts human adipose-derived stem cells to dopamine-secreting neurons. *Rejuven. Res*. 20, 309–319. doi: 10.1089/rej.2016.1887

Bouzinova, E. V., Praetorius, J., Virkki, L. V., Nielsen, S., Boron, W. F., Aalkjaer, C., et al. (2005). Na+-dependent HCO3- uptake into the rat choroid plexus epithelium is partially DIDS sensitive. *Am. J. Physiol. Cell. Physiol*. 289, C1448–C1456. doi: 10.1152/ajpcell.00313.2005

Brkic, M., Balusu, S., Van Wonterghem, E., Gorle, N., Benilova, I., Kremer, A., et al. (2015). Amyloid beta oligomers disrupt blood-CSF barrier integrity by activating matrix metalloproteinases. *J. Neurosci*. 35, 12766–12778. doi: 10.1523/JNEUROSCI.0006-15.2015

Camenga, D. L., Johnson, K. P., Alter, M., Engelhardt, C. D., Fishman, P. S., Greenstein, J. I., et al. (1986). Systemic recombinant alpha-2 interferon therapy in relapsing multiple sclerosis. *Arch. Neurol*. 43, 1239–1246. doi: 10.1001/archneur.1986.00520120023011

Carrithers, M. D., Visintin, I., Kang, S. J., and Janeway, C. A. (2000). Differential adhesion molecule requirements for immune surveillance and inflammatory recruitment. *Brain* 123, 1092–1101. doi: 10.1093/brain/123.6.1092

Chan, K. Y., Wang, W., Wu, J. J., Liu, L., Theodoratou, E., Car, J., et al. (2013). Epidemiology of Alzheimer's disease and other forms of dementia in China, 1990-2010: a systematic review and analysis. *Lancet* 381, 2016–2023. doi: 10.1016/S0140-6736(13)60221-4

Chan, Y. K., Wang, S. K., Chu, C. J., Copland, D. A., Letizia, A. J., Costa Verdera, H., et al. (2021). Engineering adeno-associated viral vectors to evade innate immune and inflammatory responses. *Sci. Transl. Med.* 13 doi: 10.1126/scitranslmed.abd3438

Chen, X., He, Y., Tian, Y., Wang, Y., Wu, Z., Lan, T., et al. (2020). Different Serotypes of Adeno-Associated Virus Vector- and Lentivirus-Mediated Tropism in Choroid Plexus by Intracerebroventricular Delivery. *Hum. Gene. Ther.* 31, 440–447. doi: 10.1089/hum.2019.300

Chodobski, A., Ghersi-Egea, J. F., Preston-Kennedy, J., Redzic, Z., Strazielle, N., Szmydynger-Chodobska, J., et al. (2019). The legacy of Malcolm Beverley Segal (1937-2019) on the science and fields concerned with choroid plexus and cerebrospinal fluid physiology. *Fluids Barriers Cns.* 16. doi: 10.1186/s12987-019-0161-6

Christensen, H. L., Paunescu, T. G., Matchkov, V., Barbuskaite, D., Brown, D., Damkier, H. H., et al. (2017). The V-ATPase is expressed in the choroid plexus and mediates cAMP-induced intracellular pH alterations. *Physiol. Rep.* 5 doi: 10.14814/phy2.13072

Cserr, H. F. (1971). Physiology of the choroid plexus. *Physiol. Rev.* 51, 273–311. doi: 10.1152/physrev.1971.51.2.273

Damkier, H. H., Brown, P. D., and Praetorius, J. (2013). Cerebrospinal fluid secretion by the choroid plexus. *Physiol. Rev.* 93, 1847–1892. doi: 10.1152/physrev.00004.2013

Damkier, H. H., Christensen, H. L., Christensen, I. B., Wu, Q., Fenton, R. A., Praetorius, J., et al. (2018). The murine choroid plexus epithelium expresses the 2Cl(-)/H+ exchanger ClC-7 and Na+/H+ exchanger NHE6 in the luminal membrane domain. *Am. J. Physiol-Cell. Ph.* 314, C439–C48. doi: 10.1152/ajpcell.00145.2017

Damkier, H. H., Prasad, V., Hubner, C. A., and Praetorius, J. (2009). Nhe1 is a luminal Na+/H+ exchanger in mouse choroid plexus and is targeted to the basolateral membrane in Ncbe/Nbcn2-null mice. *Am. J. Physiol. Cell. Physiol.* 296, C1291–C1300. doi: 10.1152/ajpcell.00062.2009

Davies, L., and Delcourt, C. (2021). Current approach to acute stroke management. *Intern. Med. J.* 51, 481–487. doi: 10.1111/imj.15273

Davis, J. D., Stern, R. A., and Flashman, L. A. (2003). Cognitive and neuropsychiatric aspects of subclinical hypothyroidism: significance in the elderly. *Curr. Psychiatry Rep.* 5, 384–390. doi: 10.1007/s11920-003-0073-6

Dewan, M. C., and Naftel, R. P. (2017). The Global Rise of Endoscopic Third Ventriculostomy with Choroid Plexus Cauterization in Pediatric Hydrocephalus. *Pediatr. Neurosurg.* 52, 401–408. doi: 10.1159/000452809

Donsante, A., Yi, L., Zerfas, P. M., Brinster, L. R., Sullivan, P., Goldstein, D. S., et al. (2011). ATP7A gene addition to the choroid plexus results in long-term rescue of the lethal copper transport defect in a Menkes disease mouse model. *Mol. Ther.* 19, 2114–2123. doi: 10.1038/mt.2011.143

Durelli, L., Bongioanni, M. R., Cavallo, R., Ferrero, B., Ferri, R., Ferrio, M. F., et al. (1994). Chronic systemic high-dose recombinant interferon alfa-2a reduces exacerbation rate, MRI signs of disease activity, and lymphocyte interferon gamma production in relapsing-remitting multiple sclerosis. *Neurology.* 44, 406–413. doi: 10.1212/WNL.44.3_Part_1.406

Elbaz, A., Carcaillon, L., Kab, S., and Moisan, F. (2016). Epidemiology of Parkinson's disease. *Rev. Neurol. (Paris).* 172, 14–26. doi: 10.1016/j.neurol.2015.09.012

Emerich, D. F., Vasconcellos, A. V., Elliott, R. B., Skinner, S. J., and Borlongan, C. V. (2004). The choroid plexus: function, pathology and therapeutic potential of its transplantation. *Expert. Opin. Biol. Ther.* 4, 1191–1201. doi: 10.1517/14712598.4.8.1191

Eslami, M., Oryan, S. H., Rahnema, M., and Bigdeli, M. R. (2021). Neuroprotective effects of normobaric hyperoxia and transplantation of encapsulated choroid plexus epithelial cells on the focal brain ischemia. *Cell. J.* 23, 303–312. doi: 10.22074/cellj.2021.7204

Fallah, A., Weil, A. G., Juraschka, K., Ibrahim, G. M., Wang, A. C., Crevier, L., et al. (2017). The importance of extent of choroid plexus cauterization in addition to endoscopic third ventriculostomy for infantile hydrocephalus: a retrospective North American observational study using propensity score-adjusted analysis. *J. Neurosurg. Pediatr.* 20, 503–510. doi: 10.3171/2017.7.PEDS16379

Fernandez-Sotos, P., Calleja, P. L. A., Lozano-Vicario, L., and Garcia-Tercero, E. (2019). del Yerro-Alvarez MJ, Lopez-Alvarez J. Posterior reversible leukoencephalopathy syndrome in a patient with Parkinson's disease and initial psychiatric symptoms: a complex clinical presentation. *Rev. Neurologia.* 68, 426–430. doi: 10.33588/rn.6810.2018435

Fullerton, H. J., Hills, N. K., Elkind, M. S. V., Dowling, M. M., Wintermark, M., Glaser, C. A., et al. (2015). Infection, vaccination, and childhood arterial ischemic stroke Results of the VIPS study. *Neurology.* 85, 1459–1466. doi: 10.1212/WNL.0000000000002065

Fullerton, H. J., Luna, J. M., Wintermark, M., Hills, N. K., Tokarz, R., Li, Y., et al. (2017). Parvovirus B19 infection in children with arterial ischemic stroke. *Stroke.* 48, 2875. doi: 10.1161/STROKEAHA.117.018272

Furber, K. L., Van Agten, M., Evans, C., Haddadi, A., Doucette, J. R., Nazarali, A. J., et al. (2017). Advances in the treatment of relapsing-remitting multiple sclerosis: the role of pegylated interferon beta-1a. *Degener. Neurol. Neuromuscul. Dis.* 7, 47–60. doi: 10.2147/DNND.S71986

Ge, R., Tornero, D., Hirota, M., Monni, E., Laterza, C., Lindvall, O., et al. (2017). Choroid plexus-cerebrospinal fluid route for monocyte-derived macrophages after stroke. *J. Neuroinflamm.* 14, 153. doi: 10.1186/s12974-017-0909-3

Ghersi-Egea, J. F., Strazielle, N., Catala, M., Silva-Vargas, V., Doetsch, F., Engelhardt, B., et al. (2018). Molecular anatomy and functions of the choroidal blood-cerebrospinal fluid barrier in health and disease. *Acta. Neuropathol.* 135, 337–361. doi: 10.1007/s00401-018-1807-1

Gonzalez, A. M., Leadbeater, W., Podvin, S., Borboa, A., Burg, M., Sawada, R., et al. (2010). Epidermal growth factor targeting of bacteriophage to the choroid plexus for gene delivery to the central nervous system *via* cerebrospinal fluid. *Brain Res.* 1359, 1–13. doi: 10.1016/j.brainres.2010.08.044

Grant, J. A. (1996). Victor Darwin Lespinasse: a biographical sketch. *Neurosurgery.* 39, 1232–1233. doi: 10.1097/00006123-199612000-00030

Haas, J., Rudolph, H., Costa, L., Faller, S., Libicher, S., Wurthwein, C., et al. (2020). The choroid plexus is permissive for a preactivated antigen-experienced memory B-cell subset in multiple sclerosis. *Front. Immunol.* 11, 618544. doi: 10.3389/fimmu.2020.618544

Haddad, M. R., Donsante, A., Zerfas, P., and Kaler, S. G. (2013). Fetal Brain-directed AAV Gene Therapy Results in Rapid, Robust, and Persistent Transduction of Mouse Choroid Plexus Epithelia. *Mol. Ther. Nucleic. Acids.* 2, e101. doi: 10.1038/mtna.2013.27

Hirano, S., Wang, X., and Suzuki, S. T. (2002). Restricted expression of protocadherin 2A in the developing mouse brain. *Brain Res. Mol. Brain Res.* 98, 119–123. doi: 10.1016/S0169-328X(01)00317-5

Hornung, M., and Sievert, H. (2021). It is time to fight ischemic stroke the best possible way. *Jacc-Cardiovasc. Inte.* 14, 793–795. doi: 10.1016/j.jcin.2021.02.017

Husted, R. F., and Reed, D. J. (1977). Regulation of cerebrospinal fluid bicarbonate by the cat choroid plexus. *J. Physiol.* 267, 411–428. doi: 10.1113/jphysiol.1977.sp011820

Jang, A., and Lehtinen, M. K. (2022). Experimental approaches for manipulating choroid plexus epithelial cells. *Fluids Barriers Cns.* 19, 36. doi: 10.1186/s12987-022-00330-2

Karimy, J. K., Zhang, J., Kurland, D. B., Theriault, B. C., Duran, D., Stokum, J. A., et al. (2017). Inflammation-dependent cerebrospinal fluid hypersecretion by the choroid plexus epithelium in posthemorrhagic hydrocephalus. *Nat. Med.* 23, 997–1003. doi: 10.1038/nm.4361

Kazemi, H., and Choma, L. (1977). H+ transport from CNS in hypercapnia and regulation of CSF [HCO3-]. *J. Appl. Physiol. Respir. Environ. Exerc. Physiol.* 42, 667–672. doi: 10.1152/jappl.1977.42.5.667

Kieseier, B. C. (2011). The mechanism of action of interferon-beta in relapsing multiple sclerosis. *CNS. Drugs.* 25, 491–502. doi: 10.2165/11591110-000000000-00000

Knobler, R. L., Panitch, H. S., Braheny, S. L., Sipe, J. C., Rice, G. P., Huddlestone, J. R., et al. (1984). Systemic alpha-interferon therapy of multiple sclerosis. *Neurology.* 34, 1273–1279. doi: 10.1212/WNL.34.10.1273

Kumar, V., Umair, Z., Kumar, S., Goutam, R. S., Park, S., Kim, J., et al. (2021). The regulatory roles of motile cilia in CSF circulation and hydrocephalus. *Fluids Barriers Cns.* 18, 31. doi: 10.1186/s12987-021-00265-0

Kunis, G., Baruch, K., Rosenzweig, N., Kertser, A., Miller, O., Berkutzki, T., et al. (2013). IFN-gamma-dependent activation of the brain's choroid plexus for CNS immune surveillance and repair. *Brain* 136, 3427–3440. doi: 10.1093/brain/awt259

Kuyama, H., Nagao, S., Tamiya, T., Nishimoto, A., Ohashi, T., Kawada, S., et al. (1987). [Choroid plexus papilloma found 6 years after initial V-P shunt treatment for hydrocephalus. Case report]. *Neurol. Med. Chir. (Tokyo).* 27, 341–346. doi: 10.2176/nmc.27.341

Li, J., Zhang, X., Guo, J., Yu, C., and Yang, J. (2021). Molecular Mechanisms and Risk Factors for the Pathogenesis of Hydrocephalus. *Front. Genet.* 12, 777926. doi: 10.3389/fgene.2021.777926

Limbrick, D. D., Morales, D. M., Shannon, C. N., Wellons, J. C., Kulkarni, A. V., Alvey, J. S., et al. (2021). Cerebrospinal fluid NCAM-1 concentration is

associated with neurodevelopmental outcome in post-hemorrhagic hydrocephalus of prematurity. *PLoS ONE* 16, e0247749. doi: 10.1371/journal.pone.0247749

Lindsey, A. E., Schneider, K., Simmons, D. M., Baron, R., Lee, B. S., Kopito, R. R., et al. (1990). Functional expression and subcellular localization of an anion exchanger cloned from choroid plexus. *Proc. Natl. Acad. Sci. U. S. A.* 87, 5278–5282. doi: 10.1073/pnas.87.14.5278

Llovera, G., Benakis, C., Enzmann, G., Cai, R. Y., Arzberger, T., Ghasemigharagoz, A., et al. (2017). The choroid plexus is a key cerebral invasion route for T cells after stroke. *Acta. Neuropathol.* 134, 851–868. doi: 10.1007/s00401-017-1758-y

Lobas, M. A., Helsper, L., Vernon, C. G., Schreiner, D., Zhang, Y., Holtzman, M. J., et al. (2012). Molecular heterogeneity in the choroid plexus epithelium: the 22-member gamma-protocadherin family is differentially expressed, apically localized, and implicated in CSF regulation. *J. Neurochem.* 120, 913–927. doi: 10.1111/j.1471-4159.2011.07587.x

Longatti, P., Basaldella, L., Orvieto, E., Dei Tos, A., and Martinuzzi, A. (2006). Aquaporin(s) expression in choroid plexus tumours. *Pediatr. Neurosurg.* 42, 228–233. doi: 10.1159/000092359

Luo, X. M., Lin, H., Wang, W., Geaney, M. S., Law, L., Wynyard, S., et al. (2013). Recovery of neurological functions in non-human primate model of Parkinson's disease by transplantation of encapsulated neonatal porcine choroid plexus cells. *J. Parkinsons. Dis.* 3, 275–291. doi: 10.3233/JPD-130214

Maimaitijiang, G., Watanabe, M., Shinoda, K., Isobe, N., Nakamura, Y., Masaki, K., et al. (2019). Long-term use of interferon-beta in multiple sclerosis increases Vdelta1(-)Vdelta2(-)Vgamma9(-) gammadelta T cells that are associated with a better outcome. *J. Neuroinflamm.* 16, 179. doi: 10.1186/s12974-019-1574-5

Matsumoto, N., Taguchi, A., Kitayama, H., Watanabe, Y., Ohta, M., Yoshihara, T., et al. (2010). Transplantation of cultured choroid plexus epithelial cells *via* cerebrospinal fluid shows prominent neuroprotective effects against acute ischemic brain injury in the rat. *Neurosci. Lett.* 469, 283–288. doi: 10.1016/j.neulet.2009.09.060

Mesquita, S. D., Ferreira, A. C., Sousa, J. C., Santos, N. C., Correia-Neves, M., Sousa, N., et al. (2012). Modulation of iron metabolism in aging and in Alzheimer's disease: relevance of the choroid plexus. *Front. Cell. Neurosci*. 6. doi: 10.3389/fncel.2012.00025

Millar, I. D., and Brown, P. D. (2008). NBCe2 exhibits a 3 HCO3(-):1 Na+ stoichiometry in mouse choroid plexus epithelial cells. *Biochem. Biophys. Res. Commun*. 373, 550–554. doi: 10.1016/j.bbrc.2008.06.053

Miyagi, Y., Natori, Y., Suzuki, S. O., Iwaki, T., Morioka, T., Arimura, K., et al. (2006). Purely cystic form of choroid plexus papilloma with acute hydrocephalus in an infant. Case report. *J. Neurosurg.* 105, 480–484. doi: 10.3171/ped.2006.105.6.480

Morales, D. M., Holubkov, R., Inder, T. E., Ahn, H. C., Mercer, D., Rao, R., et al. (2015). Cerebrospinal fluid levels of amyloid precursor protein are associated with ventricular size in post-hemorrhagic hydrocephalus of prematurity. *PLoS ONE* 10, e0115045. doi: 10.1371/journal.pone.0115045

Mortazavi, M. M., Griessenauer, C. J., Adeeb, N., Deep, A., Shahripour, R. B., Loukas, M., et al. (2014). The choroid plexus: a comprehensive review of its history, anatomy, function, histology, embryology, and surgical considerations. *Child. Nerv. Syst*. 30, 205–214. doi: 10.1007/s00381-013-2326-y

Mulroy, E., Snow, B., Bok, A., Simpson, M., Smith, A., Taylor, K. M., et al. (2021). A long-term follow-up of safety and clinical efficacy of NTCELL(R) [Immunoprotected (Alginate-encapsulated) porcine choroid plexus cells for xenotransplantation] in patients with Parkinson's disease. *Parkinsonism Relat. Disord*. 82, 128–132. doi: 10.1016/j.parkreldis.2020.12.005

Nakano, M., Hirooka, Y., Matsukawa, R., Ito, K., and Sunagawa, K. (2013). Mineralocorticoid receptors/epithelial Na(+) channels in the choroid plexus are involved in hypertensive mechanisms in stroke-prone spontaneously hypertensive rats. *Hypertens. Res*. 36, 277–284. doi: 10.1038/hr.2012.174

Narita, K., Kawate, T., Kakinuma, N., and Takeda, S. (2010). Multiple primary cilia modulate the fluid transcytosis in choroid plexus epithelium. *Traffic*. 11, 287–301. doi: 10.1111/j.1600-0854.2009.01016.x

Oi, S., Inagaki, T., Shinoda, M., Takahashi, S., Ono, S., Date, I., et al. (2011). Guideline for management and treatment of fetal and congenital hydrocephalus: Center Of Excellence-Fetal and Congenital Hydrocephalus Top 10 Japan Guideline 2011. *Childs. Nerv. Syst*. 27, 1563–1570. doi: 10.1007/s00381-011-1541-7

Ozturk, S. (2014). Epidemiology and the global burden of stroke-situation in Turkey. *World. Neurosurg.* 81, E35–E6. doi: 10.1016/j.wneu.2012.10.074

Panitch, H. S. (1987). Systemic alpha-interferon in multiple sclerosis. Long-term patient follow-up. *Arch. Neurol.* 44, 61–63. doi: 10.1001/archneur.1987.00520130047016

Perin, P., Rossetti, R., Ricci, C., Cossellu, D., Lazzarini, S., Bethge, P., et al. (2021). 3D Reconstruction of the Clarified Rat Hindbrain Choroid Plexus. *Front. Cell. Dev. Biol.* 9, 692617. doi: 10.3389/fcell.2021.692617

Petito, C. K., and Adkins, B. (2005). Choroid plexus selectively accumulates T-lymphocytes in normal controls and after peripheral immune activation. *J. Neuroimmunol*. 162, 19–27. doi: 10.1016/j.jneuroim.2004.12.020

Pople, I. K., and Ettles, D. (1995). The role of endoscopic choroid plexus coagulation in the management of hydrocephalus. *Neurosurgery*. 36, 698–701. doi: 10.1227/00006123-199504000-00009

Praetorius, J., and Damkier, H. H. (2017). Transport across the choroid plexus epithelium. *Am. J. Physiol. Cell. Physiol*. 312, C673–C86. doi: 10.1152/ajpcell.00041.2017

Praetorius, J., and Nielsen, S. (2006). Distribution of sodium transporters and aquaporin-1 in the human choroid plexus. *Am. J. Physiol. Cell. Physiol*. 291, C59–67. doi: 10.1152/ajpcell.00433.2005

Raha-Chowdhury, R., Henderson, J. W., Raha, A. A., Vuono, R., Bickerton, A., Jones, E., et al. (2019). Choroid plexus acts as gatekeeper for TREM2, abnormal accumulation of apoe, and fibrillary tau in Alzheimer's disease and in down syndrome dementia. *J. Alzheimers. Dis*. 69, 91–109. doi: 10.3233/JAD-181179

Rayasam, A., Faustino, J., Lecuyer, M., and Vexler, Z. S. (2020). Neonatal stroke and TLR1/2 ligand recruit myeloid cells through the choroid plexus in a CX3CR1-CCR2- and context-specific manner. *J. Neurosci*. 40, 3849–3861. doi: 10.1523/JNEUROSCI.2149-19.2020

Redzic, Z. B., Preston, J. E., Duncan, J. A., Chodobski, A., and Szmydynger-Chodobska, J. (2005). The choroid plexus-cerebrospinal fluid system: from development to aging. *Curr. Top. Dev. Biol.* 1–52. doi: 10.1016/S0070-2153(05)71001-2

Redzic, Z. B., and Segal, M. B. (2004). The structure of the choroid plexus and the physiology of the choroid plexus epithelium. *Adv. Drug. Deliver. Rev*. 56, 1695–1716. doi: 10.1016/j.addr.2004.07.005

Ricigliano, V., Morena, E., Colombi, A., Tonietto, M., Hamzaoui, M., Poirion, E., et al. (2021). Choroid plexus enlargement characterizes inflammatory multiple sclerosis. *Eur. J. Neurol*. 28, 140–141.

Rodriguez-Lorenzo, S., Ferreira Francisco, D. M., Vos, R., van Het Hof, B., Rijnsburger, M., Schroten, H., et al. (2020). Altered secretory and neuroprotective function of the choroid plexus in progressive multiple sclerosis. *Acta. Neuropathol. Commun*. 8, 35. doi: 10.1186/s40478-020-00903-y

Roepke, T. K., Kanda, V. A., Purtell, K., King, E. C., Lerner, D. J., Abbott, G. W., et al. (2011). KCNE2 forms potassium channels with KCNA3 and KCNQ1 in the choroid plexus epithelium. *FASEB J.* 25, 4264–4273. doi: 10.1096/fj.11-187609

Ruchoux, M. M., Rosati, C., Gelot, A., Lhuintre, Y., and Garay, R. (1992). Ultrastructural study of the choroid plexus of spontaneously hypertensive rats. *Am. J. Hypertens.* 5, 851–856. doi: 10.1093/ajh/5.11.851

Sahar, A., Feinsod, M., and Beller, A. J. (1980). Choroid plexus papilloma: hydrocephalus and cerebrospinal fluid dynamics. *Surg. Neurol.* 13, 476–478.

Schmidt, R., Ropele, S., Enzinger, C., Petrovic, K., Smith, S., Schmidt, H., et al. (2005). White matter lesion progression, brain atrophy, and cognitive decline: The Austrian Stroke Prevention Study. *Ann. Neurol.* 58, 610–616. doi: 10.1002/ana.20630

Schwartz, M., and Baruch, K. (2014). The resolution of neuroinflammation in neurodegeneration: leukocyte recruitment *via* the choroid plexus. *Embo. J.* 33, 7–20. doi: 10.1002/embj.201386609

Serot, J. M., Bene, M. C., and Faure, G. C. (2003). Choroid plexus, aging of the brain, and Alzheimer's disease. *Front. Biosci*. 8, s515–s521. doi: 10.2741/1085

Serot, J. M., Christmann, D., Dubost, T., and Couturier, M. (1997). Cerebrospinal fluid transthyretin: aging and late onset Alzheimer's disease. *J. Neurol. Neurosurg. Psychiatry*. 63, 506–508. doi: 10.1136/jnnp.63.4.506

Serot, J. M., Zmudka, J., and Jouanny, P. A. (2012). possible role for CSF turnover and choroid plexus in the pathogenesis of late onset Alzheimer's disease. *J. Alzheimers. Dis*. 30, 17–26. doi: 10.3233/JAD-2012-111964

Silva-Vargas, V., Maldonado-Soto, A. R., Mizrak, D., Codega, P., and Doetsch, F. (2016). Age-dependent niche signals from the choroid plexus regulate adult neural stem cells. *Cell. Stem. Cell*. 19, 643–652. doi: 10.1016/j.stem.2016.06.013

Silverberg, G. D., Mayo, M., Saul, T., Rubenstein, E., and McGuire, D. (2003). Alzheimer's disease, normal-pressure hydrocephalus, and senescent changes in CSF circulatory physiology: a hypothesis. *Lancet. Neurol.* 2, 506–511. doi: 10.1016/S1474-4422(03)00487-3

Skaper, S. D., Facci, L., Zusso, M., and Giusti, P. (2018). An inflammation-centric view of neurological disease: beyond the neuron. *Front. Cell. Neurosci*. 12. doi: 10.3389/fncel.2018.00072

Smith, Z. A., Moftakhar, P., Malkasian, D., Xiong, Z., Vinters, H. V., Lazareff, J. A., et al. (2007). Choroid plexus hyperplasia: surgical treatment and immunohistochemical results. Case report. *J. Neurosurg.* 107, 255–262. doi: 10.3171/PED-07/09/255

Spector, R., Keep, R. F., Snodgrass, S. R., Smith, Q. R., and Johanson, C. E. A. (2015). balanced view of choroid plexus structure and function: Focus on adult humans. *Exp. Neurol.* 267, 78–86. doi: 10.1016/j.expneurol.2015.02.032

Starkstein, S. E., Brockman, S., and Hayhow, B. D. (2012). Psychiatric syndromes in Parkinson's disease. *Curr. Opin. Psychiatr.* 25, 468–472. doi: 10.1097/YCO.0b013e3283577ed1

Stone, S. S., and Warf, B. C. (2014). Combined endoscopic third ventriculostomy and choroid plexus cauterization as primary treatment for infant hydrocephalus: a prospective North American series. *J. Neurosurg. Pediatr.* 14, 439–446. doi: 10.3171/2014.7.PEDS14152

Szmydynger-Chodobska, J., Strazielle, N., Gandy, J. R., Keefe, T. H., Zink, B. J., Ghersi-Egea, J. F., et al. (2012). Posttraumatic invasion of monocytes across the blood-cerebrospinal fluid barrier. *J. Cerebr. Blood. F. Met.* 32, 93–104. doi: 10.1038/jcbfm.2011.111

Tarkowski, E., Liljeroth, A. M., Minthon, L., Tarkowski, A., Wallin, A., Blennow, K., et al. (2003). Cerebral pattern of pro- and anti-inflammatory cytokines in dementias. *Brain Res. Bull.* 61, 255–260. doi: 10.1016/S0361-9230(03)00088-1

Wang, Y., Sabbagh, M. F., Gu, X., Rattner, A., Williams, J., Nathans, J., et al. (2019). Beta-catenin signaling regulates barrier-specific gene expression in circumventricular organ and ocular vasculatures. *Elife.* 8. doi: 10.7554/eLife.43257.035

Warf, B. C. (2005). Comparison of endoscopic third ventriculostomy alone and combined with choroid plexus cauterization in infants younger than 1 year of age: a prospective study in 550 African children. *J. Neurosurg.* 103, 475–481. doi: 10.3171/ped.2005.103.6.0475

Warf, B. C., and Kulkarni, A. V. (2010). Intraoperative assessment of cerebral aqueduct patency and cisternal scarring: impact on success of endoscopic third ventriculostomy in 403 African children. *J. Neurosurg. Pediatr.* 5, 204–209. doi: 10.3171/2009.9.PEDS09304

Wilson, G. R., Tan, J. T., Brody, K. M., Taylor, J. M., Delatycki, M. B., Lockhart, P. J., et al. (2009). Expression and localization of the Parkin co-regulated gene in mouse CNS suggests a role in ependymal cilia function. *Neurosci. Lett.* 460, 97–101. doi: 10.1016/j.neulet.2009.05.043

Wojcik, E., Carrithers, L. M., and Carrithers, M. D. (2011). Characterization of epithelial V-like antigen in human choroid plexus epithelial cells: potential role in CNS immune surveillance. *Neurosci. Lett.* 495, 115–120. doi: 10.1016/j.neulet.2011.03.051

Yamada, S., Ishikawa, M., and Nozaki, K. (2021). Exploring mechanisms of ventricular enlargement in idiopathic normal pressure hydrocephalus: a role of cerebrospinal fluid dynamics and motile cilia. *Fluids Barriers Cns.* 18 doi: 10.1186/s12987-021-00243-6

Zhang, J., Bhuiyan, M. I. H., Zhang, T., Karimy, J. K., Wu, Z., Fiesler, V. M., et al. (2020). Modulation of brain cation-Cl(-) cotransport *via* the SPAK kinase inhibitor ZT-1a. *Nat. Commun.* 11, 78. doi: 10.1038/s41467-019-13851-6

Zorad, S., Alsasua, A., and Saavedra, J. M. (1998). Decreased expression of natriuretic peptide A receptors and decreased cGMP production in the choroid plexus of spontaneously hypertensive rats. *Mol. Chem. Neuropathol.* 33, 209–222. doi: 10.1007/BF02815183

Frontiers in
Molecular Neuroscience

Leading research into the brain's molecular structure, design and function

Part of the most cited neuroscience series, this journal explores and identifies key molecules underlying the structure, design and function of the brain across all levels.

Discover the latest Research Topics

See more →

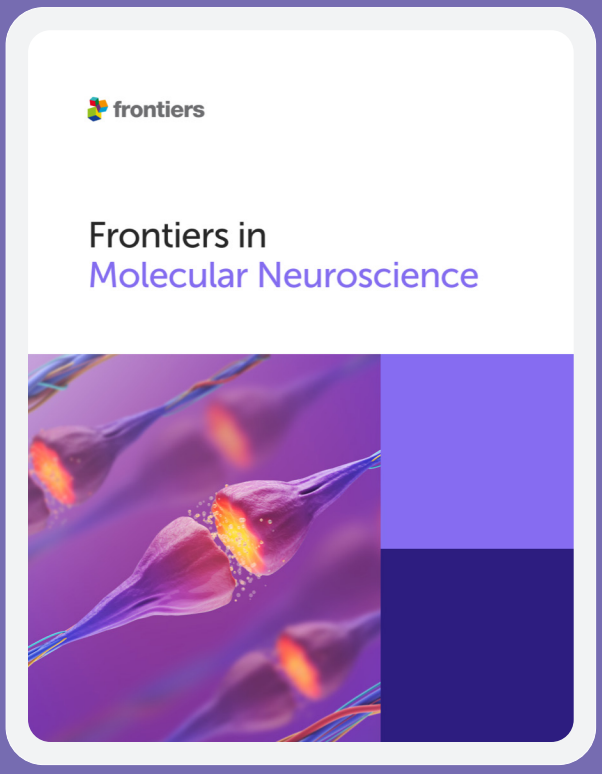

Frontiers

Avenue du Tribunal-Fédéral 34
1005 Lausanne, Switzerland
frontiersin.org

Contact us

+41 (0)21 510 17 00
frontiersin.org/about/contact